

Liver organoids, mass spectrometry, and separation science

Dissertation for the degree Philosophiae Doctor

by

Frøydis Sved Skottvoll



Department of Chemistry

Faculty of Mathematics and Natural Sciences

University of Oslo

2021

© **Frøydis Sved Skottvoll, 2022**

*Series of dissertations submitted to the
Faculty of Mathematics and Natural Sciences, University of Oslo
No. 2493*

ISSN 1501-7710

All rights reserved. No part of this publication may be
reproduced or transmitted, in any form or by any means, without permission.

Cover: Hanne Baadsgaard Utigard.
Print production: Representralen, University of Oslo.

Contents

Preface	III
List of papers	V
Summary	VII
Abbreviations	XI
Definitions	XIII
1 Introduction	1
1.1 Organoids	1
1.2 Mass spectrometry.....	5
1.2.1 Electrospray ionization mass spectrometry in bioanalysis	9
1.3 Separation prior to mass spectrometry	12
1.3.1 Liquid chromatography	12
1.3.2 Miniaturized liquid chromatography	14
1.3.3 Miniaturized separation in bioanalysis	17
1.4 Sample preparation prior to bioanalysis	19
1.4.1 Sample preparation in bottom-up proteomics	20
1.4.2 Sample preparation in small molecule bioanalysis	21
Electromembrane extraction	22
1.5 State of the art: organoids and mass spectrometry	24
1.5.1 Current challenges of mass spectrometry-based liver organoid analyses	26
2 Aim of study	27
3 Results and discussion.....	29
3.1 Liver organoids proteomics using mass spectrometry	30

3.1.1	Liver organoid and human liver tissue proteome comparison using sodium dodecyl sulfate-based sample preparation	30
3.1.2	Sodium dodecyl sulfate clearance using 96-well electromembrane extraction: a case study	34
3.2	Liver organoids small molecule drug analysis	36
3.2.1	Identifying unknown adult liver organoids neratinib drug metabolites using mass spectrometry	37
3.2.2	Establishing liver organoids heroin metabolizing properties using mass spectrometry	42
3.2.3	Challenges in small molecule conventional sample preparation	45
3.3	Parallel electromembrane extraction for high throughput liver organoids small molecule drug analysis	46
3.3.1	Optimizing parallel electromembrane extraction of heroin and metabolites	46
3.3.2	Parallel electromembrane extraction of liver organoid heroin metabolites	48
3.3.3	Miniaturized separation techniques not compatible with liver organoid small molecule analysis	50
3.4	Electromembrane extraction hyphenation with mass spectrometry for online liver organoids small molecule drug analysis	53
3.4.1	Technical setup	54
3.4.2	Proof-of-concept: online sampling and measuring of liver organoids small molecule methadone metabolites	56
3.4.3	Notes on challenges and potential related to online organoids incubation, sampling, separation and detection	59
4	Concluding remarks and future aspects	61
5	References	65

Preface

*Included in this thesis are three published papers (**Paper I, Paper II, Paper IV, Paper V**), and one submitted manuscript (**Paper III**). In addition, the author has contributed to three published papers [223, 224, 264], and one preprint [221], which are not included in the dissertation.*

The work presented in this thesis was carried out at the Department of Chemistry and Hybrid Technology Hub, HTH- *Centre of Excellence*, University of Oslo (UiO) in the period 2017-2021 under the supervision of Prof. Steven Ray Wilson and Prof. Ola Nilsen. I am forever grateful for your guidance, for providing me with challenging work, and for being a great source of inspiration. I would also like to thank Prof. Stefan Krauss for being an inspirational mentor, and for encouraging me to expand the horizon by co-organizing Nordic organ-on-a-chip symposium and hosting the Young Researcher workshop during HTH research retreats. I would also like to acknowledge UiO: Life Science, who has funded my position.

I want to acknowledge Prof. Elsa Lundanes for the support and guidance through limitless knowledge on chromatography. A big thank you to Prof. Stig Pedersen-Bjergaard for the guidance through the world of electromembrane extraction (EME) and to Dr. Gareth Sullivan for great discussions on organoid technology.

This thesis encompasses a journey of exploring bioanalytical strategies for liver organoids bioanalysis, initially with technical setup coupling a fully functional nanoLC-MS setup and method for peptide separations and protein identifications. I would like to thank Dr. Tomas Mikoviny for the support in an almost endless world of Orbitrap troubleshooting, and to Dr. Bernd Thiede for sharing knowledge on proteomic platforms and providing nanoLC-MS analyses and raw data during in-house instrumental difficulties. I would like to thank Dr. Magnus Saed Restan for discussions on SDS and EME.

Moving on to small molecule analysis, the work shifted to technical setup, method development, and troubleshooting regarding various bioanalytical techniques. I would like to thank Dr. Inger Lise Bogen for great discussions and guidance on pharmacologic topics, and Elisabeth Nerem for the technical assistance on microsomes and for running heroin UHPLC-MS analyses. A great thanks to Dr. Aleksandra Aizenshtadt and Dr. Sean Harrison for

developing organoids and for the fruitful discussions. Thanks to Dr. Matthias Stein for theoretical discussions on CE-UV and to Dr. Frederik André Hansen for the EME-discussions, and fabricating the EME-chip. I would also like to thank all co-authors for their contribution to the papers presented in this thesis.

Thanks to all my fellow colleagues and students in the bioanalytical chemistry group and the HTH center for contributing to a great working environment, especially Inge Mikalsen for reaching out on technical considerations. A special thanks to fellow colleagues Ass. Prof. Hanne Røberg-Larsen, Marita Clausen, Ph.D. candidate Christine Olsen, Henriette Engen Berg, Stian Kogler and Kristina Sæterdal for sharing advice and experiences. Thanks to master students Ida Sneis Boger for great work on organoid heroin metabolism, and Ago Mrsa for fighting it through nanoLC heroin analysis and for all the coffee walks.

Putting the academic work aside, I would like to express gratitude to the ones involved in facilitating my organizational experiences, being a board member at the Department of Chemistry, member of the faculty election board, and the Ph.D. program council at the Faculty of Mathematics and Natural Sciences.

The current work has also included popular scientific dissertation through “Kjemi Grand Prix”, “Forsker Grand Prix”, and all the invited talks that followed. A big thank you to everyone involved, especially to Yngve Vogt and to Maren Bækkelund Ellingsen.

I want to express my deepest gratitude and appreciation to all my family and friends for being encouraging and helpful during these years. A special thanks to uncle Frode, for providing endless support and care throughout this stressful time.

Johan, thank you for all the love and patience during this work. At last, this thesis is dedicated to the memory of my loving mother.



Frøydis Sved Skottvoll
Oslo, December 2021

List of papers

- I 3D cell culture models and organ-on-a-chip: Meet separation science and mass spectrometry.**
Ann Lin, Frøydis Sved Skottvoll, Simon Rayner, Stig Pedersen-Bjergaard, Gareth Sullivan, Stefan Krauss, Steven Ray Wilson, Sean Harrison. *Electrophoresis* 41, 1-2 (2020) 56-64.
- II Electromembrane extraction of sodium dodecyl sulfate from highly concentrated solutions.**
Magnus Saed Restan, Frøydis Sved Skottvoll, Henrik Jensen, Stig Pedersen-Bjergaard. *Analyst* 145, 14 (2020) 4957-4963.
- III Quantitative ramanomics for chemometric phenotyping of three-dimensional liver organoids.**
Vernon LaLone*, and Aleksandra Aizenshtadt*, John Goertz, Frøydis Sved Skottvoll, Marco Barbero Mota, Junji You, Xiaoyu Zhao, Henriette Engen Berg, Justyna Stokowiec, Minzhi Yu, Anna Schwendeman, Hanne Scholz, Steven Ray Wilson, Stefan Krauss**, and Molly Stevens**. *Manuscript submitted to Nature Biotechnology*.
- IV Electromembrane extraction and mass spectrometry for liver organoid drug metabolism studies.**
Frøydis Sved Skottvoll, Frederik André Hansen, Sean Harrison, Ida Sneis Boger, Ago Mrsa, Magnus Saed Restan, Matthias Stein, Elsa Lundanes, Stig Pedersen-Bjergaard, Aleksandra Aizenshtadt, Stefan Krauss, Gareth Sullivan, Inger Lise Bogen, Steven Ray Wilson. *Analytical Chemistry* 93, 7 (2021) 3576-3585.
- V Direct electromembrane extraction based mass spectrometry: a tool for studying drug metabolism properties of liver organoids.**
Frøydis Sved Skottvoll, Aleksandra Aizenshtadt, Frederik André Hansen, Mikel Amirola Martinez, Jannike Mørch Andersen, Inger Lise Bogen, Jörg P. Kutter, Stig Pedersen-Bjergaard, Elsa Lundanes, Stefan Krauss, Steven Ray Wilson. *Analysis & Sensing* (2022) e202100051.

Summary

Organoids are predicted to change the game of medicine by acting as an in vitro 3D representation of human organ functionality. By developing such organoids from patient derived stem cells or adult tissue one enables such as drug discovery, disease modeling and personalized medicine under more realistic conditions. Organoids are still at the developmental stage and fundamental questions concerning the functionality of the developed organoids remain to be answered. Compared to other biosamples, mass spectrometry (MS) has rarely been used in organoid analyses, especially in organ-on-a-chip systems. This thesis leverages MS and separation science for bioanalysis of liver organoids, spanning from protein identification to small molecule drug metabolite detection. With the aim of selective, high throughput liver organoid analyses and online integration, both conventional and cutting edge electromembrane extraction (EME) sample preparation approaches were explored.

The review in **Paper I** provided an overview of possible analytical tools for MS-based organoid analyses, discussing approaches for online integration. Using nano liquid chromatography MS (nanoLC-MS), the initial establishment of liver organoid untargeted proteomic functionality was linked to human liver tissue. Several proteins connected to central liver functions were identified in the liver organoids. A conventional bottom-up sample preparation procedure was applied, which included protein separation using sodium dodecyl sulfate polyacrylamide gel electrophoresis (SDS-PAGE) and removal of the MS-incompatible detergent SDS before analysis. Such conventional sample preparations steps are manual and time-consuming, and EME was explored as an alternative approach for simpler sample preparation

in **Paper II**. A fundamental study of the SDS removal using 96-well parallel-EME was conducted. Although complete SDS removal was achieved in standard solutions, the method was not found to be mature for liver organoid proteomic sample preparation and SDS removal. Hence, conventional sample preparation procedures should still be preferred for large biomolecule analysis.

Next, the drug metabolizing properties of liver organoids were assessed regarding small molecules, here tested by measuring neratinib-, heroin- and methadone metabolism. Unknown adult liver organoid neratinib metabolites were identified using capillary LC-MS (capLC-MS) in **Paper III**. In **Paper IV**, the liver organoid heroin metabolizing properties were established using conventional LC-MS, detecting liver organoid heroin phase I metabolites and low amounts of phase II metabolites. The conventional low throughput centrifugation-based sample preparation was applied for the above-mentioned small molecule studies, and again parallel-EME was explored to simplify sample preparation.

Originally shown to be a great fit with small molecule extractions, the applicability of parallel-EME with liver organoid heroin metabolism was explored in **Paper IV**. The 96-well EME setup was successfully applied for selective, parallel extraction of heroin and heroin phase I metabolites from liver organoids, using analyte optimized EME-conditions and conventional LC-MS. Capillary electrophoresis (CE) and nanoLC were explored regarding sensitivity, compatibility of the methodology of **Paper IV**, and the fit for future online analysis. However, nanoLC and CE-UV were not found to be mature for online MS-analysis and integration with EME.

The high-pressure capLC-MS measurements, low-pressure liver organoid incubation and EME sample clean up on-chip were hyphenated by a two-

position 10-port valve in **Paper V**. As a proof-of-concept, we achieved online integration of 1) organoid incubation in methadone, 2) EME-sampling, and 3) capLC-MS measurements. With the current setup we successfully mapped the methadone-metabolizing properties of adult liver organoids for 24 hours.

Using bioanalytical tools such as MS and separation sciences, we could establish that the liver organoids displayed liver organ functionality. EME combined with small molecule extractions and liver organoids were well matched and integrated online; however, EME did not prove well suited for large biomolecule sample preparation. During this thesis, the developed bioanalytical strategies for liver organoid analyses contributed to greater insight into organoid response and functionality. Hence, the developed bioanalytical strategies could be important tools in organoid development. Furthermore, online organoid integration using EME developed here could be used as a starting point towards developing future organ-on-a-chip systems integrated with mass spectrometry, which would be valuable in drug development, disease modeling, and personalized medicine.

Abbreviations

2D	two-dimensional
3D	three-dimensional
6-MAM	6-monoacetylmorphine
ACN	acetonitrile
BGE	background electrolyte
capLC	capillary liquid chromatography
CE	capillary electrophoresis
CID	collision induced dissociation
CYP	cytochromes P450
DDA	data-dependent acquisition
dEME-MS	direct electromembrane extraction mass spectrometry
DEHP	di-(2-ethylhexyl) phosphate
DESI	direct electrospray ionization
EDDP	2-ethylidene-1,5-dimethyl-3,3-diphenylpyrrolidine
ELISA	enzyme linked immunosorbent assay
EMDP	2-ethyl-5-methyl-3,3-diphenylpyrroline
EME	electromembrane extraction
ESC	embryonic stem cells
ESI	electrospray ionization
FASP	filter aided sample preparation
GC	gas chromatography
GO	gene ontology
hCE1	human carboxyl esterases 1
hCE2	human carboxyl esterases 2
HLMs	human liver microsomes
HPLC	high-performance liquid chromatography
ID	inner diameter
IS	internal standard
iPSC	induced pluripotent stem cells
LLE	liquid liquid extraction
LC	liquid chromatography
LOD	limit of detection
LOQ	limit of quantification
LPME	liquid-phase microextraction
M3G	morphine-3-glucuronide
M6G	morphine-6-glucuronide
M_M	molar mass

MP	mobile phase
MRM	multiple reaction monitoring
MS	mass spectrometry
MSI	mass spectrometry imaging
MS/MS	tandem mass spectrometry
<i>m/z</i>	mass-to-charge ratio
nanoLC	nano liquid chromatography
NPOE	2-nitrophenyl octyl ether
NPPE	2-nitrophenyl pentyl ether
OoC	organ-on-a-chip
Orbitrap	quadrupole- Orbitrap
Parallel-EME	parallel electromembrane extraction
PIS	product ion scan
PDB	protein database ID
Q	quadrupole
RP	reversed-phase
RSD	relative standard deviation
SD	standard deviation
SDS	sodium dodecyl sulfate
SDS-PAGE	sodium dodecyl sulfate polyacrylamide gel electrophoresis
SFC	supercritical fluid chromatography
SIM	selected ion monitoring
SLM	supported liquid membrane
SP	stationary phase
SPE	Solid phase extraction
SP3	single-pot, solid-phase-enhanced sample-preparation
qPCR	quantitative polymerase chain reaction
TOF	time of flight
<i>t_r</i>	retention time
UGT	uridine 5'-diphospho-glucuronosyltransferase
UHPLC	ultra-high performance liquid chromatography
<i>W_{0.5}</i>	Peak width at half peak height
ZO1	zonula occludens-1

Definitions

Acquired and copied from:

1. J. Labuda, R.P. Bowater, M. Fojta, G. Gauglitz, Z. Glatz, I. Hapala, J. Havliš, F. Kilar, A. Kilar, L. Malinovská, H.M.M. Sirén, P. Skládal, F. Torta, M. Valachovič, M. Wimmerová, Z. Zdráhal, D.B. Hibbert, *Terminology of bioanalytical methods (IUPAC Recommendations 2018)*, Pure and Applied Chemistry, 90 (2018) 1121-1198.
2. Araujo, P. *Key aspects of analytical method validation and linearity evaluation*, Journal of chromatography B, 877 (2009), 2224-2234.
3. A. Marsee et al. *Building consensus on definition and nomenclature of hepatic, pancreatic, and biliary organoids*, Cell Stem Cell, 28 (2021) 816-832.
4. International Union of Pure and Applied Chemistry (IUPAC) Gold Book. <https://goldbook.iupac.org/> (accessed on 12.10.2021).
5. Murray, Kermit K., Boyd, Robert K., Eberlin, Marcos N., Langley, G. John, Li, Liang and Naito, Yasuhide. *Definitions of terms relating to mass spectrometry (IUPAC Recommendations 2013)*, Pure and Applied Chemistry, 85 (2013) 1515-1609.

* Definition made by the author.

Biomolecule¹ “Molecule of biological origin. Most biomolecules are organic compounds present in living organisms. They may also include exogenous molecules modified by metabolism.”

Limit of Detection² “the lowest amount of analyte in a sample that can be reliably detected but not necessarily quantitated by a particular analytical method.”

Offline* When a procedure and detection are not connected in one fluidic system. The procedure is performed in a manual action by the operator.

Online* When a procedure is connected to detection in one fluidic system.

Organoid³ “Three-dimensional structure derived from pluripotent stem cells, progenitor and/or differentiated cells that self-organize through cell-cell and cell-matrix interactions to recapitulate aspects of the native tissue architecture and function in vitro.”

- Repeatability**⁴ “The closeness of agreement between independent results obtained with the same method on identical test material, under the same conditions (same operator, same apparatus, same laboratory and after short intervals of time).”
- Reproducibility**⁴ “The closeness of agreement between independent results obtained with the same method on identical test material but under different conditions (different operators, different apparatus, different laboratories and/or after different intervals of time).”
- Robustness**² “the constancy of the results when internal factors such as flow rate, column temperature, injection volume, mobile phase composition or any other variable inherent to the method of analysis are varied deliberately.”
- Ruggedness**² “the constancy of the results when external factors such as analyst, instruments, laboratories, reagents, days are varied deliberately.”
- Selectivity**⁴ “(qualitative): The extent to which other substances interfere with the determination of a substance according to a given procedure.”
- Sensitivity**⁵ **in analytical chemistry:** “The slope of the calibration curve.”

1 Introduction

1.1 Organoids

Organoids are three-dimensional (3D) tissue-like cell models developed to recapitulate the biology of human organs [1]. Compared to the established animal models or simple two-dimensional (2D) cell monolayers, organoids have the potential to give greater insight into the human organ function and response [2] and provide a promising tool to advance the future of biomedical research, e.g., in drug development, disease modeling and personalized medicine [3, 4]. Reflecting its potential, organoid technology was chosen as “Method of the Year 2017” by Nature Methods [5].

Organoids can be derived from embryonic stem cells (ESC), adult stem cells, but also from a groundbreaking technology reprogramming human somatic cells introduced by Takahashi et al. in 2006-2007, namely induced pluripotent stem cells (iPSC, **Figure 1A**) [6, 7]. Pluripotent stem cell-derived organoid formation principles involve three significant processes to mimic embryonic organ development. First, the activation or inhibition of the key signaling pathways regulating developmental patterning (using commercial morphogens and signaling inhibitors) leads to germ-layer specification (ectoderm, mesoderm, or endoderm). Secondly, terminal differentiation of the desired cell types within the organoid is developed using different media formulations (e.g., endoderm develop into intestine, stomach, lung, thyroid or liver organoids), either in 2D culture, or as 3D organoids. Organoids could be formed by aggregation of progenitors in micro cavities and/or embedding in extracellular matrix (e.g , Matrigel). Lastly, maturation of cell types of interest could be achieved by prolonged cultivation, supplementation with growth

factors and morphogens, and/or modulation of metabolic processes. Adult tissue cells can also be the source of organoid formation (**Figure 1B**), hereafter referred to as adult organoids [8]. Here, the adult tissue cells obtain 3D structures by similar procedures to that of organoid formation from stem cells, namely by aggregation or by embedding the cultures into a 3D matrix.

Organoids have been developed from a wide variety of differentiation strategies to resemble human in the micrometer scale such as the brain, heart, kidney, liver, the embryonic state, and recently endometrial organoids were derived from gland fragments recovered from menstrual flow (**Figure 2**) [9-15].

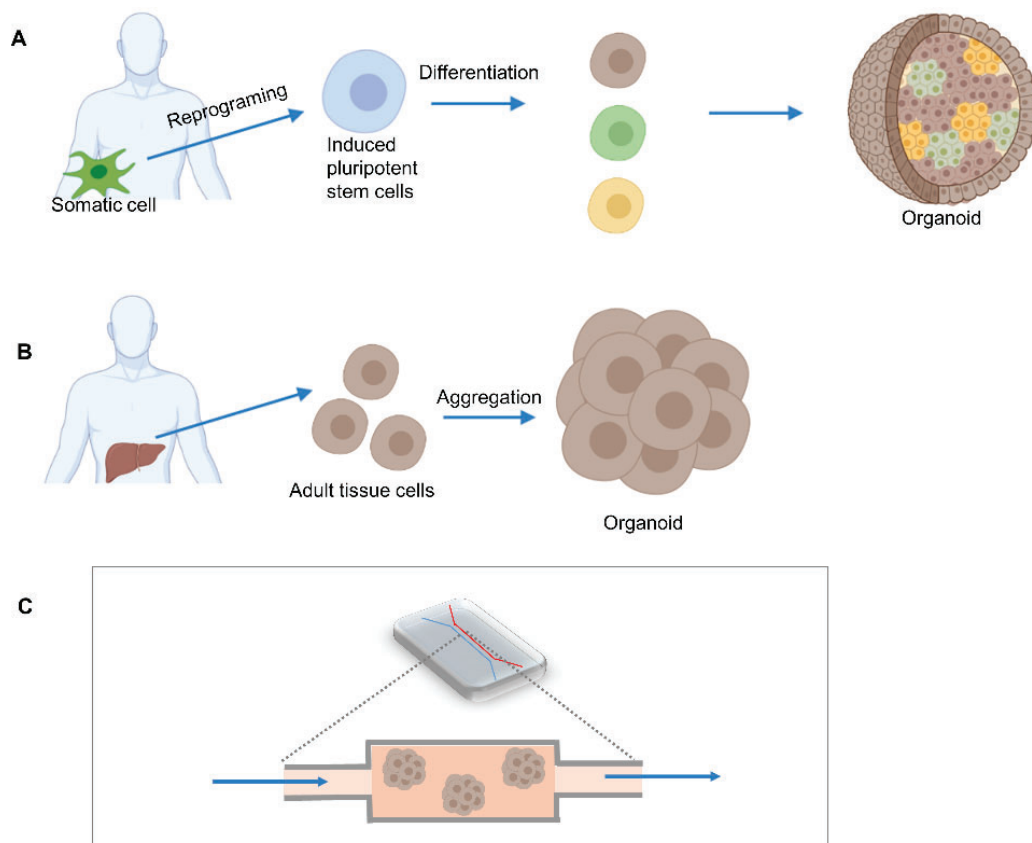


Figure 1. Schematic overview of organoid formation. A) Organoids generated from iPSC, B) adult organoids generated from adult tissue cells and C) Example of organoids integrated in a microfluidic chip. The schematic figures were partially made in BioRender.

The organoids are commonly grown in suspension. However, organoids can also be integrated in a microfluidic chip, namely organ-on-a-chip (OoC), and organoid-on-a-chip (also referred to as microphysiological systems) [16]. The organoid integration on chip enables a microfluidic controllable environment, and also facilitates the manipulation of organoids by the addition of e.g., xenobiotics, externally sourced compounds to an organism, such as drugs (Figure 1C) [17, 18].

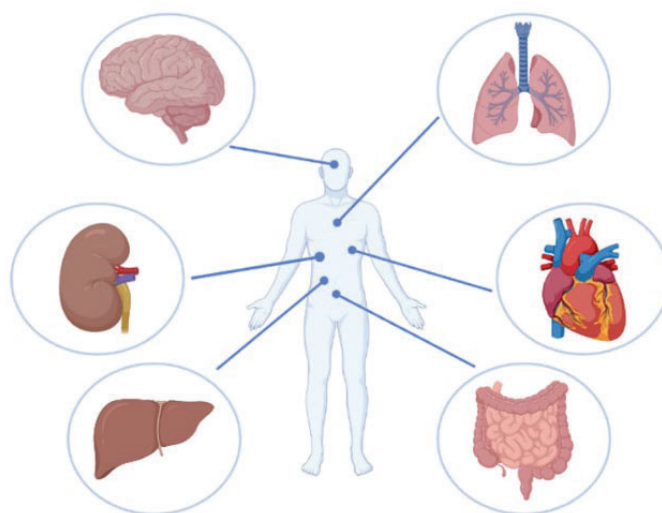


Figure 2. Schematic showing a selection of organs that organoids have been developed to resemble; brain, kidney, liver, lung, heart and intestines. The schematic figure was made in BioRender.

With the liver being the main site for drug biotransformation (hereafter called drug metabolism) [19], traditionally applied simple liver models such as primary hepatocytes, human liver microsomes (HLMs), and S9 fractions have displayed limiting organ resemblance, e.g., with regards to metabolizing properties [20]. Hence, liver organoids would be of specific interest to better model human liver functions such as drug metabolism and hepatotoxicity [21-24].

The liver organoids generated are still at the developmental stage [25, 26]. Therefore, fundamental questions on the liver organ functionality of the developed liver organoids remain to be assessed. Bioanalysis encompasses the quantitatively and or qualitatively measurement of biomolecules (e.g., amino acids, small metabolites, peptides, proteins, or drug metabolites) in biological matrices [27]. Thus, bioanalysis could give valuable information on the plethora of different cellular mechanisms related to liver organoids. However, challenges such as small sample volumes (low μL -range), low concentrations of analyte and highly complex matrices must be considered if liver organoids target molecules are to be measured in a sensitive, unbiased way. Molecular and cellular detection techniques are considered highly accepted for organoid analysis (**Figure 3AB, Paper I**). With regards to, e.g., protein expression, a variety of immunoassays are applied (such as immunofluorescence microscopy, western blot or enzyme linked immunosorbent assay, ELISA), measuring target proteins based on protein affinity to the antibody. However, the range of applications is limited to antibody availability and selectivity, and mL-scale sample volumes are often required [28, 29].

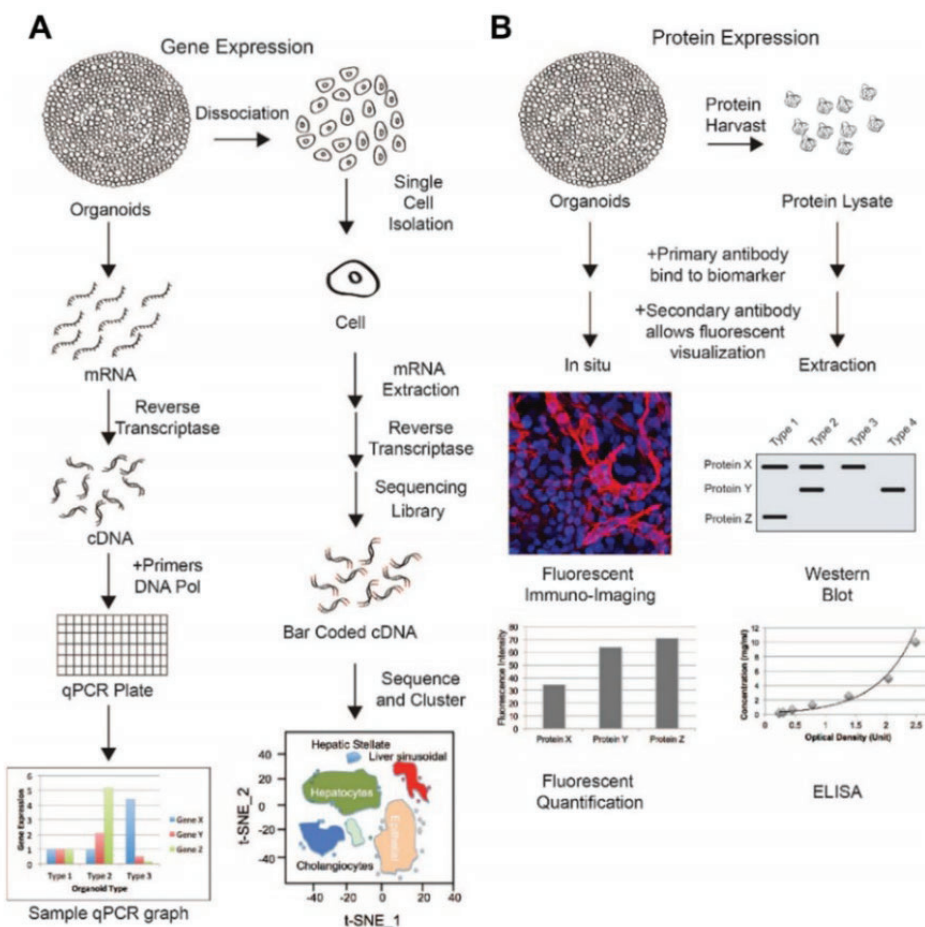


Figure 3. Characterization of organoids through biomarkers. A) Schematic of gene expression techniques quantitative polymerase chain reaction (qPCR), and single cell RNA. B) Schematic of the protein expression techniques immunofluorescence, western blot and ELISA. Reprinted with permission from WILEY-VCH Verlag GmbH & Co.

For multiplexed bioanalytical measurements of, e.g., small molecule drug metabolites [30-32] and protein analysis [33-36], together with the possibility of high throughput integration on-chip [37], the mass spectrometer would be the instrument of choice for liver organoids bioanalysis (**Paper I**).

1.2 Mass spectrometry

The mass spectrometer has evolved to be a powerful tool in a great number of scientific fields, very much including bioanalysis [38-41]. In MS, positively or negatively charged ions in vacuum are separated and measured based on the mass-to-charge ratio (m/z). The mass spectrometer is constructed from an

ion source (for molecule ionization), a mass analyzer (separation of ion m/z), and a detector (conversion of signal) (**Figure 4A**) [42].

There are different types of mass analyzers, e.g., singly operated, such as the quadrupole (Q), ion trap, and time of flight (TOF) [43]. When operated in single mode, one or a selection of target ions are guided through the mass analyzer and measured, typically using MS modes such as full scan or selected ion monitoring (SIM, **Figure 4B**).

The mass analyzers can also be geometrically placed in series (tandem mass spectrometry, MS/MS). When operated in MS/MS, the ions undergo fragmentation between the two mass analyzers, thus elucidating more structural information and providing higher selectivity compared to single mode MS [44]. Fragmentation is commonly facilitated using collision induced dissociation (CID) by collision of the analyte ions with inert gas molecules (e.g., N₂ or Ar) [45]. Examples of MS/MS configurations are the triple Q [46], and TOF-TOF, or hybrid mass analyzers such as the Q-TOF or Q-Orbitrap (Orbitrap) [47, 48]. In this thesis, the triple Q and Orbitrap were applied for targeted and untargeted measurements.

When operated in targeted MS/MS, background noise is reduced by pre-selecting one, or several target ions (precursor ions) for mass analyzer transmission, with either one, several or all m/z fragments (fragment ions) to be monitored (**Figure 4C**). Thus, increased selectivity, sensitivity, and throughput can be achieved in targeted MS/MS. One MS/MS mode when using, e.g., triple Q is multiple reaction monitoring (MRM) [49], with one or several precursor ions are fragmented into one or multiple fragment ions.

In untargeted MS/MS and, e.g., data-dependent acquisition (DDA, **Figure 4D**), the first mass analyzer performs full scan of a selected m/z range, followed by ion fragmentation based on precursor ions selected from the full scan spectrum using criteria such as signal intensity and charge state [50]. However, untargeted identifications have the drawbacks of providing low sensitivity, precision and speed compared to targeted MS/MS.

The performance of a mass spectrometer can be evaluated according to its resolving power, mass accuracy, sensitivity, and dynamic range [51, 52]. The Orbitrap is considered a high-resolution instrument platform with a fast scan rate and high mass accuracy [53-55]. With the possibility of operating in both targeted MS/MS and data dependent acquisition, the Orbitrap quickly became essential for numerous areas of research [56]. The triple Q is considered a low-resolution instrument. However the two levels of mass selection in targeted methods such as MRM allow for quantitative analyses with very high sensitivity [51].

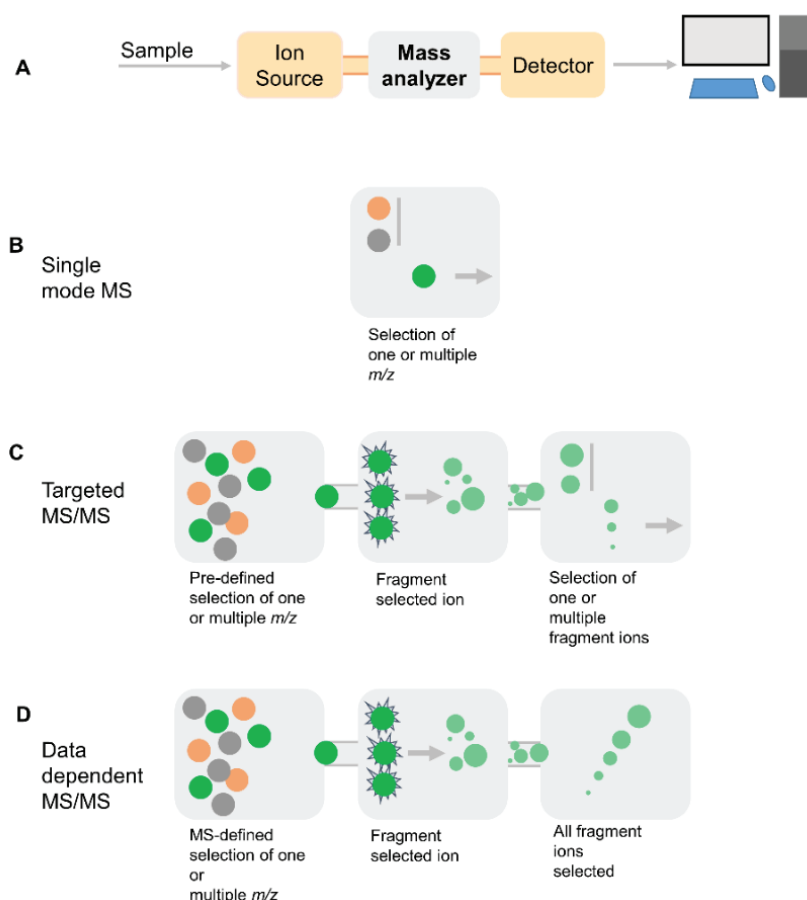


Figure 4. A) The mass spectrometric instrumental setup. B) MS operated in single mode. C) MS operated in targeted MS/MS. D) MS operated in untargeted MS/MS data dependent acquisition. (Targeted MS/MS was used in Paper III, IV and V, and untargeted DDA was used in Section 3.1.1 and Paper IV). Adapted from [44].

The MS detection relies on ionized molecules in the gaseous state. Electrospray ionization (ESI) was introduced by Yamashita and Fenn in 1984 and quickly evolved to be an essential tool in bioanalysis, facilitating the transfer of molecules in solution to molecule ions in the gas phase prior to MS detection [57-59]. Although the mass spectrometer is considered a mass-sensitive detector, ESI coupled to MS (ESI-MS) is considered a concentration-sensitive detection method [60]. Little molecule fragmentation occurs in the ESI ion source; subsequently, more structural information is kept prior to MS detection [61, 62]. Hence, ESI is considered a versatile soft ionization

technique beneficial for the determination of various molecules such as proteins, peptides, and small molecules [43, 63].

1.2.1 Electrospray ionization mass spectrometry in bioanalysis

The improvements in MS instrumental resolution and sensitivity over the past two decades have led to the facilitation of mass spectrometric elucidation of structural, quantitative, and qualitative information in proteomics. In analogy with the progress of large-scale genomics and the Human Genome Project [64], the term proteomics was introduced in 1997 by Humphery-Smith et al. [65]. The science was later described as the study of the proteome, i.e., the complete set of proteins expressed by a genome, by a cell, or a tissue [66, 67]. The Human Proteome Project was initiated in complementary to the decade of genomic research, with the goal of observing all proteins produced from the human genome [68, 69]. However, proteomes are highly complex, with protein concentration range exceeding the dynamic range of an instrument or method [51].

Both the determination of selected peptide(s) (i.e. targeted) or large scale protein identification (also termed global, discovery, untargeted, or comprehensive proteomics) can be performed [70]. There are two approaches to MS-based protein analysis; analyzing intact proteins (i.e. top-down proteomics) [27, 71], or enzymatically derived peptides (i.e. bottom-up proteomics) [27, 72], see **Section 3.1.1** and **Paper IV**, and **Section 1.4.1** for sample preparation.

The high molar mass (M_M) of a protein introduces several challenges in top-down proteomics. Proteins can be difficult to handle with limited solubility, requiring MS incompatible additives such as detergents [73]. High-resolution

MS instrumentation is also needed, to be able to distinguish between the numerous of different protein isoforms. Also, low detection limits are associated with top-down proteomics [74]. On the other hand, top-down proteomics enables the study of a protein as a whole entity, and has shown to be highly valuable in studying post translational modifications [75].

Providing lower detection limits, the small peptide M_M bottom-up proteomics is the preferred approach (**Figure 5**). Relying on peptide detection and well-established peptide libraries, DDA is commonly applied in untargeted bottom-up proteomics [76]. Trypsin cleaved peptide detection generates easily interpretable and repeatable peptide fragmentation spectra, enabling protein identification through search engines (e.g., MASCOT) peptide matches from spectral libraries such as SWISS-PROT [77, 78]. Library matched spectra lead to the identification of peptides, which are further recognized to their corresponding proteins.

Large protein identification datasets are generated, thus facilitating biological interpretation through protein analyses such as gene ontology (GO) [79], relating a protein to a specific ontology term.

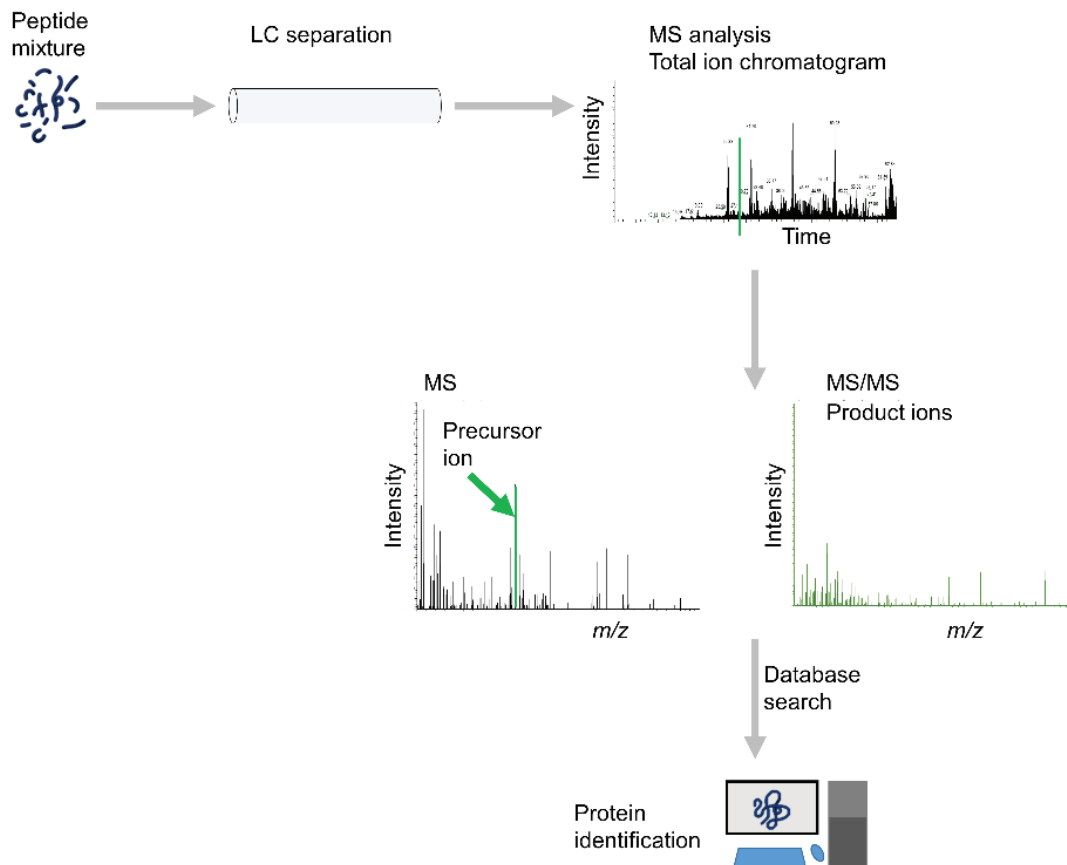


Figure 5. Illustration of the bottom-up proteomic workflow using nano liquid chromatography (nanoLC) separation and the MS analysis. Enzymatically cleaved proteins are separated on a nanoLC column, with the MS mode set to be DDA. A total ion chromatogram is acquired, and the MS and MS/MS spectra are matched against a protein sequence database of theoretical peptide product ion spectra. The outcome is the identity of peptides, further identified to their corresponding proteins. (The bottom-up proteomic workflow was used in Section 3.1.1 and Paper IV).

Salt or other compounds from biological matrices may substantially suppress or enhance analyte signal (matrix effects), consequently affecting the analyte response when using ESI-MS [80-84]. Thus, prior to ESI-MS detection, removing possibly interfering components using sample clean-up (**Section 1.4**) and additional separation steps are often required. Separation could be performed, e.g., using high-performance liquid chromatography (HPLC), hereafter called liquid chromatography (LC).

1.3 Separation prior to mass spectrometry

Different separation techniques exist, such as capillary electrophoresis (CE) and chromatography. Chromatography is the separation of several components based on the component distribution between a mobile phase (MP) and a stationary phase (SP), through, e.g., a column. The mobile phase can be a liquid (LC), gas (gas chromatography, GC), or supercritical fluid (supercritical fluid chromatography, SFC) [85, 86].

The first paper on traditional LC was published in 1908 by Tswett (for partial English summary, see [87]), and was rediscovered in the early 1930s by Kuhn and Lederer [88]. In bioanalysis of e.g. non-volatile molecules such as proteins, peptides, and many drugs, the use of LC is the method of choice compared to GC [89].

1.3.1 Liquid chromatography

In LC, a typical setup consists of a LC-pump pumping a solvent (the MP) and the sample introduced through a column, before reaching a detector (**Figure 6**) [90]. Compounds are separated by their different interactions with the SP, and move with different velocities through the column, eluting at different time points (retention time, t_r) prior to detection.

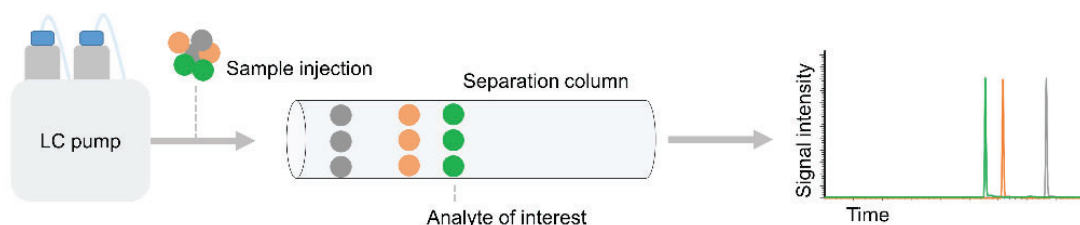


Figure 6. General principle of compound separation and detection in LC, with the analyte of interest and interferences eluting from the separation column at different time points depending on the interaction with the SP.

Reversed-phase (RP) LC is the most common separation principle for LC [91], being ESI-MS compatible, and providing high efficiency and repeatability. Compared to normal-phase LC originally applied by Tswett, where increasing analyte polarity gives greater retention, the separation principle of RP LC is considered to be the opposite, hence the name “reversed”. In RP LC, a hydrocarbon chain chemically bonded on a silica surface constitutes the SP, and increasing hydrophobicity gives greater SP retention [92, 93]. The MP is typically composed of a buffered aqueous solution mixed with an organic solvent, e.g., methanol or acetonitrile (ACN) [94, 95].

The main column format in LC is silica particle-packed columns with spherical, porous beads. However particles having a solid core and a porous layer (also called core shell particles, and other names) are also widely used [96, 97]. Particle sizes range from 2-5 μm , or sub 2 μm sized particles used in ultra-high performance liquid chromatography (UHPLC) [98].

The term band broadening is used to describe the dispersion of analyte molecules as it passes through the separation column, and the chromatographic performance of a LC column is typically evaluated based on the efficiency (N, **Equation 1**).

$$N = \frac{L}{H} \tag{Equation 1}$$

Where the increase in column efficiency increases with increasing column length (L) and decreasing plate height (H), where H can be expressed by the van Deemter equation (**Equation 2**) [99].

$$H = A + \frac{B}{u} + C u = 2\lambda dp + \frac{2\gamma D_m}{u} + \frac{f(k) dp^2 u}{D_m} \tag{Equation 2}$$

In the abbreviated version of H, A is the eddy dispersion (radial dilution) [100], B is the molecular dispersion (longitudinal) [99, 101], C is resistance to mass transfer between the SP and MP [102], and the linear velocity, u. In the extended equation of H, the λ is a constant dependent on the particle shape, d_p is the particle diameter, γ is a constant, D_m is the diffusion coefficient for a solute in the MP, and $f(k)$ is a function dependent on the retention factor, k.

1.3.2 Miniaturized liquid chromatography

LC columns can be classified based on the column inner diameter (ID) (**Table 1**) [103], and in this thesis, 0.5 mm columns are designated capillary LC (capLC). The use of narrow-bore and conventionally sized LC columns with ID in the 2-5 mm range are frequently used in analytical chemistry, designed to handle large sample volumes.

Table 1. Suggested column designation according to the column ID (mm). Adapted from [103].

Suggested column designation	Column ID (mm)
Conventional LC	3 - 5
Narrow-bore LC	2
Micro LC	0.5-1
Capillary LC	0.1-0.5
Nano LC	0.01-0.1

However, small sample sizes and analytes of low abundance could give difficulties in sensitive analyte determination using conventional/narrow-bore columns. Analyte and sample volume would be diluted inside the large ID conventional/narrow-bore columns, below the limit of detection (LOD) of the LC-MS method. Improvement in analyte signal intensity can be achieved by decreasing the ID of the separation column (**Figure 7**). The decrease in

column ID would reduce the radial dilution of the sample volume injected, and lead to theoretical enhancement in signal intensity compared to larger column ID when concentration sensitive detectors such as ESI-MS are applied [104, 105].

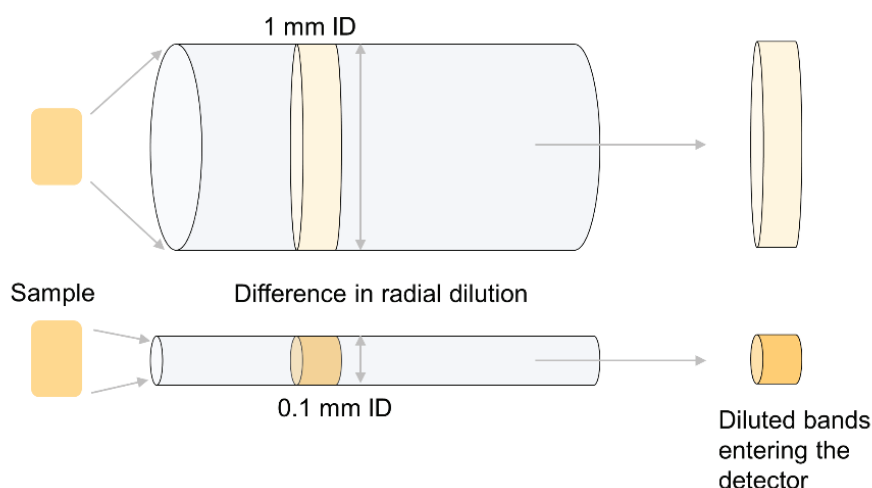


Figure 7. Illustration of sample dilution in a 1 mm ID column compared to when decreasing the column ID to 0.1 mm. Difference in column ID leads to a difference in radial dilution (and not axial dilution), and lead to 100x increase in signal intensity when entering a concentration sensitive detector. NanoLC columns were used in Section 3.1.1 and Paper IV, while capLC columns were used in Paper III and Paper V. Adapted from [105].

The chromatographic dilution at the end of a column, D , can be described by **Equation 3** [106].

$$D = \frac{C_0}{C_{\max}} = \frac{\epsilon r^2 (1+k) \sqrt{2\pi LH}}{V_{\text{inj}}} \quad \text{Equation 3}$$

Where C_0 is the initial concentration of the compound, and C_{\max} is final compound concentration at peak maximum. When particle porosity (ϵ), L , H , and the sample volume injected (V_{inj}) are kept equal, D will increase proportionally to the square of the column radius (r). The gain in signal intensity (I_{gain}) when using a narrow column (ID_{small}) compared to a large bore

column (ID_{large}) can be theoretically expressed by the downscaling factor (**Equation 4**):

$$I_{\text{gain}} = \frac{ID_{\text{large}}^2}{ID_{\text{small}}^2} \quad \text{Equation 4}$$

The decrease in mobile phase flow rate, due to the miniaturization of the LC-setup [107], reduces the need for solvent evaporation prior to ion release into the gas phase, particularly under nL/min flow conditions when nanoLC (<0.1 mm column ID) is coupled to a nano ESI source (nanoESI) [108-110]. Thus, miniaturization could also contribute to a more efficient ionization process and higher analyte signal intensity [111, 112].

The theoretical maximum injection volume is reduced to avoid a negative impact on column efficiency when miniaturizing the column ID (see Kucera in [113] for equation on packed nanoLC). However, in practice, large injection volumes are made possible through compound focusing either on-column or online solid phase extraction (SPE) using column switching techniques [114, 115]. The SPE column is commonly packed with the same SP as the analytical column and shorter in length, thus facilitating faster sample loading velocities and lower backpressure compared to the analytical column. In biological samples, polar compounds and salts are not retained on the RP SPE, reducing sample complexity prior to analytical separation and facilitating the reduction of matrix effects when coupled to ESI-MS. Thus, SPE is also considered a sample preparation technique (See **Section 1.4.2**), and is easily integrated online in systems such as LC-MS (**Section 1.5**).

1.3.3 Miniaturized separation in bioanalysis

Although recent proteomic studies using microflow LC-MS has proven promising [116, 117], nanoLC-MS has historically been the method of choice in proteomics [118-122] (**Section 3.1.1** and **Paper IV**). The use of nanoLC-MS has become interesting in the field of drug analysis and enantiomer separations [123, 124], however the nanoLC-MS for small molecule measurements is far from established (**Paper IV**). Practical difficulties during operation, small tubing being prone to clogging and low robustness and ruggedness could explain the limited use of nanoLC-MS compared to conventional LC-MS in small molecule measurements [125, 126]. A compromise between robustness and sensitivity in small molecule measurements can be made through applying microflow LC such as capLC (**Paper III** and **Paper V**) [127-131].

As an alternative to nanoLC regarding small charged molecule analysis, low pressure open tubular systems such as CE can be applied (**Paper I**, and **Paper IV**) [132, 133]. Jorgensen et al. early demonstrated in 1981, the potential of high efficiency separations in narrow bore capillaries (typically <0.1 mm) filled with background electrolyte (BGE) solution [134-136]. In CE, electrophoretic separation is achieved when the ions have different migration velocity (u), based on the force (F) exerted on the ion described in **Equation 5**:

$$F = qE \qquad \qquad \qquad \text{Equation 5}$$

Where q is the ion charge, and E is the field strength (based on the ratio of applied potential and the distance between the anode and the cathode). The migration velocity (u_m) can be further described by **Equation 6**:

$$u_m = \frac{qE}{6r\pi\eta}$$

Equation 6

The migration velocity is thus increased with increasing ion charge, field strength, and temperature (leading to decreasing viscosity, η), and decreases with increasing ion radius (r).

The high efficiency compared to LC could partly be explained by the reduction eddy dispersion, the largest contributor to band broadening in LC, due to only one flow path through the column [137]. The applied electrical field causes electroosmotic flow towards the cathode (at pH >3), thus no solvent pump is required as in LC. Hence, another contributor to high efficiency in CE compared to LC, could be the flat flow profile in CE due to the electroosmotic flow (**Figure 8**).

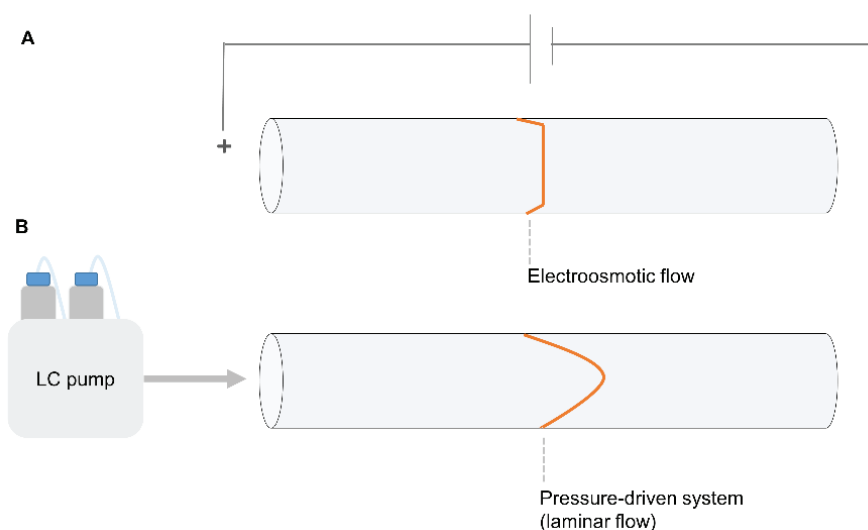


Figure 8. Illustration of the flow profiles through a capillary based on A) electroosmotic flow towards the cathode, and B) pressure driven flow. Adapted from [137].

Requiring only simple instrumentation with no solvent pump and low sample volume handling (nL-range), CE is also highly suited for analyses on-chip [138]. However, when coupled to UV-Vis detection (CE-UV), high detection

limits and consequently difficulties in detecting low abundant analytes can be a challenge (**Paper IV**). The hyphenation of MS with CE is possible through ESI. However the non ESI-compatible high salt content of the BGE, and coupling two circuits creates difficulties in integrating CE-ESI-MS [139]. However, CE has shown great applicability in various fields of bioanalysis [140, 141], e.g., drug analysis [142, 143], and proteomics [144, 145].

Even though a reduction in sample complexity is achieved through SPE-LC and other separation techniques, the crude biosamples can still contain contaminations (e.g., particles, cells, proteins) detrimental to the instrumental setup (e.g. clogging of column and tubing) and contributing to matrix effects. Therefore, additional sample preparation steps are often performed before separation and detection in bioanalysis.

1.4 Sample preparation prior to bioanalysis

When handling complex samples such as liver organoids, high contents of salts, lipids, proteins, amino acids, and cell debris are present [51]. The choice of sample preparation method prior to separation and detection depends on the compound of interest and could lead to increased selectivity and sensitivity of the method [146]. Sample preparation can be performed either offline or online to MS-detection. When performed offline, the sample preparation procedure and LC-MS are not connected in one fluidic system, and sample handling is performed in a manual action only, e.g., with the use of several pipetting steps and vial-to-vial transfer steps. When coupled online to MS detection, one or several steps of the sample preparation are coupled to LC-MS in one fluidic system, e.g., with the use of multiport valves, enabling high throughput and reducing sample loss (**Paper I**, and **Paper V**) [147].

Here, benchmark sample preparation workflows in bottom-up proteomics are briefly enclosed (applied in **Section 3.1.1** and **Paper IV**), followed by small molecule sample preparation considerations with emphasis on high throughput and online action (**Paper II- V**).

1.4.1 Sample preparation in bottom-up proteomics

In bottom-up proteomics (see **Section 1.2.1**), proteins undergoes enzymatic hydrolysis to form peptides, commonly using the highly sequence specific proteolytic enzyme trypsin [148, 149], generating peptides in the preferred mass range for MS and with easily interpretable peptide fragmentation spectra (**Figure 9**) [150]. Proteases with complementary cleavage specificities can be used to increase proteome coverage [151]. For the proteolytic enzyme to access the amino acid cleavage sites, the proteins are unfolded by reduction and alkylation of the protein thiol groups prior to enzymatic hydrolysis [152, 153]. Reduction of sample complexity is a necessity when dealing with highly complex samples, thus additional separation of protein or peptide prior to nanoLC-MS measurements is often performed [154, 155]. Sodium dodecyl sulfate (SDS) polyacrylamide gel electrophoresis (SDS-PAGE) is considered the benchmark protein separation step prior to protein hydrolysis (applied in **Section 3.1.1** and **Paper IV**) [33, 156, 157]. When operated in one dimension, proteins are migrating on a separating gel according to the difference in M_M by applying an electrical field (see **Equation 5** and **Equation 6**).

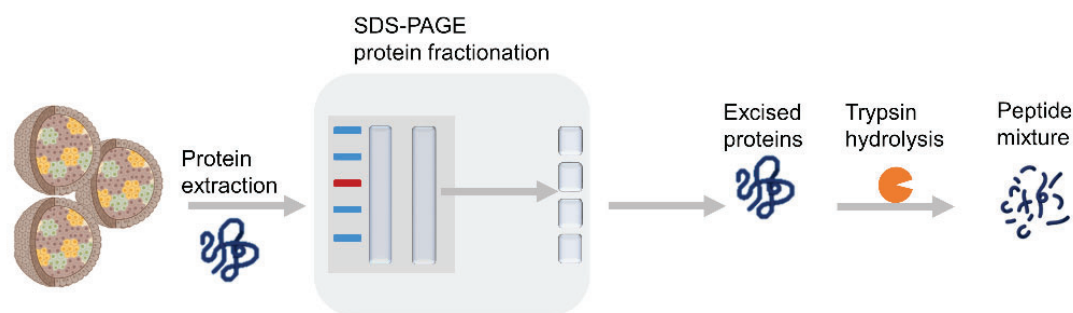


Figure 9. Example of SDS-PAGE based proteomic workflow including protein extraction from cells and tissues, followed by SDS-PAGE based protein fractionation. The excised proteins undergoes hydrolysis using trypsin, generating peptides for separation.

High concentrations of detergents or chaotropes, initially added during protein extraction to increase cell and protein solubility (e.g., SDS or urea), are associated with ESI-MS incompatibility [158, 159], and are thus commonly removed as a part of the sample preparation protocol [160]. In addition to SDS-PAGE based sample preparation protocol, numerous of other protocols for detergent removal and improving sample recovery have been introduced, e.g., filter aided sample preparation (FASP) and beads-based protocols (single-pot, solid-phase-enhanced sample-preparation, SP3) [161-164]. Removal of SDS was also explored using electromembrane extraction (EME, see **Section 1.4.2** and **Paper II**).

1.4.2 Sample preparation in small molecule bioanalysis

Conventional manual sample preparation steps typically involves simple centrifugation (**Paper III** and **Paper IV**), or small molecule extraction through partitioning liquid liquid extraction (LLE) or offline/online SPE (**Section 1.3.2**) [165-167]. However, salts are not removed when using centrifugation only, and the water-immiscible organic solvent of LLE provides low selectivity and requires an additional evaporation step prior to LC separation. Although LLE exist in 96-well format, centrifugation and LLE

are challenging to integrate in an online setup compared to the online established SPE-LC-MS. SPE is also easily miniaturized when dealing with low μL -scale sample volumes and low abundant analytes, providing selectivity by, e.g., varying the SP [147, 168, 169]. Liquid-phase microextraction (LPME) was developed as a miniaturization of LLE [170, 171]. To keep the microliter extraction solvent intact during LPME, the supported liquid membrane (SLM) was introduced as a barrier between the two liquid layers, which involves the immobilization of an organic solvent in a porous membrane [172]. However, LPME is associated with long extraction time [173].

Electromembrane extraction

Reducing the time for extraction to only a few minutes, Pedersen-Bjergaard et al. introduced EME in 2006 as a hyphenation between electrophoresis and LPME (**Paper I**) [174]. EME is considered a three phase microextraction; charged compounds are separated from an aqueous sample matrix (donor solution) to an aqueous solution (acceptor solution) by the electrophoretic migration of ions across the SLM caused by the applied potential (**Figure 10**, also based on **Equation 5** and **Equation 6**). Matrix components such as proteins and salts are separated from the charged analyte by the SLM, thus EME has shown to be a great fit for separating small hydrophobic bases or acids from complex matrices such as urine, breast milk and whole blood [175, 176]. EME can also be used for selective *removal* of unwanted compounds such as salts, detergents and phospholipids from biological samples (**Paper II**) [177-179]. When lowering the acceptor solution volume compared to donor solution volume, EME facilitates analyte enrichment.

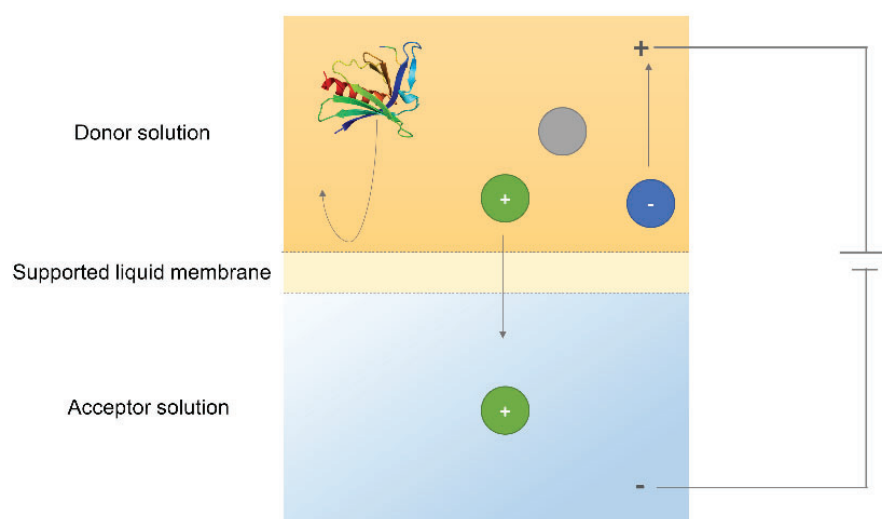


Figure 10. Principle of EME when extracting positive ions. The partitioning of positive ions into and across the SLM and to the acceptor solution assisted by an applied electrical field. Proteins, neutral small molecules and negatively charged ions in donor solution are discriminated by the hydrophobicity of the SLM.

Selective extraction with EME can be achieved by controlling the mass transfer across the SLM by varying the voltage polarity and magnitude [180], the pH conditions in the donor- and acceptor solution [181], and the SLM solvent [182]. Commonly used organic solvents for EME of nonpolar basic drugs are 2-nitrophenyl octyl ether (NPOE, **Figure 11A**) and 2-nitrophenyl pentyl ether (NPPE, **Figure 11B**) with strong hydrogen bond acceptor properties. The use of the di-(2-ethylhexyl) phosphate (DEHP, **Figure 11C**) as ionic carrier has shown to improve the partitioning of polar compounds into the SLM [183, 184].

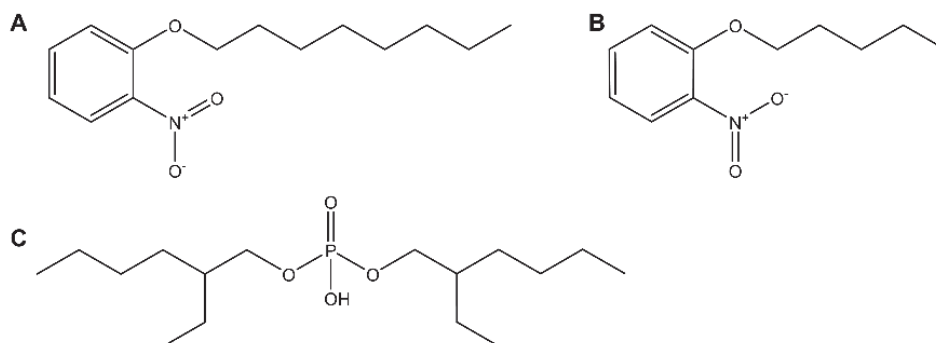


Figure 11. Chemical structure of solvents and carriers used for SLM in EME. A) The solvents NPOE, and B) NPPE. The ionic carrier C) DEHP.

EME has emerged from simple hollow fiber configurations [174], to high throughput 96-well format namely parallel-EME (**Paper II, Paper IV**) [179, 185, 186]. Additional manual sample handling steps can be fully minimized by the hyphenation of EME with MS for online measurements [187, 188] or extraction on-chip (**Paper I and Paper V**) [189-196].

1.5 State of the art: organoids and mass spectrometry

The currently developed organoids lack the structure and functional maturity of their human counterparts, and also organoid protocols show significant variations between batches. Thus, development and use of liver organoids are still in progress, calling for evaluation of the liver organ resemblance, e.g., with regards to proteomic profiling and drug metabolism using sensitive mass spectrometric analyses. In this section, recent studies on MS based liver organoid proteomics are discussed, followed by current standing of MS-based organoid drug metabolism studies, and online coupling considerations (also discussed in **Paper I**).

With regards to liver organoids proteomics functionality, MS-based untargeted proteomics have been used in a small number of studies on liver organoids, e.g., measuring extracellular matrix protein markers in liver organoids [197, 198]. Goulart et al. evaluated the impact of non-parenchymal cells for liver organoid development partly using MS-based proteomics [199]. Howell et al. performed global proteomics of murine biliary-derived hepatic organoids compared to murine liver tissue and undifferentiated organoids to assess similarity to murine liver tissue with regards to cytochromes P450 (CYP) proteins and liver biomarkers [200]. Functional annotation cluster analysis showed that proteins involved in drug metabolism by CYP450 and those involved in fatty acid, glutathione and amino acid metabolism (e.g.

glutamate dehydrogenase 1, mitochondrial, and aspartate aminotransferase, cytoplasmic) were reduced in differentiated organoids compared to liver but increased in differentiated versus undifferentiated organoids.

There are few studies utilizing LC-MS for drug metabolism measurements of organoids in general [201-203], and currently no studies, to the author's knowledge, dedicated to developing MS based metabolism measurements using liver organoids. Small molecule analysis in OoC systems is more commonly linked to offline MS measurements and simple sample centrifugation steps [204-212], with one exception (see next section) [213].

There are currently no studies on high throughput integration of organoids online with MS analysis. However, coupling of MS with on-chip simple cell handling has previously been explored with emphasis on online sample handling. Initial work by the group of Jin-Ming Lin et al. from 2010 and onwards, focused on the integration of SPE desalting prior to ESI-MS detection studying, e.g., curcumin permeability [214, 215]. The high backpressure generated by the SPE was directly coupled to the low-pressure cellular microenvironment, thus requiring low flow rate sample loading (1 $\mu\text{L}/\text{min}$) and large particle size (45 μm). Due to the incompatibility of the SPE eluent with cells, the SPE washing step was performed offline. To avoid direct cellular contact with the high-pressure of SPE-MS, Dugan et al. introduced an integrated switching valve on-chip [216]. However, incompatibility of the low-pressure chip and high-pressure SPE-MS became challenging, and 20 μm particle size SPE was needed to keep the backpressure sufficiently low for the chip integrated valves to function [216]. An early study of liver slice biochip coupled the LC-UV setup to the biochip through several stainless steel switching valves [217]. A switching valve setup coupled in series for sampling

and SPE, separated the low-pressure chip from high-pressure SPE-MS in the study of Gao et. al [218]. In this setup, challenges with detection of low abundant analytes were limited to the detection capabilities of the MS. In addition to SPE-sampling using switching valves, integration of chip-based LC separations and MS-detection were used in studying verapamil permeability in intestinal OoC [213, 219]. Although analyte detection was possible, high MS background caused by the sample matrix was observed. Thus, achieving total removal of cell medium contaminations seems to be challenging when using online SPE.

1.5.1 Current challenges of mass spectrometry-based liver organoid analyses

The main challenge enclosing the above-discussed **Section 1.5** is the little established use of MS in the liver organoid analysis, e.g., regarding untargeted protein profiling and drug metabolism studies. In addition, there are currently no studies on the hyphenation of MS to liver organoids for high throughput analysis. Previous studies of high throughput analysis using MS coupled with OoC and on-chip cell systems mainly focused on SPE extractions before MS detection. Thus, there is a need for alternative extraction setups providing higher selectivity for the liver organoid analysis of minute secretions.

2 Aim of study

MS and separation techniques such as LC are established analytical tools in bioanalysis. However, these tools are arguably underused in organoid analyses; especially in OoC systems.

The aim of this thesis was to explore MS and separation science in liver organoid bioanalysis for detecting biomolecules, spanning from protein identifications to small molecule drug metabolites. Would the liver organoids in this study display liver organ functionality? With the objective of selective, high throughput analyses and online integration of MS-based liver organoid analyses, the applicability of the sample preparation technique EME was evaluated.

The main hypothesis of this thesis is thus that LC, CE, MS, and EME enable sensitive, robust and high throughput analysis for establishing liver organoid functionality.

3 Results and discussion

To meet the aim of this thesis, challenges and possibilities with organoid based separation and MS were initially discussed in **Paper I** (see **Figure 12** for graphical overview). Liver organoids and primary liver tissue proteins were initially identified and compared by bottom-up proteomics using nanoLC-MS and SDS-PAGE based sample preparation. Parallel-EME was then explored for SDS clearance in **Paper II**. Next, the liver organoid drug metabolizing properties were assessed using centrifugation-based sample preparation. In **Paper III**, so far unknown adult liver organoid neratinib metabolites were identified using capLC-MS. The liver organoid heroin metabolizing properties were then established using benchmark UHPLC-MS in **Paper IV**. Focusing on increased throughput, **Paper IV** explored the compatibility of liver organoid heroin metabolism with 96-well parallel-EME, and separation techniques were explored regarding organoid and MS hyphenation. Finally, organoids and capLC-MS were connected using EME on-chip and a two position 10-ports valve for online measuring of adult liver organoids methadone metabolism in **Paper V**.

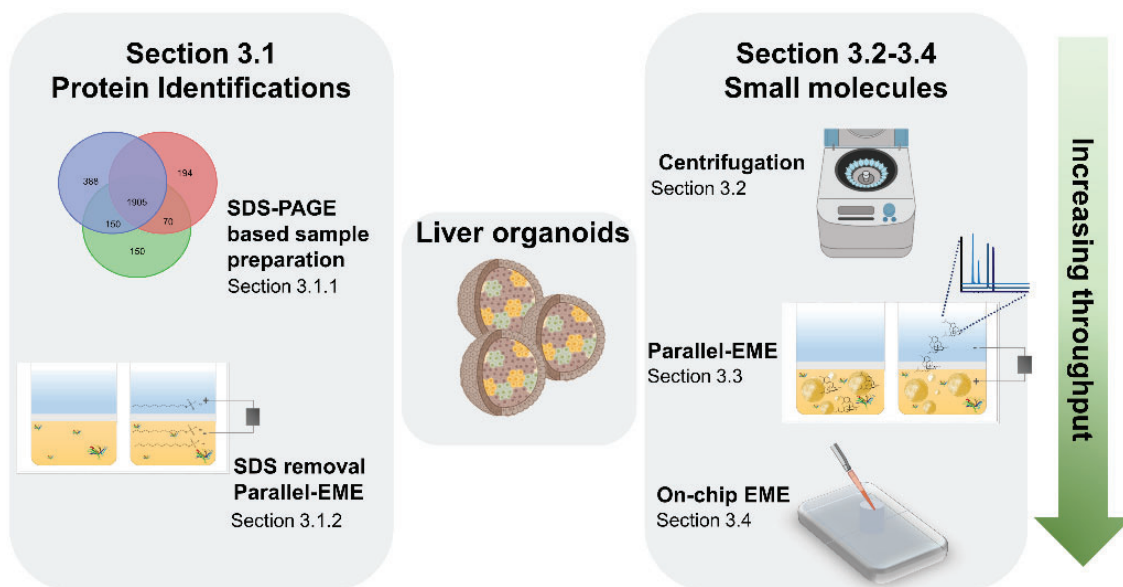


Figure 12. Graphical overview of this thesis.

3.1 Liver organoids proteomics using mass spectrometry

Although MS-based proteomics could be a valuable tool to evaluate the organ resemblance, few studies have been conducted to date (see **Section 1.5**, and **Paper I**). A new protocol for liver organoids differentiation from AG27 iPSC (see [220], for donor information) was introduced [221], using a small molecule-driven protocol as opposed to current approaches relying on growth factors. We applied bottom-up untargeted proteomics using nanoLC-MS to establish the liver traits by directly comparing the generated liver organoids to human liver tissue.

3.1.1 Liver organoid and human liver tissue proteome comparison using sodium dodecyl sulfate-based sample preparation

The scope was to use well-established proteomic platforms to, e.g., allow comparability between laboratories. Due to the high complexity and dynamic

concentration range of primary liver tissue proteins (e.g., high albumin concentrations) [222], fractionation at the protein level using benchmark SDS-PAGE based sample preparation protocol was applied, provided by Shevchenko et al. [157], and also previously used in our studies on exosomes and glioblastoma proteomes [223, 224].

Using nanoLC-MS, a total of 1003 shared proteins were identified from liver organoids and primary liver tissue (**Figure 13A**). One challenge in bottom-up proteomics and data analysis is to reduce false positive identifications, and confident protein identification is essential [225]. Thus, high level of stringency was applied through peptide and protein false discovery rate threshold of ≤ 0.01 (strict) and ≤ 0.05 (relaxed), digestion by trypsin with at most one missed cleavage and only unique peptides for proteins identification. However, it is important to state that high level of stringency also possibly leads to false negative identifications.

The shared proteins identified could be linked to central liver pathways such as amino acid biosynthesis and blood coagulation (e.g. the gene names *FGG*, *ASS1*, *GLUL*, *GOT1*, *GOT2*) (**Figure 13A**), comparable to an independent proteomic analysis performed in the same study [221]. The hierarchical branching of the heat map suggested that the outlier was the primary liver tissue sample from donor 3 (**Figure 13B**). This means that the liver organoid samples were more related to most of the primary liver tissue samples than the outlier.

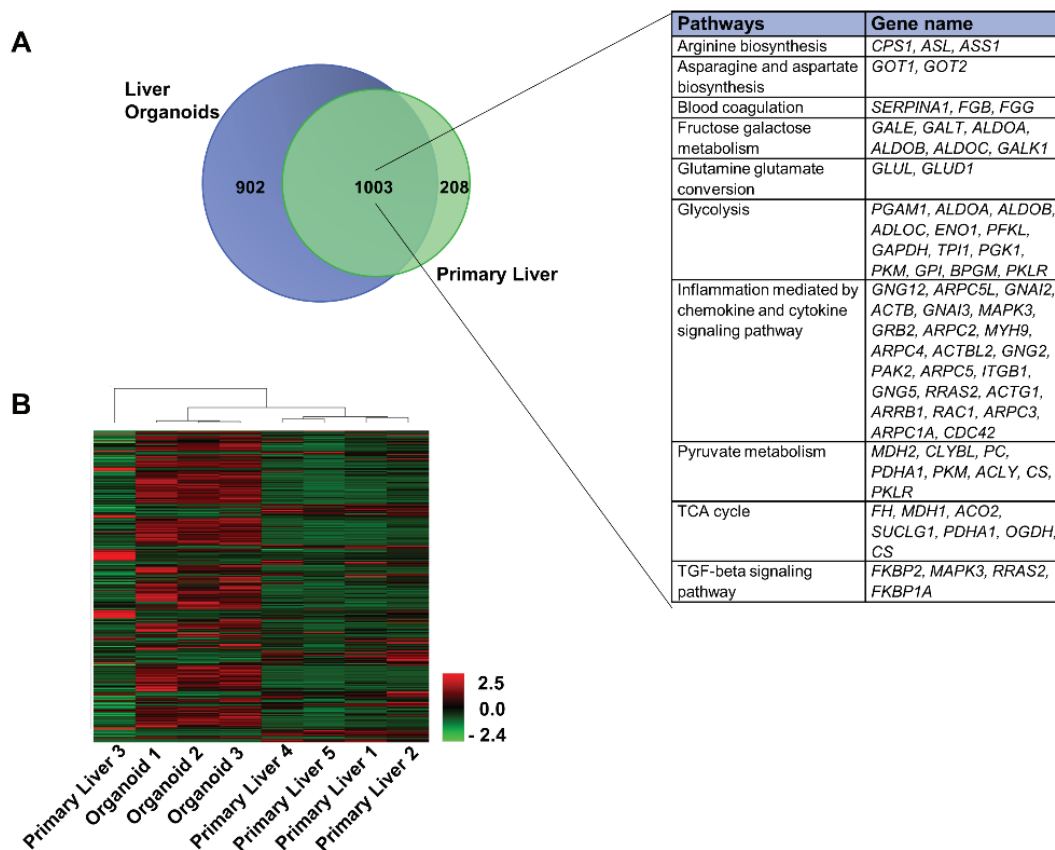


Figure 13. Untargeted proteomic analysis of liver organoids and primary liver tissue using nanoLC-MS and DDA. A) Venn diagram representing shared proteins between primary liver donors and liver organoids, with an overview of the liver related GO pathways of the shared proteins. B) Heat map of proteins identified in primary liver tissue (n=5) and liver organoids (n=3) from label-free quantification. Proteins were clustered (rows clustering) by Euclidean clustering.

Peptide separation and detection were achieved using nanoLC-MS, 0.075 mm ID commercial columns, and Q-Exactive Orbitrap (**Figure 14A-B**). However, nanoLC-MS was also performed at an external lab due to instrumental/operational challenges in-house. Difficulties during operation could vary from unstable Orbitrap MS/MS performance, nanoESI spray and nanoLC pump solvent delivery (EASY nLC 1000 pump), to easily clogged tubings, SPE and analytical columns. The difficulties during operation reflects the main drawback of nanoLC systems namely robust operation. Although nanoLC provides high sensitivity separations, the performance of mass spectrometers has been greatly improved over the past 10 years, and

sensitivity has become a less critical issue when sample quantities are not extremely scarce, hence the emergence of the robust microflow LC in proteomics [226-228].

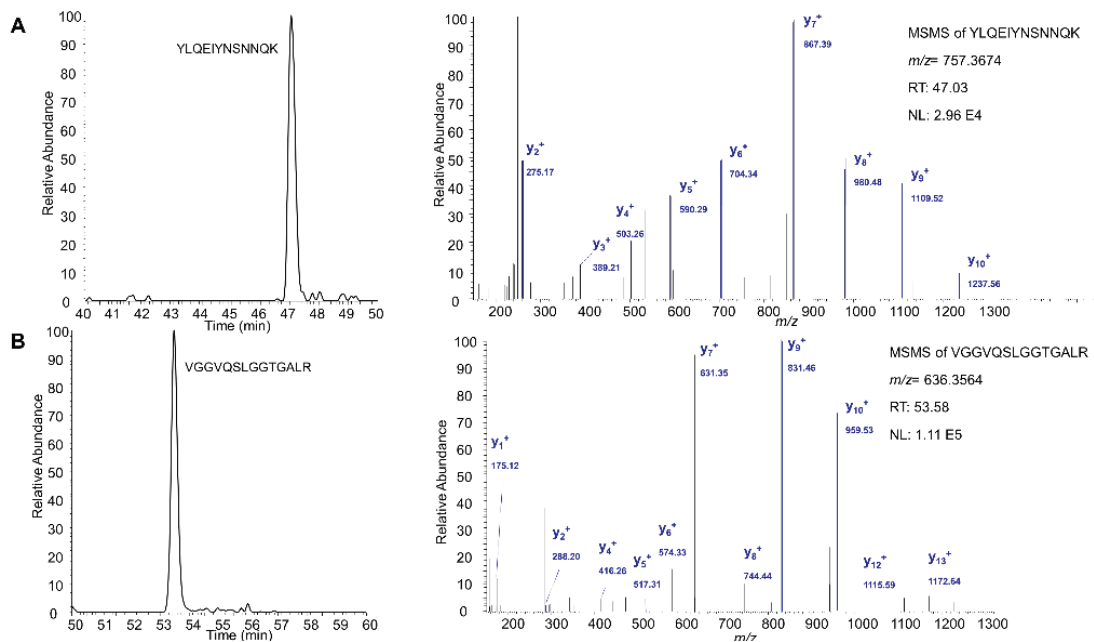


Figure 14. Extracted ion chromatogram of liver organoids identified peptides (left) and the respective peptide fragmentation spectrum (right) of proteins related to central liver pathways. **A)** The peptide YLQEIYNSNNQK (m/z 757.37) from FGG (P02679) annotated to blood coagulation, identified at charge +2. **B)** The peptide VGGVQSLGGTGALR (m/z 636.35) from GOT1 (P17174) and asparagine and aspartate biosynthesis, identified at charge +2.

The SDS-PAGE-based bottom-up proteomic sample procedure included SDS removal before ESI-MS detection, involving multiple time-consuming (>16 hours) and manual sample handling steps. Hence, conventional bottom-up preparations in proteomics are well known to provide low throughput and limited integration to automatic platforms.

To sum up: Using nanoLC-MS, the initial establishment of liver organoid untargeted proteomic functionality was linked to human liver tissue, and the

liver organoids proteins identified presented similarities to central human liver functions. However, the conventional SDS-PAGE-based sample preparation procedure provided low throughput with multiple manual sample handling steps, including SDS removal.

3.1.2 Sodium dodecyl sulfate clearance using 96-well electromembrane extraction: a case study

As discussed in **Section 1.4.1**, the use of SDS for cell lysis and protein extraction has the drawback of ESI-MS incompatibility. The use of EME is more commonly associated with small molecule *extractions* but has also been used to *remove* unwanted compounds (**Section 1.4.2**). The parallel-EME removal of SDS in 96-well format could become a novel method for proteomic sample preparation of multiplexed samples, as an alternative to existing high throughput proteomic platforms [229]. A fundamental study of SDS removal using parallel-EME was thus conducted in **Paper II** (for parallel-EME setup, see **Figure 15A-D**).

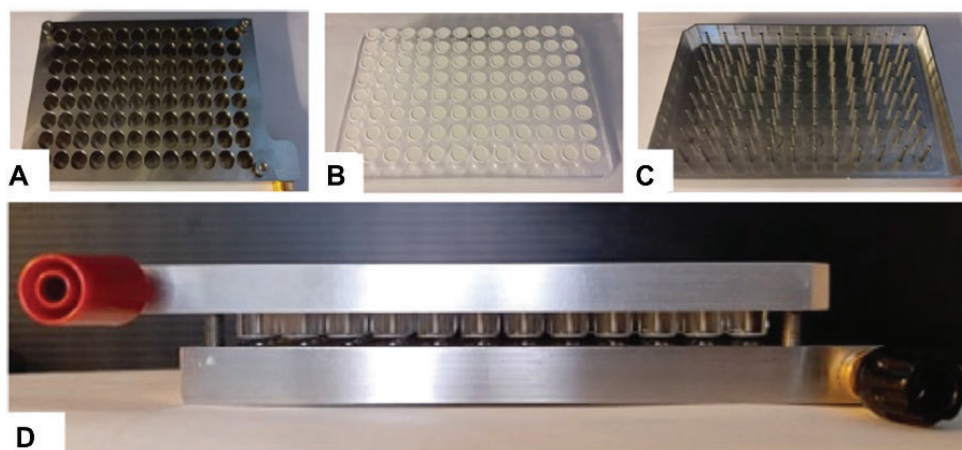


Figure 15. Experimental setup of 96-well parallel-EME, showing the A) sample reservoir plate constituting the donor solution, B) the 96-well filter plate constituting the SLM and acceptor solution, C) aluminum lid with 96 electrodes, and D) showing all plates clamped together. Reprinted with permission from The Royal Society of Chemistry.

The concentration of SDS added to promote cell lysis and protein solubility was estimated to be 0.5-1.0 %, confirmed with both in-house experiments and literature (results not shown) [230]. However, a high accumulation of SDS in the SLM was observed when extracting 0.5%-1.0% SDS, consequently limiting the SDS clearance to the SLM capacity. Increasing the membrane area of the SLM from 28 mm² to 43 mm² provided 100% clearance from 0.5% SDS after 30 minutes of EME. However, the increase of SLM surface area forced a change in the EME configuration to use pipette tips as SLM instead of 96-well parallel-EME. Furthermore, initial investigations of parallel-EME SDS removal from a simple cell lysate showed protein concentration below the detection limit in the remaining sample (**Figure 16**). Parallel-EME could alternatively be performed after protein hydrolysis of the less hydrophobic peptides to minimize the loss of proteins during extraction. Nonetheless, parallel-EME was not mature for liver organoid proteomic sample preparation and SDS removal.

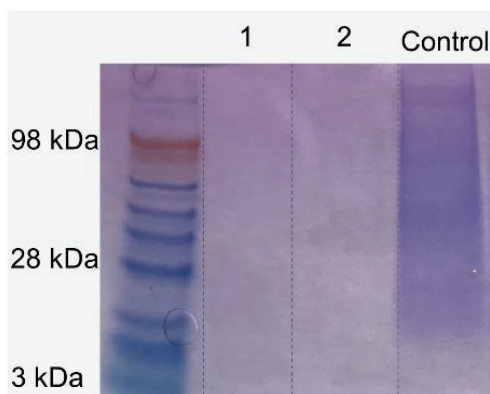


Figure 16. SDS-PAGE analysis of the extracted cell lysates (lane 1 and lane 2) after SDS removal using EME and the control cell lysate (HEK293), with Coomassie Blue staining.

To sum up: EME was explored as an approach for simpler large biomolecule sample preparation. A fundamental study of the SDS removal using 96-well

parallel-EME was conducted. Complete SDS removal was achieved, however, using a modified EME setup in a pipette tip. The parallel-EME method was not mature for liver organoid proteomic sample preparation and SDS removal. Hence, conventional sample preparation procedures are still preferred for large biomolecule analysis.

3.2 Liver organoids small molecule drug analysis

One key liver function is the ability to metabolize small molecule drugs through enzymes such as the CYP family (**Figure 17A**), human esterases (hydrolase superfamily, **Figure 17B**), and uridine 5'-diphosphoglucuronosyltransferases (UGTs, **Figure 17C**).

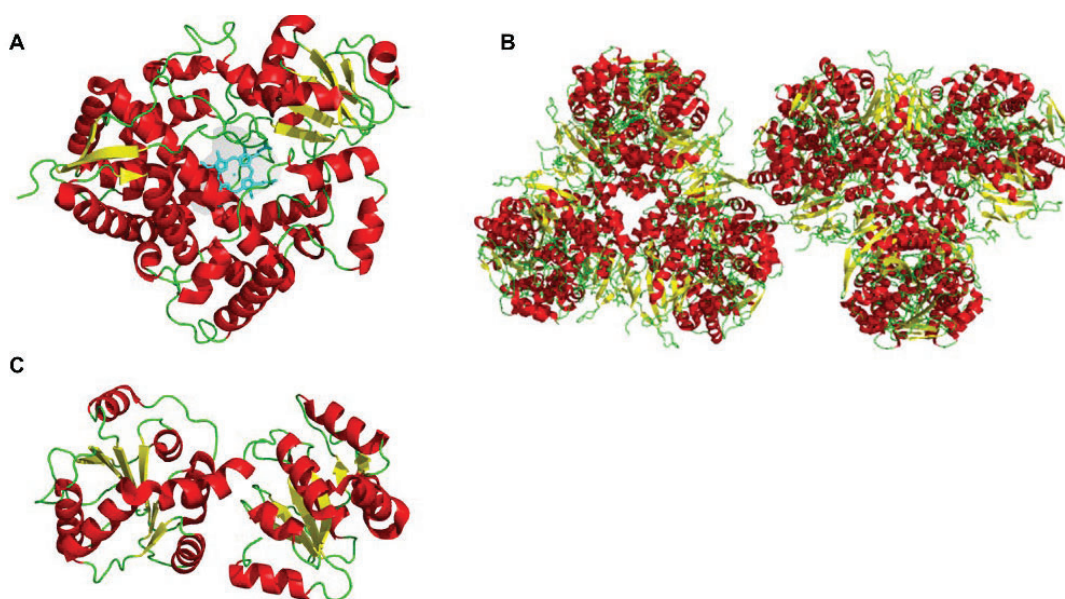


Figure 17. Crystal structure of selected liver drug metabolizing enzymes. A) CYP3A4 (protein data base ID, PDB, 1TQN), B) human liver carboxylesterase 1 (hCE1) in complexed with naloxone methiodide, a heroin analogue (PDB 1MX9), and C) the UDP-alcuronic acid binding domain of UGT2B7 (PDB 2O6L). Figures made using PyMOL.

Assessing the liver organoid metabolizing properties regarding small molecules using MS could give fundamental insight into the developmental

stage of the liver organoids generated from different cell sources in this study (**Figure 18A-B**). Using MS, liver organoid metabolizing properties were assessed regarding small molecule drugs with well-established drug metabolites (heroin in **Section 3.2.2**, and methadone in **Section 3.4**), and small molecule drugs with unknown drug metabolites (neratinib in **Section 3.2.1**).

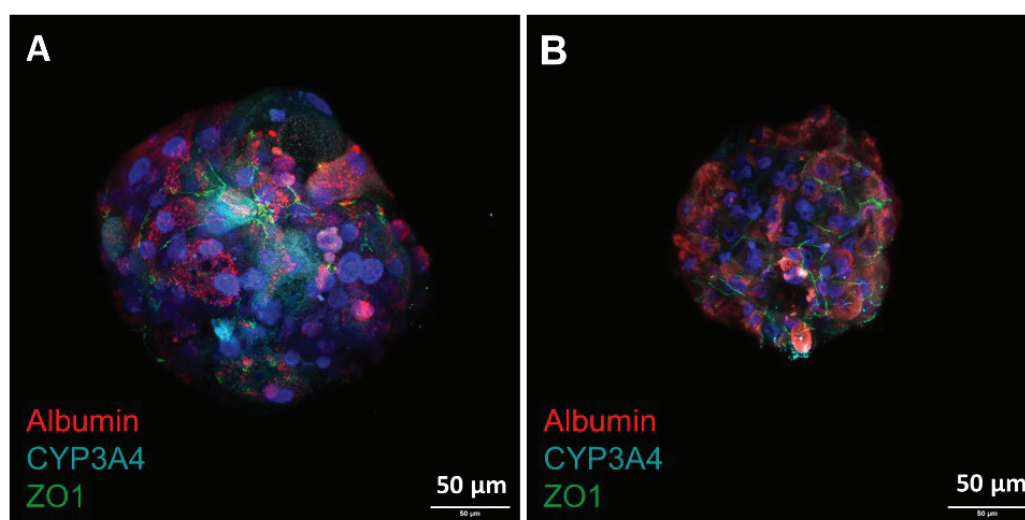


Figure 18. Representative images of whole mount staining for albumin (red), CYP3A4 (turquoise), and Zonula occludens-1 (ZO1, green) of A) adult liver organoids, and B) Liver organoids from HPSI0114i-vabj_3 iPSC. Adult liver organoids were applied in Paper III-V, iPSC derived liver organoids were applied in Section 3.1.1, Section 3.2.2, and Paper IV. Scale bar 50 µm. Photo credit: Aleksandra Aizenshtadt. Figure adapted from Paper V.

3.2.1 Identifying unknown adult liver organoids neratinib drug metabolites using mass spectrometry

In **Paper III**, we introduced quantitative Ramanomics as a bioanalytical tool for chemometric phenotyping of liver organoids. The developed methodology was demonstrated to be suited for in situ direct measurement of drug and drug metabolite accumulation of a selection of drugs with reported impact on hepatocytes (neratinib, amiodarone, nilotinib, fluticasone-propionate, ketoconazole, and methadone) within the liver organoid model systems.

Neratinib (also named nerlynx or HKI-272) was approved in 2017 by the US Food and Drug Administration for the treatment of early-stage human epidermal growth factor receptor 2 positive breast cancer (**Figure 19**) [231, 232]. The hepatotoxic effect of neratinib is not yet established; however, neratinib showed the highest intracellular metabolite accumulation and hepatotoxic effects of all the drugs studied using the developed Ramanomics methodology in **Paper III**. Nevertheless, Raman spectroscopy is not able to provide molecular structural information, consequently limited molecular information on the neratinib metabolites accumulated. Although the neratinib metabolism was early established to be CYP3A4 mediated, the current knowledge on human neratinib metabolites is limited [233]. Therefore, an MS method for identifying neratinib CYP3A4 mediated metabolites was developed, using adult liver organoids derived from patient liver tissue (called primary human hepatocyte spheroids in **Paper III**).

A literature study was conducted, showing suggested neratinib metabolites from studies using simple model systems such as monolayer cells by Aljakouch et al. and rat hepatocytes by Liu et al., using conventional LC-MS [234, 235]. In the study of Aljakouch et al., the authors suggested three metabolite candidates for neratinib CYP3A4 metabolism, detected using Raman microscopy and LC triple Q MS in monolayer breast cancer cells and small cell lung cancer cells [234]. Our initial investigations on neratinib metabolism in adult liver organoids showed overlapping Raman spectra with the study of Aljakouch et al. [234]. However, the three suggested metabolites were not detected in-house using capLC-MS (triple Q and Orbitrap) and were not detected in even simpler liver models with high enzyme concentrations such as HLMS using different MS modes (full scan, SIM or product ion scan, PIS). In addition, complete information regarding LC separation and MS

detection was lacking in the Aljakouch et al. study, questioning the reliability of the suggested neratinib metabolites.

In the study of Liu et al., the authors mapped the metabolic profile of neratinib in rat hepatocytes, bile, and urine using LC and Orbitrap MS [235]. A total of 12 metabolites were detected with high confidence by providing complete information on LC separation, structural information and suggested MS/MS fragmentation. Of them, the metabolites M3 (blue area in **Figure 19**), M10 (green area in **Figure 19**) and M12 (orange area in **Figure 19**) were unambiguously identified using in-house synthesized standards, also suggested to be present by the assessment report by the European Medicines Agency [236].

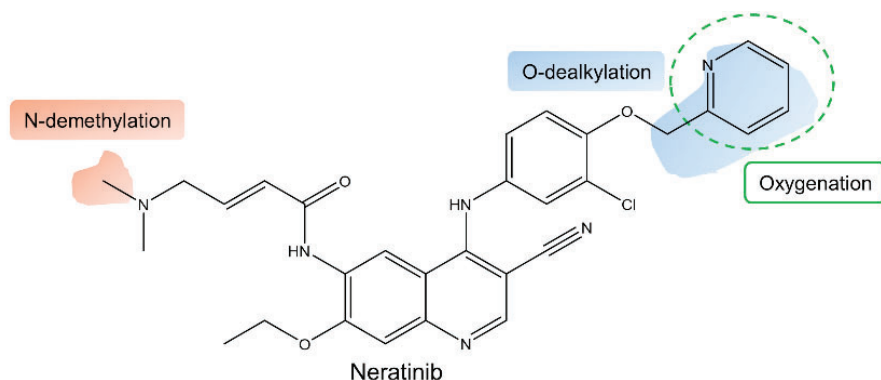


Figure 19. Schematic of neratinib (theoretical m/z 557.2) and the three possible metabolic outcomes: M3 (blue, O-dealkylation theoretical m/z 466.2), M10 (orange, N-demethylation theoretical m/z 543.2) and M12 (green, oxygenation with theoretical m/z 573.2) from [235, 236].

Based on the study of Liu et al., we initially performed incubation of neratinib in HLMs, and identified the neratinib metabolites M3, M10 and M12 using capLC-MS and different MS modes (full scan, SIM and PIS). Neratinib metabolite identification was based on the Cl isotope ion intensity ratio $[M+H+2]^+$ of 3:1, and the relative retention order to neratinib and MS/MS fragments were matched with the ones in the study of Liu et al. [235] (**Figure**

20A-D). Consequently, a sensitive MRM method was established regarding detection of M3, M10 and M12.

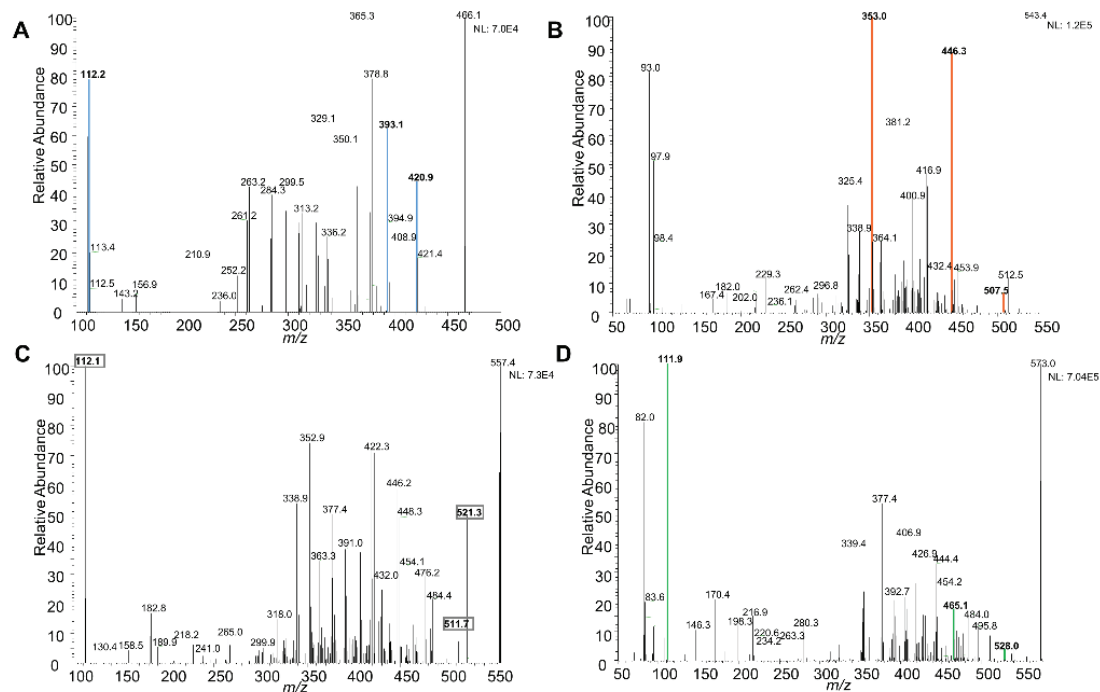


Figure 20. Selected MS/MS spectra from neratinib incubation in HLMs, showing the fragment ions from PIS of A) neratinib metabolite candidate M3 m/z 466.1 (with blue m/z used for MRM), B) neratinib metabolite candidate M10 m/z 543.4 (with orange m/z used for MRM), C) neratinib m/z 557.4 (with grey m/z used for MRM), and D) neratinib metabolite candidate M12 m/z 573.0 (with green m/z used for MRM). Acquired using capLC-MS (triple Q). Figure adapted from supplementary information in Paper III.

Separation of the analytes from interferences using capLC (0.5 mm ID) and MS, led to an identification of the three metabolites (M3, M10, and M12) in both pellet and supernatant after adult liver organoids incubation in 5 μ M neratinib for 24 hours (**Figure 21**), meaning that the adult liver organoids showed neratinib metabolizing properties. In addition, MS-analysis complemented Raman spectroscopy observations, by providing comprehensive chemical information on the neratinib metabolites present.

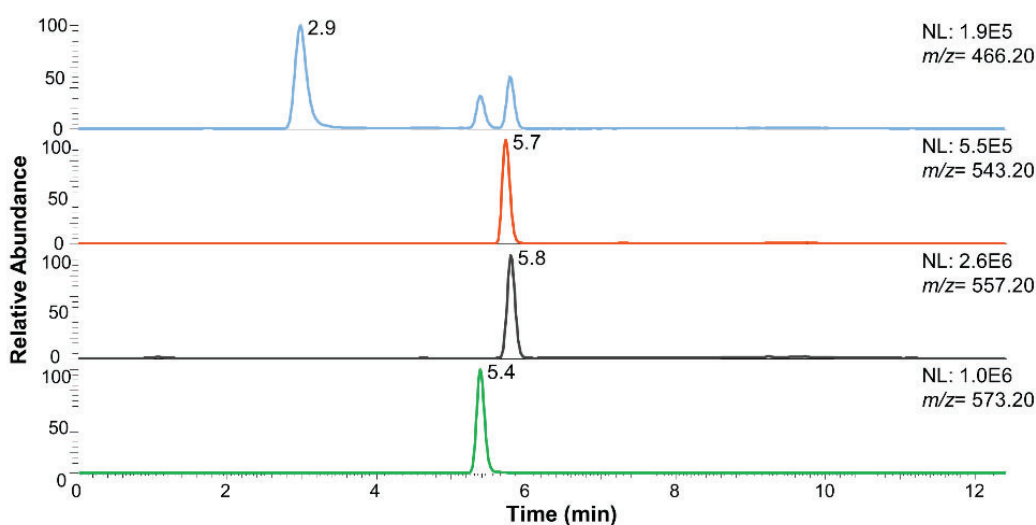


Figure 21. Extracted ion chromatograms of neratinib (black) and neratinib metabolites (M3 metabolite is marked blue, M10 is orange, and M12 green) identified in adult liver organoids after incubation for 24 hours in 5 μ M neratinib. A capLC column (HotSep® Sunniest C18, 150 x 0.5 mm, 3 μ m particles) and triple Q MS method was applied, using a gradient program ranging from 20-80% MP B in 6 minutes (5mM ammonium formate pH 3.1 as the MP A composition, and 95% ACN, 0.1% formic acid as the MP B composition). Figure adapted from supplementary information in Paper III.

In **Paper III**, neratinib metabolites were also detected in adult liver organoids influenced by a CYP3A4 inducer (rifampicin) and high lipid content (inducing steatosis, results not shown). Hence, the applicability of the capLC-MS in this study could be beneficial in studies on disease influence on neratinib drug metabolism. A combination of Raman spectroscopy and MS could also become valuable in direct measurements of OoC, either to elucidate chemical structural information in target deconvolution during drug development [237], or as imaging techniques with the use of direct ESI (DESI) for MS imaging (MSI) [238].

To sum up: The neratinib metabolizing properties of adult liver organoids were mapped, through the identification of three neratinib metabolites using capLC-MS and an optimized MRM-method.

3.2.2 Establishing liver organoids heroin metabolizing properties using mass spectrometry

Due to the well-established knowledge on the liver heroin metabolites and enzymes involved, heroin metabolizing properties of the liver organoids (from two different organoid iPSC sources) were then investigated using the well-established, conventional UHPLC-MS method used for routine clinical analysis (AG27 and HPSI0114i-vabj_3 differentiated liver organoids in **Paper IV**) [239].

Heroin was introduced in 1898 as a semi-synthesized analgesic analog to the opium extracted substance morphine, and is considered a narcotic substance [240]. In the liver, heroin is metabolized by serial steps of phase I deacetylation to 6-monoacetylmorphine (6-MAM, both spontaneously and enzymatically) and morphine (mainly enzymatically) by esterases such as human carboxyl esterases 1 or 2 (hCE1, hCE2, **Figure 22**) [239, 241-244].

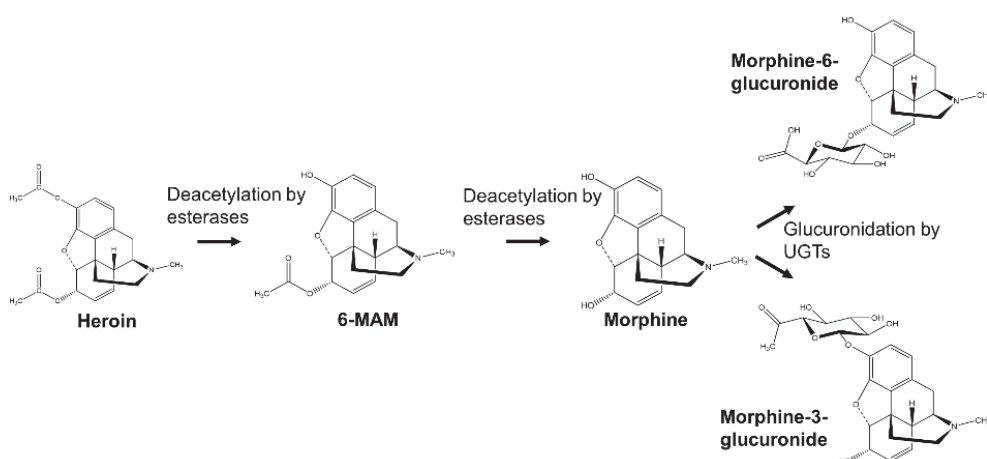


Figure 22. The human liver metabolism of heroin to its phase I metabolites 6-MAM and morphine by e.g. human carboxyl esterases (hCE), and the morphine phase II metabolites M3G and M6G mediated by UGTs. The liver organoid heroin metabolism was measured in **Paper IV**.

During heroin phase II metabolism, morphine undergoes glucuronidation to form mainly morphine-3-glucuronide (M3G), but also morphine-6-glucuronide (M6G), a reaction mediated by UGTs [245].

The UHPLC-MS method provided high resolution separations (within 5 minutes) for the heroin metabolism related analytes (**Figure 23**).

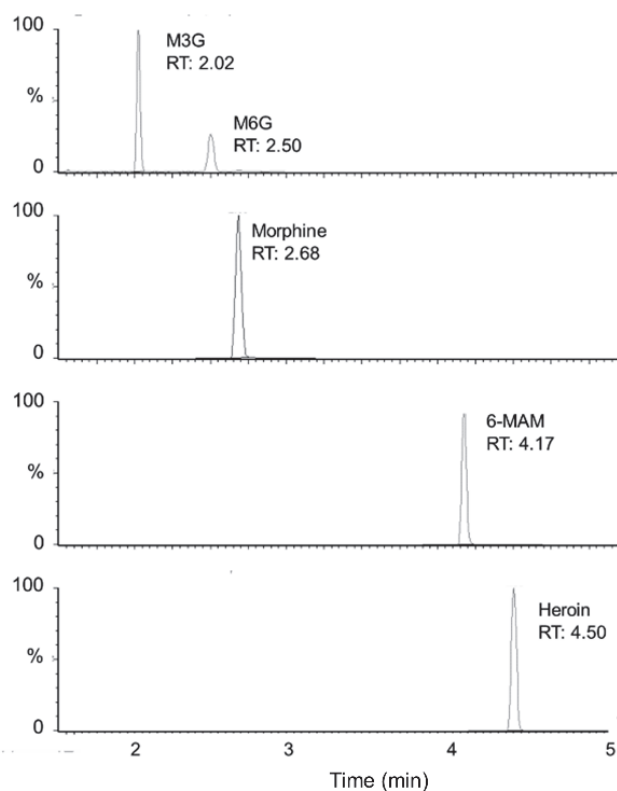


Figure 23. Extracted ion chromatogram showing the separation of the analytes M3G, M6G, morphine, 6-MAM and heroin with the use of UHPLC-MS (triple Q) and a 2.1 x 100 mm Acquity UPLC® HSS T3 C18 column with 1.8 μ m particles. The MP A consisted of 10 mM ammonium formate buffer pH 3.1 and MP B consisted of methanol. The gradient was ranging from 0-100% MP B in 4.61 min with a flow rate of 0.5 mL/min. Reprinted with permission from American Chemical Society.

After liver organoid incubation in 10 μ M heroin for 24 hours, the heroin phase I metabolites 6-MAM and morphine were successfully measured using

UHPLC-MS, meaning that liver organoids showed phase I metabolizing organotypic functions (**Paper IV**, and **Figure 24**).

Trace levels of the heroin phase II metabolites M3G (12 nM) and M6G (2 nM) were also measured after 24 hours. The low concentration levels of phase II metabolites detected were similar with the two liver organoids iPSC sources studied. Thus, the observations confirmed that the liver organoids showed traits to the human liver concerning heroin phase I and phase II metabolism. However, the kinetics were substantially slower than observed with, e.g., HLMs and S9-fractions (results not shown) [246]. A reason could be the high concentration of enzymes in the mentioned models, compared to liver organoids most likely relying on drug diffusion to reach the cells of the spherical structured organoids.

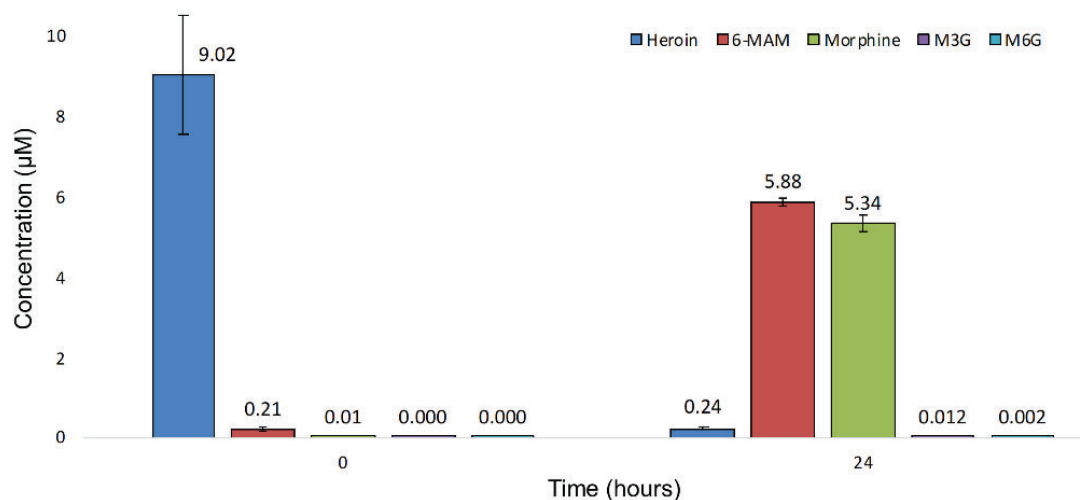


Figure 24. Liver organoid drug phase I and II metabolism measuring the concentration (μM) of heroin, 6-MAM, morphine, M3G and M6G with the use of centrifugation based sample preparation and UHPLC-MS. Liver organoids from iPSC HPSI0114i-vabj_3 (20 organoids) were incubated in 10 μM heroin for 0 and 24 hours. Each bar represent the mean (\pm standard deviation, SD) of triplicate samples. Work performed by Ida Sneis Boger, whom I supervised. Reprinted with permission from American Chemical Society.

To sum up: liver organoids showed heroin metabolizing properties to form small molecule heroin metabolites 6-MAM, morphine, M3G and M6G, measured using conventional UHPLC-MS.

3.2.3 Challenges in small molecule conventional sample preparation

The conventional low throughput centrifugation-based sample preparation was applied for the above-mentioned small molecule studies (**Paper III** and **Section 3.2.2**), involving several manual sample handling steps (**Figure 29A**). In addition, the liver organoids were grown in complex medium with high content of impurities such as salts and proteins, and the subsequent analysis would benefit from using a thorough clean-up prior to analysis. Thus, calling for a simpler sample preparation of higher selectivity and throughput.

To sum up: The universal centrifugation-based sample preparation was applied for small molecule analysis, calling for a selective, high throughput sample preparation.

3.3 Parallel electromembrane extraction for high throughput liver organoids small molecule drug analysis

Although EME was applied for SDS *removal* in **Paper II**, EME is well established for *extracting*, e.g., acidic and basic drugs, discriminating target analytes from biological matrix substances (**Section 1.4.2**). The use of EME has advanced to higher throughput platforms such as parallel-EME in 96-well format, providing fewer manual sample handling steps prior to analysis compared to centrifugation-based sample preparation (**Figure 29B**). Thus, in **Paper IV** we evaluated the fit of EME with liver organoid heroin metabolism. For this purpose, high throughput parallel-EME combined with the benchmark UHPLC-MS method, and the two liver organoids iPSC sources from **Section 3.2.2**.

3.3.1 Optimizing parallel electromembrane extraction of heroin and metabolites

Though morphine has previously been extracted using EME [247-249], EME of heroin and 6-MAM has not previously been performed. A common challenge when using EME, is the low extraction recoveries for polar analytes due to the unpolar character of the SLM (**Section 1.4.2**). Due to the trace level detection of the polar heroin phase II metabolites M3G and M6G in **Section 3.2.2**, EME conditions were not initially optimized for M3G and M6G.

EME-conditions for heroin, 6-MAM and morphine were optimized, achieving analyte selectivity by varying EME conditions such as the SLM composition, voltages applied, and the time of extraction. The optimized EME extraction parameters were evaluated to be 10% (w/w) DEHP/NPOE SLM composition, with an applied voltage of 30-50 V for 15 minutes (**Figure 25**). In literature, similar EME conditions were applied for morphine extraction [247, 248].

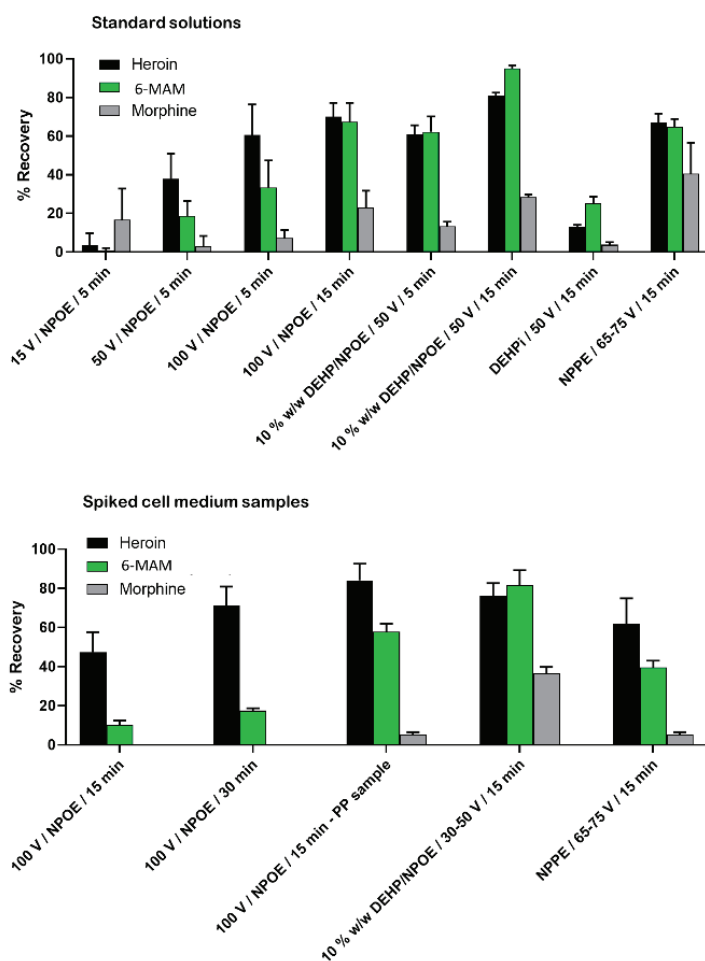


Figure 25. Analyte recovery (%) of parallel-EME under varying conditions (SLM composition, extraction voltage, and extraction time), with 5 μ M standard solutions and spiked cell medium samples using CE-UV for quantitation. Reprinted with permission from American Chemical Society.

However, differences in EME recovery for heroin (76%), 6-MAM (82%), and morphine (36%) spiked in cell medium, and poor parallel-EME sample to sample repeatability (with relative standard deviation, RSD up to 68%) in

initial liver organoid heroin small molecule extractions, contributed to inaccurate measurements. Differences in extraction efficiency using parallel-EME were thus corrected by adding isotopically labeled internal standards (IS) before extraction.

3.3.2 Parallel electromembrane extraction of liver organoid heroin metabolites

The 96-well parallel-EME was then applied for studying liver organoid heroin metabolism. Samples containing different numbers of organoids (20 and 60 organoids) from two different liver organoid iPSC sources were exposed to 10 μ M heroin for 24 hours (**Figure 26A-B**). Liver organoid samples of heroin and heroin metabolites were extracted in parallel using parallel-EME, with a sample-to-sample repeatability of 0.4%- 25% (with the exception of 6-MAM and heroin at time point 24 hours). The phase II metabolites M3G and M6G were not detected, as anticipated with the low initial morphine recovery (36%).

The observed heroin metabolism kinetics was comparable with the observations from **Figure 24**. Thus, parallel-EME was successfully applied in extracting small molecules liver organoid heroin and heroin phase I metabolites.

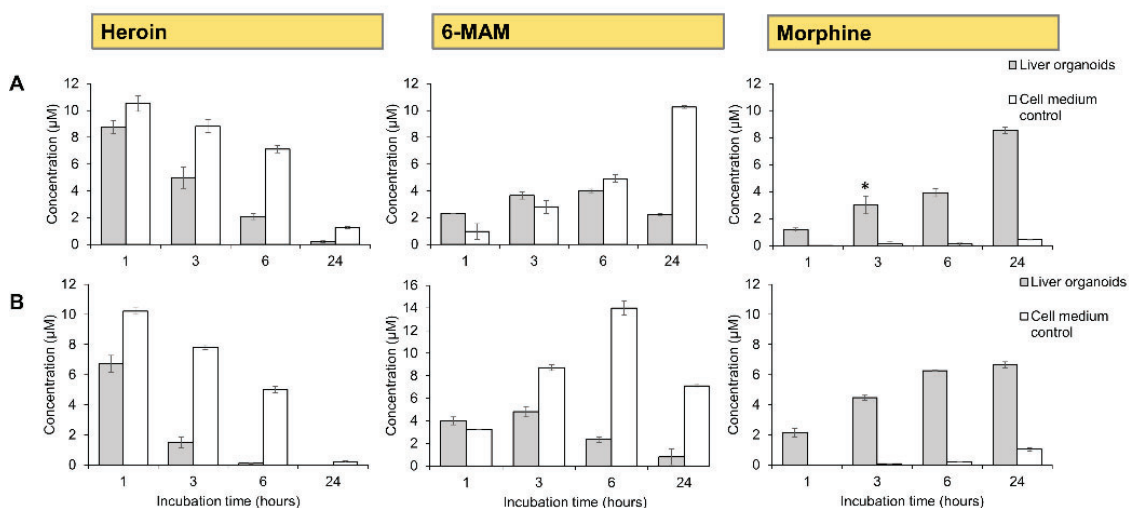


Figure 26. Concentration of heroin and metabolites (µM) in liver organoids using parallel-EME and UHPLC-MS after heroin incubation of liver organoids differentiated from the iPSC cell lines (A) AG27 (60 organoids) and (B) HPSI0114i-vabj_3 (20 organoids) in 10 µM heroin for 1, 3, 6, and 24 h. In parallel, cell medium free from organoids was used as the drug degradation control sample. Each bar represents the mean (±SD) of triplicate samples. One of the three replicates of time point 6 h liver organoids (HPSI0114i-vabj_3) was discarded. The asterisk indicates the removal of one data point due to a poor IS signal. Reprinted with permission from American Chemical Society.

The parallel-EME liver organoid methodology was established using UHPLC-MS (Section 3.2.2), providing analyte retention time repeatability with a maximum RSD of 0.07%, limit of quantification (LOQ) of 1 nM and injection volumes of 7 µL. However, similar analyte sensitivities (primarily morphine) were not achieved when we implemented the LC-MS method in-house. With the future objective of online integration of the methodology, we investigated alternative separation approaches with column IDs more suitable for high throughput and sensitive analyses of trace samples.

3.3.3 Miniaturized separation techniques not compatible with liver organoid small molecule analysis

Alternative miniaturized analytical approaches to UHPLC-MS were evaluated with regards to sensitivity, compatibility of the methodology of **Paper IV** and the fit for future online analysis.

Heroin and heroin metabolites have previously proven to be compatible with various CE and detection setups [250-253]. The EME extracted analytes from the organoid samples showed CE-UV electropherograms free from closely migrating interferences, and analyte separations within 2.5 minutes (**Figure 27**). The low injection volume (107 nL) was favorable with regards to the future handling of small organoid sample volumes. However, when coupled to UV-detection, the LOQ was estimated to be 0.5 μM for all analytes, and thus organoid incubation in 50 μM heroin was required to achieve UV-detection. In addition, indications on low robustness were observed with variations in analyte resolution affected by minor differences in sample pH.

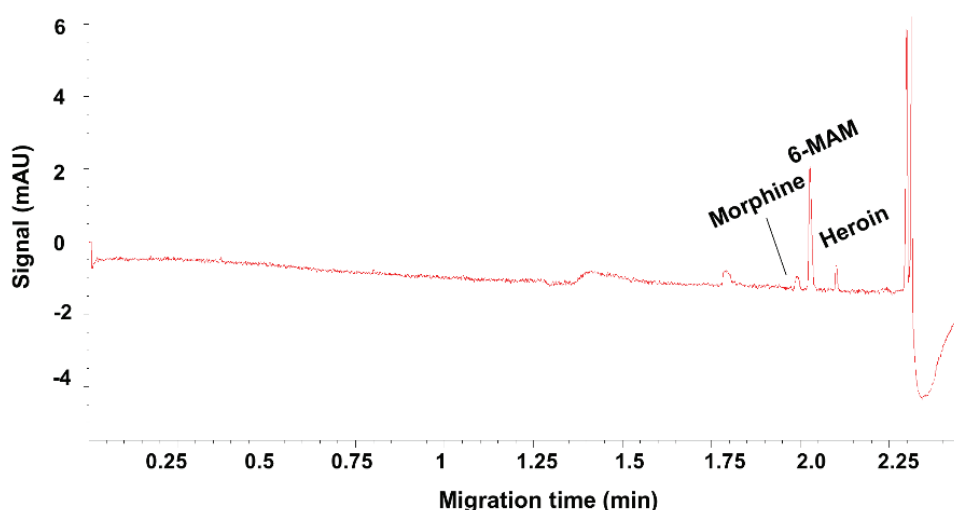


Figure 27. Electropherogram of liver organoid drug metabolism using parallel-EME and simple CE-UV using 75 μm ID fused-silica capillaries, and incubation of 60 liver organoids in 50 μM heroin for 6 hours. Sample injection was equivalent to 107 nL. Separations and measurements were performed with an applied potential of 30 kV (25°C) and at an UV-absorbance of 214 nm. Reprinted with permission from American Chemical Society.

In **Paper IV**, RP nanoLC-MS was applied in a proteomic case study of the liver organoids, identifying proteotypic peptides associated with liver heroin metabolizing enzymes (e.g., hCE1 and hCE2, results not shown). Using the same setup as for the proteomic analysis in **Section 3.1.1** and **Paper IV**, the RP nanoLC-MS system was to be evaluated for the determination of heroin, 6-MAM and morphine. The nanoLC-MS system was capable of achieving detection down to 0.95 pM for heroin and 6-MAM (1 μ L injections) while providing excellent chromatographic performance within 8 minutes (results not shown), demonstrating the potential of nanoLC for sensitive small molecule analysis.

However, as discussed in **Section 3.1.1**, similar challenges during operation were observed regarding nanoLC robustness, and poor chromatography was associated with the determination of the more polar analyte morphine. Although the polar metabolite morphine was detected using conventional and robust UHPLC-MS, morphine showed limited retention and retention repeatability using both the proteomic two-column setup and one-column setup, also when varying parameters such as LC column packing material, maximum loading pressure, and the sample loading time (**Figure 28**). Nevertheless, the methodology of **Paper IV** regarding morphine retention was not fully compatible with nanoLC, suggesting that RP nanoLC systems are not currently suited for polar metabolite studies. Future work could include assessing other RP materials more compatible with small polar analytes, e.g., phenyl-hexyl, as the phenyl groups on the SP can provide additional interactions with the aromatic rings in morphine.

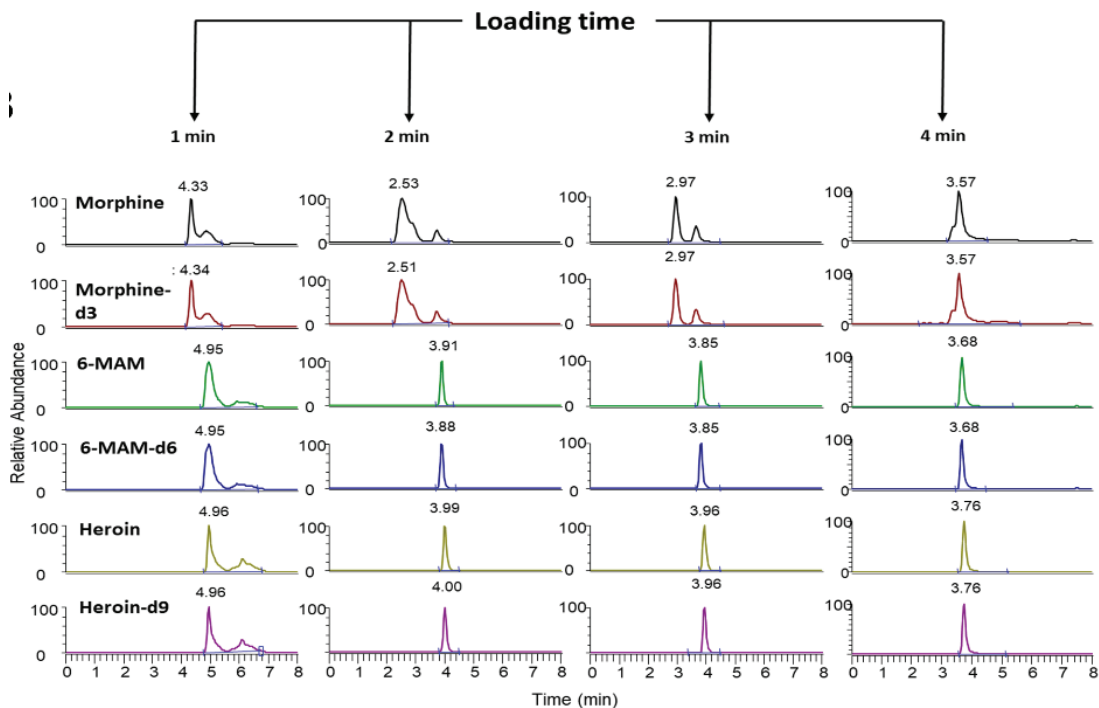


Figure 28. Extracted ion chromatogram of a 375 nM standard solution containing heroin, 6-MAM, morphine, and corresponding IS, analyzed using a one-column setup equipped with an Acclaim PepMap commercially packed analytical column with different on-column loading times (1, 2, 3, and 4 min), and injection volumes of 500 nL. Work performed by Ago Mrsa, whom I supervised. Reprinted with permission from American Chemical Society.

To sum up: High throughput parallel-EME was successfully applied in selective extraction of liver organoid heroin and heroin metabolites 6-MAM, and morphine using UHPLC-MS. CE-UV and nanoLC were explored regarding sensitivity, compatibility of the methodology, and the fit for future online analysis. The nL injection volume CE showed poor detection limits when coupled to UV detection, and although high sensitivity was achieved using nanoLC, a recurring challenge was the poor chromatographic performance of morphine.

3.4 Electromembrane extraction hyphenation with mass spectrometry for online liver organoids small molecule drug analysis

With **Paper IV** demonstrating the good fit of EME for simple and upscaled extraction of drug and drug metabolites before MS analysis, a natural next step was to bridge EME with MS for high throughput online exploration of liver organoid drug metabolizing properties, hence the aim of **Paper V**.

In 2018, Hansen et al. introduced EME on-chip and offline LC-MS, and the possibility of high analyte enrichment with only 6 nL acceptor volume [196]. Coupling organoid drug incubations with the nano-scale EME-chip and MS analysis would thus enable sensitive, real-time direct measurements of organoids and their minute secretions without multiple manual sample handling steps losing valuable sample information (**Figure 29C**). To increase the sensitivity while preserving robustness and scalability, we explored the capLC column format of 0.5 mm ID (from **Paper III**) compared to nanoLC and conventional UHPLC in **Paper IV**. Here, adult liver organoids were used, derived from a different donor tissue cell source than that in **Paper III**.

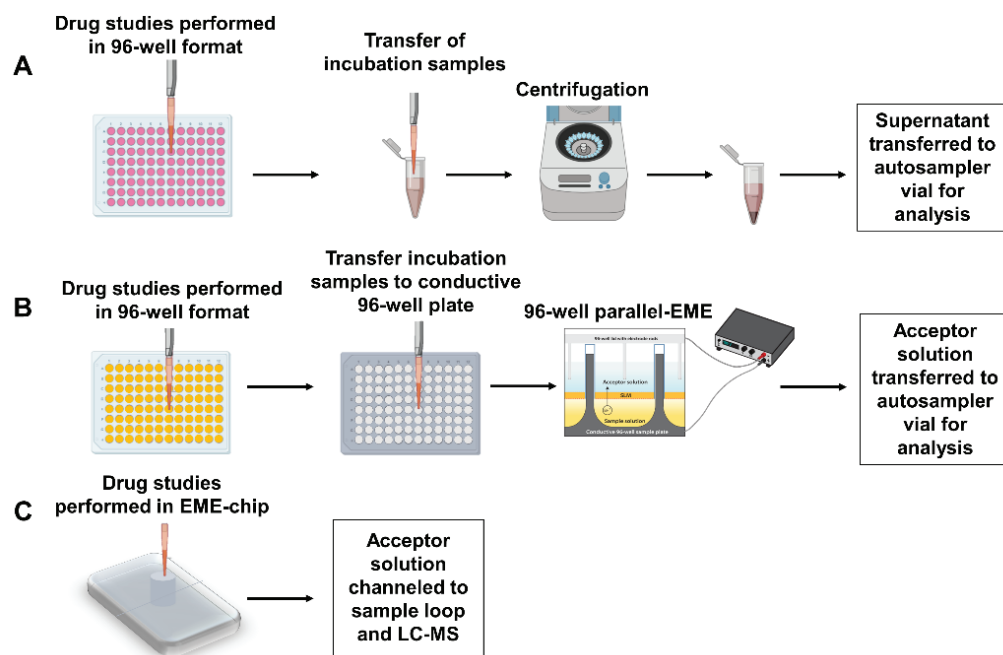


Figure 29. Schematic overview of the workflow of drug studies performed with (A) a standard sample preparation approach using centrifugation and several steps of manual pipetting prior to analysis, and (B) parallel-EME with fewer steps of manual pipetting and sample handling prior to analysis. C) Drug studies performed on chip with continuous EME extraction and no manual sample handling prior to LC-MS analysis. Figure adapted from Paper IV and Paper V. Reprinted with permission from European Chemical Societies Publishing.

3.4.1 Technical setup

In **Paper V**, a modified version of the EME-chip from [196] was fabricated, with changes such as a larger donor sample reservoir and adding a separate analyte permeable inner reservoir for organoid incubation (**Figure 30A**). Following the setup from Hansen et al. [196], the positive electrode was placed in the extraction reservoir of the EME-chip (**Figure 30A-B**), and the electrical field across the SLM to the acceptor solution was created using two stainless steel unions as negative electrodes (**Figure 30B**).

The low-pressure EME-chip and the high-pressure LC-MS setup were separated through a two position 10-ports valve (**Figure 30C-D**). In position 1 (**Figure 30C**), the EME of analytes from the extraction reservoir (donor solution) was performed, with a syringe pump continuously pumping the

extracted analytes filling the sample loop. Though extraction under stagnant conditions were associated with greater repeatability in the study of Hansen et al. [196], stagnant extraction led to clogged chip channels (100 μm x 100 μm) and connected tubing (100 μm ID) when operated under physiological conditions (37°C). The interval of the EME on-chip was set to 5 minutes (equal to 50 μL sample volume), and a sample loop of 60 μL was chosen to correct for the possible analyte band broadening in the acceptor channel previously observed [196].

In position 2 (**Figure 30D**), no EME was performed, and the acceptor solution was pumped to waste. The sample loop plug (extracted analytes in 5 mM ammonium formate pH 3.1) was pumped by the high MP organic solvent percentage from the LC-pump (MP composition of about 40% ACN in 0.1% FA, and 60% ammonium formate pH 3.1), thus enabled analyte refocusing on the analytical column before LC-separation.

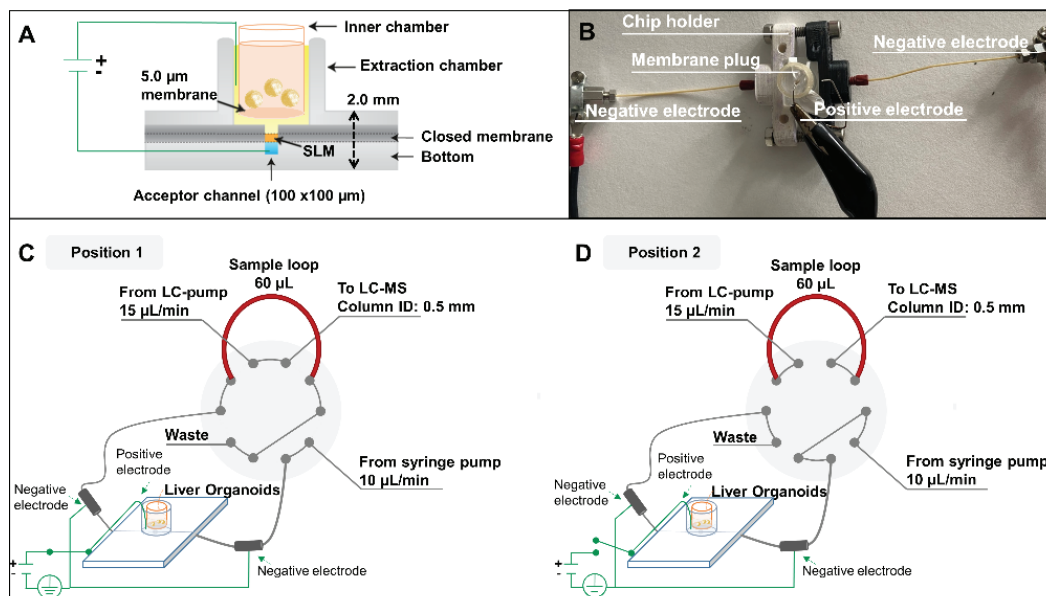


Figure 30. A) Illustration of a side-viewed cross-section of the SLM at the center of the chip. B) Top-down photograph of the EME chip assembly. C) Valve system for collecting EME extracts in a 60 μL loop, and subsequent transfer to LC-MS. In position 1- EME is performed and sample transfer to sample loop. D) In position 2- sample loading and LC-MS analysis. Figure adapted from Paper V. Reprinted with permission from European Chemical Societies Publishing.

3.4.2 Proof-of-concept: online sampling and measuring of liver organoids small molecule methadone metabolites

In **Paper IV**, the polar heroin metabolite morphine required the addition of DEHP in the SLM composition (10% DEHP/NPOE) to achieve sufficient EME recovery. However, DEHP has shown to be leaking from the SLM in sample solutions with a pH > 4 [184]. Thus, DEHP would not be favorable for EME-chip integration with physiological pH liver organoid compatible donor solutions. As morphine also indicated poor compatibility with miniaturized chromatography (**Paper IV**), heroin was not chosen as a model substance for **Paper V**.

Since the introduction of EME, methadone has frequently been used as the model drug with EME under various EME-conditions with NPOE as the SLM solvent [254, 255], also extracted in the study of Hansen et al. [196]. Methadone is mainly metabolized in the liver by CYP3A4 mediated N-demethylation to form hydrophobic metabolites 2-ethylidene-1,5-dimethyl-3,3-diphenylpyrrolidine (EDDP) and 2-ethyl-5-methyl-3,3-diphenylpyrroline (EMDP, **Figure 31**) [256-258]. The methadone metabolites EDDP and EMDP have also previously been shown to be compatible with EME [188, 259]. Thus, methadone was chosen as a model substance for **Paper V**.

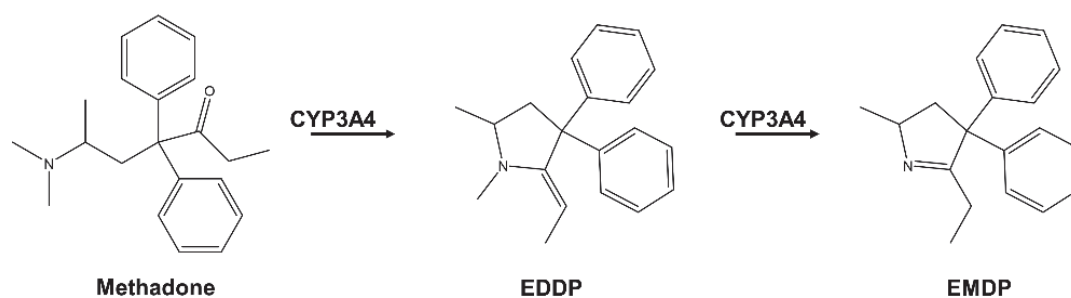


Figure 31. Human liver metabolism of methadone to form EDDP and EMDP, a reaction mediated by CYP3A4. Methadone was used as drug substrate for liver organoid metabolism measurement in Paper V.

With the current EME-chip setup coupled online to capLC and triple Q MS, detection down to sub 100 pM was achieved for methadone and EDDP. For proof-of-concept, we used the current setup for online extraction and measurements of small molecule drug metabolites studying methadone metabolism in adult liver organoids. The organoid reservoir was filled with 50 adult liver organoids, and organoid incubation was performed in 1 μM methadone for 24 hours (37°C, with agitation), as in accordance with **Section 3.2** and **Paper IV**. Introducing the methodology direct EME-MS (dEME-MS); on-chip EME, sample loading and capLC-MS separation and detection was performed automatically for 11 time points (compared to < 4 time points in **Paper IV**). Analyte selectivity was enabled through EME, capLC separation, and MS analyte specific MRM-transitions. The use of capLC chromatography also showed to be compatible with the current setup, with methadone width at the half peak height ($W_{0.5}$) of 10-11 seconds and analyte retention time repeatability of < 0.4% (**Figure 32**).

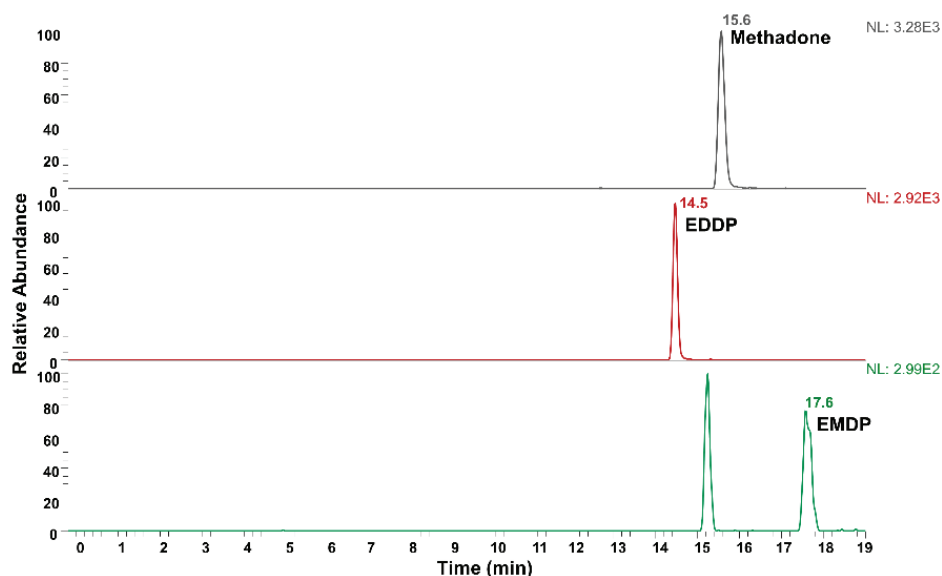


Figure 32. Extracted ion chromatogram of methadone, EDDP and EMDP in EME-chip extracted liver organoids after 24 hours of incubation in 1 μ M methadone using capLC-MS. Gradient start was at 11 min starting from 40-80% MP B in 3.5 min (5mM ammonium formate pH 3.1 as the MP A composition, and 95% acetonitrile, 0.1% formic acid as the MP B composition). The signal delay to the MS was 1.1 minutes. Figure adapted from Paper V. Reprinted with permission from European Chemical Societies Publishing.

Using dEME-MS, the methadone metabolism in adult liver organoids ($n=4$) was mapped, showing increasing metabolite formation to EDDP and EMDP with decreasing peak area of methadone, consistent with literature (**Figure 33**) [260-262]. However, with variances (\pm SD) anticipated at this prototype stage.

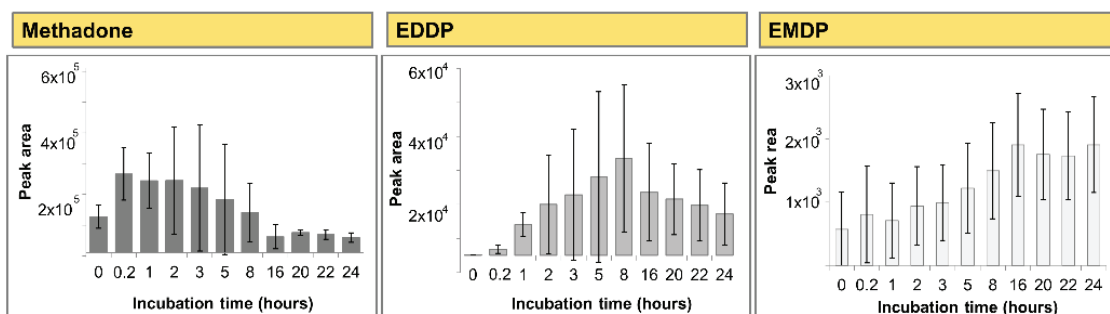


Figure 33. Mean peak area (\pm SD) of methadone and metabolites from the four studies of adult liver organoids drug metabolism in 1 μ M methadone using incubation and EME on-chip, and continuous sample transfer and capLC-MS measurements. Measurements were undertaken at the following time points; 0 hours, 20 min, 1, 2, 3, 5, 8, 16, 20, 22 and 24 hours. Time points 8, 20, 22 and 24 was not measured in one of the four studies due to operational difficulties. Figure adapted from supplementary materials in Paper V. Reprinted with permission from European Chemical Societies Publishing.

3.4.3 Notes on challenges and potential related to online organoids incubation, sampling, separation and detection

The reason for the significant variations in signal intensity during operation described in the previous section could reflect the numerous challenges related to the online integration of organoid incubation, sampling, separation, and measurement. As previously mentioned, the EME-chip and chip-connected tubing were observed to be prone to clogging during operation under physiological conditions (37°C). Although tubing with a larger ID was applied (originally 0.13 mm, changed to 0.39 mm ID), the clogging of chip channels and tubing was a recurring challenge. In addition, rupture of the SLM porous membrane of the chip was also observed, suspected to be due to increased backpressure. Future improvements could include implementing commercial LC-fittings that connect the EME-chip to the valve system for more operational friendly upscaling of the EME-chip setup.

As the expression level and metabolic activity of CYP3A4 and other drug metabolizing enzymes are highly donor-specific, the high variability in signal intensity could also be explained by the use of adult liver organoids from different donors. Day-to-day variabilities in MS signal intensity made absolute quantification challenging, in addition to the possible variations in chip-to-chip extraction efficiency (observed in [196]). As in **Section 3.3.1**, the observed variations can be corrected by adding IS to the acceptor solution, essential for future absolute quantification of the conceptual setup.

Nevertheless, dEME-MS was capable of automated and selective drug monitoring of drug metabolism in liver organoids, and the conceptual work of **Paper III** can be further assessed for a range of unpolar drugs and drug metabolites of telltale traits of enzyme activity (e.g., tolbutamide for

CYP2C9). Optimizing the SLM composition to better fit polar small molecule drugs (e.g. phenacetin as telltale of CYP1A2) and also polar endogenous metabolites (e.g., metabolomics-on-a-chip) would broaden the applicability of the conceptual work of dEME-MS, for future automated drug discovery efforts [263].

We have also previously investigated a column format selective for drug targeting (monolithic support immobilized with a Wnt pathway inhibitor) that could be further explored for implementation [264]. Furthermore, design adjustments to the dEME-MS platform should be made to fit the hyphenation to organ-on-a-chip devices better. For direct plug-and-play connection to the organ-on-a-chip, the EME-chip inlet could be designed to fit the outlet of the organ-on-a-chip. An alternative design concept to explore could be “EME in a tubing” directly coupled to the organ-on-a-chip outlet using fittings.

To sum up: Proof-of-concept dEME-MS was successfully applied in mapping adult liver organoid methadone metabolism. The low-pressure EME chip was bridged with the high-pressure capLC-MS through a two position 10-port valve, ensuring online sampling and measurement of the EME-extracts for 24 hours.

4 Concluding remarks and future aspects

This thesis explores the use of MS and separation sciences to assess liver organoid functionality by measuring biomolecules, spanning from proteins to small molecule drug metabolites. High throughput sampling was successfully achieved using parallel-EME and EME on-chip for selective small molecule extraction. However, parallel-EME was not found to be mature for large biomolecule sample preparation.

The proteomic functionality of the liver organoids was mapped and compared to human liver tissue using SDS-PAGE protein fractionation and nanoLC-MS. 1003 identified proteins were shared between liver tissue and liver organoids. Several proteins connected to central liver functions were identified in the liver organoids. However, the conventional sample preparation procedure entailed multiple sample handling steps and low throughput. Parallel-EME could become a novel method for SDS-removal during proteomic sample preparation of multiplexed samples in 96-well format. Thus, a fundamental study of SDS removal using EME was conducted. Complete SDS removal was achieved with an increase in SLM surface area using a modified EME setup in a pipette tip. However, the parallel-EME method was not found mature for liver organoid large biomolecule sample preparation and SDS removal.

Next, the liver organoid metabolizing properties were assessed by measuring neratinib-, heroin- and methadone metabolism. Adult liver organoids neratinib metabolizing properties were established by identifying unknown human neratinib metabolites using capLC-MS. Next, the heroin metabolizing properties of liver organoids were assessed using UHPLC-MS, identifying

both heroin phase I metabolites 6-MAM, morphine, and traces of the phase II metabolites M6G and M3G. Conventional low throughput centrifugation-based sample preparation was applied for the above-mentioned small molecule studies.

Minimizing the manual sample handling steps, 96-well EME was successfully applied for liver organoid extraction of heroin and phase I metabolites using conventional LC-MS. CE and nanoLC were tested for sensitivity, compatibility of the current methodology, and the fit for future online analysis. The nL injection volume CE showed poor detection limits when coupled to UV detection. Although high sensitivity was achieved using nanoLC, a recurring challenge was the poor chromatographic performance of morphine. Thus, nanoLC and CE-UV were not found to be mature for increased throughput and online MS-analysis.

The capLC-MS and small molecule analysis were hyphenated, enabling separation of the high-pressure capLC and the low-pressure liver organoids incubation through EME on-chip and continuous sampling using a two-position 10-port valve. As a proof-of-concept, adult liver organoid methadone metabolizing properties were monitored for 24 hours, with 11 online measurements showing EDDP and EMDP methadone metabolite formations. Future improvements on the EME-chip architecture and connections should be made for increased robustness of the online EME-chip capLC-MS. The dEME-MS setup can be further assessed for other drugs and metabolites of telltale traits of enzyme activity.

The liver organoids in this study displayed liver organ functionality, here presented through different bioanalytical tools. Although EME was not well

suites for large biomolecule sample preparation, EME combined with small-molecule extractions and liver organoids were well-matched and integrated online to capLC-MS. During this thesis, the developed bioanalytical strategies contributed to greater insight into organoid response and functionality, and could be a powerful tool in improving organoid development. Thus, the work presented could add to organoid bioanalytical technology in future drug development, disease modeling, and personalized medicine.

5 References

- [1] J. Kim, B.-K. Koo, J.A. Knoblich, *Human organoids: model systems for human biology and medicine*, *Nature Reviews Molecular Cell Biology*, 21 (2020) 571-584.
- [2] L. Schyschka, J.J.M. Sánchez, Z. Wang, B. Burkhardt, U. Müller-Vieira, K. Zeilinger, A. Bachmann, S. Nadalin, G. Damm, A.K. Nussler, *Hepatic 3D cultures but not 2D cultures preserve specific transporter activity for acetaminophen-induced hepatotoxicity*, *Archives of Toxicology*, 87 (2013) 1581-1593.
- [3] T. Takahashi, *Organoids for drug discovery and personalized medicine*, *Annual Review of Pharmacology and Toxicology*, 59 (2019) 447-462.
- [4] M. Hofer, M.P. Lutolf, *Engineering organoids*, *Nature Reviews Materials*, 6 (2021) 402-420.
- [5] *Method of the Year 2017: Organoids*, *Nature Methods*, 15 (2018) 1-1.
- [6] K. Takahashi, K. Tanabe, M. Ohnuki, M. Narita, T. Ichisaka, K. Tomoda, S. Yamanaka, *Induction of pluripotent stem cells from adult human fibroblasts by defined factors*, *Cell*, 131 (2007) 861-872.
- [7] K. Takahashi, S. Yamanaka, *Induction of pluripotent stem cells from mouse embryonic and adult fibroblast cultures by defined factors*, *Cell*, 126 (2006) 663-676.
- [8] A. Marsee, F.J.M. Roos, M.M.A. Verstegen, A. Marsee, F. Roos, M. Verstegen, H. Clevers, L. Vallier, T. Takebe, M. Huch, W.C. Peng, S. Forbes, F. Lemaigre, E. de Koning, H. Gehart, L. van der Laan, B. Spee, S. Boj, P. Baptista, K. Schneeberger, C. Soroka, M. Heim, S. Nuciforo, K. Zaret, Y. Saito, M. Lutolf, V. Cardinale, B. Simons, S. van Ijzendoorn, A. Kamiya, H. Chikada, S. Wang, S.J. Mun, M.J. Son, T.T. Onder, J. Boyer, T. Sato, N. Georgakopoulos, A. Meneses, L. Broutier, L. Boulter, D. Grün, J. Ijzermans, B. Artegiani, R. van Boxtel, E. Kuijk, G. Carpino, G. Peltz, J. Banales, N. Man, L. Aloia, N. LaRusso, G. George, C. Rimland, G. Yeoh, A. Grappin-Botton, D. Stange, N. Prior, J.E.E. Tirnitz-Parker, E. Andersson, C. Braconi, N. Hannan, W.-Y. Lu, S. Strom, P. Sancho-Bru, S. Ogawa, V. Corbo, M. Lancaster, H. Hu, S. Fuchs, D. Hendriks, H. Gehart, E. de Koning, F. Lemaigre, S.J. Forbes, W.C. Peng, M. Huch, T. Takebe, L. Vallier, H. Clevers, L.J.W. van der Laan, B. Spee, *Building consensus on definition and nomenclature of hepatic, pancreatic, and biliary organoids*, *Cell Stem Cell*, 28 (2021) 816-832.
- [9] M.A. Lancaster, M. Renner, C.-A. Martin, D. Wenzel, L.S. Bicknell, M.E. Hurlles, T. Homfray, J.M. Penninger, A.P. Jackson, J.A. Knoblich,

- Cerebral organoids model human brain development and microcephaly*, Nature, 501 (2013) 373-379.
- [10] K.R. Stevens, K.L. Kreutziger, S.K. Dupras, F.S. Korte, M. Regnier, V. Muskheli, M.B. Nourse, K. Bendixen, H. Reinecke, C.E. Murry, *Physiological function and transplantation of scaffold-free and vascularized human cardiac muscle tissue*, Proceedings of the National Academy of Sciences, 106 (2009) 16568-16573.
- [11] B.D. Humphreys, *Kidney structures differentiated from stem cells*, Nature Cell Biology, 16 (2014) 19-21.
- [12] T. Takebe, K. Sekine, M. Enomura, H. Koike, M. Kimura, T. Ogaeri, R.-R. Zhang, Y. Ueno, Y.-W. Zheng, N. Koike, *Vascularized and functional human liver from an iPSC-derived organ bud transplant*, Nature, 499 (2013) 481-484.
- [13] M.A. Lancaster, J.A. Knoblich, *Organogenesis in a dish: Modeling development and disease using organoid technologies*, Science, 345 (2014) 1247125.
- [14] B. Sozen, V. Jorgensen, B.A.T. Weatherbee, S. Chen, M. Zhu, M. Zernicka-Goetz, *Reconstructing aspects of human embryogenesis with pluripotent stem cells*, Nature Communications, 12 (2021) 1-13.
- [15] T. Cindrova-Davies, X. Zhao, K. Elder, C.J.P. Jones, A. Moffett, G.J. Burton, M.Y. Turco, *Menstrual flow as a non-invasive source of endometrial organoids*, Communications Biology, 4 (2021) 1-8.
- [16] S.E. Park, A. Georgescu, D. Huh, *Organoids-on-a-chip*, Science, 364 (2019) 960-965.
- [17] T. Takebe, B. Zhang, M. Radisic, *Synergistic engineering: Organoids meet organs-on-a-chip*, Cell Stem Cell, 21 (2017) 297-300.
- [18] L.A. Low, C. Mummery, B.R. Berridge, C.P. Austin, D.A. Tagle, *Organs-on-chips: into the next decade*, Nature Reviews Drug Discovery, 20 (2021) 345-361.
- [19] P.B. Watkins, *Drug metabolism by cytochromes P450 in the liver and small bowel*, Gastroenterology Clinics of North America, 21 (1992) 511-526.
- [20] J.P. Cotovio, T.G. Fernandes, *Production of human pluripotent stem cell-derived hepatic cell lineages and liver organoids: current status and potential applications*, Bioengineering, 7 (2020).
- [21] M.A. Baxter, C. Rowe, J. Alder, S. Harrison, K.P. Hanley, B.K. Park, N.R. Kitteringham, C.E. Goldring, N.A. Hanley, *Generating hepatic cell lineages from pluripotent stem cells for drug toxicity screening*, Stem Cell Research, 5 (2010) 4-22.
- [22] R. Kia, R.L.C. Sison, J. Heslop, N.R. Kitteringham, N. Hanley, J.S. Mills, B.K. Park, C.E.P. Goldring, *Stem cell-derived hepatocytes as a*

- predictive model for drug-induced liver injury: are we there yet?*, British Journal of Clinical Pharmacology, 75 (2013) 885-896.
- [23] E. Milner, M. Ainsworth, M. McDonough, B. Stevens, J. Buehrer, R. Delzell, C. Wilson, J. Barnhill, *Emerging three-dimensional hepatic models in relation to traditional two-dimensional In vitro assays for evaluating drug metabolism and hepatotoxicity*, Medicine in Drug Discovery, 8 (2020) 100060, DOI: 10.1016/j.medidd.2020.100060.
- [24] A. Brooks, X. Liang, Y. Zhang, C.-X. Zhao, M.S. Roberts, H. Wang, L. Zhang, D.H.G. Crawford, *Liver organoid as a 3D in vitro model for drug validation and toxicity assessment*, Pharmacological Research, 169 (2021) 105608, DOI: 10.1016/j.phrs.2021.105608.
- [25] M. Baxter, S. Withey, S. Harrison, C.-P. Segeritz, F. Zhang, R. Atkinson-Dell, C. Rowe, D.T. Gerrard, R. Sison-Young, R. Jenkins, J. Henry, A.A. Berry, L. Mohamet, M. Best, S.W. Fenwick, H. Malik, N.R. Kitteringham, C.E. Goldring, K. Piper Hanley, L. Vallier, N.A. Hanley, *Phenotypic and functional analyses show stem cell-derived hepatocyte-like cells better mimic fetal rather than adult hepatocytes*, Journal of Hepatology, 62 (2015) 581-589.
- [26] T. Shinozawa, H.Y. Yoshikawa, T. Takebe, *Reverse engineering liver buds through self-driven condensation and organization towards medical application*, Developmental Biology, 420 (2016) 221-229.
- [27] J. Labuda, R.P. Bowater, M. Fojta, G. Gauglitz, Z. Glatz, I. Hapala, J. Havliš, F. Kilar, A. Kilar, L. Malinovská, H.M.M. Sirén, P. Skládal, F. Torta, M. Valachovič, M. Wimmerová, Z. Zdráhal, D.B. Hibbert, *Terminology of bioanalytical methods (IUPAC Recommendations 2018)*, Pure and Applied Chemistry, 90 (2018) 1121-1198.
- [28] T.G. Cross, M.P. Hornshaw, *Can LC and LC-MS ever replace immunoassays?*, Journal of Applied Bionalysis, 2 (2016) 108-116.
- [29] J. Bordeaux, A.W. Welsh, S. Agarwal, E. Killiam, M.T. Baquero, J.A. Hanna, V.K. Anagnostou, D.L. Rimm, *Antibody validation*, BioTechniques, 48 (2010) 197-209.
- [30] X. Liu, L. Jia, *The conduct of drug metabolism studies considered good practice (I): Analytical systems and in vivo studies*, Current Drug Metabolism, 8 (2007) 815-821.
- [31] E.J. Want, A. Nordström, H. Morita, G. Siuzdak, *From exogenous to endogenous: The inevitable imprint of mass spectrometry in Metabolomics*, Journal of Proteome Research, 6 (2007) 459-468.
- [32] C. Prakash, C.L. Shaffer, A. Nedderman, *Analytical strategies for identifying drug metabolites*, Mass Spectrometry Reviews, 26 (2007) 340-369.
- [33] R. Aebersold, M. Mann, *Mass spectrometry-based proteomics*, Nature, 422 (2003) 198-207.

- [34] T.C. Walther, M. Mann, *Mass spectrometry-based proteomics in cell biology*, Journal of Cell Biology, 190 (2010) 491-500.
- [35] A. Bensimon, A.J.R. Heck, R. Aebersold, *Mass spectrometry-based proteomics and network biology*, Annual Review of Biochemistry, 81 (2012) 379-405.
- [36] A. Gonneaud, C. Asselin, F. Boudreau, F.-M. Boisvert, *Phenotypic analysis of organoids by proteomics*, Proteomics, 17 (2017) 1700023, DOI: 10.1002/pmic.201700023.
- [37] X. Feng, B.-F. Liu, J. Li, X. Liu, *Advances in coupling microfluidic chips to mass spectrometry*, Mass Spectrometry Reviews, 34 (2015) 535-557.
- [38] J.J. Thomson, *Rays of positive electricity and their application to chemical analysis*, Longmans, Green & Co, London, England, 1913.
- [39] J.C. Holmes, F.A. Morrell, *Oscillographic mass spectrometric monitoring of gas chromatography*, Applied Spectroscopy, 11 (1957) 86-87.
- [40] R.S. Gohlke, *Time-of-flight mass spectrometry and gas-liquid partition chromatography*, Analytical Chemistry, 31 (1959) 535-541.
- [41] R.T. Kelly, *Single-cell proteomics: progress and prospects*, Molecular & Cellular Proteomics, 19 (2020) 1739-1748.
- [42] M.A. Grayson, *Measuring mass: from positive rays to proteins*, Chemical Heritage Press, Philadelphia, 2002.
- [43] A. El-Aneed, A. Cohen, J. Banoub, *Mass spectrometry, review of the basics: Electrospray, MALDI, and commonly used mass analyzers*, Applied Spectroscopy Reviews, 44 (2009) 210-230.
- [44] E. de Hoffmann, *Tandem mass spectrometry: A primer*, Journal of Mass Spectrometry, 31 (1996) 129-137.
- [45] R.G. Cooks, *Special feature: Historical. collision-induced dissociation: readings and commentary*, Journal of Mass Spectrometry, 30 (1995) 1215-1221.
- [46] R.A. Yost, C.G. Enke, *Selected ion fragmentation with a tandem quadrupole mass spectrometer*, Journal of the American Chemical Society, 100 (1978) 2274-2275.
- [47] A. Makarov, *Electrostatic axially harmonic orbital trapping: a high-performance technique of mass analysis*, Analytical Chemistry, 72 (2000) 1156-1162.
- [48] S. Eliuk, A. Makarov, *Evolution of orbitrap mass spectrometry instrumentation*, Annual Review of Analytical Chemistry, 8 (2015) 61-80.
- [49] K.K. Murray, *The term 'multiple reaction monitoring' is recommended*, Rapid Communications in Mass Spectrometry, 29 (2015) 1926-1928.
- [50] A. Kalli, G.T. Smith, M.J. Sweredoski, S. Hess, *Evaluation and optimization of mass spectrometric settings during data-dependent*

- acquisition mode: Focus on LTQ-Orbitrap mass analyzers*, Journal of Proteome Research, 12 (2013) 3071-3086.
- [51] B. Domon, R. Aebersold, *Mass spectrometry and protein analysis*, Science, 312 (2006) 212-217.
- [52] A.G. Brenton, A.R. Godfrey, *Accurate mass measurement: Terminology and treatment of data*, Journal of the American Society for Mass Spectrometry, 21 (2010) 1821-1835.
- [53] Q. Hu, R.J. Noll, H. Li, A. Makarov, M. Hardman, R. Graham Cooks, *The Orbitrap: a new mass spectrometer*, Journal of Mass Spectrometry, 40 (2005) 430-443.
- [54] A. Makarov, E. Denisov, O. Lange, S. Horning, *Dynamic range of mass accuracy in LTQ orbitrap hybrid mass spectrometer*, Journal of the American Society for Mass Spectrometry, 17 (2006) 977-982.
- [55] M. Mann, N.L. Kelleher, *Precision proteomics: The case for high resolution and high mass accuracy*, Proceedings of the National Academy of Sciences, 105 (2008) 18132-18138.
- [56] R.H. Perry, R.G. Cooks, R.J. Noll, *Orbitrap mass spectrometry: Instrumentation, ion motion and applications*, Mass Spectrometry Reviews, 27 (2008) 661-699.
- [57] M. Yamashita, J.B. Fenn, *Electrospray ion source. Another variation on the free-jet theme*, The Journal of Physical Chemistry, 88 (1984) 4451-4459.
- [58] J.B. Fenn, M. Mann, C.K. Meng, S.F. Wong, C.M. Whitehouse, *Electrospray ionization for mass spectrometry of large biomolecules*, Science, 246 (1989) 64-71.
- [59] N.B. Cech, C.G. Enke, *Practical implications of some recent studies in electrospray ionization fundamentals*, Mass Spectrometry Reviews, 20 (2001) 362-387.
- [60] P.L. Urban, *Clarifying misconceptions about mass and concentration sensitivity*, Journal of Chemical Education, 93 (2016) 984-987.
- [61] M. Dole, L.L. Mack, R.L. Hines, R.C. Mobley, L.D. Ferguson, M.B. Alice, *Molecular beams of macroions*, The Journal of Chemical Physics, 49 (1968) 2240-2249.
- [62] A.P. Bruins, *Mechanistic aspects of electrospray ionization*, Journal of Chromatography A, 794 (1998) 345-357.
- [63] B.N. Pramanik, A.K. Ganguly, M.L. Gross, *Applied electrospray mass spectrometry: practical spectroscopy*, CRC Press, New York, 2002.
- [64] E.S. Lander, L.M. Linton, B. Birren, C. Nusbaum, M.C. Zody, J. Baldwin, K. Devon, K. Dewar, M. Doyle, W. FitzHugh, R. Funke, D. Gage, K. Harris, A. Heaford, J. Howland, L. Kann, J. Lehoczky, R. LeVine, P. McEwan, K. McKernan, J. Meldrim, J.P. Mesirov, C. Miranda, W. Morris, J. Naylor, C. Raymond, M. Rosetti, R. Santos, A. Sheridan, C. Sougnez, N. Stange-Thomann, N. Stojanovic, A. Subramanian, D. Wyman, J. Rogers, J.

Sulston, R. Ainscough, S. Beck, D. Bentley, J. Burton, C. Clee, N. Carter, A. Coulson, R. Deadman, P. Deloukas, A. Dunham, I. Dunham, R. Durbin, L. French, D. Grafham, S. Gregory, T. Hubbard, S. Humphray, A. Hunt, M. Jones, C. Lloyd, A. McMurray, L. Matthews, S. Mercer, S. Milne, J.C. Mullikin, A. Mungall, R. Plumb, M. Ross, R. Shownkeen, S. Sims, R.H. Waterston, R.K. Wilson, L.W. Hillier, J.D. McPherson, M.A. Marra, E.R. Mardis, L.A. Fulton, A.T. Chinwalla, K.H. Pepin, W.R. Gish, S.L. Chissoe, M.C. Wendl, K.D. Delehaunty, T.L. Miner, A. Delehaunty, J.B. Kramer, L.L. Cook, R.S. Fulton, D.L. Johnson, P.J. Minx, S.W. Clifton, T. Hawkins, E. Branscomb, P. Predki, P. Richardson, S. Wenning, T. Slezak, N. Doggett, J.-F. Cheng, A. Olsen, S. Lucas, C. Elkin, E. Uberbacher, M. Frazier, R.A. Gibbs, D.M. Muzny, S.E. Scherer, J.B. Bouck, E.J. Sodergren, K.C. Worley, C.M. Rives, J.H. Gorrell, M.L. Metzker, S.L. Naylor, R.S. Kucherlapati, D.L. Nelson, G.M. Weinstock, Y. Sakaki, A. Fujiyama, M. Hattori, T. Yada, A. Toyoda, T. Itoh, C. Kawagoe, H. Watanabe, Y. Totoki, T. Taylor, J. Weissenbach, R. Heilig, W. Saurin, F. Artiguenave, P. Brottier, T. Bruls, E. Pelletier, C. Robert, P. Wincker, A. Rosenthal, M. Platzer, G. Nyakatura, S. Taudien, A. Rump, D.R. Smith, L. Doucette-Stamm, M. Rubenfield, K. Weinstock, H.M. Lee, J. Dubois, H. Yang, J. Yu, J. Wang, G. Huang, J. Gu, L. Hood, L. Rowen, A. Madan, S. Qin, R.W. Davis, N.A. Federspiel, A.P. Abola, M.J. Proctor, B.A. Roe, F. Chen, H. Pan, J. Ramser, H. Lehrach, R. Reinhardt, W.R. McCombie, M. de la Bastide, N. Dedhia, H. Blöcker, K. Hornischer, G. Nordsiek, R. Agarwala, L. Aravind, J.A. Bailey, A. Bateman, S. Batzoglou, E. Birney, P. Bork, D.G. Brown, C.B. Burge, L. Cerutti, H.-C. Chen, D. Church, M. Clamp, R.R. Copley, T. Doerks, S.R. Eddy, E.E. Eichler, T.S. Furey, J. Galagan, J.G.R. Gilbert, C. Harmon, Y. Hayashizaki, D. Haussler, H. Hermjakob, K. Hokamp, W. Jang, L.S. Johnson, T.A. Jones, S. Kasif, A. Kasprzyk, S. Kennedy, W.J. Kent, P. Kitts, E.V. Koonin, I. Korf, D. Kulp, D. Lancet, T.M. Lowe, A. McLysaght, T. Mikkelsen, J.V. Moran, N. Mulder, V.J. Pollara, C.P. Ponting, G. Schuler, J. Schultz, G. Slater, A.F.A. Smit, E. Stupka, J. Szustakowki, D. Thierry-Mieg, J. Thierry-Mieg, L. Wagner, J. Wallis, R. Wheeler, A. Williams, Y.I. Wolf, K.H. Wolfe, S.-P. Yang, R.-F. Yeh, F. Collins, M.S. Guyer, J. Peterson, A. Felsenfeld, K.A. Wetterstrand, R.M. Myers, J. Schmutz, M. Dickson, J. Grimwood, D.R. Cox, M.V. Olson, R. Kaul, C. Raymond, N. Shimizu, K. Kawasaki, S. Minoshima, G.A. Evans, M. Athanasiou, R. Schultz, A. Patrinos, M.J. Morgan, *Initial sequencing and analysis of the human genome*, Nature, 409 (2001) 860-921.

[65] I. Humphery-Smith, S.J. Cordwell, W.P. Blackstock, *Proteome research: complementarity and limitations with respect to the RNA and DNA worlds*, Electrophoresis, 18 (1997) 1217-1242.

- [66] M.R. Wilkins, J.-C. Sanchez, A.A. Gooley, R.D. Appel, I. Humphery-Smith, D.F. Hochstrasser, K.L. Williams, *Progress with proteome projects: Why all proteins expressed by a genome should be identified and how to do it*, *Biotechnology and Genetic Engineering Reviews*, 13 (1996) 19-50.
- [67] N.L. Anderson, N.G. Anderson, *Proteome and proteomics: New technologies, new concepts, and new words*, *Electrophoresis*, 19 (1998) 1853-1861.
- [68] Y.-K. Paik, S.-K. Jeong, G.S. Omenn, M. Uhlen, S. Hanash, S.Y. Cho, H.-J. Lee, K. Na, E.-Y. Choi, F. Yan, F. Zhang, Y. Zhang, M. Snyder, Y. Cheng, R. Chen, G. Marko-Varga, E.W. Deutsch, H. Kim, J.-Y. Kwon, R. Aebersold, A. Bairoch, A.D. Taylor, K.Y. Kim, E.-Y. Lee, D. Hochstrasser, P. Legrain, W.S. Hancock, *The chromosome-centric human proteome project for cataloging proteins encoded in the genome*, *Nature biotechnology*, 30 (2012) 221-223.
- [69] M.-S. Kim, S.M. Pinto, D. Getnet, R.S. Nirujogi, S.S. Manda, R. Chaerkady, A.K. Madugundu, D.S. Kelkar, R. Isserlin, S. Jain, J.K. Thomas, B. Muthusamy, P. Leal-Rojas, P. Kumar, N.A. Sahasrabudhe, L. Balakrishnan, J. Advani, B. George, S. Renuse, L.D.N. Selvan, A.H. Patil, V. Nanjappa, A. Radhakrishnan, S. Prasad, T. Subbannayya, R. Raju, M. Kumar, S.K. Sreenivasamurthy, A. Marimuthu, G.J. Sathe, S. Chavan, K.K. Datta, Y. Subbannayya, A. Sahu, S.D. Yelamanchi, S. Jayaram, P. Rajagopalan, J. Sharma, K.R. Murthy, N. Syed, R. Goel, A.A. Khan, S. Ahmad, G. Dey, K. Mudgal, A. Chatterjee, T.-C. Huang, J. Zhong, X. Wu, P.G. Shaw, D. Freed, M.S. Zahari, K.K. Mukherjee, S. Shankar, A. Mahadevan, H. Lam, C.J. Mitchell, S.K. Shankar, P. Satishchandra, J.T. Schroeder, R. Sirdeshmukh, A. Maitra, S.D. Leach, C.G. Drake, M.K. Halushka, T.S.K. Prasad, R.H. Hruban, C.L. Kerr, G.D. Bader, C.A. Iacobuzio-Donahue, H. Gowda, A. Pandey, *A draft map of the human proteome*, *Nature*, 509 (2014) 575-581.
- [70] M. Beck, M. Claassen, R. Aebersold, *Comprehensive proteomics*, *Current Opinion in Biotechnology*, 22 (2011) 3-8.
- [71] J.C. Tran, L. Zamdborg, D.R. Ahlf, J.E. Lee, A.D. Catherman, K.R. Durbin, J.D. Tipton, A. Vellaichamy, J.F. Kellie, M. Li, C. Wu, S.M. Sweet, B.P. Early, N. Siuti, R.D. LeDuc, P.D. Compton, P.M. Thomas, N.L. Kelleher, *Mapping intact protein isoforms in discovery mode using top-down proteomics*, *Nature*, 480 (2011) 254-258.
- [72] D.F. Hunt, J.R. Yates, J. Shabanowitz, S. Winston, C.R. Hauer, *Protein sequencing by tandem mass spectrometry*, *Proceedings of the National Academy of Sciences*, 83 (1986) 6233-6237.
- [73] Z.R. Gregorich, Y. Ge, *Top-down proteomics in health and disease: Challenges and opportunities*, *Proteomics*, 14 (2014) 1195-1210.

- [74] P.D. Compton, L. Zamdborg, P.M. Thomas, N.L. Kelleher, *On the scalability and requirements of whole protein mass spectrometry*, *Analytical Chemistry*, 83 (2011) 6868-6874.
- [75] T.K. Toby, L. Fornelli, N.L. Kelleher, *Progress in top-down proteomics and the analysis of proteoforms*, *Annual Review of Analytical Chemistry*, 9 (2016) 499-519.
- [76] N.W. Bateman, S.P. Goulding, N.J. Shulman, A.K. Gadok, K.K. Szumlinski, M.J. MacCoss, C.C. Wu, *Maximizing peptide identification events in proteomic workflows using data-dependent acquisition (dda)* *Molecular & Cellular Proteomics*, 13 (2014) 329-338.
- [77] J.K. Eng, A.L. McCormack, J.R. Yates, *An approach to correlate tandem mass spectral data of peptides with amino acid sequences in a protein database*, *Journal of the American Society for Mass Spectrometry*, 5 (1994) 976-989.
- [78] C. O'Donovan, M.J. Martin, A. Gattiker, E. Gasteiger, A. Bairoch, R. Apweiler, *High-quality protein knowledge resource: SWISS-PROT and TrEMBL*, *Briefings in Bioinformatics*, 3 (2002) 275-284.
- [79] G.O. Consortium, *The Gene Ontology (GO) database and informatics resource*, *Nucleic acids research*, 32 (2004) D258-D261.
- [80] P. Kebarle, L. Tang, *From ions in solution to ions in the gas phase—the mechanism of electrospray mass spectrometry*, *Analytical Chemistry*, 65 (1993) 972A-986A.
- [81] L. Tang, P. Kebarle, *Dependence of ion intensity in electrospray mass spectrometry on the concentration of the analytes in the electrosprayed solution*, *Analytical Chemistry*, 65 (1993) 3654-3668.
- [82] T.M. Annesley, *Ion suppression in mass spectrometry*, *Clinical Chemistry*, 49 (2003) 1041.
- [83] C.R. Mallet, Z. Lu, J.R. Mazzeo, *A study of ion suppression effects in electrospray ionization from mobile phase additives and solid-phase extracts*, *Rapid Communications in Mass Spectrometry*, 18 (2004) 49-58.
- [84] A. Van Eeckhaut, K. Lanckmans, S. Sarre, I. Smolders, Y. Michotte, *Validation of bioanalytical LC–MS/MS assays: Evaluation of matrix effects*, *Journal of Chromatography B*, 877 (2009) 2198-2207.
- [85] I. Špánik, A. Machyňáková, *Recent applications of gas chromatography with high-resolution mass spectrometry*, *Journal of Separation Science*, 41 (2018) 163-179.
- [86] A. Dispas, H. Jambo, S. André, E. Tyteca, P. Hubert, *Supercritical fluid chromatography: a promising alternative to current bioanalytical techniques*, *Bioanalysis*, 10 (2018) 107-124.
- [87] A. Ihde, *Michael Tswett's first paper on chromatography by Gerhard Hesse; Herbert Weil; The elements of chromatography by Trevor Illtyd Williams*, *Isis: A journal of the History of Science Society*, 47 (1956) 93-94.

- [88] R. Kuhn, E. Lederer, *Fraktionierung und isomerisierung des carotins*, *Naturwissenschaften*, 19 (1931) 306-306.
- [89] S.K. Grebe, R.J. Singh, *LC-MS/MS in the clinical laboratory - where to from here?*, *The Clinical Biochemist Reviews*, 32 (2011) 5-31.
- [90] P. Jandera, G. Henze, *Liquid chromatography, 1. Fundamentals, history, instrumentation, materials*, John Wiley & Sons, Weinheim, Germany, 2000.
- [91] G.A. Howard, A.J.P. Martin, *The separation of the C12-C18 fatty acids by reversed-phase partition chromatography*, *Biochemical Journal*, 46 (1950) 532-538.
- [92] C. Horvath, W. Melander, I. Molnar, *Liquid chromatography of ionogenic substances with nonpolar stationary phases*, *Analytical Chemistry*, 49 (1977) 142-154.
- [93] J.G. Dorsey, K.A. Dill, *The molecular mechanism of retention in reversed-phase liquid chromatography*, *Chemical Reviews*, 89 (1989) 331-346.
- [94] M.C. García, *The effect of the mobile phase additives on sensitivity in the analysis of peptides and proteins by high-performance liquid chromatography–electrospray mass spectrometry*, *Journal of Chromatography B*, 825 (2005) 111-123.
- [95] R. Kostianen, T.J. Kauppila, *Effect of eluent on the ionization process in liquid chromatography–mass spectrometry*, *Journal of Chromatography A*, 1216 (2009) 685-699.
- [96] R. Hayes, A. Ahmed, T. Edge, H. Zhang, *Core–shell particles: Preparation, fundamentals and applications in high performance liquid chromatography*, *Journal of Chromatography A*, 1357 (2014) 36-52.
- [97] N. Tanaka, D.V. McCalley, *Core–shell, ultrasmall particles, monoliths, and other support materials in high-performance liquid chromatography*, *Analytical Chemistry*, 88 (2016) 279-298.
- [98] U.D.N. Jeffrey R. Mazzeo, Marianna Kele, Robert S. Plumb, *Advancing LC performance with smaller particles and higher pressure*, *Analytical Chemistry*, 77 (2005) 460 A-467 A.
- [99] J.J. van Deemter, F.J. Zuiderweg, A. Klinkenberg, *Longitudinal diffusion and resistance to mass transfer as causes of nonideality in chromatography*, *Chemical Engineering Science*, 5 (1956) 271-289.
- [100] J.C. Giddings, *'Eddy' diffusion in chromatography*, *Nature*, 184 (1959) 357-358.
- [101] E. Kučera, *Contribution to the theory of chromatography: Linear non-equilibrium elution chromatography*, *Journal of Chromatography A*, 19 (1965) 237-248.
- [102] F. Gritti, G. Guiochon, *Mass transfer kinetics, band broadening and column efficiency*, *Journal of Chromatography A*, 1221 (2012) 2-40.

- [103] Y. Saito, K. Jinno, T. Greibrokk, *Capillary columns in liquid chromatography: between conventional columns and microchips*, Journal of Separation Science, 27 (2004) 1379-1390.
- [104] J.P. Vissers, *Recent developments in microcolumn liquid chromatography*, Journal of Chromatography A, 856 (1999) 117-143.
- [105] S.R. Wilson, T. Vehus, H.S. Berg, E. Lundanes, *Nano-LC in proteomics: recent advances and approaches*, Bioanalysis, 7 (2015) 1799-1815.
- [106] J.P. Vissers, H.A. Claessens, C.A. Cramers, *Microcolumn liquid chromatography: instrumentation, detection and applications*, Journal of Chromatography A, 779 (1997) 1-28.
- [107] J. Chervet, M. Ursem, J. Salzmann, *Instrumental requirements for nanoscale liquid chromatography*, Analytical Chemistry, 68 (1996) 1507-1512.
- [108] M.S. Wilm, M. Mann, *Electrospray and Taylor-Cone theory, Dole's beam of macromolecules at last?*, International Journal of Mass Spectrometry and Ion Processes, 136 (1994) 167-180.
- [109] M.R. Emmett, R.M. Caprioli, *Micro-electrospray mass spectrometry: ultra-high-sensitivity analysis of peptides and proteins*, Journal of the American Society for Mass Spectrometry, 5 (1994) 605-613.
- [110] T. Köcher, P. Pichler, M. De Pra, L. Rieux, R. Swart, K. Mechtler, *Development and performance evaluation of an ultralow flow nanoliquid chromatography-tandem mass spectrometry set-up*, Proteomics, 14 (2014) 1999-2007.
- [111] A. Schmidt, M. Karas, T. Dülcks, *Effect of different solution flow rates on analyte ion signals in nano-ESI MS, or: when does ESI turn into nano-ESI?*, Journal of the American Society for Mass Spectrometry, 14 (2003) 492-500.
- [112] Y. Shen, R. Zhao, S.J. Berger, G.A. Anderson, N. Rodriguez, R.D. Smith, *High-efficiency nanoscale liquid chromatography coupled on-line with mass spectrometry using nanoelectrospray ionization for proteomics*, Analytical Chemistry, 74 (2002) 4235-4249.
- [113] J. Šesták, D. Moravcová, V. Kahle, *Instrument platforms for nano liquid chromatography*, Journal of Chromatography A, 1421 (2015) 2-17.
- [114] M. Rogeberg, H. Malerod, H. Roberg-Larsen, C. Aass, S.R. Wilson, *On-line solid phase extraction-liquid chromatography, with emphasis on modern bioanalysis and miniaturized systems*, Journal of Pharmaceutical and Biomedical Analysis, 87 (2014) 120-129.
- [115] A.J. Oosterkamp, E. Gelpí, J. Abian, *Quantitative peptide bioanalysis using column-switching nano liquid chromatography/mass spectrometry*, Journal of Mass Spectrometry, 33 (1998) 976-983.

- [116] J. Lenčo, M. Vajrychová, K. Pimková, M. Prokšová, M. Benková, J. Klimentová, V. Tambor, O. Soukup, *Conventional-flow liquid chromatography–mass spectrometry for exploratory bottom-up proteomic analyses*, *Analytical Chemistry*, 90 (2018) 5381-5389.
- [117] Y. Bian, R. Zheng, F.P. Bayer, C. Wong, Y.-C. Chang, C. Meng, D.P. Zolg, M. Reinecke, J. Zecha, S. Wiechmann, S. Heinzlmeir, J. Scherr, B. Hemmer, M. Baynham, A.-C. Gingras, O. Boychenko, B. Kuster, *Robust, reproducible and quantitative analysis of thousands of proteomes by micro-flow LC–MS/MS*, *Nature Communications*, 11 (2020) 157, DOI: 10.1038/s41467-019-13973-x.
- [118] M. Wilm, M. Mann, *Analytical properties of the nanoelectrospray ion source*, *Analytical Chemistry*, 68 (1996) 1-8.
- [119] C.L. Gatlin, G.R. Kleemann, L.G. Hays, A.J. Link, J.R. Yates, *Protein identification at the low femtomole level from silver-stained gels using a new fritless electrospray interface for liquid chromatography–microspray and nanospray mass spectrometry*, *Analytical Biochemistry*, 263 (1998) 93-101.
- [120] A.J. Link, J. Eng, D.M. Schieltz, E. Carmack, G.J. Mize, D.R. Morris, B.M. Garvik, J.R. Yates, *Direct analysis of protein complexes using mass spectrometry*, *Nature biotechnology*, 17 (1999) 676-682.
- [121] H.D. Meiring, E. van der Heeft, G.J. ten Hove, A.P.J.M. de Jong, *Nanoscale LC–MS(n): Technical design and applications to peptide and protein analysis*, *Journal of Separation Science*, 25 (2002) 557-568.
- [122] Y. Ishihama, *Proteomic LC–MS systems using nanoscale liquid chromatography with tandem mass spectrometry*, *Journal of Chromatography A*, 1067 (2005) 73-83.
- [123] I. Sierra, M.L. Marina, D. Pérez-Quintanilla, S. Morante-Zarcelero, M. Silva, *Approaches for enantioselective resolution of pharmaceuticals by miniaturised separation techniques with new chiral phases based on nanoparticles and monoliths*, *Electrophoresis*, 37 (2016) 2538-2553.
- [124] J. Alcántara-Durán, D. Moreno-González, M. Beneito-Cambra, J.F. García-Reyes, *Dilute-and-shoot coupled to nanoflow liquid chromatography high resolution mass spectrometry for the determination of drugs of abuse and sport drugs in human urine*, *Talanta*, 182 (2018) 218-224.
- [125] A.J. Chetwynd, A. David, *A review of nanoscale LC-ESI for metabolomics and its potential to enhance the metabolome coverage*, *Talanta*, 182 (2018) 380-390.
- [126] K. Lanckmans, A. Van Eeckhaut, S. Sarre, I. Smolders, Y. Michotte, *Capillary and nano-liquid chromatography–tandem mass spectrometry for the quantification of small molecules in microdialysis samples: Comparison with microbore dimensions*, *Journal of Chromatography A*, 1131 (2006) 166-175.

- [127] X. Duan, B. Weinstock-Guttman, H. Wang, E. Bang, J. Li, M. Ramanathan, J. Qu, *Ultrasensitive quantification of serum vitamin D metabolites using selective solid-phase extraction coupled to microflow liquid chromatography and isotope-dilution mass spectrometry*, *Analytical Chemistry*, 82 (2010) 2488-2497.
- [128] C.C. Christianson, C.J.L. Johnson, S.R. Needham, *The advantages of microflow LC–MS/MS compared with conventional HPLC–MS/MS for the analysis of methotrexate from human plasma*, *Bioanalysis*, 5 (2013) 1387-1396.
- [129] A. Uclés Moreno, S. Herrera López, B. Reichert, A. Lozano Fernández, M.D. Hernando Guil, A.R. Fernández-Alba, *Microflow liquid chromatography coupled to mass spectrometry—An approach to significantly increase sensitivity, decrease matrix effects, and reduce organic solvent usage in pesticide residue analysis*, *Analytical Chemistry*, 87 (2015) 1018-1025.
- [130] Z. Márta, B. Bobály, J. Fekete, B. Magda, T. Imre, K.V. Mészáros, M. Bálint, P.T. Szabó, *Simultaneous determination of thirteen different steroid hormones using micro UHPLC-MS/MS with on-line SPE system*, *Journal of Pharmaceutical and Biomedical Analysis*, 150 (2018) 258-267.
- [131] S. Geller, H. Lieberman, A. Kloss, A.R. Ivanov, *A systematic approach to development of analytical scale and microflow-based liquid chromatography coupled to mass spectrometry metabolomics methods to support drug discovery and development*, *Journal of Chromatography A*, 1642 (2021) 462047, DOI: 10.1016/j.chroma.2021.462047.
- [132] R.K. Harstad, A.C. Johnson, M.M. Weisenberger, M.T. Bowser, *Capillary electrophoresis*, *Analytical Chemistry*, 88 (2016) 299-319.
- [133] Z. Gao, W. Zhong, *Recent (2018–2020) development in capillary electrophoresis*, *Analytical and Bioanalytical Chemistry*, (2021) 1-16, DOI: 10.1007/s00216-021-03290-y.
- [134] J.W. Jorgenson, K.D. Lukacs, *Zone electrophoresis in open-tubular glass capillaries*, *Analytical Chemistry*, 53 (1981) 1298-1302.
- [135] J.W. Jorgenson, K.D. Lukacs, *High-resolution separations based on electrophoresis and electroosmosis*, *Journal of Chromatography A*, 218 (1981) 209-216.
- [136] P.G. Righetti, *Electrophoresis: The march of pennies, the march of dimes*, *Journal of Chromatography A*, 1079 (2005) 24-40.
- [137] S.F.Y. Li, *Capillary electrophoresis: principles, practice and applications*, Elsevier Science Publishers B.V., Amsterdam, The Netherlands, 1992.
- [138] X. Ou, P. Chen, X. Huang, S. Li, B.-F. Liu, *Microfluidic chip electrophoresis for biochemical analysis*, *Journal of Separation Science*, 43 (2020) 258-270.

- [139] G. Bonvin, J. Schappler, S. Rudaz, *Capillary electrophoresis–electrospray ionization-mass spectrometry interfaces: Fundamental concepts and technical developments*, *Journal of Chromatography A*, 1267 (2012) 17-31.
- [140] R. Ramautar, G.W. Somsen, G.J. de Jong, *CE–MS for metabolomics: Developments and applications in the period 2014–2016*, *Electrophoresis*, 38 (2017) 190-202.
- [141] R.L.C. Voeten, I.K. Ventouri, R. Haselberg, G.W. Somsen, *Capillary electrophoresis: Trends and recent advances*, *Analytical Chemistry*, 90 (2018) 1464-1481.
- [142] M. Langmajerová, R. Řemínek, M. Pelcová, F. Foret, Z. Glatz, *Combination of on-line CE assay with MS detection for the study of drug metabolism by cytochromes P450*, *Electrophoresis*, 36 (2015) 1365-1373.
- [143] C. Fanali, G. D'Orazio, A. Gentili, S. Fanali, *Potentiality of miniaturized techniques for the analysis of drugs of abuse*, *Electrophoresis*, (2021) DOI: 10.1002/elps.202100150.
- [144] A.A.M. Heemskerk, A.M. Deelder, O.A. Mayboroda, *CE–ESI-MS for bottom-up proteomics: Advances in separation, interfacing and applications*, *Mass Spectrometry Reviews*, 35 (2016) 259-271.
- [145] A. Latosinska, J. Siwy, H. Mischak, M. Frantzi, *Peptidomics and proteomics based on CE-MS as a robust tool in clinical application: The past, the present, and the future*, *Electrophoresis*, 40 (2019) 2294-2308.
- [146] M.M. Moein, A. El Beqqali, M. Abdel-Rehim, *Bioanalytical method development and validation: Critical concepts and strategies*, *Journal of Chromatography B*, 1043 (2017) 3-11.
- [147] H. Roberg-Larsen, S.R. Wilson, E. Lundanes, *Recent advances in on-line upfront devices for sensitive bioanalytical nano LC methods*, *TrAC Trends in Analytical Chemistry*, 136 (2021) 116190, DOI: 10.1016/j.trac.2021.116190.
- [148] J.P. Abita, M. Delaage, M. Lazdunski, J. Savrda, *The mechanism of activation of trypsinogen*, *European Journal of Biochemistry*, 8 (1969) 314-324.
- [149] J.V. Olsen, S.-E. Ong, M. Mann, *Trypsin cleaves exclusively C-terminal to arginine and lysine residues*, *Molecular & Cellular Proteomics*, 3 (2004) 608-614.
- [150] D.L. Tabb, Y. Huang, V.H. Wysocki, J.R. Yates, *Influence of basic residue content on fragment ion peak intensities in low-energy collision-induced dissociation spectra of peptides*, *Analytical Chemistry*, 76 (2004) 1243-1248.
- [151] L. Tsiatsiani, A.J.R. Heck, *Proteomics beyond trypsin*, *The FEBS Journal*, 282 (2015) 2612-2626.

- [152] W.W. Cleland, *Dithiothreitol, a new protective reagent for SH groups**, *Biochemistry*, 3 (1964) 480-482.
- [153] S. Suttapitugsakul, H. Xiao, J. Smeeckens, R. Wu, *Evaluation and optimization of reduction and alkylation methods to maximize peptide identification with MS-based proteomics*, *Molecular BioSystems*, 13 (2017) 2574-2582.
- [154] S. Camerini, P. Mauri, *The role of protein and peptide separation before mass spectrometry analysis in clinical proteomics*, *Journal of Chromatography A*, 1381 (2015) 1-12.
- [155] L. Reubsæet, M.J. Sweredoski, A. Moradian, B. Lomenick, R. Eggleston-Rangel, S.D. Garbis, *Nano volume fractionation strategy for dilute-and-shoot injections in off-line loss-less proteomic workflows for extensive protein identifications of ultra-low sample amounts*, *Journal of Chromatography A*, 1609 (2020) 460507, DOI: 10.1016/j.chroma.2019.460507.
- [156] A. Shevchenko, M. Wilm, O. Vorm, M. Mann, *Mass spectrometric sequencing of proteins from silver-stained polyacrylamide gels*, *Analytical Chemistry*, 68 (1996) 850-858.
- [157] A. Shevchenko, H. Tomas, J. Havli, J.V. Olsen, M. Mann, *In-gel digestion for mass spectrometric characterization of proteins and proteomes*, *Nature Protocols*, 1 (2007) 2856-2860.
- [158] R.R.O. Loo, N. Dales, P.C. Andrews, *Surfactant effects on protein structure examined by electrospray ionization mass spectrometry*, *Protein Science*, 3 (1994) 1975-1983.
- [159] D. Botelho, M.J. Wall, D.B. Vieira, S. Fitzsimmons, F. Liu, A. Doucette, *Top-down and bottom-up proteomics of SDS-containing solutions following mass-based separation*, *Journal of Proteome Research*, 9 (2010) 2863-2870.
- [160] R.M. Tubaon, P.R. Haddad, J.P. Quirino, *Sample clean-up strategies for ESI mass spectrometry applications in bottom-up proteomics: Trends from 2012 to 2016*, *Proteomics*, 17 (2017) 1700011, DOI: 10.1002/pmic.201700011.
- [161] J.R. Wiśniewski, A. Zougman, N. Nagaraj, M. Mann, *Universal sample preparation method for proteome analysis*, *Nature Methods*, 6 (2009) 359-362.
- [162] M.S. Bereman, J.D. Egertson, M.J. MacCoss, *Comparison between procedures using SDS for shotgun proteomic analyses of complex samples*, *Proteomics*, 11 (2011) 2931-2935.
- [163] C.S. Hughes, S. Foehr, D.A. Garfield, E.E. Furlong, L.M. Steinmetz, J. Krijgsveld, *Ultrasensitive proteome analysis using paramagnetic bead technology*, *Molecular Systems Biology*, 10 (2014) 757, DOI: 10.15252/msb.20145625.

- [164] M. Sielaff, J. Kuharev, T. Bohn, J. Hahlbrock, T. Bopp, S. Tenzer, U. Distler, *Evaluation of FASP, SP3, and iST protocols for proteomic sample preparation in the low microgram range*, Journal of Proteome Research, 16 (2017) 4060-4072.
- [165] J. Blanchard, *Evaluation of the relative efficacy of various techniques for deproteinizing plasma samples prior to high-performance liquid chromatographic analysis*, Journal of Chromatography B: Biomedical Sciences and Applications, 226 (1981) 455-460.
- [166] C. Bylda, R. Thiele, U. Kobold, D.A. Volmer, *Recent advances in sample preparation techniques to overcome difficulties encountered during quantitative analysis of small molecules from biofluids using LC-MS/MS*, Analyst, 139 (2014) 2265-2276.
- [167] F.A. Hansen, S. Pedersen-Bjergaard, *Emerging extraction strategies in analytical chemistry*, Analytical Chemistry, 92 (2020) 2-15.
- [168] T. Bouvarel, N. Delaunay, V. Pichon, *Selective extraction of cocaine from biological samples with a miniaturized monolithic molecularly imprinted polymer and on-line analysis in nano-liquid chromatography*, Analytica Chimica Acta, 1096 (2020) 89-99.
- [169] J.Y. Lee, J.S. Yang, S.M. Park, S.K. Byeon, M.H. Moon, *On-line high speed lipid extraction for nanoflow liquid chromatography-tandem mass spectrometry*, Journal of Chromatography A, 1464 (2016) 12-20.
- [170] M.A. Jeannot, F.F. Cantwell, *Solvent microextraction into a single drop*, Analytical Chemistry, 68 (1996) 2236-2240.
- [171] H. Liu, P.K. Dasgupta, *Analytical chemistry in a drop. Solvent extraction in a microdrop*, Analytical Chemistry, 68 (1996) 1817-1821.
- [172] S. Pedersen-Bjergaard, K.E. Rasmussen, *Liquid-liquid-liquid microextraction for sample preparation of biological fluids prior to capillary electrophoresis*, Analytical Chemistry, 71 (1999) 2650-2656.
- [173] N. Drouin, P. Kubáň, S. Rudaz, S. Pedersen-Bjergaard, J. Schappler, *Electromembrane extraction: Overview of the last decade*, TrAC, Trends in Analytical Chemistry, 113 (2019) 357-363.
- [174] S. Pedersen-Bjergaard, K.E. Rasmussen, *Electrokinetic migration across artificial liquid membranes: New concept for rapid sample preparation of biological fluids*, Journal of Chromatography A, 1109 (2006) 183-190.
- [175] A. Gjelstad, K.E. Rasmussen, S. Pedersen-Bjergaard, *Electromembrane extraction of basic drugs from untreated human plasma and whole blood under physiological pH conditions*, Analytical and Bioanalytical Chemistry, 393 (2009) 921-928.
- [176] I.J.Ø. Kjelsen, A. Gjelstad, K.E. Rasmussen, S. Pedersen-Bjergaard, *Low-voltage electromembrane extraction of basic drugs from biological samples*, Journal of Chromatography A, 1180 (2008) 1-9.

- [177] P. Kubáň, *Salt removal from microliter sample volumes by multiple phase microelectromembrane extractions across free liquid membranes*, *Analytical Chemistry*, 89 (2017) 8476-8483.
- [178] L. Vårdal, A. Gjelstad, C. Huang, E.L. Øiestad, S. Pedersen-Bjergaard, *Efficient discrimination and removal of phospholipids during electromembrane extraction from human plasma samples*, *Bioanalysis*, 9 (2017) 631-641.
- [179] M.S. Restan, M.E. Pedersen, H. Jensen, S. Pedersen-Bjergaard, *Electromembrane extraction of unconjugated fluorescein isothiocyanate from solutions of labeled proteins prior to flow induced dispersion analysis*, *Analytical Chemistry*, 91 (2019) 6702-6708.
- [180] N.C. Domínguez, A. Gjelstad, A.M. Nadal, H. Jensen, N.J. Petersen, S.H. Hansen, K.E. Rasmussen, S. Pedersen-Bjergaard, *Selective electromembrane extraction at low voltages based on analyte polarity and charge*, *Journal of Chromatography A*, 1248 (2012) 48-54.
- [181] M.S. Restan, H. Jensen, X. Shen, C. Huang, Ø.G. Martinsen, P. Kubáň, A. Gjelstad, S. Pedersen-Bjergaard, *Comprehensive study of buffer systems and local pH effects in electromembrane extraction*, *Analytica Chimica Acta*, 984 (2017) 116-123.
- [182] C. Huang, A. Gjelstad, S. Pedersen-Bjergaard, *Organic solvents in electromembrane extraction: recent insights*, *Reviews in Analytical Chemistry*, 35 (2016) 169-183.
- [183] C. Huang, K.F. Seip, A. Gjelstad, S. Pedersen-Bjergaard, *Electromembrane extraction of polar basic drugs from plasma with pure bis(2-ethylhexyl) phosphite as supported liquid membrane*, *Analytica Chimica Acta*, 934 (2016) 80-87.
- [184] F.A. Hansen, P. Kubáň, E.L. Øiestad, S. Pedersen-Bjergaard, *Electromembrane extraction of highly polar bases from biological samples – Deeper insight into bis(2-ethylhexyl) phosphate as ionic carrier*, *Analytica Chimica Acta*, 1115 (2020) 23-32.
- [185] L.E.E. Eibak, K.E. Rasmussen, E.L. Øiestad, S. Pedersen-Bjergaard, A. Gjelstad, *Parallel electromembrane extraction in the 96-well format*, *Analytica Chimica Acta*, 828 (2014) 46-52.
- [186] N. Drouin, J.-F. Mandscheff, S. Rudaz, J. Schappler, *Development of a new extraction device based on parallel-electromembrane extraction*, *Analytical Chemistry*, 89 (2017) 6346-6350.
- [187] D. Fuchs, H. Jensen, S. Pedersen-Bjergaard, C. Gabel-Jensen, S.H. Hansen, N.J. Petersen, *Real time extraction kinetics of electro membrane extraction verified by comparing drug metabolism profiles obtained from a flow–flow electro membrane extraction-mass spectrometry system with LC–MS*, *Analytical Chemistry*, 87 (2015) 5774-5781.

- [188] D. Fuchs, C. Gabel-Jensen, H. Jensen, K.D. Rand, S. Pedersen-Bjergaard, S.H. Hansen, N.J. Petersen, *Direct coupling of a flow–flow electromembrane extraction probe to LC-MS*, *Analytica Chimica Acta*, 905 (2016) 93-99.
- [189] N.J. Petersen, H. Jensen, S.H. Hansen, S.T. Foss, D. Snakenborg, S. Pedersen-Bjergaard, *On-chip electro membrane extraction*, *Microfluidics and Nanofluidics*, 9 (2010) 881-888.
- [190] N.J. Petersen, S.T. Foss, H. Jensen, S.H. Hansen, C. Skonberg, D. Snakenborg, J.P. Kutter, S. Pedersen-Bjergaard, *On-chip electro membrane extraction with online ultraviolet and mass spectrometric detection*, *Analytical Chemistry*, 83 (2011) 44-51.
- [191] N.J. Petersen, J.S. Pedersen, N.N. Poulsen, H. Jensen, C. Skonberg, S.H. Hansen, S. Pedersen-Bjergaard, *On-chip electromembrane extraction for monitoring drug metabolism in real time by electrospray ionization mass spectrometry*, *Analyst*, 137 (2012) 3321-3327.
- [192] Y. Abdossalami Asl, Y. Yamini, S. Seidi, B. Ebrahimpour, *A new effective on chip electromembrane extraction coupled with high performance liquid chromatography for enhancement of extraction efficiency*, *Analytica Chimica Acta*, 898 (2015) 42-49.
- [193] Y.A. Asl, Y. Yamini, S. Seidi, *A novel approach to the consecutive extraction of drugs with different properties via on chip electromembrane extraction*, *Analyst*, 141 (2016) 311-318.
- [194] Y.A. Asl, Y. Yamini, S. Seidi, M. Rezazadeh, *Simultaneous extraction of acidic and basic drugs via on-chip electromembrane extraction*, *Analytica Chimica Acta*, 937 (2016) 61-68.
- [195] M. Karami, Y. Yamini, Y. Abdossalami Asl, M. Rezazadeh, *On-chip pulsed electromembrane extraction as a new concept for analysis of biological fluids in a small device*, *Journal of Chromatography A*, 1527 (2017) 1-9.
- [196] F.A. Hansen, D. Sticker, J.P. Kutter, N.J. Petersen, S. Pedersen-Bjergaard, *Nanoliter-scale electromembrane extraction and enrichment in a microfluidic chip*, *Analytical Chemistry*, 90 (2018) 9322-9329.
- [197] Y. Jin, J. Kim, J.S. Lee, S. Min, S. Kim, D.-H. Ahn, Y.-G. Kim, S.-W. Cho, *Vascularized liver organoids generated using Induced hepatic tissue and dynamic liver-specific microenvironment as a drug testing platform*, *Advanced Functional Materials*, 28 (2018) 1801954, DOI: 10.1002/adfm.201801954.
- [198] F. Michielin, G.G. Giobbe, C. Luni, Q. Hu, I. Maroni, M.R. Orford, A. Manfredi, L. Di Filippo, A.L. David, D. Cacchiarelli, P. De Coppi, S. Eaton, N. Elvassore, *The microfluidic environment reveals a hidden role of self-organizing extracellular matrix in hepatic commitment and organoid*

- formation of hiPSCs*, Cell Reports, 33 (2020) 108453, DOI: 10.1016/j.celrep.2020.108453.
- [199] E. Goulart, L.C. de Caires-Junior, K.A. Telles-Silva, B.H.S. Araujo, G.S. Kobayashi, C.M. Musso, A.F. Assoni, D. Oliveira, E. Caldini, J.A. Gerstenhaber, S. Raia, P.I. Lelkes, M. Zatz, *Adult and iPSC-derived non-parenchymal cells regulate liver organoid development through differential modulation of Wnt and TGF- β* , Stem Cell Research & Therapy, 10 (2019) 258, DOI: 10.1186/s13287-019-1367-x.
- [200] L. Howell, R.E. Jenkins, S. Lynch, C. Duckworth, B. Kevin Park, C. Goldring, *Proteomic profiling of murine biliary-derived hepatic organoids and their capacity for drug disposition, bioactivation and detoxification*, Archives of Toxicology, 95 (2021) 2413-2430.
- [201] W. Lu, E. Rettenmeier, M. Paszek, M.-F. Yueh, R.H. Tukey, J. Trotter, O. Barbier, S. Chen, *Crypt organoid culture as an in vitro model in drug metabolism and cytotoxicity studies*, Drug Metabolism and Disposition, 45 (2017) 748-754.
- [202] R.J. Mills, B.L. Parker, G.A. Quaipe-Ryan, H.K. Voges, E.J. Needham, A. Bornot, M. Ding, H. Andersson, M. Polla, D.A. Elliott, L. Drowley, M. Clausen, A.T. Plowright, I.P. Barrett, Q.-D. Wang, D.E. James, E.R. Porrello, J.E. Hudson, *Drug screening in human PSC-cardiac organoids identifies pro-proliferative compounds acting via the mevalonate pathway*, Cell Stem Cell, 24 (2019) 895-907.
- [203] S. Yoshida, H. Miwa, T. Kawachi, S. Kume, K. Takahashi, *Generation of intestinal organoids derived from human pluripotent stem cells for drug testing*, Scientific Reports, 10 (2020) 5989, DOI: 10.1038/s41598-020-63151-z.
- [204] J.A. Brown, S.G. Codreanu, M. Shi, S.D. Sherrod, D.A. Markov, M.D. Neely, C.M. Britt, O.S. Hoilett, R.S. Reiserer, P.C. Samson, L.J. McCawley, D.J. Webb, A.B. Bowman, J.A. McLean, J.P. Wikswo, *Metabolic consequences of inflammatory disruption of the blood-brain barrier in an organ-on-chip model of the human neurovascular unit*, Journal of Neuroinflammation, 13 (2016) 306, DOI: 10.1186/s12974-016-0760-y.
- [205] U. Sarkar, K.C. Ravindra, E. Large, C.L. Young, D. Rivera-Burgos, J. Yu, M. Cirit, D.J. Hughes, J.S. Wishnok, D.A. Lauffenburger, L.G. Griffith, S.R. Tannenbaum, *Integrated assessment of diclofenac biotransformation, pharmacokinetics, and omics-based toxicity in a three-dimensional human liver-immunocompetent co culture system*, Drug Metabolism and Disposition, 45 (2017) 855-866.
- [206] T. Satoh, S. Sugiura, K. Shin, R. Onuki-Nagasaki, S. Ishida, K. Kikuchi, M. Kakiki, T. Kanamori, *A multi-throughput multi-organ-on-a-chip system on a plate formatted pneumatic pressure-driven medium circulation platform*, Lab on a Chip, 18 (2018) 115-125.

- [207] C.D. Edington, W.L.K. Chen, E. Geishecker, T. Kassis, L.R. Soenksen, B.M. Bhushan, D. Freake, J. Kirschner, C. Maass, N. Tsamandouras, J. Valdez, C.D. Cook, T. Parent, S. Snyder, J. Yu, E. Suter, M. Shockley, J. Velazquez, J.J. Velazquez, L. Stockdale, J.P. Papps, I. Lee, N. Vann, M. Gamboa, M.E. LaBarge, Z. Zhong, X. Wang, L.A. Boyer, D.A. Lauffenburger, R.L. Carrier, C. Communal, S.R. Tannenbaum, C.L. Stokes, D.J. Hughes, G. Rohatgi, D.L. Trumper, M. Cirit, L.G. Griffith, *Interconnected microphysiological systems for quantitative biology and pharmacology studies*, Scientific Reports, 8 (2018) 4530, DOI: 10.1038/s41598-018-22749-0eek.
- [208] X. Wang, M. Cirit, J.S. Wishnok, L.G. Griffith, S.R. Tannenbaum, *Analysis of an integrated human multiorgan microphysiological system for combined tolcapone metabolism and brain metabolomics*, Analytical Chemistry, 91 (2019) 8667-8675.
- [209] K. Eckstrum, A. Striz, M. Ferguson, Y. Zhao, B. Welch, N. Solomotis, N. Olejnik, R. Sprando, *Utilization of a model hepatotoxic compound, diglycolic acid, to evaluate liver Organ-Chip performance and in vitro to in vivo concordance*, Food and Chemical Toxicology, 146 (2020) 111850, DOI: 10.1016/j.fct.2020.111850.
- [210] A. Rubiano, A. Indapurkar, R. Yokosawa, A. Miedzik, B. Rosenzweig, A. Arefin, C.M. Moulin, K. Dame, N. Hartman, D.A. Volpe, M.K. Matta, D.J. Hughes, D.G. Strauss, T. Kostrzewski, A.J.S. Ribeiro, *Characterizing the reproducibility in using a liver microphysiological system for assaying drug toxicity, metabolism, and accumulation*, Clinical and Translational Science, 14 (2021) 1049-1061.
- [211] F. Yin, X. Zhang, L. Wang, Y. Wang, Y. Zhu, Z. Li, T. Tao, W. Chen, H. Yu, J. Qin, *HiPSC-derived multi-organoids-on-chip system for safety assessment of antidepressant drugs*, Lab on a Chip, 21 (2021) 571-581.
- [212] C. Görgens, A.P. Ramme, S. Guddat, Y. Schrader, A. Winter, E.-M. Dehne, R. Horland, M. Thevis, *Organ-on-a-chip: Determine feasibility of a human liver microphysiological model to assess long-term steroid metabolites in sports drug testing*, Drug Testing and Analysis, (2021) 1-8.
- [213] P. de Haan, M.J.C. Santbergen, M. van der Zande, H. Bouwmeester, M.W.F. Nielen, E. Verpoorte, *A versatile, compartmentalised gut-on-a-chip system for pharmacological and toxicological analyses*, Scientific Reports, 11 (2021) 4920, DOI: 10.1038/s41598-021-84187-9.
- [214] D. Gao, H. Wei, G.-S. Guo, J.-M. Lin, *Microfluidic cell culture and metabolism detection with electrospray ionization quadrupole time-of-flight mass spectrometer*, Analytical Chemistry, 82 (2010) 5679-5685.
- [215] D. Gao, H. Liu, J.-M. Lin, Y. Wang, Y. Jiang, *Characterization of drug permeability in Caco-2 monolayers by mass spectrometry on a membrane-based microfluidic device*, Lab on a Chip, 13 (2013) 978-985.

- [216] C.E. Dugan, J.P. Grinias, S.D. Parlee, M. El-Azzouny, C.R. Evans, R.T. Kennedy, *Monitoring cell secretions on microfluidic chips using solid-phase extraction with mass spectrometry*, *Analytical and Bioanalytical Chemistry*, 409 (2017) 169-178.
- [217] P.M. van Midwoud, J. Janssen, M.T. Merema, I.A. de Graaf, G.M. Groothuis, E. Verpoorte, *On-line HPLC analysis system for metabolism and inhibition studies in precision-cut liver slices*, *Analytical Chemistry*, 83 (2011) 84-91.
- [218] C.C. Marasco, J.R. Enders, K.T. Seale, J.A. McLean, J.P. Wikswo, *Real-time cellular exometabolome analysis with a microfluidic-mass spectrometry platform*, *PLoS One*, 10 (2015) e0117685, DOI: 10.1371/journal.pone.0117685.
- [219] M.J.C. Santbergen, M. van der Zande, A. Gerssen, H. Bouwmeester, M.W.F. Nielen, *Dynamic in vitro intestinal barrier model coupled to chip-based liquid chromatography mass spectrometry for oral bioavailability studies*, *Analytical and Bioanalytical Chemistry*, 412 (2020) 1111-1122.
- [220] *Donor information, human induced pluripotent stem cell line AG27*. <https://hpscereg.eu/cell-line/UIOi001-A>. (Accessed 16.02.2022).
- [221] S.P. Harrison, R. Sillar, Y. Tanaka, Y. Xiang, B. Patterson, H. Kempf, E. Melum, K. Åsrud, M.E. Chollet, E. Andersen, P.M. Sandset, S. Baumgarten, F. Bonanini, D. Kurek, S. Mathapati, R. Almaas, K. Sharma, S.R. Wilson, F.S. Skottvoll, I.C. Boger, I.L. Bogen, T.A. Nyman, J.J. Wu, A. Bezrouk, D. Cizkova, J. Mokry, R. Zweigerdt, I.-H. Park, G.J. Sullivan, *Scalable production of tissue-like vascularised liver organoids from human PSCs*, *bioRxiv*, (2020) 2020.12.02.406835.
- [222] G.L. Corthals, V.C. Wasinger, D.F. Hochstrasser, J.-C. Sanchez, *The dynamic range of protein expression: A challenge for proteomic research*, *Electrophoresis*, 21 (2000) 1104-1115.
- [223] I.C. Hvinden, H.E. Berg, D. Sachse, E. Skaga, F.S. Skottvoll, E. Lundanes, C.J. Sandberg, E.O. Vik-Mo, F. Rise, S.R. Wilson, *Nuclear magnetic resonance spectroscopy to identify metabolite biomarkers of nonresponsiveness to targeted therapy in glioblastoma tumor stem cells*, *Journal of Proteome Research*, 18 (2019) 2012-2020.
- [224] F.S. Skottvoll, H.E. Berg, K. Bjørseth, K. Lund, N. Roos, S. Bekhradnia, B. Thiede, C. Sandberg, E.O. Vik-Mo, H. Roberg-Larsen, B. Nyström, E. Lundanes, S.R. Wilson, *Ultracentrifugation versus kit exosome isolation: nanoLC-MS and other tools reveal similar performance biomarkers, but also contaminations*, *Future Science OA*, 5 (2018) FSO359, DOI: 10.4155/fsoa-2018-0088.
- [225] E.J. Dupree, M. Jayathirtha, H. Yorkey, M. Mihasan, B.A. Petre, C.C. Darie, *A critical review of bottom-up proteomics: The good, the bad, and the future of this field*, *Proteomes*, 8 (2020).

- [226] A.S. Hebert, A.L. Richards, D.J. Bailey, A. Ulbrich, E.E. Coughlin, M.S. Westphall, J.J. Coon, *The one hour yeast proteome**, *Molecular & Cellular Proteomics*, 13 (2014) 339-347.
- [227] E. Shishkova, Alexander S. Hebert, Joshua J. Coon, *Now, more than ever, proteomics needs better chromatography*, *Cell Systems*, 3 (2016) 321-324.
- [228] Y. Bian, F.P. Bayer, Y.-C. Chang, C. Meng, S. Hoefler, N. Deng, R. Zheng, O. Boychenko, B. Kuster, *Robust microflow LC-MS/MS for proteome analysis: 38 000 runs and counting*, *Analytical Chemistry*, 93 (2021) 3686-3690.
- [229] J.R. Krieger, L.E. Wybenga-Groot, J. Tong, N. Bache, M.S. Tsao, M.F. Moran, *Evosep one enables robust deep proteome coverage using tandem mass tags while significantly reducing instrument time*, *Journal of Proteome Research*, 18 (2019) 2346-2353.
- [230] R.E. Farrell, *RNA Methodologies Chapter 7 - Resilient Ribonucleases*, in: R.E. Farrell (Ed.), *RNA Methodologies* Academic Press, San Diego, 2010, pp. 155-172.
- [231] E.D. Deeks, *Neratinib: First global approval*, *Drugs*, 77 (2017) 1695-1704.
- [232] H. Singh, A.J. Walker, L. Amiri-Kordestani, J. Cheng, S. Tang, P. Balcazar, K. Barnett-Ringgold, T.R. Palmby, X. Cao, N. Zheng, Q. Liu, J. Yu, W.F. Pierce, S.R. Daniels, R. Sridhara, A. Ibrahim, P.G. Kluetz, G.M. Blumenthal, J.A. Beaver, R. Pazdur, *U.S. Food and Drug Administration approval: Neratinib for the extended adjuvant treatment of early-stage HER2-positive breast cancer*, *Clinical Cancer Research*, 24 (2018) 3486-3491.
- [233] B. Hug, R. Abbas, C. Leister, J. Burns, D. Sonnichsen, *A single-dose, crossover, placebo- and moxifloxacin-controlled study to assess the effects of neratinib (HKI-272) on cardiac repolarization in healthy adult subjects*, *Clinical Cancer Research*, 16 (2010) 4016-4023.
- [234] K. Aljakouch, T. Lehtonen, H.K. Yosef, M.K. Hammoud, W. Alsaïdi, C. Kötting, C. Mügge, R. Kourist, S.F. El-Mashtoly, K. Gerwert, *Raman microspectroscopic evidence for the metabolism of a tyrosine kinase inhibitor, neratinib, in cancer cells*, *Angewandte Chemie International Edition*, 57 (2018) 7250-7254.
- [235] W. Liu, S. Li, Y. Wu, X. Yan, Y.M. Zhu, J.H. Huang, Z. Chen, *Metabolic profiles of neratinib in rat by using ultra-high-performance liquid chromatography coupled with diode array detector and Q-Exactive Orbitrap tandem mass spectrometry*, *Biomedical Chromatography*, 32 (2018) e4272, DOI: 10.1002/bmc.4272.

- [236] Nerlynx: EPAR- Public assessment report, 2018.
https://www.ema.europa.eu/en/documents/assessment-report/nerlynx-epar-public-assessment-report_en.pdf. (Accessed 25.10 2021).
- [237] A.K. Meher, Y.-C. Chen, *Combination of raman spectroscopy and mass spectrometry for online chemical analysis*, Analytical Chemistry, 88 (2016) 9151-9157.
- [238] L.E. Flint, G. Hamm, J.D. Ready, S. Ling, C.J. Duckett, N.A. Cross, L.M. Cole, D.P. Smith, R.J.A. Goodwin, M.R. Clench, *Characterization of an aggregated three-dimensional cell culture model by multimodal mass spectrometry imaging*, Analytical Chemistry, 92 (2020) 12538-12547.
- [239] R. Karinen, J.M. Andersen, Å. Ripel, I. Hasvold, A.B. Hopen, J. Mørland, A.S. Christophersen, *Determination of heroin and its main metabolites in small sample volumes of whole blood and brain tissue by reversed-phase liquid chromatography-tandem mass spectrometry*, Journal of Analytical Toxicology, 33 (2009) 345-350.
- [240] W. Sneader, *The discovery of heroin*, The Lancet, 352 (1998) 1697-1699.
- [241] E.L. Way, J.W. Kemp, J.M. Young, D.R. Grassetti, *The pharmacologic effects of heroin IX relationship to its rate of biotransformation*, Journal of Pharmacology and Experimental Therapeutics, 129 (1960) 144-154.
- [242] U. Boerner, S. Abbott, R.L. Roe, *The metabolism of morphine and heroin in man*, Drug Metabolism Reviews, 4 (1975) 39-73.
- [243] L.M. Kamendulis, M.R. Brzezinski, E.V. Pindel, W.F. Bosron, R.A. Dean, *Metabolism of cocaine and heroin is catalyzed by the same human liver carboxylesterases*, Journal of Pharmacology and Experimental Therapeutics, 279 (1996) 713-717.
- [244] M.R. Brzezinski, B.J. Spink, R.A. Dean, C.E. Berkman, J.R. Cashman, W.F. Bosron, *Human liver carboxylesterase hCE-1: binding specificity for cocaine, heroin, and their metabolites and analogs*, Drug Metabolism and Disposition, 25 (1997) 1089-1096.
- [245] A.N. Stone, P.I. Mackenzie, A. Galetin, J.B. Houston, J.O. Miners, *Isoform selectivity and kinetics of morphine 3-and 6-glucuronidation by human UDP-glucuronosyltransferases: evidence for atypical glucuronidation kinetics by UGT2B7*, Drug Metabolism and Disposition, 31 (2003) 1086-1089.
- [246] Y. Qian, T.K. Gilliland, J.S. Markowitz, *The influence of carboxylesterase 1 polymorphism and cannabidiol on the hepatic metabolism of heroin*, Chemico-Biological Interactions, 316 (2020) 108914.
- [247] Y. Yamini, A. Pourali, S. Seidi, M. Rezazadeh, *Electromembrane extraction followed by high performance liquid chromatography: an efficient method for extraction and determination of morphine, oxymorphone, and*

- methylmorphine from urine samples*, *Analytical Methods*, 6 (2014) 5554-5565.
- [248] H. Ahmar, H. Tabani, M. Hossein Koruni, S.S.H. Davarani, A.R. Fakhari, *A new platform for sensing urinary morphine based on carrier assisted electromembrane extraction followed by adsorptive stripping voltammetric detection on screen-printed electrode*, *Biosensors and Bioelectronics*, 54 (2014) 189-194.
- [249] A. Rahimi, S. Nojavan, H. Tabani, *Inside gel electromembrane extraction: A novel green methodology for the extraction of morphine and codeine from human biological fluids*, *Journal of Pharmaceutical and Biomedical Analysis*, 184 (2020) 113175, DOI: 10.1016/j.jpba.2020.113175.
- [250] S. Emara, I. Darwish, D. Youssef, T. Masujima, *On the perspectives of capillary electrophoresis modes for the determination of morphine in human plasma without sample pretreatment*, *Biomedical Chromatography*, 18 (2004) 21-27.
- [251] A. Alnajjar, J.A. Butcher, B. McCord, *Determination of multiple drugs of abuse in human urine using capillary electrophoresis with fluorescence detection*, *Electrophoresis*, 25 (2004) 1592-1600.
- [252] T.A. Isbell, E.C. Strickland, J. Hitchcock, G. McIntire, C.L. Colyer, *Capillary electrophoresis-mass spectrometry determination of morphine and its isobaric glucuronide metabolites*, *Journal of Chromatography B*, 980 (2015) 65-71.
- [253] Z. Aturki, S. Fanali, A. Rocco, *Online sample concentration and analysis of drugs of abuse in human urine by micelle to solvent stacking in capillary zone electrophoresis*, *Electrophoresis*, 37 (2016) 2875-2881.
- [254] M.S. Restan, Ø. Skjærvø, Ø.G. Martinsen, S. Pedersen-Bjergaard, *Towards exhaustive electromembrane extraction under stagnant conditions*, *Analytica Chimica Acta*, 1104 (2020) 1-9.
- [255] L. Vårdal, E.L. Øiestad, A. Gjelstad, H. Jensen, S. Pedersen-Bjergaard, *Electromembrane extraction with solvent modification of the acceptor solution: improved mass transfer of drugs of abuse from human plasma*, *Bioanalysis*, 11 (2019) 755-771.
- [256] D.E. Moody, M.E. Alburges, R.J. Parker, J.M. Collins, J.M. Strong, *The involvement of cytochrome P450 3A4 in the N-demethylation of l- α -acetylmethadol (LAAM), norLAAM, and methadone*, *Drug Metabolism and Disposition*, 25 (1997) 1347-1353.
- [257] D.J.R. Foster, A.A. Somogyi, F. Bochner, *Methadone N-demethylation in human liver microsomes: lack of stereoselectivity and involvement of CYP3A4*, *British Journal of Clinical Pharmacology*, 47 (1999) 403-412.
- [258] R.J. Dinis-Oliveira, *Metabolomics of methadone: clinical and forensic toxicological implications and variability of dose response*, *Drug Metabolism Reviews*, 48 (2016) 568-576.

- [259] D. Fuchs, S. Pedersen-Bjergaard, H. Jensen, K.D. Rand, S. Honoré Hansen, N.J. Petersen, *Fully automated electro membrane extraction autosampler for LC–MS systems allowing soft extractions for high-throughput applications*, *Analytical Chemistry*, 88 (2016) 6797-6804.
- [260] D.E. Moody, W.B. Fang, S.-N. Lin, D.M. Weyant, S.C. Strom, C.J. Omiecinski, *Effect of rifampin and nelfinavir on the metabolism of methadone and buprenorphine in primary cultures of human hepatocytes*, *Drug Metabolism and Disposition*, 37 (2009) 2323-2329.
- [261] J. De Vos, J. Ufkes, H. van Wilgenburg, P. Geerlings, W. van den Brink, *Pharmacokinetics of methadone and its primary metabolite in 20 opiate addicts*, *European Journal of Clinical Pharmacology*, 48 (1995) 361-366.
- [262] A. Ferrari, C.P.R. Coccia, A. Bertolini, E. Sternieri, *Methadone—metabolism, pharmacokinetics and interactions*, *Pharmacological Research*, 50 (2004) 551-559.
- [263] G. Schneider, *Automating drug discovery*, *Nature Reviews Drug Discovery*, 17 (2018) 97-113.
- [264] C. Olsen, F.S. Skottvoll, O.K. Brandtzaeg, C. Schnaars, P. Rongved, E. Lundanes, S.R. Wilson, *Investigating monoliths (vinyl azlactone-co-ethylene dimethacrylate) as a support for enzymes and drugs, for proteomics and drug-target studies*, *Frontiers in Chemistry*, 7 (2019) DOI: 10.3389/fchem.2019.00835.

Ann Lin^{1,2}
 Frøydis Sved Skottvoll^{1,3}
 Simon Rayner^{1,4}
 Stig Pedersen-Bjergaard⁵
 Gareth Sullivan^{1,6,7,8,9} 
 Stefan Krauss^{1,10}
 Steven Ray Wilson^{1,3} 
 Sean Harrison¹

¹Hybrid Technology Hub-Centre of Excellence, Institute of Basic Medical Sciences, Faculty of Medicine, University of Oslo, Oslo, Norway

²Department of Genetics, Stanford University, CA, USA

³Department of Chemistry, University of Oslo, Oslo, Norway

⁴Department of Medical Genetics, Oslo University Hospital and University of Oslo, Oslo, Norway

⁵School of Pharmacy, University of Oslo, Oslo, Norway

⁶Norwegian Center for Stem Cell Research, University of Oslo, Oslo, Norway

⁷Department of Molecular Medicine, Institute of Basic Medical Sciences, University of Oslo, Oslo, Norway

⁸Institute of Immunology, Oslo University Hospital, Oslo, Norway

⁹Department of Pediatric Research, Oslo University Hospital, Oslo, Norway

¹⁰Unit for Cell Signaling, Department of Immunology and Transfusion Medicine, Oslo University Hospital, Oslo, Norway

Received May 3, 2019

Revised September 12, 2019

Accepted September 19, 2019

1 Introduction

Drug discovery and development is a lengthy and costly process that involves several preclinical stages, including target validation, hit to lead optimization, adsorption, distribution, metabolism, and excretion studies, pharmacodynamics stud-

Correspondence: Prof. Steven Ray Wilson, Department of Chemistry, University of Oslo, Post Box 1033, Blindern, NO-0315 Oslo, Norway

E-mail: stevenw@kjemi.uio.no

Abbreviations: EME, electromembrane extraction; ESCs, embryonic stem cells; HSCs, hepatic stellate cells; iPSCs, induced pluripotent stem cells; OTLC, open tubular LC; SLM, supported liquid membrane

Review

3D cell culture models and organ-on-a-chip: Meet separation science and mass spectrometry

In vitro derived simplified 3D representations of human organs or organ functionalities are predicted to play a major role in disease modeling, drug development, and personalized medicine, as they complement traditional cell line approaches and animal models. The cells for 3D organ representations may be derived from primary tissues, embryonic stem cells or induced pluripotent stem cells and come in a variety of formats from aggregates of individual or mixed cell types, self-organizing in vitro developed “organoids” and tissue mimicking chips. Microfluidic devices that allow long-term maintenance and combination with other tissues, cells or organoids are commonly referred to as “microphysiological” or “organ-on-a-chip” systems. Organ-on-a-chip technology allows a broad range of “on-chip” and “off-chip” analytical techniques, whereby “on-chip” techniques offer the possibility of real time tracking and analysis. In the rapidly expanding tool kit for real time analytical assays, mass spectrometry, combined with “on-chip” electrophoresis, and other separation approaches offer attractive emerging tools. In this review, we provide an overview of current 3D cell culture models, a compendium of current analytical strategies, and we make a case for new approaches for integrating separation science and mass spectrometry in this rapidly expanding research field.

Keywords:

Chromatography / Electrophoresis / Mass spectrometry / Organ on a chip / Organoid
 DOI 10.1002/elps.201900170

ies, and in vitro toxicity testing before the drug can proceed through the investigational new drug stage to clinical trials [1, 2]. Most experimental drugs fail before reaching clinical trials. Further significant termination of new drugs occurs during latter stages of clinical trials. Only around 10% of all drugs that enter phase I clinical trial succeed in obtaining the United States Food and Drug Administration approval while over half of the drugs tested in phase III trials spanning from 1998–2008 fail due to inadequate preclinical efficacy and drug toxicity [3, 4].

Numerous studies have highlighted culprits which are contributing to the low efficacy and high toxicity of drugs

Color online: See article online to view Figs. 1, 2, and 4 in color.

entering preclinical testing [5]. In particular, it has been pointed out that cells that are used in preclinical drug validation assays (e.g. immortalized cell lines and cancer cell lines) frequently do not reflect the physiology, complexity, and diversity of a corresponding cell in healthy humans. Cell lines have altered biochemical pathways due to the culturing process or the disease state of the donor from which they were derived. Mouse and other animal models better reflect the complexity of the human body, but their physiology diverges from the human state and they fail to capture the heterogeneity of the human population. In addition, the field lacks appropriate mouse models for a significant spectrum of human disease conditions. Finally, extensive animal experiments, as required for preclinical drug testing, raise ethical issues. Hence, there has been an increasing demand for developing novel experimental models that may help to better map potential patient responses to experimental drugs during preclinical drug development. A currently explored strategy in this direction is to increase the complexity of an *ex vivo* cellular system to better reflect aspects of the human physiology relevant to the drug discovery and validation process [6,7]. Hence, traditional 2D-cultivated cell cultures are expanded into barrier structures comprising of two cell layers that may include several cell types separated by a membrane, 3D structures that may contain a number of cell types in a specific spatial arrangement, and combined systems that comprise several cellular systems [7,8]. By combining the advances in cell engineering with microfluidic technology and lab-on-a-chip [9,10], different chip-based cell microenvironments have evolved and facilitated miniaturized *in vitro* studies over the past two decades [11,12].

Recent examples for cell barrier structures are lung-on-a-chip [13,14], and gut-on-a-chip systems [15,16]. Examples for 3D structures that may be relevant for drug testing are neural organoids [17,18], 3D muscle structures [19,20], liver organoids and liver-on-a-chip models [21,22], islets [23], and white adipocyte tissue-on-a-chip [24]. Examples for combined structures may be a gut-on-a-chip coupled to a liver-on-a-chip to model drug adsorption and metabolism [25], a liver-on-a-chip combined with a heart-on-a-chip to model cardio-toxicity [26], and a tumor-on-a-chip combined with components of the immune systems in fluidic compartments [27].

The biological material for barrier structures, 3D cultures, and multi-organ systems “on chip” can vary. Frequently, immortalized cell lines such as human hepatic (HepG2) cells, human intestinal (Caco-1) cells, or human vascular endothelial cells are used [25]. Such cell lines provide a controlled and reproducible source of biological material at the cost of compromised physiological activity. Cells can also be derived, either in a terminally differentiated state such as human hepatocytes, or as cells differentiated from adult stem cell pools such as mesenchymal stem cell derived chondrocytes, osteoblast, and adipocytes. Further promising source for functional cells are human embryonic stem cells (ESCs) and human induced pluripotent stem cells (iPSCs) [28]. Both stem cell types can in principle be differentiated into all types of cells present in the human body. However, many differenti-

ation protocols require further elaboration and differentiated cells or tissue derived from ESCs or iPSCs lack the maturity and physiological activity of adult tissue, and commonly lack the correct spatial arrangement that is characteristic of mature tissue [29]. Despite these pitfalls, iPSC technology not only allows for the creation of a representative system for functional organs, but – since iPSCs can be derived from any subject, control or diseased – it also enables genotypic personalization [6]. Hence, the field works towards exploring future preclinical drug testing on healthy and diseased 3D models with the perspective of allowing researchers to extrapolate how patients may respond to a plethora of drugs in a healthy state, and at various stages of their personal disease progression.

2 Drug development and disease modeling *in vitro*

There are many variations of 3D cell culture, though some are distinctly more organotypic than others, by virtue of being formed through developmentally recognizable stages [30], in contrast to aggregates or spheroids [31], while some lie between the two such as the liver buds from the Takebe group, a mixture of iPSC specified hepatic endoderm with cell lines condensed to mimic the early points in organogenesis [32]. A distinct subset of 3D cell culture, organoids are self-organized tissue systems derived from stem cells including iPSCs, ESCs, and *in vivo* derived progenitor populations. They can reflect much of the complexity of the organ they model, or present with certain aspects of the organ, for example producing only specific types of cells, i.e. LGR5 derived single cell liver organoids [33]. They can be distinguished from Organ-on-chip technology that relies on engineering specific complexity or features into the system, such as distinct spatial separation of different cell types and/or extra cellular matrices, in order to model a key organ or tissue function or subunit. An advantage of organoid cultures, compared to monolayer culture systems, is that it provides an environment allowing cell-cell interactions to be established, therefore mimicking the *in vivo* situation, such as the correct orientation and polarity of cells and formation of structures, where they begin to take on the properties of smaller tissue subunits. For example, a number of labs have produced cerebral organoids using PSCs, which recapitulate developmental processes and importantly the organization of a developing human brain including acquisition of cell polarity and distinct neuronal zones [34–37]. While intestinal organoids present with polarized columnar epithelium containing enterocytes, goblet, Paneth, and enteroendocrine cells, they also develop characteristic villus structures and proliferative crypt zones expressing stem cell markers, which are representative traits of the human intestine [38–40]. Hepatic organoids have been demonstrated that form both hepatocytes and cholangiocytes and their organization into physiologically relevant structures in a single protocol, where non-organoid derivation of these cell types requires separate protocols [41].

In general, 3D cultures containing multiple cell lineages have advantages over co-culture based on monolayer systems. An example is demonstrated by Coll and colleagues' cultured spheroids consisting of iPSC derived hepatic stellate cells (HSCs) and the immortalized "hepatocytes like" cell line HepaRG cells. They observed a quiescent phenotype from the HSCs in the aggregates as well as an increased hepatocyte specific gene expression in the HepaRGs [31]. These co-cultures can then be used to model liver fibrosis caused by activation of the HSCs in the liver, which can lead to cirrhosis and hepatocellular carcinoma. Treatment of these co-cultures with fibrogenic and hepatotoxic compounds resulted in signs of fibrosis such as HSC activation, extracellular matrix secretion, and deposition which are absent from mono-cultures of these cells, highlighting the interaction between the two cell types within the spheres and showing their use as disease and toxicity models.

Many diseases, however, would be unsuitable for modeling in an aggregate system, such as the one used above, as they are caused by changes in the arrangement of cells or 3D structure of solid organs during development. Here, the self-organizing complexity of organoids is a necessity. For example, hepatobiliary organoids were used in a study by Guan and colleagues to model Alagille syndrome, which presents with impaired bile duct formation and many facets of biliary atresia in patients. The study used iPSCs harboring a mutation in the JAG1 gene to generate hepatobiliary organoids and the model recapitulated many of the defects observed in patients including impaired biliary development, revealing that it is not caused by immune mediated damage [41].

To develop and utilize 3D organoids and organ-on-a-chip technology to their full potential, it is important to understand the current development state of the technology and the analytical possibilities that it provides. In this review, we will discuss how extraction and separation science (based on chromatography and electrophoresis) and MS techniques may become central tools in tomorrow's drug discovery and validation studies in microphysiological systems. As of today, the coupling of, e.g. electrophoresis and organoids/organ-on-a-chips are hardly described in literature, so this review is intended to serve as an introduction to new possibilities.

Since organoid technology is at a relatively early stage in its development, the accepted characterization and analysis parameters for organoids are currently evolving. To date, a number of accepted molecular, cellular, and next generation analyses are carried out, including: reverse transcription-quantitative polymerase chain reaction against established developmentally relevant genes, western blot analysis, microscopy including confocal, spinning disc and light sheet, flow cytometry, ELISA and now single cell RNA sequencing is becoming the bench mark (Fig. 1). These are used to study the development and validate the differentiation of 3D cultures as well as to assess the effects of assays in the context of disease modeling, etc. However, bioanalytical techniques such as chromatography, electrophoresis, and MS are still little used in organoid analysis. Below, we discuss opportunities for these approaches.

3 The small size of an organoid: challenges and opportunities for micro-separations

Organoids are typically very small, e.g. in the millimeter scale or below. Hence, there are significant challenges in performing sensitive analysis of organoids, in regards to both the organoid itself, and perhaps even more challenging, the minute secretions of an organoid. Conventional LC–MS systems will arguably pose difficulties in organoid analysis, as they are primarily developed for far larger sample sizes. Specifically, conventional LC–MS systems often feature separation columns that have 1–2.1 mm i.d.. Although these columns are robust and reproducibly manufactured, there lies a disadvantage in that the wider the i.d., the more a sample is diluted during chromatography. This can be detrimental to sensitivity when a concentration-sensitive detection system such as electrospray-MS is employed [42]. Sample dilution does not have to be an issue when ample amounts of sample are available, but when very limited samples are to be processed, a reduction in column i.d. may be preferred. This is one of the reasons why proteomics is often performed with narrow LC columns, e.g. the nano-LC format (about 0.05–0.1 mm column i.d.). It can however be mentioned that larger column i.d. are also used for proteomics, in compromises between sensitivity and robustness, but also because of improvements in ESI hardware. In routine drug analysis laboratories, narrow column i.d. are often regarded as being impractical, due to the difficulties of handling the small-scale hardware and nL– μ L/min flow rates. However, to perform analyses related to organoids, narrow LC columns may be the only choice (and hence an important application area for the technology). Also, organoid/organ-on-a-chip researchers are already working with low flow fluidic systems, so the realities of narrow LC may be simpler to accept, as was the case in proteomics.

Nano-LC–MS based proteomics is a beneficial tool in organoid analyses typically relying on the analysis of peptides enzymatically digested from their proteins of origin ("bottom-up" proteomics) [43]. When additional pre-fractionation techniques are employed, nano-LC–MS analyses have led to the identification and quantification of over 7000 proteins in different organoid materials (e.g. intestinal-, pancreatic-, mammary- and tumor and healthy colon organoids) [44–47]. For example, Cristobal et al. assessed the proteomic heterogeneity between patient-derived human colorectal tumor and healthy organoids using nano-LC–MS. The proteomic study recapitulated previous genetic experiments demonstrating that down-regulation of the protein MSH3 correlates with colorectal cancer tumorigenesis. Furthermore, the results from the nano-LC–MS analysis also revealed discrepancies between proteomic and transcriptome trends within patient-derived human colorectal tumor. This is illustrated by results from the nano-LC–MS experiment revealing down-regulation of proteins such as PMS2, MSH3, MLH1, and RPL22 in colorectal cancer cells which were not observed from previous transcriptomic studies [47]. Thus, not only did the study demonstrate the bio-variability between individuals, but it

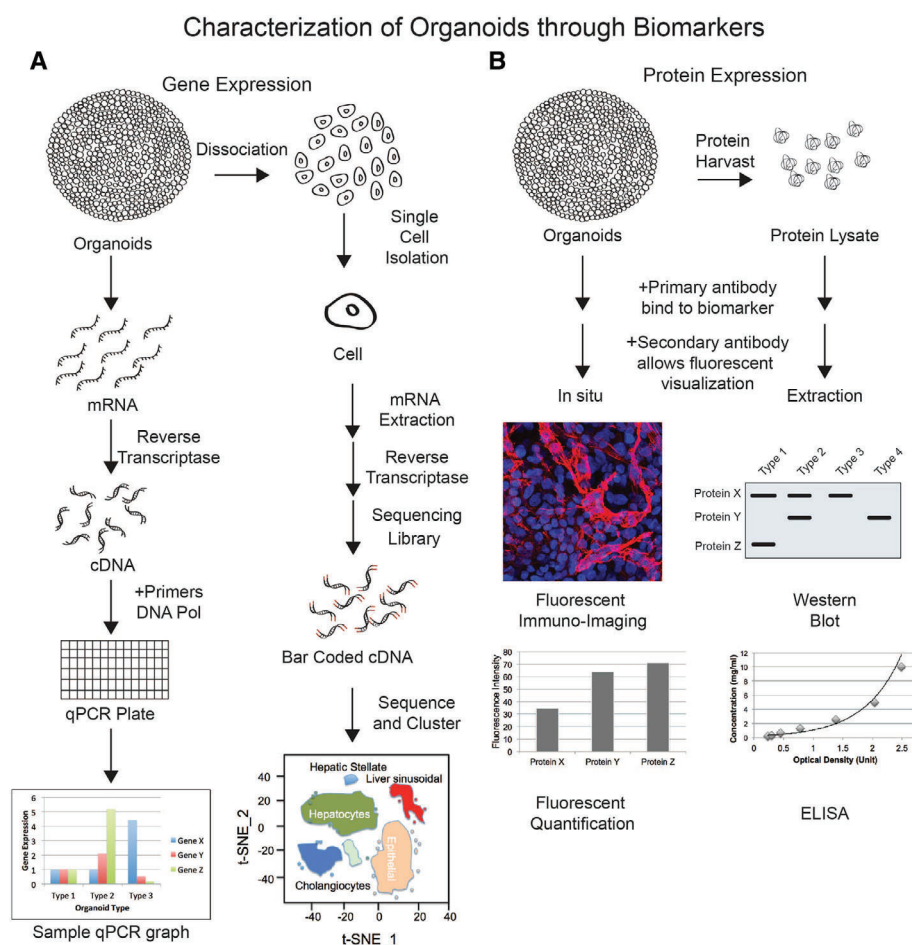


Figure 1. (A) Schematic of transcriptomic techniques, qPCR and single cell RNA sequencing, used in the characterization of organoids. (B) Schematic of proteomic techniques used to quantify biomarker expression in organoids.

also emphasized the importance of using proteomic profiling in addition to transcriptomic analysis in personalized medicine studies using patient-derived organoids. It is noteworthy that organoid proteomics is far more underway than organoid metabolomics (see Species-specific enhancement of enterohemorrhagic *E. coli* pathogenesis mediated by microbiome metabolites for an example of the latter [48]). We believe that a key reason may be that metabolomics (in addition to being less established than proteomics in general) is almost always performed with conventional LC–MS systems, which is limited regarding small samples. Could smaller systems be used for organoid metabolomics? Perhaps, considering that small-scale LC metabolomics has success in recent small-sample applications [49, 50].

However, we predict a need for even more sensitive analytical techniques than “regular” nano-LC. As with the larger i.d. systems, regular nano-LC columns are typically packed with porous particles that feature a hydrophobic stationary phase. As a result of technological development, the particles used today are around 2 μm in size, as opposed to 3–5 μm about 10–15 years ago. Smaller particles are associated with improved chromatography, but generate high back-pressures that require dedicated solvent delivery pumps. In addition, when particles are too small, frictional heating effects and par-

ticle stability can become factors. Therefore, particle-based columns are somewhat of a bottleneck for small-sample analysis, e.g. place limits on how narrow a separation column can be. An alternative to packed columns may be using open tubular LC (OTLC). OTLC columns, which are significantly smaller in scale compared to nano-LC are quite rarely used. An OTLC column is between 5 and 10 μm i.d., and operates at pL-low nL/min flow rates. This makes OTLC highly demanding to operate, but benefits include excellent chromatography and sensitivity. For example, Vehus et al. were able to detect attogram-scale amounts of metabolites using a 10 μm i.d. OTLC column, which were about two orders better compared to other reports with larger columns. The authors also showed that OTLC columns are versatile, with the same column performing well for bottom-up as well as top-down analysis of proteins. OTLC columns are also highly suited for coupling with online sample preparation, e.g. SPE for removing salts and other potential contaminations, and immobilized enzyme reactors for more automated proteomics [51]. In other words, OTLC is a potential candidate for coupling with organoid-related analysis, but is very far from being considered a routine tool.

Other open tubular options include CE. CE has long been known for its excellent separation properties. It is also

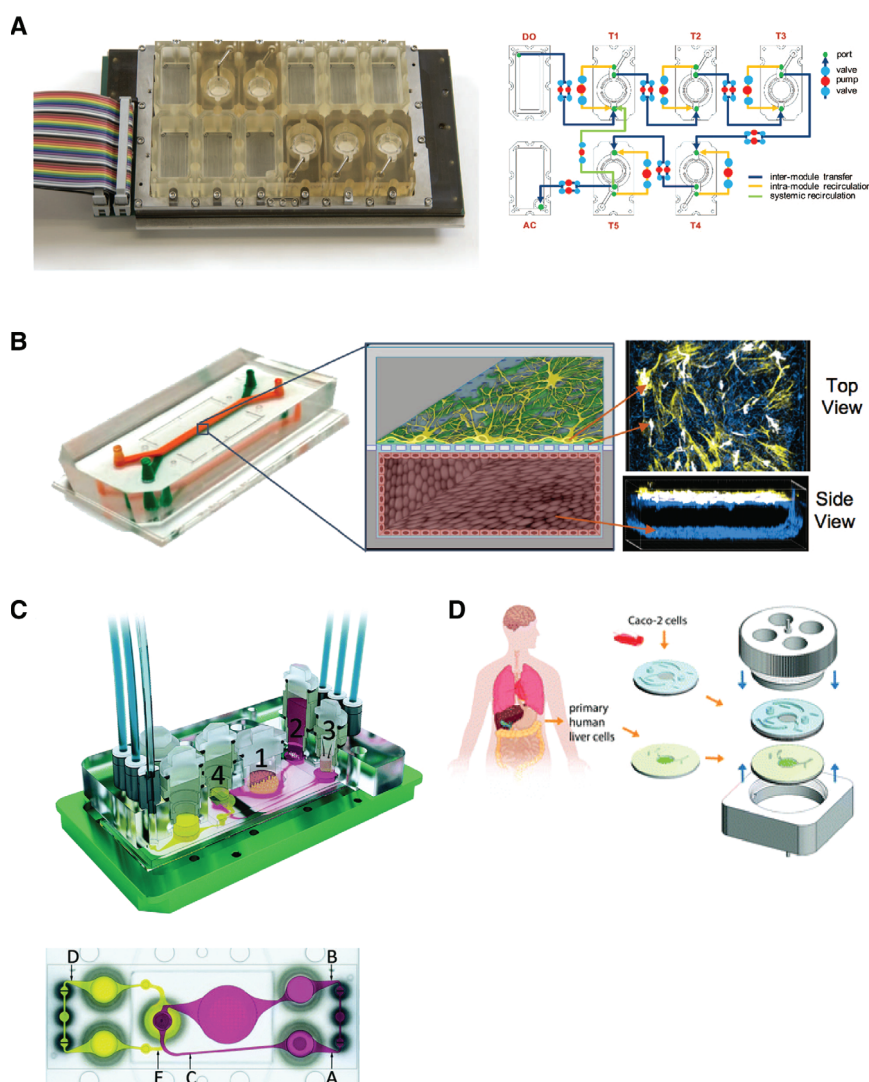


Figure 2. (A) EVATAR, a microfluidic culture model of the human reproductive tract. Images are from ref.64; see also ref.65. (B) Reconstitution of the human blood brain barrier, in an organ chip microfluidic device. Photograph (left), schematic illustration (middle), and immunofluorescence micrographs are from “Hypoxia-enhanced Blood-Brain Barrier Chip recapitulates human barrier function, drug penetration, and antibody shuttling properties” [66]. Reproduced with permission from the authors (the copyright holders of this BiorXiv preprint). (C) Top: Microfluidic device of a four-organ system representing the excretory system, which includes intestine (1), liver (2), skin (3), and kidney (4) tissue. Bottom: Horizontal view of the chip displaying three points of measurement (A, B, and C) in the surrogate blood circuit and two points of measurement (D, E) in the excretory circuit. Images are from “A four-organ-chip for interconnected long-term co-culture of human intestine, liver, skin and kidney equivalents” [67]; Reproduced by permission of The Royal Society of Chemistry. (D) Organ-on-CHIP containing co-culture of gastric intestinal tract epithelium and 3D primary liver tissue. Images are from “Modular, pumpless body-on-a-chip platform for the co-culture of GI tract epithelium and 3D primary liver tissue” [68]; Reproduced by permission of The Royal Society of Chemistry.

commonly associated with chip-based systems [52, 53]. Although CE in many instances out-competed LC in terms of separation capabilities, the latter has been the tool of choice for most bio-analysts. A key reason may be that LC is compatible with ESI-MS, while the electrolyte solutions of CE have been far more difficult to couple with MS detection. However, CE–ESI–MS can prove highly sensitive analysis. In addition, it has been shown that CE–ESI–MS has excellent potential for analysis of intact proteins [54, 55], fulfilling a prediction by James Jorgenson in his pioneering work in developing CE. Considering that CE is capable of, e.g. drug analysis [56], metabolomics [57], proteomics [58], and is “chip-ready”, CE could very well be a natural partner in organoid analysis.

4 On-chip technology: challenges and opportunities for online MS analysis

Major advantages of microfluidic devices include automatable manipulation and on-line or “on chip” analysis (see

Fig. 2). On-line is a highly familiar term to analysts and separation scientists, as well as the associated pro’s and con’s. Advantages of online action can include rapid and precise analysis, with reduced chances of outside contaminations. Disadvantages can include decreased flexibility, poor robustness due to clogging and incompatibility of solvents when two or more fluidic systems are to be hyphenated [59]. It is therefore possible that all these traits will be present when organ-on-a-chip and nano-LC–MS are to be coupled on-line. For example, the organ-on-a-chip will typically have an oxygenated medium consisting of, e.g. salts and serum, components that can cause interferences in LC–MS. Therefore, a modulation system for bridging the OoC system to the nano-LC–MS system can be necessary. A system by Elisabeth Verpoorte and co-workers for drug metabolism studies of liver slices will be a likely template (Figure 3) [60]. Here, a medium fraction is sent to one storage loop, while a previously “looped” fraction is sent to an LC–UV system for measuring metabolites. Such a modulation system allows for two solvent systems to operate simultaneously without a large degree of mixing. These

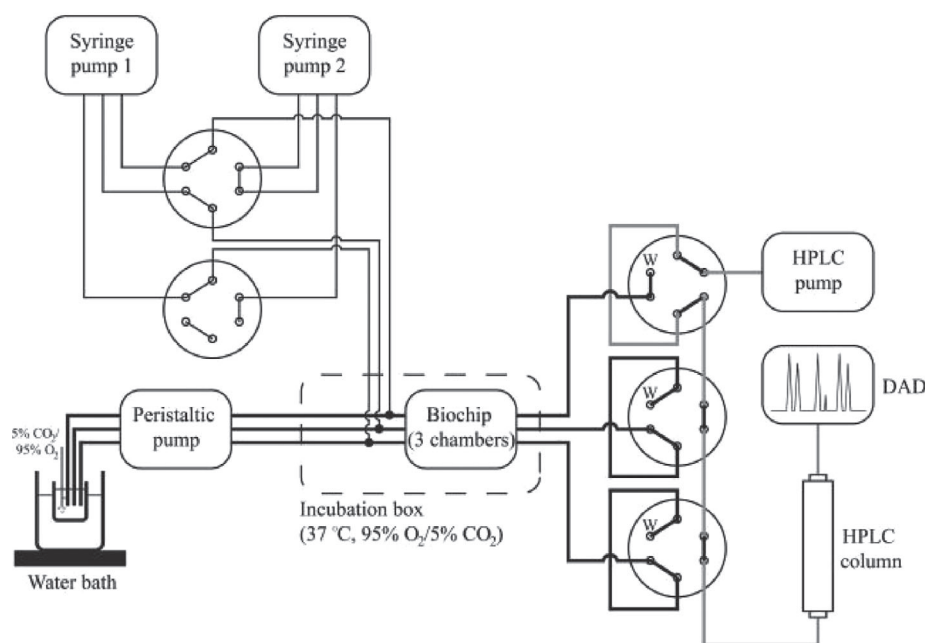


Figure 3. System for metabolism and inhibition studies of precision-cut liver slices in a microfluidic device, online coupled with LC. Preproduced with permission from “On-line HPLC analysis system for metabolism and inhibition studies in precision-cut liver slices” [60]. Copyright (2019) American chemical society.

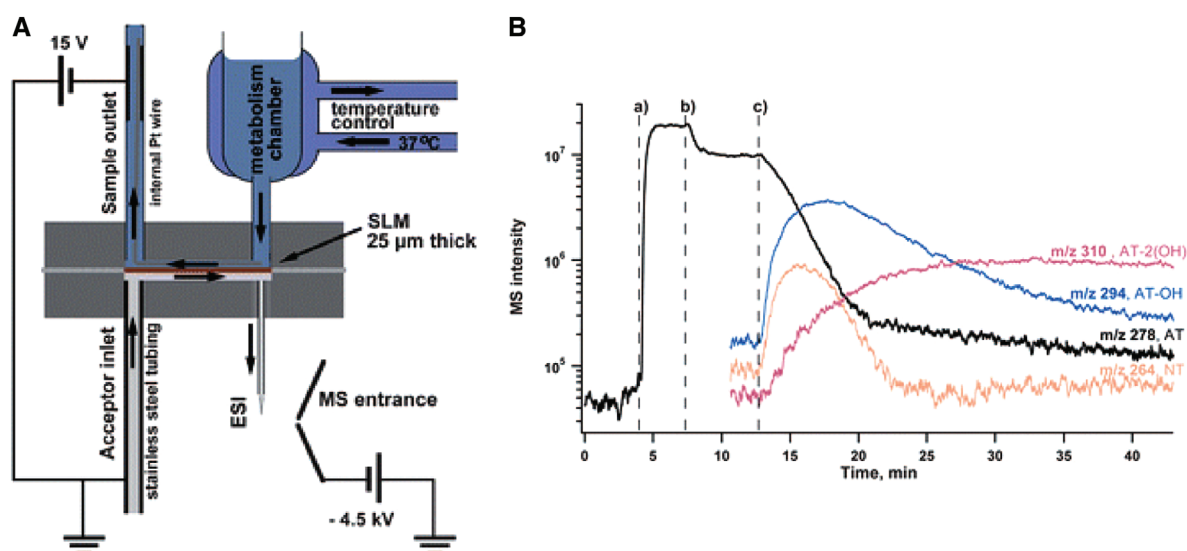


Figure 4. System for the online monitoring of microsome drug metabolism-MS directly with on-chip electromembrane extraction. Image from “On-chip electromembrane extraction for monitoring drug metabolism in real time by ESI-MS” [63]. Reproduced by permission of The Royal Society of Chemistry.

systems remind of 2D LC systems. The described system should be well suited for miniaturization to narrow columns and for MS detection. In addition, more variants can be tested, for example replacing the loops with SPE columns for even more selective handling [61].

However, both the loop and SPE variant may be prone to clogging and perturbing from media proteins, e.g. a relatively high concentration of albumin. Therefore, alternatives to the 2-stage chromatography approaches systems can be investigated. One option is online electromembrane extraction (EME) systems. Fundamentally, EME can be considered as electrophoresis across an oil membrane, and there has been

considerable interest for this concept in recent years [62]. Figure 4A exemplifies the potential, where EME was used in combination with ESI-MS for continuous and on-line monitoring of microsome drug metabolism [63]. In-vitro metabolism of drug substances was performed in a small temperature-controlled metabolism chamber, open to air and located on a microchip for EME. During the metabolic reaction, reaction mixture was continuously perfused at 20 $\mu\text{L}/\text{min}$ into the microchip. Inside the EME microchip, the reaction mixture was in contact with a supported liquid membrane (SLM), comprised of 0.2 μL of 2-nitrophenyl octyl ether immobilized in the pore of a porous membrane of

polypropylene (25 µm thickness). On the other side of the SLM, 100 mM formic acid was pumped continuously with a flow rate of 20 µL/min. This liquid served as acceptor phase. A DC electrical potential was applied across the SLM using small platinum wires in reaction mixture and acceptor phase, and these were connected to an external power supply. By application of 15 V, parent drug substance and metabolites in the reaction mixture were prone to electro-kinetic migration, and were extracted across the SLM and into the acceptor phase. The acceptor phase was pumped continuously into the mass spectrometer, and by such the concentration of parent drug and metabolites were monitored unremittingly as shown in Figure 4B. Buffer components, enzymes, proteins, and other species from the rat liver microsomes used in the reaction mixture were effectively discriminated by the lipophilic SLM, and these matrix components were not introduced into the mass spectrometer. Thus, contamination of the mass spectrometer and serious ion suppression was avoided. We believe that the online EME concept, which has been demonstrated with microsomes and metabolism studies, can be transferred to organoid analysis as well.

5 Concluding remarks

Organoids and organ-on-a-chip systems are predicted to be the key tools in drug discovery and disease modeling in the upcoming years. The limited amounts of sample and on-line features, along with the need for versatile and comprehensive analysis, points to a natural partnership with mass spectrometry and separation science (especially miniaturized systems). Various omics approaches are already being undertaken offline, but there are especially many opportunities for online coupling. Online organ-on-a-chip MS will be most straightforward for small molecules, e.g. drugs and metabolites. Online proteomics will be more challenging, as protein cleavage to MS-detectable peptides must likely be done in reactors. Immobilized enzyme reactors are indeed available, but are far from becoming routine and robust tools for high throughput organoid analysis.

Finally, we would like to comment on how the output of complete organoid/analysis systems will be handled. Another way in which organ-on-a-chip is distinguished from standard life science experiments is much of the experiment is defined in digital form. For example, chip design is typically defined in CAD files that are sent to 3D printers. Similarly, both on board and offline sensors process signals to record information in digital format. This provides exciting opportunities in how data can be utilized in the organ-on-a-chip universe. In standard life science experiments, data analysis is performed after an experiment has been completed and the processed results are then used to answer a specific scientific question. In the organ-on-a-chip universe, the data encompasses the entire process, from component and experimental design to raw sensor data and processed experimental results. If data can be integrated through introduction of well-defined standards, it becomes feasible to consider artificial intelligence

approaches that allow data to be used in a feedback process. In such an approach data could be used to iteratively introduce design modifications (for example, changes to chip profiles or sensor/chip/cell combinations) that leads to optimised designs for specific purposes.

Financial support from UiO:Life Science is gratefully acknowledged. This work was also partially supported by the Research Council of Norway through its Centre of Excellence scheme, project number 262613. This work has also received financial support from the Olav Thon Foundation and the US-Norway Fulbright Foundation.

The authors have declared no conflict of interest.

6 References

- [1] Scannell, J. W., Blanckley, A., Boldon, H., Warrington, B., *Nat. Rev. Drug Discov.* 2012, 11, 191–200.
- [2] Roy, A., *High-Throughput* 2018, 7, 4.
- [3] Hwang, T. J., Carpenter, D., Lauffenburger, J. C., Wang, B., Franklin, J. M., Kesselheim, A. S., *JAMA Intern. Med.* 2016, 176, 1826–1833.
- [4] Fogel, D. B., *Contemp. Clin. Trials Commun.* 2018, 11, 156–164.
- [5] Wong, C. H., Siah, K. W., Lo, A. W., *Biostatistics* 2019, 20, 273–286.
- [6] Jodat, Y. A., Kang, M. G., Kiaee, K., Kim, G. J., Martinez, A. F. H., Rosenkranz, A., Bae, H., Shin, S. R., *Curr. Pharm. Des.* 2018, 24, 5471–5486.
- [7] Ishida, S., *Drug Metab. Pharmacokinet.* 2018, 33, 49–54.
- [8] Li, M., Izpisua Belmonte, J. C., *N. Engl. J. Med.* 2019, 380, 569–579.
- [9] Whitesides, G. M., *Nature* 2006, 442, 368–373.
- [10] Sosa-Hernández, J. E., Villalba-Rodríguez, A. M., Romero-Castillo, K. D., Aguilar-Aguila-Isaías, M. A., García-Reyes, I. E., Hernández-Antonio, A., Ahmed, I., Sharma, A., Parra-Saldívar, R., Iqbal, H. M. N., *Micromachines (Basel)*. 2018, 9, pii: E536.
- [11] Kimura, H., Sakai, Y., Fujii, T., *Drug Metab. Pharmacokinet.* 2018, 33, 43–48.
- [12] Zhang, B., Radisic, M., *Lab Chip* 2017, 17, 2395–2420.
- [13] Zhang, M., Xu, C., Jiang, L., Qin, J., *Toxicol. Res.* 2018, 7, 1048–1060.
- [14] Stucki, A. O., Stucki, J. D., Hall, S. R., Felder, M., Mermoud, Y., Schmid, R. A., Geiser, T., Guenat, O. T., *Lab Chip* 2015, 15, 1302–1310.
- [15] Bein, A., Shin, W., Jalili-Firoozinezhad, S., Park, M. H., Sontheimer-Phelps, A., Tovaglieri, A., Chalkiadaki, A., Kim, H. J., Ingber, D. E., *Cell. Mol. Gastroenterol. Hepatol.* 2018, 5, 659–668.
- [16] Helm, M. W. van der, Henry, O. Y. F., Bein, A., Hamkins-Indik, T., Cronce, M. J., Leineweber, W. D., Odijk, M., Meer, A. D. van der, Eijkel, J. C. T., Ingber, D. E., Berg, A. van den, Segerink, L. I., *Lab Chip* 2019, 19, 452–463.
- [17] Haring, A. P., Sontheimer, H., Johnson, B. N., *Stem Cell Rev. Rep.* 2017, 13, 381–406.
- [18] Miccoli, B., Braeken, D., Li, Y.-C. E., *Curr. Pharm. Des.* 2018, 24, 5419–5436.

- [19] Agarwal, A., Goss, J. A., Cho, A., McCain, M. L., Parker, K. K., *Lab Chip* 2013, **13**, 3599–3608.
- [20] Wan, H., Gu, C., Gan, Y., Wei, X., Zhu, K., Hu, N., Wang, P., *Curr. Pharm. Des.* 2018 **24**, 5375–5385.
- [21] Danoy, M., Bernier, M. L., Kimura, K., Poulain, S., Kato, S., Mori, D., Kido, T., Plessy, C., Kusuhara, H., Miyajima, A., Sakai, Y., Leclerc, E., *Biotechnol. Bioeng.* 2019, **116**, 1762–1776.
- [22] Camp, J. G., Sekine, K., Gerber, T., Loeffler-Wirth, H., Binder, H., Gac, M., Kanton, S., Kageyama, J., Damm, G., Seehofer, D., Belicova, L., Bickle, M., Barsacchi, R., Okuda, R., Yoshizawa, E., Kimura, M., Ayabe, H., Taniguchi, H., Takebe, T., Treutlein, B., *Nature* 2017, **546**, 533–538.
- [23] Tao, T., Wang, Y., Chen, W., Li, Z., Su, W., Guo, Y., Deng, P., Qin, J., *Lab Chip* 2019, **19**, 948–958.
- [24] Loskill, P., Sezhan, T., Tharp, K. M., Lee-Montiel, F. T., Jeeawoody, S., Reese, W. M., Zushin, P.-J. H., Stahl, A., Healy, K. E., *Lab Chip* 2017, **17**, 1645–1654.
- [25] Chen, H. J., Miller, P., Shuler, M. L., *Lab Chip* 2018, **18**, 2036–2046.
- [26] Oleaga, C., Riu, A., Rothemund, S., Lavado, A., McAleer, C. W., Long, C. J., Persaud, K., Narasimhan, N. S., Tran, M., Roles, J., Carmona-Moran, C. A., Sasserath, T., Elbrecht, D. H., Kumanchik, L., Bridges, L. R., Martin, C., Schnepfer, M. T., Ekman, G., Jackson, M., Wang, Y. I., Note, R., Langer, J., Teissier, S., Hickman, J. J., *Biomaterials* 2018, **182**, 176–190.
- [27] Nguyen, M., De Ninno, A., Mencattini, A., Mermet-Meillon, F., Fornabaio, G., Evans, S. S., Cossutta, M., Khira, Y., Han, W., Sirven, P., Pelon, F., Di Giuseppe, D., Bertani, F. R., Gerardino, A., Yamada, A., Descroix, S., Soumelis, V., Mechta-Grigoriou, F., Zalcman, G., Camonis, J., Martinelli, E., Businaro, L., Parrini, M. C., *Cell Rep.* 2018, **25**, 3884–3893.e3.
- [28] Karagiannis, P., Takahashi, K., Saito, M., Yoshida, Y., Okita, K., Watanabe, A., Inoue, H., Yamashita, J. K., Todani, M., Nakagawa, M., Osawa, M., Yashiro, Y., Yamanaka, S., Osafune, K., *Physiol. Rev.* 2019, **99**, 79–114.
- [29] Shinozawa, T., Yoshikawa, H. Y., Takebe, T., *Dev. Biol.* 2016, **420**, 221–229.
- [30] Eiraku, M., Watanabe, K., Matsuo-Takasaki, M., Kawada, M., Yonemura, S., Matsumura, M., Wataya, T., Nishiyama, A., Muguruma, K., Sasai, Y., *Cell Stem Cell* 2008, **3**, 519–532.
- [31] Coll, M., Perea, L., Boon, R., Leite, S. B., Vallverdú, J., Mannaerts, I., Smout, A., El Taghdouini, A., Blaya, D., Rodrigo-Torres, D., Graupera, I., Aguilar-Bravo, B., Chesne, C., Najimi, M., Sokal, E., Lozano, J. J., Grunsvan, L. A. van, Verfaillie, C. M., Sancho-Bru, P., *Cell Stem Cell* 2018, **23**, 101–113.e7.
- [32] Takebe, T., Enomura, M., Yoshizawa, E., Kimura, M., Koike, H., Ueno, Y., Matsuzaki, T., Yamazaki, T., Toyohara, T., Osafune, K., Nakauchi, H., Yoshikawa, H. Y., Taniguchi, H., *Cell Stem Cell* 2015, **16**, 556–565.
- [33] Huch, M., Dorrell, C., Boj, S. F., Es, J. H. van, Li, V. S. W., Wetering, M. van de, Sato, T., Hamer, K., Sasaki, N., Finegold, M. J., Haft, A., Vries, R. G., Grompe, M., Clevers, H., *Nature* 2013, **494**, 247–250.
- [34] Lancaster, M. A., Renner, M., Martin, C.-A., Wenzel, D., Bicknell, L. S., Hurlles, M. E., Homfray, T., Penninger, J. M., Jackson, A. P., Knoblich, J. A., *Nature* 2013, **501**, 373–379.
- [35] Jo, J., Xiao, Y., Sun, A. X., Cukuroglu, E., Tran, H.-D., Göke, J., Tan, Z. Y., Saw, T. Y., Tan, C.-P., Lokman, H., Lee, Y., Kim, D., Ko, H. S., Kim, S.-O., Park, J. H., Cho, N.-J., Hyde, T. M., Kleinman, J. E., Shin, J. H., Weinberger, D. R., Tan, E. K., Je, H. S., Ng, H.-H., *Cell Stem Cell* 2016, **19**, 248–257.
- [36] Qian, X., Nguyen, H. N., Song, M. M., Hadiono, C., Ogdan, S. C., Hammack, C., Yao, B., Hamersky, G. R., Jacob, F., Zhong, C., Yoon, K.-J., Jeang, W., Lin, L., Li, Y., Thakor, J., Berg, D. A., Zhang, C., Kang, E., Chickering, M., Nauen, D., Ho, C.-Y., Wen, Z., Christian, K. M., Shi, P.-Y., Maher, B. J., Wu, H., Jin, P., Tang, H., Song, H., Ming, G.-L., *Cell* 2016, **165**, 1238–1254.
- [37] Marchetto, M. C. N., Carroumeu, C., Acab, A., Yu, D., Yeo, G. W., Mu, Y., Chen, G., Gage, F. H., Muotri, A. R., *Cell* 2010, **143**, 527–539.
- [38] Spence, J. R., Mayhew, C. N., Rankin, S. A., Kuhar, M. F., Vallance, J. E., Tolle, K., Hoskins, E. E., Kalinichenko, V. V., Wells, S. I., Zorn, A. M., Shroyer, N. F., Wells, J. M., *Nature* 2011, **470**, 105–109.
- [39] Sato, T., Vries, R. G., Snippert, H. J., Wetering, M. van de, Barker, N., Stange, D. E., Es, J. H. van, Abo, A., Kujala, P., Peters, P. J., Clevers, H., *Nature* 2009, **459**, 262–265.
- [40] Wells, J. M., Spence, J. R., *Development* 2014, **141**, 752–760.
- [41] Guan, Y., Xu, D., Garfin, P. M., Ehmer, U., Hurwitz, M., Enns, G., Michie, S., Wu, M., Zheng, M., Nishimura, T., Sage, J., Peltz, G., *JCI Insight.* 2017, **2**, 94954.
- [42] Wilson, S. R., Vehus, T., Berg, H. S., Lundanes, E., *Bioanalysis* 2015, **7**, 1799–1815.
- [43] Dakic, V., Minardi Nascimento, J., Costa Sartore, R., Maciel, R. de M., Araujo, D. B. de, Ribeiro, S., Martins-de-Souza, D., Rehen, S. K., *Sci. Rep.* 2017, **7**, 12863.
- [44] Lindeboom, R. G., Voorthuijsen, L. van, Oost, K. C., Rodríguez-Colman, M. J., Luna-Velez, M. V., Furlan, C., Baraille, F., Jansen, P. W., Ribeiro, A., Burgering, B. M., Snippert, H. J., Vermeulen, M., *Mol. Syst. Biol.* 2018, **14**, e8227.
- [45] Williams, K. E., Lemieux, G. A., Hassis, M. E., Olshen, A. B., Fisher, S. J., Werb, Z., *Proc. Natl. Acad. Sci. USA* 2016, **113**, E1343–E1351.
- [46] Boj, S. F., Hwang, C.-I., Baker, L. A., Chio, I. I. C., Engle, D. D., Corbo, V., Jager, M., Ponz-Sarvisé, M., Tiriác, H., Spector, M. S., Gracanin, A., Oni, T., Yu, K. H., van Boxtel, R., Huch, M., Rivera, K. D., Wilson, J. P., Feigin, M. E., Öhlund, D., Handly-Santana, A., Ardito-Abraham, C. M., Ludwig, M., Elyada, E., Alagesan, B., Biffi, G., Yordanov, G. N., Delcuze, B., Creighton, B., Wright, K., Park, Y., Morsink, F. H. M., Molenaar, I. Q., Borel Rinkes, I. H., Cuppen, E., Hao, Y., Jin, Y., Nijman, I. J., Iacobuzio-Donahue, C., Leach, S. D., Pappin, D. J., Hammell, M., Klimstra, D. S., Basturk, O., Hruban, R. H., Offerhaus, G. J., Vries, R. G. J., Clevers, H., Tuveson, D. A., *Cell* 2015, **160**, 324–338.
- [47] Cristobal, A., Toorn, H. W. P. van den, Wetering, M. van de, Clevers, H., Heck, A. J. R., Mohammed, S., *Cell Rep.* 2017, **18**, 263–274.

- [48] Tovaglieri, A., Sontheimer-Phelps, A., Geirnaert, A., Prantil-Baun, R., Camacho, D. M., Chou, D. B., Jalili-Firoozinezhad, S., Wouters, T. de, Kasendra, M., Super, M., Cartwright, M. J., Richmond, C. A., Breault, D. T., Lacroix, C., Ingber, D. E., *Microbiome* 2019, 7, 43.
- [49] Vehus, T., Roberg-Larsen, H., Waaler, J., Aslaksen, S., Krauss, S., Wilson, S. R., Lundanes, E., *Sci. Rep.* 2016, 6, 37507.
- [50] Roberg-Larsen, H., Lund, K., Seterdal, K. E., Solheim, S., Vehus, T., Solberg, N., Krauss, S., Lundanes, E., Wilson, S. R., *J. Steroid Biochem. Mol. Biol.* 2017, 169, 22–28.
- [51] Hustoft, H. K., Vehus, T., Brandtzaeg, O. K., Krauss, S., Greibrokk, T., Wilson, S. R., Lundanes, E., *PLoS One* 2014, 9, e106881.
- [52] Benz, C., Boomhoff, M., Appun, J., Schneider, C., Belder, D., *Angew. Chem., Int. Ed.* 2015, 54, 2766–2770.
- [53] Wu, D., Qin, J., Lin, B., *J. Chromatogr. A* 2008, 1184, 542–559.
- [54] Zhao, Y., Sun, L., Zhu, G., Dovichi, N. J., *J. Proteome Res.* 2016, 15, 3679–3685.
- [55] Lubeckyj, R. A., McCool, E. N., Shen, X., Kou, Q., Liu, X., Sun, L., *Anal. Chem.* 2017, 89, 12059–12067.
- [56] Langmajerová, M., Řemínek, R., Pelcová, M., Foret, F., Glatz, Z., *Electrophoresis* 2015, 36, 1365–1373.
- [57] Ramautar, R., Somsen, G. W., Jong, G. J. de, *Electrophoresis* 2017, 38, 190–202.
- [58] Heemskerk, A. A. M., Deelder, A. M., Mayboroda, O. A., *Mass Spectrometry Rev.* 2016, 35, 259–271.
- [59] Rogeberg, M., Malerod, H., Roberg-Larsen, H., Aass, C., Wilson, S. R., *J. Pharm. Biomed. Anal.* 2014, 87, 120–129.
- [60] Midwoud, P. M. van, Janssen, J., Merema, M. T., Graaf, I. A. M. de, Groothuis, G. M. M., Verpoorte, E., *Anal. Chem.* 2011, 83, 84–91.
- [61] Malerod, H., Lundanes, E., Greibrokk, T., *Anal. Meth.* 2010, 2, 110–122.
- [62] Huang, C., Chen, Z., Gjelstad, A., Pedersen-Bjergaard, S., Shen, X., *Trends Anal. Chem.* 2017, 95, 47–56.
- [63] Petersen, N. J., Pedersen, J. S., Poulsen, N. N., Jensen, H., Skonberg, C., Hansen, S. H., Pedersen-Bjergaard, S., *Analyst* 2012, 137, 3321–3327.
- [64] EVATAR TECHNOLOGY | Woodruff Lab <https://www.woodrufflab.org/EvatarTechnology> [accessed Apr 15, 2019].
- [65] Xiao, S., Coppeta, J. R., Rogers, H. B., Isenberg, B. C., Zhu, J., Olalekan, S. A., McKinnon, K. E., Dokic, D., Rashedi, A. S., Haisenleder, D. J., Malpani, S. S., Arnold-Murray, C. A., Chen, K., Jiang, M., Bai, L., Nguyen, C. T., Zhang, J., Laronda, M. M., Hope, T. J., Maniar, K. P., Pavone, M. E., Avram, M. J., Sefton, E. C., Getsios, S., Burdette, J. E., Kim, J. J., Borenstein, J. T., Woodruff, T. K., *Nat. Commun.* 2017, 8, 14584.
- [66] Park, T.-E., Mustafaoglu, N., Herland, A., Hasselkus, R. M., Mannix, R., FitzGerald, E. A., Prantil-Baun, R., Watters, A., Henry, O., Benz, M., Sanchez, H., McCrea, H. J., Christova Goumnerova, L., Song, H. W., Palecek, S. P., Shusta, E., Ingber, D. E., *bioRxiv* 2018 <https://doi.org/10.1101/482463>.
- [67] Maschmeyer, I., Lorenz, A. K., Schimek, K., Hasenberg, T., Ramme, A. P., Hübner, J., Lindner, M., Drewell, C., Bauer, S., Thomas, A., Sambo, N. S., Sonntag, F., Lauster, R., Marx, U., *Lab Chip* 2015, 15, 2688–2699.
- [68] Esch, M. B., Ueno, H., Applegate, D. R., Shuler, M. L., *Lab Chip* 2016, 16, 2719–2729.

II



Cite this: *Analyst*, 2020, **145**, 4957

Electromembrane extraction of sodium dodecyl sulfate from highly concentrated solutions

Magnus Saed Restan,^a Frøydis Sved Skottvoll,^b Henrik Jensen^c and Stig Pedersen-Bjergaard  ^{a,c}

This fundamental work investigated the removal of sodium dodecyl sulfate (SDS) from highly concentrated samples by electromembrane extraction (EME). SDS concentrations were in the range of 0.1–1.0% w/v, covering both sub- and super-critical micellar concentrations (CMC). Under optimal conditions, we extracted SDS from 100 μL aqueous sample, through 3 μL supported liquid membrane (SLM) and into 200 μL 10 mM NaOH in water as waste solution. The SLM comprised 1.0% w/w Aliquat 336 in 1-nonanol, and extraction voltage was 5 V. From 0.1% SDS samples, EME removed 100% during 30 minutes operation (100% clearance). SDS concentration above the critical micellar concentration (CMC) challenged the capacity of the system. Thus, to reach 100% clearance from 0.5% samples, we extracted for 120 minutes and replenished the SLM after 60 minutes. Increasing the membrane area of the SLM from 28 mm^2 to 43 mm^2 provided 100% clearance from 0.5% samples after 30 min EME. Complete clearance of 1.0% SDS samples was not achieved under the tested conditions, and maximal clearance was 60%. Mass balance experiments demonstrated that most of the removed SDS is trapped in the SLM, rather than transferring to the waste solution. For super-CMC samples, aggregation of SDS in the SLM exceeded the SLM capacity and impeded further mass transfer.

Received 30th March 2020,
Accepted 13th May 2020

DOI: 10.1039/d0an00622j

rsc.li/analyst

1. Introduction

Electromembrane extraction (EME) was introduced in 2006¹ and provided a new approach to microextraction utilizing an electrical field as the main driving force. EME can be considered as a hybrid between liquid-phase microextraction (LPME)² and electrophoresis and is performed in a three-phase system with an aqueous sample (donor) solution, an aqueous acceptor solution, and an organic solvent immobilized inside the pores of a porous membrane sandwiched in between. The latter is termed a supported liquid membrane (SLM) and acts as a barrier between the two aqueous phases (sample and acceptor). Electrodes are placed in the sample and acceptor, and the electrical field is applied using an external power supply. Charged substances of interest (target substances) thus transfer from the sample, through the SLM, and into the acceptor by electrokinetic migration. In order to promote electrokinetic migration, the sample and acceptor are neutral or acidic for EME of basic substances, and the cathode

is located in the acceptor. For EME of acidic substances, the sample and acceptor are neutral or alkaline, and the anode is in the acceptor. The electrical field improves extraction kinetics, and the operator controls the selectivity by the polarity and magnitude of the electrical field, by the chemical composition of the SLM, and by pH. EME is compatible with complex real samples and can provide highly purified extracts.

To date, EME has been used for the extraction of hydrophilic drugs,³ hydrophobic drugs,⁴ acidic and basic drugs,^{5,6} metals,^{7,8} peptides,⁹ inorganic ions,¹⁰ contaminants in environmental samples¹¹ and wastewaters,¹² and drugs and drugs of abuse in whole blood,¹³ plasma¹⁴ and saliva.¹⁵ In general, target substances have been at the trace level, corresponding to ng ml^{-1} (ref. 5 and 16–21) or low $\mu\text{g ml}^{-1}$ concentrations.^{22–25} Under such conditions, the individual phases of the EME system are far from saturation.

Recent work reported on EME of propranolol and probenecid templates used in the synthesis of molecularly imprinted polymers (MIPs), at the 1–1000 $\mu\text{g mL}^{-1}$ level.²⁶ In these experiments, the flux of target ions ($\mu\text{g cm}^{-2} \text{min}^{-1}$) through the SLM was less than expected, based on the flux at lower concentrations and the area of the SLM. Lower mass transfer capacity was due to saturation of the SLM and to excessive boundary layer conditions in the donor/SLM interface. Another research reported on EME of selected basic drugs (haloperidol, amitriptyline, fluoxetine, and sertraline) at the

^aDepartment of Pharmacy, University of Oslo, P.O. Box 1068, Blindern, 0316 Oslo, Norway. E-mail: stigpe@farmasi.uio.no

^bDepartment of Chemistry, University of Oslo, P.O. Box 1033, Blindern, 0315 Oslo, Norway

^cDepartment of Pharmacy, Faculty of Health and Medical Sciences, University of Copenhagen, Universitetsparken 2, 2100 Copenhagen, Denmark

0.5–200 $\mu\text{g ml}^{-1}$ level.²⁷ Again, mass transfer apparently decreased with increasing concentration levels. A third paper reported on EME of sodium chloride, with concentrations up to 500 mM NaCl (29 mg mL^{-1}).²⁸

Conceptually, EME research focuses on the extraction of target analytes from real samples and into pure buffer solution, followed by an instrumental analysis of the latter. This mode of EME is termed *extraction mode*. Potentially, EME can be used in a different way, namely to remove abundant matrix components from real samples prior to instrumental analysis of the latter. In this approach, termed *removal mode*, the acceptor serves as waste solution. EME in removal mode is not common, but the literature describes the removal of salt from micro-liter volumes of biological fluids,²⁸ removal of phospholipids from plasma samples,²⁹ and removal of fluorescein isothiocyanate (FITC) from tagged protein solutions.²⁵ Potentially, there are many similar applications where EME in removal mode may play a future role, including removal of surfactants from protein solutions prior to analysis by chromatography and mass spectrometry. However, the development of such applications requires additional fundamental knowledge. In particular, experiences above 1 mg mL^{-1} , where the system is close to saturation, are important to understand.

The purpose of the current fundamental paper was to investigate EME at 1–10 mg mL^{-1} concentrations. Attention was on mass transfer as a function of high concentration, to develop a better understanding of concentration limits related to EME in removal mode. Sodium dodecyl sulfate (SDS) was chosen as a target substance. SDS is an anionic detergent, and at the 0.02% level it has been reported to enhance mass transfer in EME.³⁰ However, much more commonly, SDS is used with biological cell samples during cell lysis to solubilize membrane and intracellular proteins.³¹ In order to promote lysis, the concentration of SDS added to biological cell samples is 0.5–1.0% (5–10 mg mL^{-1}).³² This high concentration is undesirable in the final analysis due to its detrimental effects on chromatographic columns and contribution to ion suppression in mass spectrometry.³³

2. Experimental

2.1. Chemicals and solutions

Stains-All (1-ethyl-2-[3-(1-ethylnaphtho[1,2-*d*]thiazolin-2-ylidene)-2-methylpropenyl]-naphtho[1,2-*d*]thiazolium bromide, 3,3'-diethyl-9-methyl-4,5,4',5'-dibenzothiacarbocyanine), SDS, 2-nitrophenyl octyl ether (NPOE), 1-octanol, 1-nonanol, 1-decanol, and 2-decanone were purchased from Sigma Aldrich (St Louis, MO, USA). *N,N*-Dimethyl-formamide was purchased from Merck (Kenilworth, New Jersey, USA), Aliquat 366 was from Cognis Corporation (Cincinnati, Ohio, USA), NaOH was from VWR International (Radnor, PA, USA), and deionized water was obtained from a Milli-Q water purification system (Molsheim, France).

1.0 g of SDS was dissolved in 10 mM NaOH for the preparation of 1.0% w/v stock solution. All stock solutions were

stored at room temperature and protected from light. Working solutions were freshly prepared before experiments by dilution of the stock solutions with the same solvent. Preparation of Stains-All working solution was a 1 : 64 dilution of a stock solution, containing 2 mg mL^{-1} Stain-All in *N,N*-dimethyl-formamide, with deionized water. New stock solutions were prepared monthly and stored in darkness at 4 °C while working solutions were prepared daily right before measurements.

2.2. UV-spectrophotometry

Quantification of SDS was conducted on a Beckman 530 UV/Vis Spectrophotometer (Beckman Coulter, Fullerton, CA, USA), using a 10 × 10 mm quartz cuvette (Hellma Analytics, Mulheim, Germany). Calibration and verification of the instrument were according to the European Pharmacopeia. Quantification of SDS involved pipetting 1 μL solution into a quartz cuvette, preloaded with 3 mL Stains-All working solution, and measuring the absorbance at 438 nm.^{34,35}

2.3. Electromembrane extraction (EME)

Equipment used for EME has been described previously (Fig. 1).²⁵ In brief, a laboratory built stainless steel plate with 0.5 mL wells served as a compartment for the waste solutions and as an electrode (96-well waste reservoir plate). A 96-well MultiScreen-IP filter plate with 100 μm thick polyvinylidene fluoride (PVDF) filter membranes of 0.45 μm pore size (Merck Millipore Ltd, Carrigtwohill, Ireland) served as a compartment for the samples (96-well filter plate) and SLMs. A laboratory built aluminum plate with 96 rods tailor-made for the wells of the filter plate served as the second electrode (96-electrode plate). A model ES 0300-0.45 (Delta Elektronika BV, Zierikzee, The Netherlands) was used as a power supply, and a Vibramax 100 Heidolph shaking board (Kellheim, Germany) was used to agitate the entire extraction system.

EME involved the following procedure for each sample: (a) pipetting 200 μL of 10 mM NaOH into the 96-well waste reservoir plate, (b) pipetting 3 μL organic solvent onto the filter membrane of the 96-well filter plate, and (c) pipetting 100 μL sample into the 96-well filter plate. Subsequently, we clamped the 96-well waste reservoir plate and filter plate and placed the 96-electrode plate on top. The rod electrodes of the electrode plate were then in contact with the samples. Finally, we connected the power supply to the waste reservoir plate (anode) and the electrode plate (cathode), and we conducted EME by simultaneous application of voltage and agitation.

2.4. Electromembrane extraction (EME) with an extended SLM area

EME with an extended SLM area was according to previous work.³⁶ In brief, a 100 μm thick porous Accurel PP 1E (R/P) polypropylene membrane (Membrana, Wuppertal, Germany) was fastened to the wide end of a 10–1000 μL pipette tip and sealed with a soldering iron. The total surface area of the membrane was measured as 43 mm^2 . A 0.5 mm hole was drilled in the bottom of a 2 mL Eppendorf tube, and a silver electrode (0.5 mm diameter) was inserted and fastened with

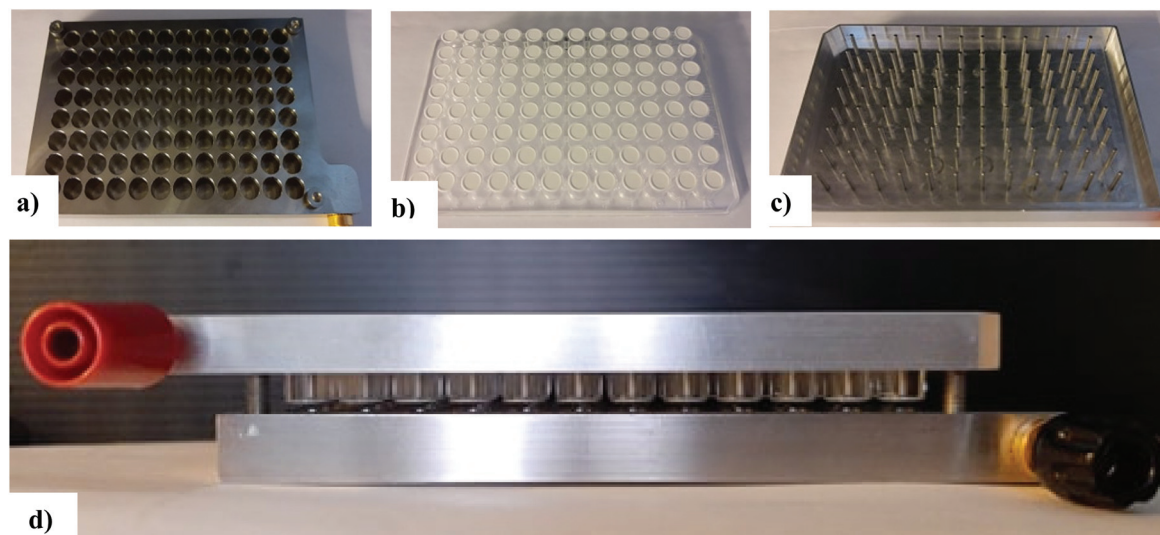


Fig. 1 96-Well EME setup. (a) 96-well waste reservoir plate, (b) 96-well filter plate, (c) 96-electrode plate, and (d) all plates clamped.

superglue. 500 μL 10 mM NaOH was pipetted into the Eppendorf tube and served as waste solution. Subsequently, the membrane was inserted into the Eppendorf tube, with a 3 mm clearance to the waste solution. 100 μL sample solution was pipetted on top of the membrane, and a silver electrode was placed in contact with the sample solution. The electrodes were connected to a power supply and the extraction setup was agitated during extraction.

2.5. Calculations

For the calculation of SDS clearance, we used the following equation:

$$\text{Clearance} = \left(\frac{-n_{\text{S,Original}} - n_{\text{S,Final}}}{n_{\text{S,Original}}} \right) \times 100\% \quad (1)$$

Here, $n_{\text{S,Original}}$ was the number of moles of SDS in the original sample prior to EME, and $n_{\text{S,Final}}$ was the number of moles of SDS left in the sample after EME.

3. Results and discussion

3.1. Operational principle

Fig. 1 illustrates the electromembrane extraction (EME) system used in this work. The complete setup consisted of a metallic 96-well waste reservoir plate, a 96-well filter plate, a 96-electrode plate, an agitator, and a power supply. The waste solution and electrode plates were laboratory-made, while the other items were commercially available. First, we pipetted 3 μL of organic solvent to a filter in the 96-well filter plate. The organic solvent immobilized in the pores due to capillary forces and served as a supported liquid membrane (SLM). Second, we pipetted 100 μL aqueous sample containing SDS into the 96-well filter plate above the SLM. Third, we pipetted 200 μL of waste solution (water or 10 mM NaOH) to a well at a corresponding position in the 96-well waste solution plate.

Finally, we clamped together the three plates like a sandwich and placed them on the agitator. We connected the power supply with the waste solution plate and the electrode plate, and we applied voltage and agitation simultaneously to initiate extraction. For the extraction of SDS (negatively charged), the waste solution plate served as the anode (+) and the electrode plate served as the cathode (-).

3.2. Extraction under sub-critical micellar concentrations

SDS forms micelles in water at concentrations higher than 0.237%.³⁷ In a first set of experiments, we performed EME from samples under sub-critical micellar conditions with 0.1% SDS (1 mg mL⁻¹) in pure water. The concentration level of SDS was between 10³ and 10⁶ times higher than typical concentrations of target substances in published EME articles.^{5,22} From previous EME experiments, alcohols are ideal SLM solvents for the extraction of negatively charged analytes.³⁸ This is mainly due to the hydrogen bond donor properties of alcohols, which promote partition of negatively charged analytes (hydrogen bond acceptors) into the SLM. Since the SLM acts as a barrier between the aqueous sample and the waste solution, the solvent should be immiscible with water in order to avoid leakage. On the other hand, $\log P$ should not exceed 5.5 in order to facilitate partition of charged compounds into the SLM.³⁹ Considering these factors, we tested 1-octanol, 1-nonanol, and 1-decanol for the extraction of SDS (Fig. 2). EME with 1-octanol as the SLM gave an SDS clearance of 64% after 10 minutes with 25 V. The higher alcohols 1-nonanol and 1-decanol were less efficient and provided 47% and 29% clearance, respectively. These differences were most likely due to differences in viscosity and polarity of the solvents, which in turn affected SDS diffusion and partition. We tested NPOE and 2-decanone, which are common EME solvents, under similar extraction conditions, but they were as expected less efficient than the alcohols (data not shown). Although we observed the

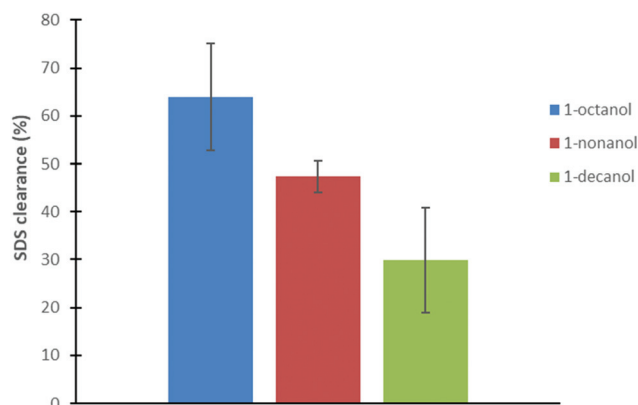


Fig. 2 SDS clearance with different SLMs. Sample solution: 100 μL 0.1% SDS in 10 mM NaOH, waste solution: 200 μL 10 mM NaOH, SLM: 3 μL organic solvent, extraction time: 10 min. Error bars represent standard deviation (SD, $n = 3$).

highest SDS clearance with 1-octanol, we continued with 1-nonanol as the SLM due to lower solubility in water. This improved the stability of the EME system as evidenced by stable extraction current as monitored during EME (current profile).

In the following experiment, we extended the extraction time from 10 to 30 minutes with 1-nonanol as the SLM. However, this did not improve the SDS clearance and the system removed no more than 50% of total SDS from the sample. Based on previous experience, the phase transfer catalyst Aliquat 336 (A336) was added to the SLM.²⁵ A336 is a lipophilic quaternary ammonium chloride salt that facilitates partition of negatively charged compounds through ionic interactions. This involves exchange of chloride ions with SDS during transfer across the SLM. With the addition of 1.0% (w/w) A336 to 1-nonanol, the SDS clearance reached 100% after 30 minutes of extraction (Fig. 3). Because the electrical resistance of the SLM decreased due to A336, the voltage was lowered to 5 V to avoid excessive electrolysis and potential

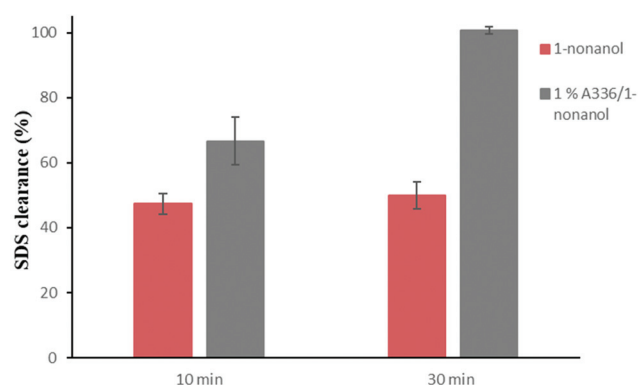


Fig. 3 SDS clearance without and with Aliquat 336 in the SLM. Sample solution: 100 μL 0.1% SDS in 10 mM NaOH, waste solution: 200 μL 10 mM NaOH, SLM: 3 μL 1-nonanol or 1.0% A336/1-nonanol, extraction time: 10 or 30 min. Error bars represent standard deviation (SD, $n = 3$).

Joule heating.⁴⁰ The average current profile for each extraction well was 40 μA after initial voltage application, followed by a slow decrease and stabilizing at approximately 30 μA . As a rule of thumb, current levels of 50 μA per extraction well should be avoided.⁴¹

3.3. Extraction under super-critical micellar concentrations

In the next series of experiments, we conducted EME from 0.5 and 1.0% solutions of SDS. Now SDS was above the critical micellar concentration (CMC). EME was conducted for 30 minutes at 5 V, with 1.0% A336 in 1-nonanol as the SLM. Surprisingly, even though the SLM was in contact with a soap-type sample solution, the SLM remained intact. Clearly, capillary forces strongly immobilized the organic solvent in the porous structure of the PVDF filters. This was evident from the stable current profile throughout the extraction and visual inspection. The EME performance was lower above the CMC, and SDS clearance was 55% and 25% for 0.5 and 1.0% SDS, respectively.

In the following experiments, we tested different approaches to increase SDS clearance from super-critical micellar concentrations. First, we increased the A336 concentration from 1.0 and up to 10% (w/w). The resistance decreased with increasing concentration of A336, and therefore voltage was decreased to 1–2 V. Similar current profiles measured with 1.0% A336 in the SLM were achieved. Interestingly, clearance was almost unaffected by the increased level of A336. Thus, while mass transfer increased significantly up to 1.0% of A336, there was no major gain above this level. Second, we replaced the waste solution after 15 minutes, but SDS clearance remained unaffected. Third, we tested replenishment of the SLM after 15 minutes, and this gave some improvement of SDS clearance. Finally, we increased the extraction time to 120 minutes with replenishment of the SLM after 60 minutes, and this provided 100% SDS clearance from 0.5% samples. When the same conditions were applied to 1.0% SDS, the clearance was 60%. With 0.5 and 1.0% samples, the appearance of the SLM changed from transparent to cloudy white during the extraction. This cloudiness was more prevalent at higher concentrations of A336 in the SLM, and it was absent when we used pure 1-nonanol as the SLM.

3.4. Mass balance considerations

To understand the observations above, we performed a set of mass balance experiments. Both the sample and the waste solution were analyzed after extraction and based on mass balance the content of SDS trapped in the SLM was calculated. As shown in Table 1, we detected no SDS in 0.1% ($\approx 1 \text{ mg mL}^{-1}$) samples after 30 minutes of EME. This confirmed 100% clearance as discussed above. Surprisingly, we detected no SDS in the waste solution. Thus, the total amount of SDS (= 0.1 mg) was trapped in the SLM. Since the volume of the SLM was 3 μL , the final SDS concentration in the SLM was 33 mg mL^{-1} .

In the following experiment, we conducted EME from 0.5% samples ($\approx 5 \text{ mg mL}^{-1}$). With this experiment, we exceeded the capacity of the system, and SDS clearance decreased to 55%.

Table 1 Distribution of SDS after 3-phase EME

SDS concentration	With voltage			Without voltage		
	0.1%	0.5%	1.0%	0.1%	0.5%	1.0%
Sample	≤0.01%	45%	71%	50%	73%	81%
SLM	99.99%	47%	23%	50%	27%	19%
Waste solution	≤0.01%	8%	5%	≤0.01%	≤0.01%	≤0.01%

SDS content in the SLM is calculated by measurements performed on donor and waste solution after EME. SLM: 100% – donor concentration (%) – acceptor concentration (%). Sample: 100 μL SDS in 10 mM NaOH, SLM: 3 μL 1% A336/1-nonanol, waste solution: 200 μL 10 mM NaOH, and extraction time: 30 min ($n = 3$).

Consequently, 45% of total SDS (total SDS = 0.5 mg) remained in the sample after extraction. With 0.5% samples, we detected 8% of the total SDS in the waste solution. Based on mass balance calculation, the SLM trapped 47% of total SDS. From 1.0% samples (total SDS = 1.0 mg), 71% of total SDS was left in the sample, 5% was detected in the waste solution, and 24% was trapped in the SLM. With both 0.5 and 1.0% samples, the SDS concentration in the SLM increased up to 80 mg mL^{-1} , and SDS concentration was about 0.5 mg mL^{-1} in the waste solution. The data with 0.5 and 1.0% samples were thus consistent.

The solubility of SDS in aqueous solution is more than 200 mg mL^{-1} ,⁴² and therefore we initially considered aqueous 10 mM NaOH as an appropriate waste solution. However, we performed a simple liquid–liquid extraction experiment, with SDS in water as the aqueous phase and 1-nonanol with 1.0% A336 as the organic phase, and this demonstrated very high partition into the organic phase (partition coefficient higher than 1000). This is in accordance with the literature.⁴² Thus, due to strong partition into the SLM, SDS transferred rapidly into the SLM, but for the same reason, transfer into the waste solution was strongly limited.

Due to the strong partition into the SLM, we repeated the mass balance experiment above without voltage (0 V). With all SDS concentrations, the SDS clearance was lower without voltage. Interestingly, without voltage, we were unable to detect SDS in the waste solution. This confirmed that the electrical field influenced the SDS partition.

3.5. Experiences with two-phase EME

Because transfer from the SLM to waste solution limited clearance capacity, we investigated a two-phase EME system in a separate set of experiments. We conducted EME from 1.0% and 0.5% SDS samples for 30 minutes, with 1-nonanol + 1.0% A336 serving both as the SLM and as the waste solution. The total volume of the organic phase was 275 μL . The electrical resistance was higher in the two-phase system, and therefore we increased the voltage to 30 V. This provided a current level of 40 μA per well, which was similar to that reported by experiments discussed in previous sections. Table 2 summarizes the experimental results. From 0.5% samples, SDS clearance was 75%, while the value decreased to 10% for 1.0% SDS samples. Conducting the same experiments with a closed circuit and 0 V, to evaluate contribution from pure diffusion, provided

Table 2 Distribution of SDS after 2-phase EME

SDS concentration	With voltage		Without voltage	
	0.5%	1.0%	0.5%	1.0%
Sample	25%	90%	51%	75%
SLM/waste solution	75%	10%	49%	25%

SDS content in the SLM is calculated by measurements performed on donor and waste solution after EME. SLM: 100% – donor concentration (%) – acceptor concentration (%). Sample: 100 μL SDS in 10 mM NaOH, SLM: 3 μL % A336/1-nonanol, waste solution: 275 μL 1% A336/1-nonanol, and extraction time: 30 min ($n = 3$).

slightly better results for the 1.0% SDS sample (25% clearance) while worse for the 0.5% sample (49% clearance).

Considering the high solubility of SDS in 1.0% A336/1-nonanol, the poor clearance both with and without voltage was surprising. However, due to the relatively large volume of organic solvents in the system, the electrical field (V cm^{-1}) in the organic phase was less than that in the 3-phase system. This probably reduced the electrokinetic transport of SDS into the organic phase. Furthermore, the fraction of organic solvents immobilized in the filter was stagnant during extraction and this seriously limited mass transfer. Thus, the mass transfer capacity of the SLM was the main bottleneck when the system was applied at high concentrations of SDS.

3.6. Experiences with an extended SLM area

In order to evaluate the SDS clearance as a function of SLM surface area, we conducted a new set of experiments with a modified EME setup. This provided an SLM area of 43 cm^2 , as compared to 28 cm^2 in the previous experiments. The membrane was made of polypropylene, which together with polyvinylidene difluoride are the most common membranes in EME. The polypropylene membrane was attached to the head of a pipette tip and functioned as a SLM and reservoir for the sample solution as described in the Experimental section. With the increase in the surface area, 10 μL organic solvent was immobilized within the pores of the SLM. As expected, with the increased SLM area, the SDS clearance increased. With 10 μL 10% A336/1-nonanol as the SLM, a voltage of 1 V, and 30 min extraction, no SDS was detected in the 0.5% SDS samples after EME. Thus, the system completely removed

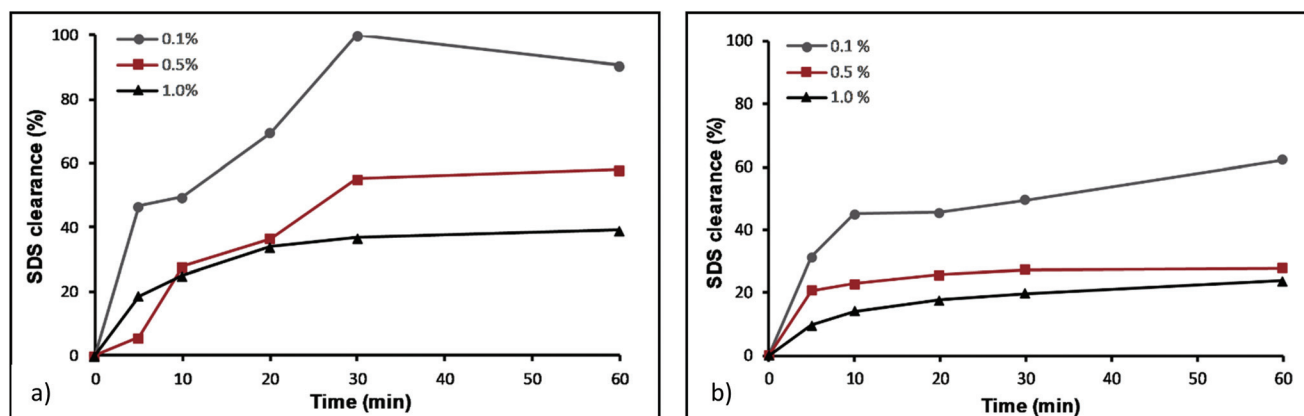


Fig. 4 SDS clearance as a function of extraction time. (a) SDS clearance with voltage and (b) SDS clearance without voltage. Sample: 100 μ L 0.1, 0.5, 1.0% SDS in 10 mM NaOH, waste solution: 200 μ L NaOH, SLM: 3 μ L 1.0% A336/1-nonanol, voltage: 5 V. RSD ($n = 3$) < 15% for all time measurements.

0.5% SDS. With 1.0% SDS, clearance was now increased to 46%.

3.7. Impact of the electrical field

To assess the impact of the electrical field on the SDS clearance, we conducted a final set of time experiments with and without voltage. The extraction conditions were similar to the ones used in section 3.4. The results are presented in Fig. 4. Both with and without voltage, SDS mass transfer was fast the first 5–10 minutes, and SDS clearance increased until 30 min and then leveled off. Thus, extending the extraction time to 60 min gave only negligible gain in SDS clearance. A comparison of data showed that kinetics was more or less unaffected by the electrical field. This is consistent with the hypothesis above that the limit of the system is the SLM capacity. However, with voltage, the clearance was significantly higher than that without voltage. This supports the fact that partition of SDS into the SLM is favored by the electrical field. Clearly, even at very high concentrations, where the extraction system was close to saturation, there are still important benefits from application of voltage across the SLM.

4. Conclusion

The present work has for the first time demonstrated removal of sodium dodecylsulfate (SDS) using electromembrane extraction (EME). Highly concentrated samples of 0.1–1.0% SDS represented both sub- and super-critical micellar concentrations. Complete SDS removal was achieved for 0.1% SDS samples using 1.0% of the ionic phase transfer catalyst Aliquat 336 in 1-nonanol as the supported liquid membrane (SLM). Complete removal of SDS from 0.5 and 1.0% samples proved more challenging, and mass transfer suffered from accumulation of SDS within the SLM. Replenishment of the SLM or increasing the surface area circumvented some of these issues and complete removal was achieved for 0.5% SDS samples.

Based on the experiences from this work, EME removal of SDS shows potential. However, due to complexity, and to obtain a full understanding of fundamentals, we currently conducted experiments with pure solutions of SDS only. Therefore, forthcoming research should test the concept with real protein samples (biological samples), to evaluate performance under the influence of a complex biological matrix, and to study the behavior of target proteins. The experiences from this work have also improved upon the understanding of EME at very high concentration levels. Under such conditions, the benefit of the electrical field and electro-kinetic migration is less, compared with similar systems operated purely by diffusion. Similar observations are reported for a few other model compounds in the literature, and may be inherently connected with EME.

Conflicts of interest

The authors declare no conflict of interest.

Acknowledgements

Financial support from UiO: Life Science is gratefully acknowledged. This work was also partially supported by the Research Council of Norway through its Centre of Excellence scheme, project number 262613.

References

- 1 S. Pedersen-Bjergaard and K. E. Rasmussen, *J. Chromatogr., A*, 2006, **1109**, 183–190.
- 2 S. Pedersen-Bjergaard and K. E. Rasmussen, *Anal. Chem.*, 1999, **71**, 2650–2656.
- 3 S. Seidi, Y. Yamini and M. Rezazadeh, *J. Pharm. Biomed. Anal.*, 2011, **56**, 859–866.

- 4 S. S. H. Davarani, A. M. Najarian, S. Nojavan and M.-A. Tabatabaei, *Anal. Chim. Acta*, 2012, **725**, 51–56.
- 5 M. R. Payán, M. Á. B. López, R. F. Torres, M. V. Navarro and M. C. Mochón, *Talanta*, 2011, **85**, 394–399.
- 6 P. Kuban and P. Bocek, *J. Chromatogr. A*, 2014, **1337**, 32–39.
- 7 C. Basheer, S. H. Tan and H. K. Lee, *J. Chromatogr., A*, 2008, **1213**, 14–18.
- 8 P. Kubáň, L. Strieglerová, P. Gebauer and P. Boček, *Electrophoresis*, 2011, **32**, 1025–1032.
- 9 C. X. Huang, A. Gjelstad and S. Pedersen-Bjergaard, *Anal. Chim. Acta*, 2015, **853**, 328–334.
- 10 H. Nsubuga, C. Basheer, M. M. Bushra, M. H. Essa, M. H. Omar and A. M. Shemsi, *J. Chromatogr. B: Anal. Technol. Biomed. Life Sci.*, 2016, **1012**, 1–7.
- 11 H. Tabani, A. R. Fakhari and E. Zand, *Anal. Methods*, 2013, **5**, 1548–1555.
- 12 M. Rezazadeh, Y. Yamini and S. Seidi, *J. Sep. Sci.*, 2012, **35**, 571–579.
- 13 R. E. Jamt, A. Gjelstad, L. E. Eibak, E. L. Oiestad, A. S. Christophersen, K. E. Rasmussen and S. Pedersen-Bjergaard, *J. Chromatogr. A*, 2012, **1232**, 27–36.
- 14 C. X. Huang, A. Gjelstad, K. F. Seip, H. Jensen and S. Pedersen-Bjergaard, *J. Chromatogr., A*, 2015, **1425**, 81–87.
- 15 Y. Liu, X. L. Zhang, L. Guo, Y. Zhang, Z. Li, Z. Y. Wang, M. F. Huang, C. Yang, J. N. Ye and Q. C. Chu, *Talanta*, 2014, **128**, 386–392.
- 16 J. Lee, F. Khalilian, H. Bagheri and H. K. Lee, *J. Chromatogr. A*, 2009, **1216**, 7687–7693.
- 17 K. Alhooshani, C. Basheer, J. Kaur, A. Gjelstad, K. E. Rasmussen, S. Pedersen-Bjergaard and H. K. Lee, *Talanta*, 2011, **86**, 109–113.
- 18 Z. Hu, H. Chen, C. Yao and Y. Zhu, *J. Chromatogr. Sci.*, 2011, **49**, 617–621.
- 19 M. Rezazadeh, Y. Yamini and S. Seidi, *J. Chromatogr. B: Anal. Technol. Biomed. Life Sci.*, 2011, **879**, 1143–1148.
- 20 S. Seidi, Y. Yamini, A. Heydari, M. Moradi, A. Esrafilii and M. Rezazadeh, *Anal. Chim. Acta*, 2011, **701**, 181–188.
- 21 X. L. Zhang, H. T. Zhang, Y. Liu, L. Guo, J. N. Ye and Q. C. Chu, *Chin. J. Chem.*, 2015, **33**, 235–240.
- 22 S. Seidi, Y. Yamini, A. Saleh and M. Moradi, *J. Sep. Sci.*, 2011, **34**, 585–593.
- 23 A. Slampova and P. Kuban, *Anal. Chem.*, 2017, **89**, 12960–12967.
- 24 P. Norouzi, M. Rezaei Akmal, Z. Mofidi, B. Larijani, M. R. Ganjali and M. Ebrahimi, *Microchem. J.*, 2019, **148**, 759–766.
- 25 M. S. Restan, M. E. Pedersen, H. Jensen and S. Pedersen-Bjergaard, *Anal. Chem.*, 2019, **91**, 6702–6708.
- 26 B. Lin, L. B. Wan, X. J. Sun, C. X. Huang, S. Pedersen-Bjergaard and X. T. Shen, *J. Membr. Sci.*, 2018, **568**, 30–39.
- 27 L. Wan, B. Lin, R. Zhu, C. Huang, S. Pedersen-Bjergaard and X. Shen, *Anal. Chem.*, 2019, **91**, 8267–8273.
- 28 P. Kubáň, *Anal. Chem.*, 2017, **89**, 8476–8483.
- 29 L. Vardal, A. Gjelstad, C. Huang, E. L. Oiestad and S. Pedersen-Bjergaard, *Bioanalysis*, 2017, **9**, 631–641.
- 30 P. Zahedi, S. S. H. Davarani, H. R. Moazami and S. Nojavan, *J. Pharm. Biomed. Anal.*, 2016, **117**, 485–491.
- 31 S. M. Hengel, E. Floyd, E. S. Baker, R. Zhao, S. Wu and L. Pasa-Tolic, *Proteomics*, 2012, **12**, 3138–3142.
- 32 R. E. Farrell, in *RNA Methodologies*, ed. R. E. Farrell, Academic Press, San Diego, 4th edn, 2010, pp. 155–172, DOI: 10.1016/B978-0-12-374727-3.00007-3.
- 33 D. Botelho, M. J. Wall, D. B. Vieira, S. Fitzsimmons, F. Liu and A. Doucette, *J. Proteome Res.*, 2010, **9**, 2863–2870.
- 34 K. R. Rupprecht, E. Z. Lang, S. D. Gregory, J. M. Bergsma, T. D. Rae and J. R. Fishpaugh, *Anal. Biochem.*, 2015, **486**, 78–80.
- 35 F. Rusconi, É. Valton, R. Nguyen and E. Dufourc, *Anal. Biochem.*, 2001, **295**, 31–37.
- 36 C. Huang, L. E. Eibak, A. Gjelstad, X. Shen, R. Trones, H. Jensen and S. Pedersen-Bjergaard, *J. Chromatogr. A*, 2014, **1326**, 7–12.
- 37 P. Mukerjee and K. J. Myse, *J. Pharm. Sci.*, 1972, **61**, 319–319.
- 38 C. Huang, A. Gjelstad and S. Pedersen-Bjergaard, *Rev. Anal. Chem.*, 2016, **35**, 169–183.
- 39 C. Huang, A. Gjelstad and S. Pedersen-Bjergaard, *J. Membr. Sci.*, 2017, **526**, 18–24.
- 40 P. Kubáň and P. Boček, *J. Chromatogr., A*, 2015, **1398**, 11–19.
- 41 S. Pedersen-Bjergaard, C. Huang and A. Gjelstad, *J. Pharm. Anal.*, 2017, **7**, 141–147.
- 42 J. M. Pollard, A. J. Shi and K. E. Göklen, *J. Chem. Eng. Data*, 2006, **51**, 230–236.

III

Quantitative Ramanomics for chemometric phenotyping of three-dimensional liver organoids.

Vernon LaLone^{1,2,*} and Aleksandra Aizenshtadt^{3*}, John Goertz¹, Frøydis Sved Skottvoll⁴, Marco Barbero Mota¹, Junji You¹, Xiaoyu Zhao¹, Henriette Engen Berg⁴, Justyna Stokowiec³, Minzhi Yu^{5,6}, Anna Schwendeman^{5,6}, Hanne Scholz^{3,8,9}, Steven Ray Wilson^{3,4}, Stefan Krauss^{3,7**}, and Molly Stevens^{1,2**}

¹Department of Materials, Department of Bioengineering and Institute of Biomedical Engineering, Imperial College London, London, SW7 2AZ, UK.

²Hybrid Technology Hub-Centre of Excellence, Imperial College London, London, SW7 2AZ, UK.

³Hybrid Technology Hub-Centre of Excellence, Institute of Basic Medical Sciences, Faculty of Medicine, University of Oslo, P.O. Box 1112 Blindern, NO-0317 Oslo, Norway.

⁴Department of Chemistry, University of Oslo, P.O. Box 1033, Blindern, NO-0315 Oslo, Norway.

⁵Department of Pharmaceutical Sciences, University of Michigan, Ann Arbor, Michigan 48109, USA.

⁶Biointerfaces Institute, University of Michigan, Ann Arbor, Michigan 48109, USA.

⁷Department of Immunology and Transfusion Medicine, Oslo University Hospital, P.O. Box 4950 Nydalen, 0424, Oslo, Norway.

⁸Department of Transplant Medicine, Oslo University Hospital, Oslo, Norway.

⁹Institute for Surgical Research, Oslo University Hospital, Oslo, Norway.

*shared first authorship

**shared senior authorship

Abstract

Quantitative chemometric imaging tools for validating the composition, functional maturity, disease progression and response to therapeutic interventions are of significant interest in the rapidly expanding organoid arena. Raman spectral imaging (RSI) allows high-content, label-free detection of tell-tale biomolecules, but requires reliable quantification of deconvoluted spectra to unfold its full potential. Herein, we first develop an integrated bioanalytical methodology, qRamanomics, to qualify RSI as a tool for quantitative chemotyping by abundance and distribution of major classes of biomolecules. Next, we apply qRamanomics to 3D liver organoids to assess specimen variation, chemometric distribution, and maturity. We then demonstrate the utility of qRamanomics for identifying biomolecular response signatures from a panel of liver altering drugs, probing drug-induced compositional changes in 3D liver organoids followed by *in situ* monitoring of drug metabolism/accumulation. qRamanomics comprises an important step in expanding RSI technology towards quantitative label-free interrogation of 3D biological specimens.

Introduction

There is a significant need for development of reliable human organ representations (termed organoids) that provide bio-relevant model systems with foreseeable utility in drug discovery and disease modelling. Induced pluripotent stem cell (iPSC) technology enables *in vitro* development of human organoids that show features of the organs they represent. However, most current organoids lack the structure and functional maturity of their human counterparts and show significant intra- and inter-batch variations. Hence, there is a need for advancing supervised organoid characterization, including their response to therapeutic interventions, by applying high-content and high-resolution imaging tools¹.

Confocal Raman spectral imaging (RSI), measuring predominantly the vibrational modes of molecules, can enable high content label-free visualization of a wide span of molecules in biological specimen without sample preparation. This phenomenon may be exploited in fixed and living tissues as the emitted spectral information is reported to remain consistent². Recently, RSI has been successfully applied for assessing cell differentiation³⁻⁵, and for quantitative characterization of tissue-engineered and native cartilage and bone⁶⁻⁸. Furthermore, the utility of RSI was demonstrated through direct measurements of drugs and drug metabolites, with sub-cellular resolution, in selected cell lines including cancer cells (BaF3/BCR-ABL1, SK-BR-3, NCI-H1975, Calu-3) and macrophages (raw 264.7)⁹⁻¹². Despite this progress, the full potential of biospecimen analysis by RSI is hindered by a modest sensitivity and demanding unmixing of signals derived from complex biological matrices. In addition, reliable quantification has been challenging. As a significant step to address these challenges, quantitative volumetric Raman imaging (qVRI) was previously developed for analysis of individual mesenchymal stem cells in 3D biomaterials¹³ offering volumetric insight into the size of subcellular features without, however, providing information of local concentrations of biomolecules. The role of localized concentrations and biomolecular density at the single-cell and subcellular levels is gaining attention as a relevant phenotypic parameter important to cell-type specific functions^{14,15}. Quantitation at the single-cell level remains a topic of debate throughout the Raman community due to the absence of reliable calibration standards and standardized preprocessing algorithms^{16,17}.

Building on the work of LaLone et al.¹⁸ and Kuzmin, Pliss and Prasad¹⁹ we herein present the development of a robust calibrated bioanalytical platform for quantitative chemometric phenotyping by confocal RSI of biological specimen ranging from single cells to complex 3D organoids. The methodology, termed quantitative Ramanomics (qRamanomics), allows direct structural and quantitative compositional characterization of biological specimens in absolute biochemical measurements with nanoscale spatial resolution²⁰. We apply qRamanomics to iPSC-derived 3D hepatic organoids, benchmarked to primary human hepatocyte spheroids, with the goal of interrogating their state of maturation, response to drug challenges and drug metabolism. Our work addresses a currently unmet analytical need and paves the way for further advances in supervised organoid development and tracking.

Results

Quantitative chemometric phenotyping of distribution, abundance, and co-localization of all major class of biomolecules in 3D biospecimens - qRamanomics.

To develop a strategy for quantitative chemometric unmixing of Raman spectra from organoids, we designed a 3D tissue phantom calibration technology which enables direct simultaneous measurement of absolute local concentrations of the most abundant biomolecular components and sequestered xenobiotics.

First, a spectral pre-processing algorithm to normalize and correct for liquid water signal was developed and employed to prepare all Raman data presented in this study in a robust and repeatable manner (Fig. 1a). Employing the OH stretch band in Raman spectra of liquid water ($3,400\text{ cm}^{-1}$)²¹, all analyte Raman signals were normalized relative to the aqueous matrix, thereby accounting and correcting for singularities of each data voxel. The underlying assumption was that the water content remains constant within the excitation voxel sampling volume (~ 5 femtolitres) across linear quantitation ranges of biomolecule concentration. However, when an analyte concentration exceeds aqueous solubility, phase separation may occur and, in this case, the quantitative accuracy of the model becomes difficult to verify with this current iteration of calibration technology. Nevertheless, measurements beyond the upper range of biomolecule calibration standard phantoms are presented under the assumption that linearity remains constant.

Next, common biomolecular components of eukaryotic cells were formulated as single-component and multi-component tissue phantoms containing a range of concentrations of proteins (10-300 mg/mL), saturated (5-80 mg/mL) and monounsaturated (5-50 mg/mL) lipids, DNA (10-60 mg/mL), and glycogen (10-100 mg/mL) in PBS to represent 3D tissue phantoms. The poor solubility of lipids in aqueous media was resolved by employing formulated saturated (DPPC) and monounsaturated (POPC) synthetic high-density lipoprotein nanodiscs (sHDLs) of ~ 10 nm particle diameter as previously described¹⁸. The nanoscale particle size distribution of DPPC and POPC sHDLs was comparable to albumin and substantially smaller than conventional tissue phantom intra-lipid emulsions as revealed by dynamic light scattering (DLS). This allowed dissolution of lipids up to 80 mg/mL and facilitated miscibility with other biomolecules at varying concentrations in PBS (Fig. 1b)²². 3D phantoms were subsequently analysed in z-dimension to assess the depth-dependant depletion of scattered Raman signals and served as quantitative calibration standards for Raman cytometry.

Analysis of the 3D tissue phantoms was carried out using the state-of-the-art confocal Raman chemical imaging system (WITec, Ulm, Germany, Model alpha300RA) in reflected analysis mode, whereby an excitation laser scans the specimen of interest from above and scattered Raman signals are emitted and acquired back through the same objective lens (Fig. 1c). This approach enabled calibration imaging datasets elucidating sample homogeneity and signal interference profiles as a function of 3D imaging depth. The signal-to-noise ratio (SNR) was calculated as a function of depth across various concentrations and compositions of tissue phantoms. The calibration was repeated across concentration ranges for protein, DPPC, POPC, DNA, and glycogen. Pre-processed spectra yielded linear relationships across relevant ranges of concentrations. To estimate normalized Raman intensity per mg/mL, unit-scaled reference spectra were generated from linear relationships of pre-processed spectra across bio-relevant concentration ranges (Fig. 1d). The complete unit-scaled reference

spectral model accurately identified and deconvoluted single-component tissue phantom data with minimal errors using linear combination modelling approaches. Bayesian model fitting enabled accuracy and precision confidence assessments across measured concentration ranges (Fig. 1e and Extended Data Fig. 1a) and specificity in complex multi-component mixtures for model validation (Fig. 1f and Extended Data Fig. 1b). The two most important sources of potential error in this calibration system were the accuracy of actual concentrations in the calibration standards (i.e., “ground truth”) and misfitting errors associated with statistical unmixing of preprocessed Raman spectra. Regardless, the fundamental linear theory presented herein establishes a robust framework for quantitative analysis of 3D biospecimens.

Quantitative high-content assessment of 3D liver biospecimens by qRamanomics.

To demonstrate the potential of qRamanomics, primary human hepatocyte spheroids (3D PHH) and iPSC-derived hepatocyte-like cell containing organoids (3D iHLC) were generated using modified differentiation protocols to ensure functional maturation (Fig. 2a). 3D Raman hyperspectral image datasets were acquired from both models via continuous scanning of laser voxel in raster pattern across a series of image planes in a z-stack achieving optimal possible spatial resolution of ~500 nm in x-y and ~1 μm in z-plane. The depth of reliable data acquisition was limited to 50 μm to ensure adequate SNR for accurate spectral unmixing and quantification. This approach allowed reliable acquisition of high-content Raman hyperspectral datasets with nanoscale spatial resolution (Fig. 2b). The complete specimen dataset presented in this work was pre-processed as described above (up to 30,000 spectra per specimen). Endmember spectra were identified and classified as “pure” component signals and identities were assigned according to typical biomolecule signatures, apart from nucleic acids (N.A.) as these compounds nearly always associate with various proteins (histones, ribosomes, etc.) within typical eukaryotic cells (Fig. 2c). All endmember reference spectra were unit-scaled according to the calibration model (Fig. 2d) and used to translate the specimen spectral data into local concentration measurements of proteins, lipids (saturated, monounsaturated, unsaturated), nucleic acids, glycogen, and cytochrome c (cyt c). The cyt c signal was included in the quantitative model by dissolving 100 $\mu\text{g}/\text{mL}$ cytochrome c in PBS to elucidate the concentration-dependent signal intensity (a.u. per $\mu\text{g}/\text{mL}$). The quantitative data set was subsequently combined into a 3D representation showing the spatial distribution and relation of each component (Fig. 2e). Adjusting the acquisition spatial resolution and voxel dwell time (spectral integration time) enabled SNR improvement and resolution of intracellular features such as nuclei, organelles, and lipid droplets (Fig. 2f).

We next employed the qRamanomics methodology for high-content quantitative comparison of 3D PHH and 3D iHLC specimens to determine quantitative and qualitative differences between both. 3D PHHs were created by standardized hepatocyte aggregation²³. 3D iHLC were generated as highly reproducible 3D structures with significant metabolic maturity²³ (Extended Data Fig. 2a-c). 3D iHLC faithfully expressed hepatocyte-specific markers (Fig. 3a, c) and produced albumin at comparable levels as 3D PHH (n = 3) while the concentration of urea remained ~50 % lower than in 3D PHH cultures (Fig. 3d). A comprehensive proteomics analysis confirmed that 3D iHLC closely resembled 3D PHH (Fig. 3b and Extended Data Fig. 2e,f) and demonstrated the presence of most phase I enzymes, as well as phase II enzymes and transporters (Fig. 3b). 3D iHLC exhibit CYP3A4 and CYP1A2 enzymatic activity, albeit at a level lower than in PHH spheroids (Fig. 3e). Hence, our differentiation protocol allowed

generation of 3D hepatic representations suitable for the testing of qRamanomics as a benchmarking tool.

For comparing of 3D iHLC and 3D PHH by qRamanomics a total of >130 hyperspectral images were pre-processed and deconvoluted to quantitatively map density distribution of biomolecules in 3D (Fig. 3f). Despite variance in spheroid-to-spheroid size (Extended Data Fig. 2e, %CV from 63 to 82% for iHLC, from 64% to 90% for PHH, depending on iPSC line and donor correspondingly), distribution of measurements remained consistent within each group and revealed statistically significant tell-tale differences between 3D PHHs and 3D iHLCs (Fig. 3g, Extended Data Fig.3.), allowing chemometric benchmarking of heterogeneity and maturation markers at a sub-cellular level.

Spatial correlation chemometric heat maps provided a derivative measurement of a 3D specimen's composition and allowed a deeper understanding of molecular content distribution (Fig. 3h)²⁴⁻²⁶. Generated chemometric scatter plots show total lipid, glycogen, and cyt c levels plotted against the local protein content, the conventional standard for normalization in traditional bulk biochemical assays (Fig. 3i). Furthermore, the scatter plots visualized the chemometric phenotype and homogeneity therein of iHLC as compared to PHH, providing data-rich, label-free, direct characterization of 3D tissue representations with foreseeable utility as a quality control tool.

In summary, qRamanomics revealed similar patterns of glycogen accumulation between 3D iHLC and 3D PHH, an important hallmark of hepatocytes functionality and essential for the maintenance of glucose homeostasis. No significant differences were observed in total lipid content. Remarkably, qRamanomics identified similar levels of cyt c, the mitochondrial respiratory chain heme protein in 3D PHHs and iHLCs, indicating a substantial maturity of the iHLC generated with our protocol. Proteomics confirmed presence of citric cycle enzymes and mitochondrial respiratory chain components in 3D iHLC (Extended Data Fig. 2d). Oxidative phosphorylation is characteristic for metabolism of differentiated and adult cells, while fetal and stem cells mostly rely on glycolytic metabolism^{28,52}. However, qRamanomics revealed lower protein concentration, a marker for functional activity, per iHLC organoids as compared to the benchmark PHH spheroids. Lower protein concentrations were subsequently confirmed by UV-spectroscopy and proteomics (Fig. 3b).

qRamanomics reveals compositional phenotypic changes in 3D liver representations in response to drug exposure.

Next, we applied the platform for quantitative chemometric phenotyping of 3D PHHs and 3D iHLCs upon exposure to a panel of drugs with reported impact on hepatocytes. Hitherto, coherent anti-Stokes Raman spectroscopy (CARS) has only been used for quasi-quantitative imaging drug-induced lipid accumulation in the mouse liver²⁷.

3D PHHs and 3D iHLCs were exposed to 10 μ M amiodarone, nilotinib, fluticasone-propionate, ketoconazole, neratinib, and methadone for 48 h prior to analysis. qRamanomics elucidated drug-specific compositional changes induced in 3D PHH and 3D iHLC (Fig. 4, Extended Data Fig. 4 and Extended Data Fig. 5, correspondingly). We faithfully observed a drug-specific modulation of lipid content in all treatment groups, with marked increases in the amiodarone- and nilotinib-treated groups^{28,29} (Fig. 4b). Moreover, elevated levels of glycogen, as well as changes in cyt c levels (Fig.4b) and its co-localization with DNA, proteins, and lipids were seen in drug-treated groups (Fig.4a). Hepatic

carbohydrate metabolism, including glycogen accumulation is reported to be impaired by pathological processes and xenobiotic exposure⁴⁵⁻⁵⁰. Hence, qRamanomics offers a powerful tool for the further studying of drug/disease-induced changes in hepatic carbohydrate metabolism. Except level of glycogen accumulation (lower in 3D iHLC as compared to 3D PHH) drug-induced changes in both liver models were similar, suggesting drug responses in iHLCs closely mimicked those in PHHs.

We next analysed in more detail the alterations after exposure to 10 μ M amiodarone - a commonly used model hepatotoxic drug³⁶ leading to microvesicular steatosis and phospholipidosis^{37,38} (Extended Data Fig. 6d-e). Accordingly, quantitative 3D chemical maps illustrated changes of monounsaturated lipids in the amiodarone-treated 3D PHH and 3D iHLCs (Fig. 4c,d, Extended Data Fig. 5a) with consistent increase of lipid-containing voxel frequency. Among all tested drugs, amiodarone treatment induced the most significant changes in glycogen (increase) and cyt c concentrations (decrease) (Fig. 4e). Decrease in cyt c content may be a consequence of previously described amiodarone-induced mitochondrial toxicity and an inhibition of the mitochondrial respiratory chain³⁹. To the best of our knowledge, amiodarone-induced glycogenesis has not yet been reported. Significantly elevated glycogen and decreased cyt c were also observed in 3D PHHs treated with ketoconazole. qRamanomics results were confirmed by measuring a decrease in ATP content and albumin production in 3D PHHs and iHLCs (Extended Data Fig. 6b,c). While the mechanistic link between drug induced toxicity and intracellular drug-lipid accumulation, as well as glycogen accumulation, is not currently well understood, qRamanomics is well-suited as a bioanalytical tool to further explore drug induced quantitative chemometric alterations in unprecedented resolution.

In situ detection of xenobiotic deposits.

Beyond biomolecular phenotyping upon drug exposure, qRamanomics enables direct measurement of contextual drug and metabolite accumulation within cells. Unique molecular vibrations arising from xenobiotics can be set in context with the above deconvoluted and quantifiable biomolecule spectra. Herein we report the first spectroscopic evidence of xenobiotic deposits of amiodarone and fluticasone detectable by RSI within the 3D biospecimens along with evidence of nilotinib and neratinib accumulation (Fig. 5a-d) while no deposits were detected in the ketoconazole or methadone treatment groups (Extended Data Fig. 4, Extended Data Fig. 5). Kernel-density probability estimates for unmixed deposit spectra revealed composition and relative abundance of deposit-associated biomolecular matrices. Each compound exhibited unique drug-biomolecule complexes as determined by the relative abundance of lipid/protein in each pixel, thereby further elucidating xenobiotic-cell interactions. Subtracting the biomolecule signals from detected deposits provided spectra for “pure” unmixed deposits. Comparison of unmixed deposit spectra with parent drug reference spectra revealed differences attributable to changes in molecular bond/structure of molecule, as was the case for nilotinib, fluticasone-propionate, and neratinib. These spectroscopic changes could be evidence of drug metabolism as previously described for neratinib in cancer cells¹².

On the example of neratinib and its metabolites we investigated xenobiotics accumulation in further detail in 3D liver representations. The presence of neratinib and its metabolites was independently confirmed in both organoid pellets and supernatant by high performance liquid chromatography-mass spectrometry (LC-MS) (Extended Data Fig. 7f, Supplementary Fig. 2). Due to the wavelength of the fluorescence signals of neratinib, Raman data were acquired with a 785 nm excitation laser (instead

of 532 nm as previously described) and quantified using the qVRI. Raman image segmentation using ilastik software⁴⁰ allowed 3D visualization (Fig. 5e) and volumetric measurements of the neratinib metabolite deposits (Fig. 5f) and revealed deposits smaller than the volume of typical hepatocytes (<3500 μm^3) indicative of intracellular localization (Fig. 5g). High-resolution qVRI imaging enabled clear distinction of nuclei and verified particle size distribution measurements (Fig. 5h). The strong fluorescence signal of neratinib/metabolites allowed an independent confirmation of neratinib/metabolite accumulation by confocal imaging (Extended Data Fig. 7c) which unlike RSI, cannot reveal chemical composition of deposits and is applicable for a limited number of drugs with strong fluorescence (from our panel – only neratinib). Nevertheless, confocal microscopy reveals an accumulation of xenobiotics in lysosomes as marked by the lysosomal membrane protein LAMP1 (Extended Data Fig. 7d). High-resolution qVRI also suggested that larger deposits represent metabolites excreted into the bile canaliculi-like structures, observed in both 3D PHHs and 3D iHLC (Extended Data Fig. 7e). Therefore, lysosomal accumulation and phospholipidosis (Extended Data Fig. 6a,b) are proposed as possible mechanisms of neratinib-induced toxicity⁴¹.

In summary, for drugs identifiable by RSI, a label-free spatial and temporal “snap-shot” of a drug's presence and processing is now available, comprising factors including drug/metabolite abundance and spatial distribution in the context of drug-induced changes in 3D hepatic representations.

Conclusion

qRamanomics provides a novel solution to address the current need for quantitative in-depth chemotypic characterization of 3D tissue representations with unprecedented resolution and represents a significant advancement in the field of Raman-based biomedical research. Further development of instrumental calibration technology is still necessary to facilitate inter-laboratory comparisons of Raman cytometry data and harmonize Ramanomics at the global level⁴². qRamanomics opens the doors of scientific perception to the unadulterated biomolecular realm within living cells and tissues, thereby enabling more stringent development of 3D bioengineered living systems. As a next step, the technology described here will be advanced towards measurements on living 3D structures to enable chemotyping and benchmarking of living organoid cultures.

References

1. Yin, X. *et al.* Engineering Stem Cell Organoids. *Cell Stem Cell* **18**, 25–38 (2016).
2. Meade, A. D. *et al.* Studies of chemical fixation effects in human cell lines using Raman microspectroscopy. *Analytical and Bioanalytical Chemistry* **396**, 1781–1791 (2010).
3. Hsu, C.-C. *et al.* A single-cell Raman-based platform to identify developmental stages of human pluripotent stem cell-derived neurons. *Proceedings of the National Academy of Sciences* **117**, 18412 (2020).
4. Giuseppe, P. *et al.* Spectroscopic label-free microscopy of changes in live cell chromatin and biochemical composition in transplantable organoids. *Science Advances* **7**, eabj2800 (2021).

5. Geng, J. *et al.* Tracking the Differentiation Status of Human Neural Stem Cells through Label-Free Raman Spectroscopy and Machine Learning-Based Analysis. *Analytical Chemistry* **93**, 10453–10461 (2021).
6. Albro, M. B. *et al.* Raman spectroscopic imaging for quantification of depth-dependent and local heterogeneities in native and engineered cartilage. *npj Regenerative Medicine* **3**, 3 (2018).
7. Gentleman, E. *et al.* Comparative materials differences revealed in engineered bone as a function of cell-specific differentiation. *Nature Materials* **8**, 763–770 (2009).
8. Bergholt, M. S. *et al.* Raman Spectroscopy Reveals New Insights into the Zonal Organization of Native and Tissue-Engineered Articular Cartilage. *ACS Central Science* **2**, 885–895 (2016).
9. Fu, D. *et al.* Imaging the intracellular distribution of tyrosine kinase inhibitors in living cells with quantitative hyperspectral stimulated Raman scattering. *Nature Chemistry* **6**, 614–622 (2014).
10. Woldemichael, T. *et al.* Reverse Engineering the Intracellular Self-Assembly of a Functional Mechanopharmaceutical Device. *Scientific Reports* **8**, 2934 (2018).
11. Baik, J. & Rosania, G. R. Molecular Imaging of Intracellular Drug–Membrane Aggregate Formation. *Molecular Pharmaceutics* **8**, 1742–1749 (2011).
12. Aljakouch, K. *et al.* Raman Microspectroscopic Evidence for the Metabolism of a Tyrosine Kinase Inhibitor, Neratinib, in Cancer Cells. *Angewandte Chemie International Edition* **57**, 7250–7254 (2018).
13. Kallepitis, C. *et al.* Quantitative volumetric Raman imaging of three dimensional cell cultures. *Nature Communications* **8**, 14843 (2017).
14. Oh, S. *et al.* Protein and Lipid Mass Concentration Measurement in Tissues by Stimulated Raman Scattering Microscopy. *bioRxiv* 629543 (2021) doi:10.1101/629543.
15. Neurohr, G. E. & Amon, A. Relevance and Regulation of Cell Density. *Trends in Cell Biology* **30**, 213–225 (2020).
16. Storey, E. E. & Helmy, A. S. Optimized preprocessing and machine learning for quantitative Raman spectroscopy in biology. *Journal of Raman Spectroscopy* **50**, 958–968 (2019).
17. Afseth, N. K., Segtnan, V. H. & Wold, J. P. Raman Spectra of Biological Samples: A Study of Preprocessing Methods. *Applied Spectroscopy* **60**, 1358–1367 (2006).
18. LaLone, V. *et al.* Inkjet-printed micro-calibration standards for ultraquantitative Raman spectral cytometry. *Analyst* **144**, 3790–3799 (2019).
19. Kuzmin, A., Pliss, A. & Prasad, P. Ramanomics: New Omics Disciplines Using Micro Raman Spectrometry with Biomolecular Component Analysis for Molecular Profiling of Biological Structures. *Biosensors* **7**, 52 (2017).
20. Ember, K. J. I. *et al.* Raman spectroscopy and regenerative medicine: a review. *npj Regenerative Medicine* **2**, 12 (2017).

21. Hu, Q., Zhao, H. & Ouyang, S. Understanding water structure from Raman spectra of isotopic substitution H₂O/D₂O up to 573 K. *Physical Chemistry Chemical Physics* **19**, 21540–21547 (2017).
22. Kuai, R., Ochyl, L. J., Bahjat, K. S., Schwendeman, A. & Moon, J. J. Designer vaccine nanodiscs for personalized cancer immunotherapy. *Nature Materials* **16**, 489–496 (2017).
23. Overeem, A. W. *et al.* Pluripotent stem cell-derived bile canaliculi-forming hepatocytes to study genetic liver diseases involving hepatocyte polarity. *Journal of Hepatology* **71**, 344–356 (2019).
24. Ma, C. *et al.* Single cell Raman spectroscopy to identify different stages of proliferating human hepatocytes for cell therapy. *Stem Cell Research & Therapy* **12**, 555 (2021).
25. Giuseppe, P. *et al.* Spectroscopic label-free microscopy of changes in live cell chromatin and biochemical composition in transplantable organoids. *Science Advances* **7**, eabj2800 (2021).
26. Levchenko, S. M., Kuzmin, A. N., Pliss, A., Qu, J. & Prasad, P. N. Macromolecular Profiling of Organelles in Normal Diploid and Cancer Cells. *Analytical Chemistry* **89**, 10985–10990 (2017).
27. Le, T. T., Ziemba, A., Urasaki, Y., Brotman, S. & Pizzorno, G. Label-free Evaluation of Hepatic Microvesicular Steatosis with Multimodal Coherent Anti-Stokes Raman Scattering Microscopy. *PLoS ONE* **7**, e51092 (2012).
28. Sadiq, S. *et al.* Nilotinib-induced metabolic dysfunction: insights from a translational study using in vitro adipocyte models and patient cohorts. *Leukemia* **33**, 1810–1814 (2019).
29. Antonini, J. M. & Reasor, M. J. Accumulation of amiodarone and desethylamiodarone by rat alveolar macrophages in cell culture. *Biochemical Pharmacology* **42**, S151–S156 (1991).
30. Breccia, M. *et al.* Impaired fasting glucose level as metabolic side effect of nilotinib in non-diabetic chronic myeloid leukemia patients resistant to imatinib. *Leukemia Research* **31**, 1770–1772 (2007).
31. Torres, M. & López, D. Liver glycogen storage associated with uncontrolled type 1 diabetes mellitus. *Journal of Hepatology* **35**, 538 (2001).
32. Zdenek Racil *et al.* Mechanism of impaired glucose metabolism during nilotinib therapy in patients with chronic myelogenous leukemia. *Haematologica* **98**, e124–e126 (2013).
33. Allende, D. S. *et al.* Glycogenesis is common in nonalcoholic fatty liver disease and is independently associated with ballooning, but lower steatosis and lower fibrosis. *Liver International* **41**, 996–1011 (2021).
34. Chatila, R. & West, B. A. Hepatomegaly and Abnormal Liver Tests Due to Glycogenesis in Adults with Diabetes. *Medicine* **75**, (1996).
35. He, F. *et al.* NRF2 activates growth factor genes and downstream AKT signaling to induce mouse and human hepatomegaly. *Journal of Hepatology* **72**, 1182–1195 (2020).
36. Szalowska, E., van der Burg, B., Man, H.-Y., Hendriksen, P. J. M. & Peijnenburg, A. A. C. M. Model Steatogenic Compounds (Amiodarone, Valproic Acid, and Tetracycline) Alter Lipid Metabolism by Different Mechanisms in Mouse Liver Slices. *PLoS ONE* **9**, e86795 (2014).

37. Anthérieu, S., Rogue, A., Fromenty, B., Guillouzo, A. & Robin, M.-A. Induction of vesicular steatosis by amiodarone and tetracycline is associated with up-regulation of lipogenic genes in heparg cells. *Hepatology* **53**, 1895–1905 (2011).
38. Hinkovska-Galcheva, V. *et al.* Inhibition of lysosomal phospholipase A2 predicts drug-induced phospholipidosis. *Journal of Lipid Research* **62**, (2021).
39. Felser, A., Blum, K., Lindinger, P. W., Bouitbir, J. & Krähenbühl, S. Mechanisms of Hepatocellular Toxicity Associated with Dronedarone—A Comparison to Amiodarone. *Toxicological Sciences* **131**, 480–490 (2013).
40. Berg, S. *et al.* ilastik: interactive machine learning for (bio)image analysis. *Nature Methods* **16**, 1226–1232 (2019).
41. Paracha, N. *et al.* Evaluating the clinical effectiveness and safety of various HER2-targeted regimens after prior taxane/trastuzumab in patients with previously treated, unresectable, or metastatic HER2-positive breast cancer: a systematic review and network meta-analysis. *Breast Cancer Research and Treatment* **180**, 597–609 (2020).
42. Guo, S. *et al.* Comparability of Raman Spectroscopic Configurations: A Large Scale Cross-Laboratory Study. *Analytical Chemistry* **92**, 15745–15756 (2020).
43. Liu, W. *et al.* Metabolic profiles of neratinib in rat by using ultra-high-performance liquid chromatography coupled with diode array detector and Q-Exactive Orbitrap tandem mass spectrometry. *Biomedical Chromatography* **32**, e4272 (2018).

Methods

Biomolecular tissue phantoms as 3D quantitative calibration standards.

Tissue phantoms are artificial structures that mimic tissue-like properties, commonly mechanical or optical, in a reliable and reproducible way, widely used to test instrumental performance. Aqueous-based gels containing known concentrations of the most abundant cellular biomolecules were formulated in PBS. Bovine serum albumin (BSA) (Sigma Aldrich) was selected as protein representative due to its inexpensiveness, high water solubility and miscibility with other biomolecules. Synthetic high-density lipoproteins (sHDL) composed of 22A peptide (PVLDLFRELLNELLEALKQKLK) and DPPC or POPC were prepared by a co-lyophilization procedure. Briefly, peptide and phospholipid were dissolved in glacial acetic acid, mixed at 1:2 wt/wt ratio, and lyophilized overnight. The powder was rehydrated with water to make 80 mg mL⁻¹ (based on DPPC concentration) sHDL or 50 mg mL⁻¹ (based on POPC concentration) and thermocycled. For DPPC the procedure was between 50 °C (10 min) and room temperature (10 min) thrice and for POPC it was room temperature (10 min) and ice bath (10 min) thrice to facilitate sHDL formation. The resulting HDL complexes were diluted to 1 mg mL⁻¹ (based on peptide concentration) with water and analyzed by gel permeation chromatography (GPC) for purity using 7.8 mm × 30 cm Tosoh TSK gel G3000SWxl column (Tosoh Bioscience) with 1 mL min⁻¹ flow rate (PBS pH 7.4). Free peptide and sHDL peaks were detected at 220 nm. The sHDL hydrodynamic diameters were determined in water at 1 mg mL⁻¹ by dynamic light scattering (DLS) using a Zetasizer Nano ZSP, Malvern Instruments (Westborough, MA). The volume intensity average values (±SD) were reported.

Intralipid 20% (Sigma-Aldrich, I141-100ML) was initially employed as lipid reference but was excluded from the model due to quantitative inconsistencies resulting from larger particle size of the emulsion formulation as compared with HDLs. In the case of nucleic acids, commercially available salmon testes DNA (Sigma-Aldrich, St. Louis, MO, USA) was diluted in deionized water at 50 °C and pH 8 prior to gelation. BSA and IL were also subjected to dynamic light scattering (DLS) analysis (Zetasizer Nanoseries, Malvern Instruments, Ltd) to ensure homogeneity and discard molecular aggregation. Cytochrome c (cyt c) signals were included in the quantitative model (after detection in biological specimens) by dissolving 100 µg/mL cytochrome c (Sigma-Aldrich, C3131-50MG) in PBS to elucidate the concentration-dependent signal intensity (a.u. per µg/mL). Cyt c signals are commonly reported in various biospecimens and yield signals ~1,000-fold stronger than other biomolecules due to resonance Raman effect when excited with 532 nm light^{1,2,3}.

Raman spectral acquisition.

All spectra were acquired using a WITec alpha 300 R+ Raman confocal microspectrometer (Ulm, Germany) equipped with a piezoelectric stage (UHTS 300, WITec, GmbH.), 50X air objective lens (Zeiss EC EPIPLAN, N.A. = 0.75), 63x water immersive objective lens (Zeiss W Plan Aplanachromat 63X, N.A = 1), green solid-state excitation laser ($\lambda = 532$ nm, 32 mW, WITec, GmbH.) and an imaging spectrograph (Newton, Andor Technology Ltd. UK) equipped with a 600 groove/mm grating and a thermoelectrically cooled (60 °C) charged-coupled detector (CCD) optically connected to the objective through a 10 μ m diameter single mode silica fiber-optic cable. This setup enabled acquisition of spectral data across a wavenumber range from 0-3600 cm^{-1} . Raman depth scans of tissue phantom calibration set were performed by first locating the highest SNR laser focal plane for sample excitation at the tissue phantom surface, followed by continuous scanning data acquisition through the depth profile of interest at each x-z position. Similarly, z-stacks for quantitative chemometric profiling were acquired sequentially with 10 μ m step size, starting from the sample surface. Each stack was acquired in raster pattern as a 100*100 x-y 2D hyperspectral image with 2 μ m spatial resolution. In all cases, the excitation laser intensity was kept constant between sample scans, as well as integration time of 0.25 s.

Spectral preprocessing.

All acquired Raman spectra were preprocessed in WITec ProjectFIVE 5.2 and Matlab following the same pipeline on a per pixel basis: cosmic ray removal (filter size: 4; dynamic factor: 4.1), setting minimum value in Rayleigh region (-150 - 50 cm^{-1}) to zero (detector dark current to zero), normalization setting the main water peak average value (3220–3420 cm^{-1}) equal to one, matrix/medium background subtraction using a matrix blank (i.e., 1 % agarose (w/v) in PBS), and rolling circle baseline correction (shape size: 300) to remove any other non-specific background signal artifacts. Finally, all spectra were cropped from 400 - 3100 cm^{-1} while also ignoring the biological "silent region" from subsequent unmixing (1800 - 2700 cm^{-1}).

Spectral unmixing via linear combination modelling.

The spectroscopic unmixing problem for any Raman spectrum can be described as

$$\mathbf{y}_i = \mathbf{X}\boldsymbol{\beta}_i + \mathbf{e}_i \quad (2)$$

or in matrix form as

$$\mathbf{Y} = \mathbf{X}\mathbf{B} + \mathbf{E} \quad (3)$$

Where \mathbf{y}_i is the i -th $m \times 1$ sample spectrum of the unfolded Raman image dataset; \mathbf{X} is the $m \times n$ calibration dataset matrix; $\boldsymbol{\beta}_i$ the i -th $n \times 1$ mixing coefficient vector and \mathbf{e}_i the i -th $m \times 1$ unmodeled residual vector. Within this linear algebra framework, to obtain $\boldsymbol{\beta}_i$ estimations,

$$\hat{\mathbf{y}}_i = \mathbf{X}\hat{\boldsymbol{\beta}}_i \quad (4)$$

as

$$\mathbf{e}_i = \mathbf{y}_i - \hat{\mathbf{y}}_i \quad (5)$$

Thus

$$\hat{\boldsymbol{\beta}}_i = (\mathbf{X}^T \mathbf{X})^{-1} \mathbf{X}^T \mathbf{y}_i \quad (6)$$

where $\hat{\beta}_i$ and \hat{y}_i are the algorithmic model estimations of β_i and y_i respectively. There are several ways of computing equation (6), although for simplicity and interpretability, in this study we use ordinary least squares with non-negativity constraint on $\hat{\beta}_i$. Once the Raman spectral unmixing is performed, the estimated coefficient values ($\hat{\beta}_i$) provide a map/image of the biochemical concentration distribution of each endmember throughout the sample.

Using this mathematical formulation as a mean to estimate chemical concentrations from Raman spectra carries an implicit assumption: the relationship between the concentration of an analyte and its corresponding Raman signal must be linear. Consequently, mixtures spectra are considered as ideal additions of each component's Raman fingerprint scaled by a coefficient that is directly correlated to its concentration. This assumption has been proved in several different scenarios^{4,5}, however, when dealing with biochemical samples, small alterations to the individual concentration-Raman signal patterns may arise due to molecular interactions among bio-molecular species. To account for these potential effects within our linear model, chemical mixtures were also included in the calibration set at different concentration combinations.

Three-dimensional Raman chemical imaging of iHLC organoids and PHH spheroids.

Upon maturation, all specimens were fixed with paraformaldehyde (PFA) 4 % (v/v) and embedded in 1 % (w/v) agarose (Sigma-Aldrich, A0701-25G) microwells with phosphate-buffered saline (PBS) (pH 7.4, Gibco) for immobilization in hydrated state during chemical imaging⁹⁻¹². Using 63X water immersion objective, 50 μm deep Z-stack scans were acquired with X-Y step size of 2 μm , Z step size of 10 μm , and integration time of 0.25 s per voxel. Total image size was dependant on each organoids' physical dimensions, ranging from 100-180 * 150-250 pixels, but keeping X-Y and Z resolution at 2 and 10 μm respectively. Additionally, organoid image stacks were subjected to SNR thresholding to remove all voxels where maxima in the high wavenumber region (2800 – 3100 cm^{-1}) were less than 10-fold the standard deviation observed across the baseline of Raman-silent region (2200 – 2600 cm^{-1}) of same spectra to ensure only high SNR spectral data was included in the quantitative analysis. Each hyperspectral image in every stack was preprocessed as described and run through the selected statistical unmixing algorithm. Thereupon, pseudo-colour images were generated using the resulting lipid, protein, glycogen, and nucleic acids unmixing coefficients and plotted across the scan area to create 2D biochemical maps. Finally, the z-stack of biomolecular distribution maps were loaded into ICY 2.0.3.0 for rendering of 3D quantitative chemical images.

Quantitative volumetric Raman imaging (qVRI) for neratinib assessment in 3D PHHs and 3D iHLCs.

Due to neratinib's intrinsic fluorescence under 532 nm excitation, we employed a 785 nm laser as alternative Raman excitation source. The limited spectral range of 785 nm near-infrared detector (400 – 2300 cm^{-1}) as compared to 532 nm Raman system (0 – 3600 cm^{-1}), prevented spectral normalization to water signal (3,400 cm^{-1}). Alternatively, standard normal variate scaling was utilized to account for sample-to-sample and depth-dependent signal variations. Endmembers were extracted as references, and all were normalized accordingly before linear combination unmixing as previously described. The main difference here is the deconvolved coefficients no longer contain quantitative concentration information as previously described for qRamanomics. Regardless, the relative abundance (now in arbitrary units, a.u.) of each biomolecular analyte may be mapped throughout the specimens. ilastik⁴⁰

machine learning software was used to train a random forest model to classify subcellular regions of interest as cytoplasm, lipid droplets, drug/metabolite deposits, and nuclei and segment the 3D images accordingly. It should be noted that although this method offers volumetric insight into the size and abundance of intracellular features, it lacks the ability to quantify absolute local concentrations throughout the specimen. Finally, 3D object analysis was performed using ImageJ to generate particle size distribution measurements.

Generation of human primary hepatic spheroids (3D PHH).

Cryopreserved primary human hepatocytes (Gibco, catalogue no. HMCPSQ, lot HU8339-A (PHH_1), Lonza, catalogue no. HUCPG, lot HUM180201A (PHH_2) and Gibco, catalogue no. HMCPSQ, lot HU8287 (PHH_3)) were thawed in the Hepatocytes thaw media (Gibco, catalogue no. CM7500) according to manufacturer's protocol. Moreover, one sample of PHH (donor 73 years old, male) was obtained from the Department of Clinical Science, Intervention and Technology (CLINTEC), Division of Transplantation Surgery, Karolinska Institutet (Stockholm, Sweden). The regional committee for medical and health research ethics in Norway approved the use of human material (REK 50786). Uniform PHH spheroids were created by aggregation in ultra-low attachment micro-wells (Corning, catalogue no. 4440) or in house-made agarose microwells - a format in which PHHs showed stable functionality over at least 7 days as described before⁶ (Extended Data Fig. 2g). Briefly, cells were plated into microwells at the concentration of 1000 viable cells per microwell and were centrifuged at 100 g for 2 min. For the first 3 days PHH were cultured in the Williams E medium (Thermo Fisher Scientific, catalogue no. A1217601) supplemented with 7 % FBS (Thermo Fisher Scientific, catalogue no. 41400045), 2 mM L-glutamine (Thermo Fisher Scientific, catalogue no. 35050038), 10 µg/ml insulin, 5.5 µg/ml transferrin, 6.7 ng/ml sodium selenite (Thermo Fisher Scientific, catalogue no. 41400045) and 0.1 µM dexamethasone (Sigma Aldrich, catalogue no. D4902). From day 4 onwards, the FBS concentration was gradually decreased till 1% (v/v). Spheroids were maintained in serum free media from day 7 for up to 2 weeks.

Differentiation of human iPSC derived 3D iHLCs.

Human induced pluripotent stem cells (iHLC_1: WTC-11, Coriell Institute for Medical Research; iHLC_2: WTSli013-A and iHLC_3: WTSli028-A, Wellcome Trust Sanger Institute) were cultured in E8 media (Thermo Fisher Scientific, catalogue no. A1517001) on plates coated with 0.1% (v/v) Geltrex (Thermo Fisher Scientific, catalogue no. A1413201) in a humidified 37 °C, 5% CO₂ incubator. Cells were passaged using 0,5mM EDTA (Thermo Fisher Scientific) in DPBS and replated as small clumps at a dilution 1:3-1:5. Quality control, performed after thawing of cells, included flow cytometry, qPCR, immunofluorescent imaging for pluripotency markers and karyotyping.

3D hepatic spheroids were generated using modification of previously published protocols^{7,8}. Briefly, iPSC were differentiated toward definitive endoderm in IMDM/F12 media containing 1% (v/v) lipid concentrate (Thermo Fisher Scientific, catalogue no. 11905031), 100 µg/ml transferrin, 3 µM CHIR99021 (Tocris Bioscience, catalogue no. 4423), 50 nM PI-103 (Tocris Bioscience, catalogue no. 2930) and 100 ng/ml activin A (Peprotech, catalogue no. 120-14P) for 24 h and 100 ng/ml activin A for subsequent 48 h. The definitive endoderm cells were treated with 10 ng/mL FGF2 (Peprotech, catalogue no. 100-18B) and 20 ng/mL BMP4 (Peprotech, catalogue no. 120-05) in IMDM/F12 medium supplemented with 1% (v/v) N-2 (Thermo Fisher Scientific, catalogue no. 17502-048), 1% (v/v) B-27

minus vitamin A (Thermo Fisher Scientific, catalogue no. 12587010) and 1% (v/v) lipid concentrate, then with 5 μ M A8301 (Stem Cell Technologies, catalogue no. 72022), 20 ng/mL HGF (PeproTech, catalogue no. 100-39H), 20 ng/mL BMP4, 1% (v/v) B-27 with vitamin A for 3 more days and with 25 ng/mL HGF, 1% (v/v) DMSO for another 5 days. At day 12, cells were detached and aggregated in the agarose U bottom microwells in the presence of 25 ng/mL HGF, 0.1 μ M Dexamethasone, 0.5% (v/v) ITS, 0.1% (v/v) lipids concentrate, 100 μ M Ascorbic acid-2 phosphate (AAP), 1% (v/v) B-27 (without vitamin A) and 1% (v/v) N-2. After formation of spheroids at day 13, media was replaced with William's E media, supplemented with 5% (v/v) FBS, 20 ng/ml HGF and 10 ng/ml oncostatin M (PeproTech, catalogue no. 300-10), 1% (v/v) ITS, 100 μ M AAP, 0.1 μ M Dexamethasone. For further maturation, organoids were cultured in microwells in William's E media, supplemented with 1% (v/v) ITS, 0.1 μ M Dexamethasone, 20 ng/ml Oncostatin M and 1% (v/v) MEM Non-Essential Amino Acids Solution (Thermo Fisher Scientific, catalogue no. 11140050), for another 10 days. At day 18, organoids were additionally incubated for 1 h in the same medium supplemented with 5% (v/v) of Geltrex.

Drug treatment.

Neratinib (catalogue no. S2150), nilotinib (catalogue no. S1033), ketoconazole (catalogue no. S1353), amiodarone HCl (catalogue no. S1979) and fluticasone propionate (catalogue no. S1992) were obtained from Selleckchem, Methadone stock solution (1 mg/ml) was provided by Department of Chemistry, University of Oslo. Stock solutions of drugs were prepared in DMSO in concentration 10 mM. 3D PHH (at day 7 after thawing) and 3D iHLC (after 24 days of differentiation) were incubated with indicated compounds for 24 h and 48 h, diluted in the concentration 10 μ M in serum-free William's E media, supplemented with 1 % ITS, 0.1 μ M Dexamethasone. Control organoids were incubated in the same medium with 0.1 % DMSO.

RNA extraction and real-time polymerase chain reaction (PCR).

RNA was isolated using RNeasy Micro kit (Qiagen) or TRIzol reagent (Thermo Fisher) according to the manufacturer's protocol. RNA concentration and purity was determined using NanoDrop ND-1000 spectrophotometer (Thermo Fisher Scientific). cDNA was synthesized using High-Capacity cDNA Reverse Transcription Kit (Thermo Fisher Scientific, catalogue no. 4368814). Gene expression analysis was performed using a TaqMan Universal mix on a TaqMan ViiA7 Real Time PCR System. Used primers are listed in the Supplementary table 1. PPIA and GAPDH were used as endogenous control. Level of expression of genes of interest were quantified by ddCt with normalization to iHLC differentiated from the WTSli028-A iPSC line (iHLC_3), and with normalization to control organoids for drug treatment. Data represent three donor PHH samples, and iHLCs differentiated from 3 cell lines.

ELISA.

Albumin content in the supernatant media was assayed with Human Albumin ELISA Quantitation Set (Bethyl Laboratories, catalogue no. E88-129). For the comparison between drug treated groups with control PHH or iHLC albumin concentration was normalized to the 3D spheroid/organoid total area as determined from bright field imaging using Fiji software. For the comparison between iHLC and PHH albumin concentration was normalized to the total protein content, Pierce™ BCA Protein Assay Kit (Thermo Fisher Scientific) according to the vendor instruction.

Immunofluorescence staining and microscopy.

Organoids were fixed in 4% (w/v) PFA for 30 min on the orbital shaker. Each step was followed by 3 washings (each 5 min) in DPBS using an orbital shacking. Permeabilization and blocking was performed by incubation in PBS with 1% (m/v) BSA (Sigma Aldrich), 0.2% (v/v) Tritox-X100 (Sigma Aldrich) and 0.5% (v/v) DMSO at RT for 2 h on the orbital shaker. Staining with primary antibodies was performed for 24 h (at 4 °C) with subsequently 2 h incubation with secondary antibodies (Jackson ImmunoResearch, West Grove, PA) diluted with 1 % BSA, 0.1 % Tritox-X100 in PBS. Primary antibodies (Ab) used in this study: rabbit polyclonal Ab to human serum albumin (Abcam, catalogue no. ab2406, 1:400), goat polyclonal antibody to ZO-1 (Thermo Fisher Scientific, catalogue no. PA5-19090, 1:200), mouse monoclonal Ab to CYP3A4 (3H8) (Invitrogen, catalogue no. MA5-17064, 1:250), mouse monoclonal Ab to MRP2 (Abcam, catalogue no. ab3373, 1:400); secondary Ab used in this study: Alexa Fluor® 488 AffiniPure Donkey Anti-Goat IgG (H+L) (catalogue no. 705-545-147, 1:300), Cy™3 AffiniPure Donkey Anti-Rabbit IgG (H+L) (catalogue no. 711-165-152, 1:400), Alexa Fluor® 647 AffiniPure Donkey Anti-Mouse IgG (H+L) (catalogue no. 715-605-150, 1:400) (all secondary Ab are from Jackson ImmunoResearch). Nuclear counterstaining was performed with 1 µg/mL Hoechst 33258 (Sigma Aldrich) for 5 min at RT. Confocal microscopy was performed on a Zeiss 700 laser scanning confocal microscope and Andor Dragonfly Spinning Disk Confocal microscope using standard filters sets and laser lines with a 40x and 63x oil immersion objective. For the detection of neratinib fluorescence, we used imaging with excitation by UV at 350 nm and emission in far-red spectrum, 650-670 nm, that allowed distinguishing between neratinib and Hoechst 33258 signals. Images were acquired using Zen software (Zeiss) as Z-stacks with 2 µm spacing between stacks and Dragonfly software with 0.5 µm spacing correspondingly. The confocal images were analyzed using Fiji software¹³. Confocal images are displayed as a resulting Z-stack of half of spheroid.

Viability and hepatotoxicity.

ATP content was evaluated using Cell Titer-Glo® 3D Cell Viability Assay (Promega) according to manufacturer's instructions. Briefly, 50 µl of the reagent was added to individual spheroids in 100 µl of culture medium. To facilitated lysis, organoids were vortexed for 1 min and the plate was incubated at 37 °C in 5% CO₂ for 20 min with subsequent luminescent signal measurement using GloMax® Multiplus Plate Reader/Luminometer (Promega). The changes in viability are represented as % compared to viability of control spheroids/organoids. The viability of organoids after 48 h of incubation with tested compounds was visualized using a LIVE/DEAD® assay (Thermo Fisher Scientific) as described by the manufacturer. Briefly, organoids were washed in D-PBS and incubated for 30 min at 37 °C in a 5 % CO₂ incubator in 1 mL of culture media containing 1 µL of calcein AM solution and 5 µL of ethidium homodimer-1 solution. Stained spheroids/organoids were analyzed using a fluorescence microscope (Zeiss).

Cytochrome CYP3A4 and CYP1A2 activity.

Cytochrome CYP3A4 and CYP1A2 enzymatic activities of 3D PHHs and 3D iHLCs were measured using P450-Glo™ Assay with Luciferin-IPA (catalogue no. V9001) and Luciferin-1A2 (catalogue no. V8771) correspondingly (Promega, Sweden). For the induction of CYP3A4 activity, organoids were treated with 50 µM of rifampicin for 24 h prior the analysis. For the induction of CYP1A2 activity organoids were treated with 100 µM of omeprazole for 24 h prior the analysis. Relative luminescence was normalized to total protein content, measured by Pierce™ BCA Protein Assay Kit (Thermo Fisher Scientific) according to the vendor instruction.

Transporter activity.

Spheroids/organoids were incubated with 10 μ M 5(6)-carboxy-2',7'-dichlorofluorescein diacetate (CDFDA) (Sigma Aldrich, catalogue no. 21882) for 30 min at 37 °C in the 5 % CO₂ atmosphere. Nuclei were counterstained with 1 μ g/mL Hoechst 33342. Cultures were washed with PBS containing calcium and magnesium. Imaging was performed in William's E media without phenol red, but containing 5 mM of HEPES using a Zeiss LSM 700 confocal microscope after 5, 15 and 30 min after washing at 37 °C.

Phospholipidosis assay.

The HCS LipidTOX™ Phospholipidosis Detection Reagents (PLD) (Thermo Fisher Scientific, catalogue no. H34350) accumulation was monitored in real time using Incucyte live imaging visualization system. For real-time experiments spheroids were generated in 96 wells ultra-low attachment U-bottom plate with initial plating density of 1000 cells per well. PLD accumulation data is represented by mean fluorescence signal per well. Total accumulation of PLD after 48 h of drug exposure was verified using Andor Dragonfly Spinning Disk Confocal microscope. Z-stack of half of spheroid was taken with spacing 1 μ m.

Proteomic liquid chromatography-tandem mass spectrometry (LC-MS/MS) analysis.

Pelleted iHLC organoids generated from 3 cell lines (iHLC_1: WTC-11, WiCell; iHLC_2: WTSli013-A and iHLC_3: WTSli028-A, Wellcome Trust Sanger Institute) and cryopreserved primary human hepatocytes (Gibco, lot HU8287 (PHH_3)) (all ~100 000-300 000 cells) were washed once with DPBS (final volume ~15 μ L), before lysing and digestion. Sample preparation was performed according to the protocol for sample preparation by Easy Extraction and Digestion (SPEED) by Doellinger et al.¹⁴, with a modified reduction and alkylation step: reduction was performed by adding DL-dithiothreitol (Merck, catalogue nr. D5545) to a final concentration of 10 mM before incubation at 56 °C / 900 rpm for 25 min in a thermoshaker (Grant instruments), and alkylation was performed by adding iodoacetamide (Merck, catalogue no. I1149) to a total concentration of 20 mM before incubation at room temperature / 900 rpm for 30 min in the thermoshaker (in the dark). Samples were digested with 6 μ g trypsin () overnight in the thermoshaker at 37 °C / 700 rpm. To terminate protease activity, trifluoroacetic acid was added to a final concentration of 1 % (v/v) and the peptide extracts were concentrated to dryness using a Concentrator plus from Eppendorf (Hamburg). The dried extracts were dissolved in 100 μ L LC-MS grade water with 0.25 % (v/v) heptafluorobutyric acid before sample clean up. Cleanup was performed using 100 μ L BondElute C18 solid-phase extraction columns from Agilent (Santa Clara) according to the attached protocol and eluted into 100 μ L acetonitrile/water/formic acid (60/40/0.1, v/v/v) in 1.5 mL Eppendorf Protein-LoBind tubes. The two aliquots of each sample were combined and concentrated to dryness in the Concentrator plus, and the final peptide extracts were dissolved in 4 μ L LC-MS grade water containing 0.1 % (v/v) formic acid.

The protein extracts were analyzed by LC-MS/MS using the timsTOF Pro (Bruker Daltonik) mass spectrometer which was coupled online to a nanoElute nanoflow liquid chromatography system (Bruker Daltonik) via a Captive Spray nanoelectrospray ion source. The peptides were separated on a reversed-phase C18 column (25 cm x 75 μ m, 1.6 μ m, Ion Optics (Fitzroy) at 50 °C). Mobile phase A contained LC-MS grade water with 0.1 % (v/v) formic acid, and acetonitrile with 0.1 % (v/v) formic acid was used as mobile phase B. The peptides were separated by a linear gradient from 0 – 35 % mobile phase B over 54 min at a flow rate of 300 nL/min at a column temperature of 50 °C. MS acquisition

was performed in data-dependent acquisition parallel accumulation-serial fragmentation (DDA-PASEF) mode. An injection volume of 2 μ L was used.

The LC-MS data were searched against the human UniProt database (20,431 entries), with PEAKS X+ software version 10.5 (Bioinformatics Solutions). The following parameters were used: digestion enzyme, trypsin; maximum missed cleavage, 1; fragment ion mass error tolerance, 0.03 Da; parent ion error tolerance, 15 ppm. Oxidation of methionine, carbamidomethyl formation on cysteines, and acetylation of the N-terminus was specified as variable modifications and the maximum number of posttranslational modifications (PTMs) was set to 2. A false-discovery rate of 1 % was applied to the datasets. Label-free quantification (LFQ) using the PEAKS X+ software was performed using proteins containing at least 1 peptide in both groups (iHLC_1 and PHH) with a significance ≥ 0 and FDR of 5 %. Peptides were filtered, retaining peptides with a $2 \leq \text{charge} \leq 5$, quality ≥ 0 , and area ≥ 0 . Normalization to the total protein intensity was performed (intensity of the PHH reduced by a factor of 5.6 compared to that of iHLC_1).

Drug metabolism in microsomes.

Human liver microsomes (XTremme Pool 200 Human, Tebu-bio, Lot nr: 1710084) were stored at -80 °C. NADPH regeneration solution (final concentration 1.3 mM NADP⁺, 3.3 mM glucose-6-phosphate, 0.4 U/mL glucose-6-phosphate dehydrogenase, 3.3 mM MgCl₂) and human liver microsomes (final concentration 1 mg protein/mL) were pre-incubated to 37 °C for 15 min in a shaking water bath. The reaction was initiated by addition of neratinib or amiodarone (final concentration of 5 μ M in a total volume of 100 μ L) and stopped after 0, 20, and 60 min by addition of ice-cold formic acid (FA, final concentration 0.11 M). The samples were centrifuged at 14500 \times g and 4 °C for 10 min and the supernatants were transferred to autosampler vials. Drug degradation control samples, without human liver microsomes, were performed in parallel to evaluate the stability of neratinib at the incubation conditions.

Neratinib and amiodarone metabolites detection by LC-MS.

PHH spheroids were incubated in 5 μ M neratinib or 10 μ M amiodarone in serum-free William's E medium supplemented with 0.1 μ M dexamethasone and 1% (v/v) ITS for 6 and 24 h. Metabolism was stopped by adding FA to a final concentration of 0.11 M, and the plates were frozen at -80 °C. In parallel, samples of cell medium without organoids (n = 3) were used as drug degradation control samples. The samples were centrifuged at 14500 \times g and 4 °C for 10 min. The supernatant was diluted 10x in 0.1% (v/v) FA prior to analysis. The pellet was washed three times in PBS, followed by the addition of 100 μ L type I. Rapidly, pellet and liquid were transferred to Eppendorf tubes and then placed in an ultrasonic bath for further preparation, applying a variant of procedure described before¹⁵, to reduce sample heating; in the bath, the cells were subjected to ultrasonic treatment for 30 s on/30 s off 10 times, taking a total of 10 min. Detection of neratinib metabolites was achieved with an Agilent 1100 series pump equipped with an Agilent 1200 autosampler from Agilent Technologies. The autosampler and pump was coupled to Quantiva (triple quadrupole) MS with an electrospray ionization (ESI) interface from Thermo Fisher Scientific. Separation was performed using a HotSep® Sunniest C18 analytical column (150 \times 0.5 mm, 3 μ m particles and 120 Å pores) from GT Septech Teknolab (Ski, Norway). The Agilent 1100 series pump was equipped with two solvent compartments (A and B), where A contained 5 mM ammonium formate pH 3.1 (w/v) and B contained 0.1 % FA in LC-MS grade water and acetonitrile (5/95, v/v). A linear gradient was applied ranging from

20 % to 80 % B in 6 min at a flow rate of 15 μ L/min, and the injection volume was 3 μ L. The ion spray voltage was set to 3.5 kV, the sheath- and aux gas was set to 7 arb and 5 arb, and the vaporizer temperature was set to 33 °C. The MS operated in positive mode, with multiple reaction monitoring (MRM) transitions of neratinib and metabolites obtained from neratinib metabolite detection in neratinib incubated human liver microsomes. The neratinib metabolite identification quality control was based on the characteristic Cl isotope intensity ratio of 3:1, and the retention time order and MS/MS fragments were matched with the study of Liu et al.⁴³. The MRM transitions and collision energies (ce) for neratinib, Peak 3 (m/z 557.2 > 112.2, 512.2, and 521.3 at 20 V), Peak 1 (m/z 466.2 > 112.8, 393.1, and 421.2 at 20 V), Peak 2 (m/z 543.2 > 353.0 at 37 V, and 543.2 > 446.1, and 507.5 at 20 V), Peak 4 (m/z 573.2 > 464.3, 528.3, and 111.9 at 20 V). Solvent gradients and MS acquisition was controlled by the Agilent LC software (Chemstation).

Amiodarone metabolite detection was achieved with ESI-MS (triple quadrupole Quantiva, Thermo Fisher Scientific), and direct injection using a Fusion 101 syringe pump from Chemyx Inc (Stafford, TX). Here, the flow rate was 5 μ L/min, the ion spray voltage was set to 4.5 kV, the sheath- and aux gas was set to 3 arb and 5 arb, and the vaporizer temperature was set to 33 °C. The MS operated in positive mode.

Statistics.

Statistical analyses and graphs generation were performed using GraphPad PRISM 7 (GraphPad Software Inc.). Unless specifically stated, a two-tailed, paired *t*-test (with unequal variances) was applied for the comparison of two groups. For more than two groups, a one-way ANOVA analysis was applied. The data are presented as mean \pm SD. Statistical significance was assigned as not significant (NS) $P > 0.05$; * $P \leq 0.05$; ** $P \leq 0.01$; *** $P \leq 0.001$; **** $P \leq 0.0001$.

Data and code availability

Research raw data and scripts are available upon request from rdm-enquiries@imperial.ac.uk.

Acknowledgements

The work was supported by the Research Council of Norway through its Centre of Excellence scheme, project number 262613 and from the UiO:Life Science program. V.L. acknowledges support from H2020 through the Individual Marie Skłodowska-Curie Fellowship ‘UltraRamanomics’ under grant agreement no. 890854. J.G. acknowledges support from the National Institute of General Medical Sciences of the National Institutes of Health under Award Number F32GM131594. M.M.S. was funded by the grant from the UK Regenerative Medicine Platform “Acellular / Smart Materials – 3D Architecture” (MR/R015651/1), the Wellcome Trust Senior Investigator Award (098411/Z/12/Z) and the Royal Academy of Engineering Chair in Emerging Technologies award (CiET2021\94). S.R.W. is a member of the National Network of Advanced Proteomics Infrastructure (NAPI), which is funded by the Research Council of Norway INFRASTRUKTUR-program (project number: 295910). Quality control of iPSC lines was partially performed at The Norwegian Center for Stem Cell Research. We thank Dr. Ewa C. S. Ellis at Liver Cell Laboratory, Department of Clinical Science, Intervention and Technology, Karolinska University Hospital Huddinge for obtaining the primary hepatocytes. We thank Dr. Bernd

Thiede at the Department of Biosciences, University of Oslo for the performing of LC-MS/MS runs for proteomics analysis. For the purpose of open access, the author has applied a Creative Commons Attribution (CC BY) licence to any Author Accepted Manuscript version arising from this submission.

Contributions

V.L. and A.A. designed and planned the study, analyzed and interpreted the data. A.A. performed all cell culture and biochemical assays. V.L., M.B.M., and J.Y. acquired all Raman data. V.L., M.B.M, J.Y., and X.Z. performed Raman data preprocessing and analysis. F.S.S. and S.R.W. performed LC-MS analysis of drug metabolism. J.G. performed Bayesian modelling for method validation. H.E.B. performed proteome analysis. J.S. performed iPSC lines culture and assisted in biochemical assays. M.Y. and A.S. provided sHDLs and material characterization. S.R.W., H.S., S.K. and M.M.S. provided scientific discussions and contributed to writing the manuscript. S.K. and M.M.S. supervised study, provided conceptual advice and financial support. V.L., A.A., S.K. wrote the article. All authors reviewed the manuscript.

Competing interests.

The authors declare no competing interests

Quantitative Ramanomics for chemometric phenotyping of three-dimensional liver organoids

Vernon LaLone^{1*} and Aleksandra Aizenshtadt^{2*}, John Goertz¹, Frøydis Sved Skottvoll³, Marco Barbero Mota¹, Junji You¹, Xiaoyu Zhao¹, Henriette Engen Berg³, Justyna Stokowicz², Minzhi Yu^{4,5}, Anna Schwendeman^{4,5}, Hanne Scholz^{2,7,8}, Steven Ray Wilson^{2,3}, Stefan Krauss^{2,6**}, and Molly M. Stevens^{1**}

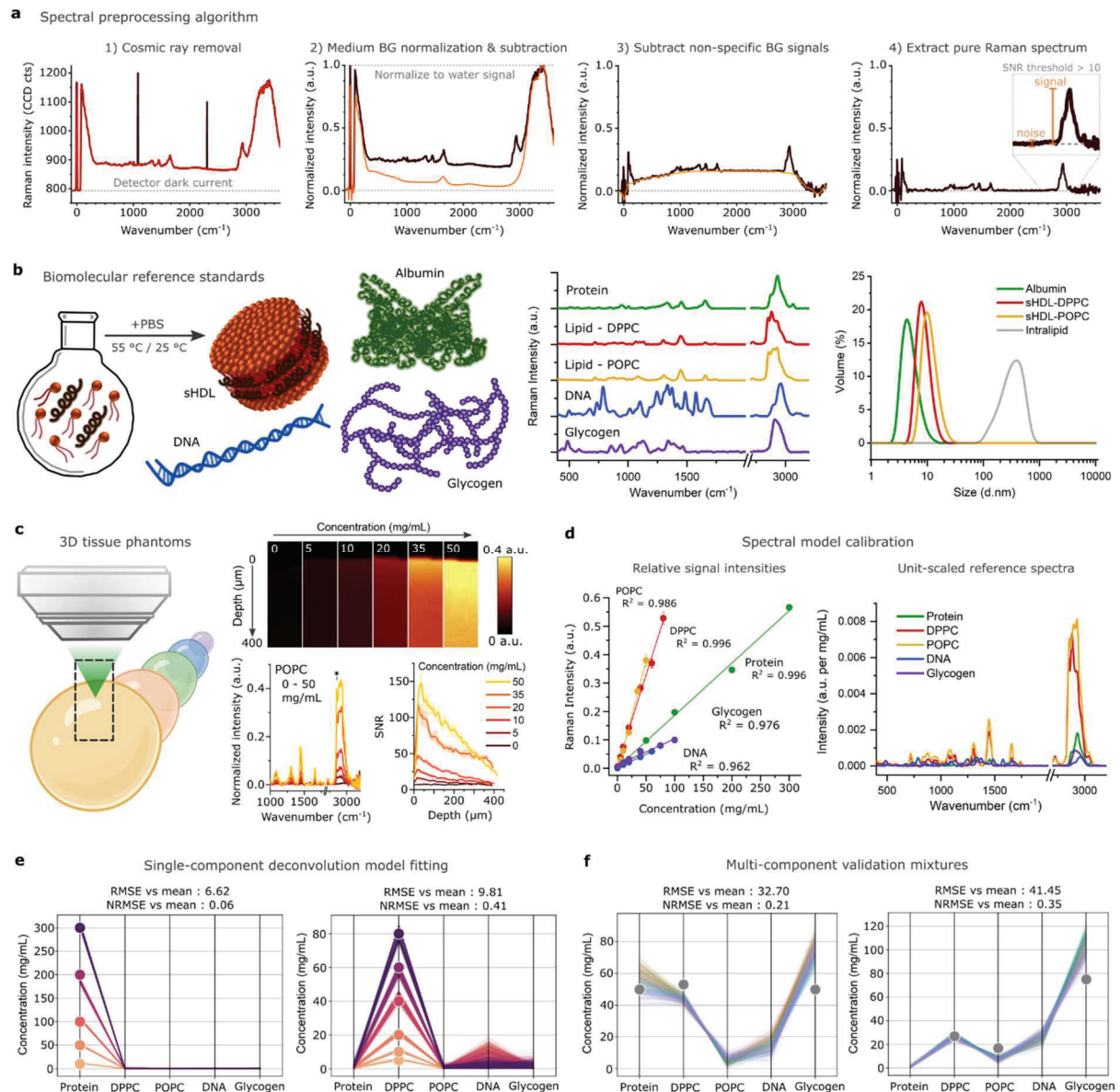


Fig. 1. Methodology for spectral preprocessing and quantitative calibration of reference model using biomolecular tissue phantoms. **a**, Spectral preprocessing algorithm employing the water signal as an internal standard for all measurements. **b**, sHDLs enable mixing of lipid species with other classes of biomolecules in aqueous mediums. Reference spectra for each major distribution normalized to maximum peak height. Particle size distribution of sHDLs compared with albumin solutions and intralipid emulsions by DLS. **c**, 3D tissue phantoms elucidate linear range of quantitation for each analyte (shown for POPC) and allow for depth-dependent signal interference studies. **d**, Signal intensities vary for each major class of biomolecules and reference spectra are scaled accordingly to extract the unit-scaled (a.u. per 1 mg/mL) spectra for each. **e**, Linear combination modelling enables accurate quantitation across single-component concentration ranges and **f**, specificity in complex multi-component mixtures. Points represent theoretical concentrations and lines show measurement fits for select calibration standards. See Extended Data Fig. 1 for complete calibration panel.

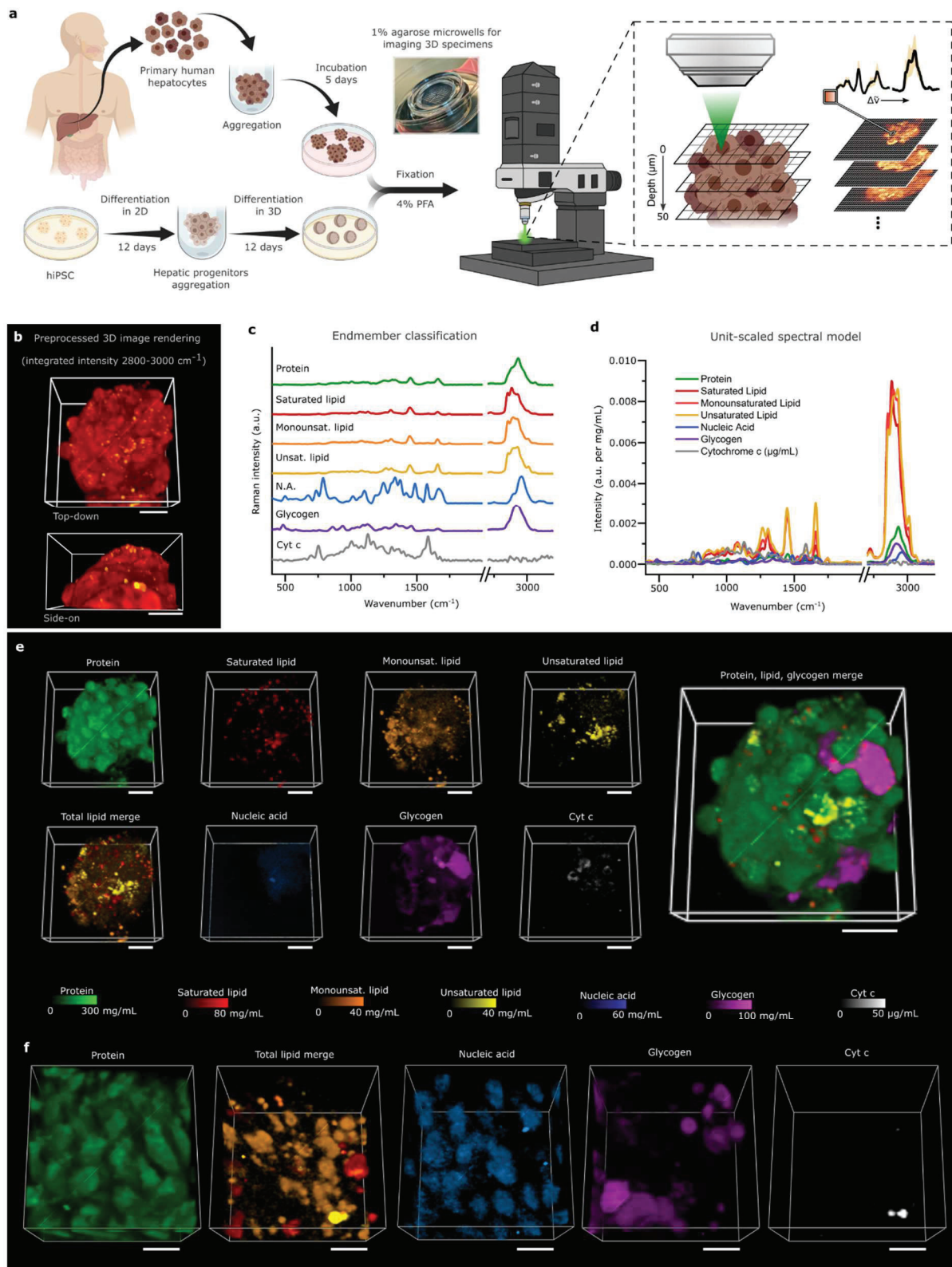


Fig. 2. qRamanomics platform for chemometric phenotyping of 3D biospecimens enables quantitative assessment of distribution, abundance, and colocalization of biomolecules. **a**, Workflow for the formation and Raman analysis of 3D PHH spheroids and 3D iHLC organoids. Cell/organoid graphics created with BioRender.com. **b**, 3D images of 3D PHH spheroid generated from preprocessed spectra showing total signal acquired in high wavenumber region ($2800\text{--}3000\text{ cm}^{-1}$). Scale bars = $50\ \mu\text{m}$. **c**, Endmember spectra extracted from complete control dataset ($n = 20$ spheroids/organoids from 3 donors and 1 hiPSC line; $>30,000$ spectra per spheroid/organoid) to generate representative model and classified according to major biomolecular class. **d**, Endmember spectra were scaled according to calibration to generate unit-scaled (a.u. per mg/mL or $1\ \mu\text{g/mL}$ for cyt c) spectral model for quantitative deconvolution of biospecimen datasets. **e**, High-content qRamanomics imaging reveals distribution of molecular content throughout 3D PHH spheroid. Scale bars = $50\ \mu\text{m}$. **f**, High-resolution imaging requires longer acquisition times and allows intracellular distribution of biomolecular content. Scale bars = $10\ \mu\text{m}$.

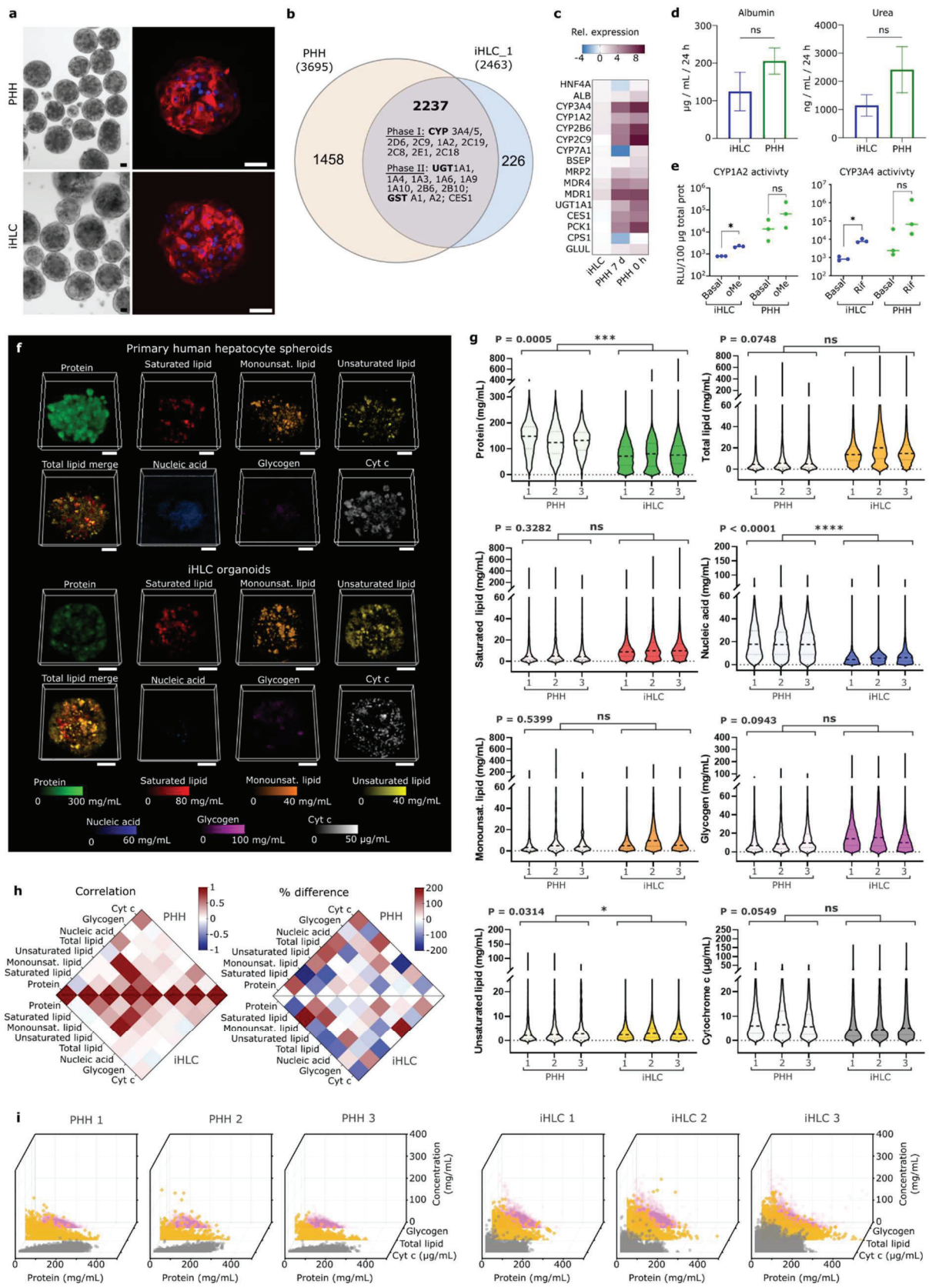


Fig. 3. qRamanomics enables quantitative high-content composition comparison between primary human hepatocyte spheroids and induced hepatocyte-like cell organoids. **a**, Representative bright field, and immunofluorescence (red – albumin) images of 3D PHHs and 3D iHLCs. Scale bar = 50 μ m. **b**, Venn diagram of proteins detected in PHH ($n = 1$ donor) and iHLC organoids ($n = 1$ cell line). **c**, The heatmap shows mean relative expression of selected hepatocyte-specific genes given as Log₂, iHLC organoids generated from iPSC line WTSii028-A (iHLC_3) were used for the normalization. **d**, Secretion of albumin and urea in PHH and iHLC organoids, $n = 3$ donor PHH, $n = 3$ cell lines iHLC (3 replicates for each). Data represented as mean \pm SD. Significance was calculated by nested two-tailed t-test (albumin $p=0,177$, urea $p=0,107$). **e**, Basal and induced cytochromes P450 activity. Data represented as mean for 3 donors of 3D PHHs and 3 independent

differentiations of iHLC. Significance determined by multiple t test, using the Holm-Sidak method, * $p < 0.05$. *f*, High-content quantitative Ramanomic imaging reveals distribution of molecular content throughout 3D PHH spheroids from a single donor ($n = 3$) and 3D iHLC organoids ($n = 3$). Scale bars = 50 μm . *g*, Inter-spheroid/organoid repeatability within and between specimen groups. Nested t-test revealed significant differences in protein, unsaturated lipid, and nucleic acid content between 3D PHH and 3D iHLC samples. *h*, Pearson's correlation chemometric heatmaps illustrate colocalization of various molecular components and % difference between PHH and iHLC. *i*, Single-pixel local concentration correlation plots for total lipid, glycogen, and cyt c vs. protein measurements (mg/mL for all; cyt c reported in $\mu\text{g/mL}$).

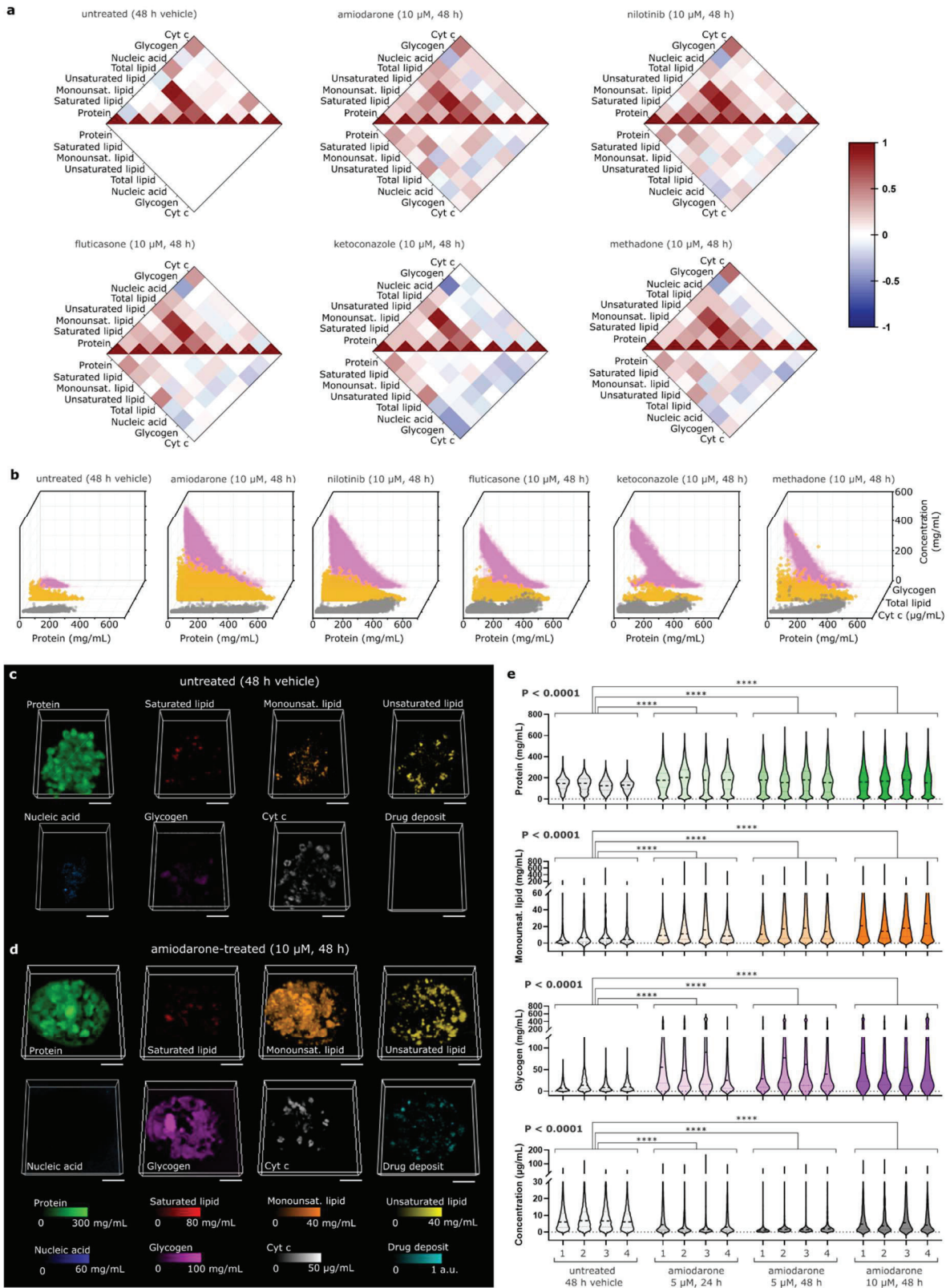


Fig. 4. qRamanomics reveals high-content compositional phenotypic changes in response to drug treatment. **a**, Drug-specific changes in compositional phenotype for amiodarone, nilotinib, fluticasone-propionate, ketoconazole, and methadone-treated 3D PHHs by quantitative high content correlation analysis ($n = 4$ spheroids per group). Top half of plots shows Pearson's correlation and bottom half shows absolute difference compared to untreated control. **b**, Frequency distribution plots of total lipid, glycogen, and cytochrome *c* vs. protein content for representative drug-treated samples. High-content chemometric profiling of individual control (48 h vehicle treatment, **c**) and amiodarone-treated (10 μM , 48 h, **d**) 3D PHHs. Amiodarone induces significant measurable changes in biomolecular composition of 3D PHH spheroids. Scale bars = 50 μm . **e**, Analysis demonstrates repeatability across multiple spheroids from each sample group.

Nested one-way ANOVA followed by Kruskal-Wallis multiple comparisons were significant (n = 137,374 protein, 118,193 monounsaturated lipid, 124,697 glycogen, and 60,003 cyt c measurements from 16 different 3D PHH spheroids).

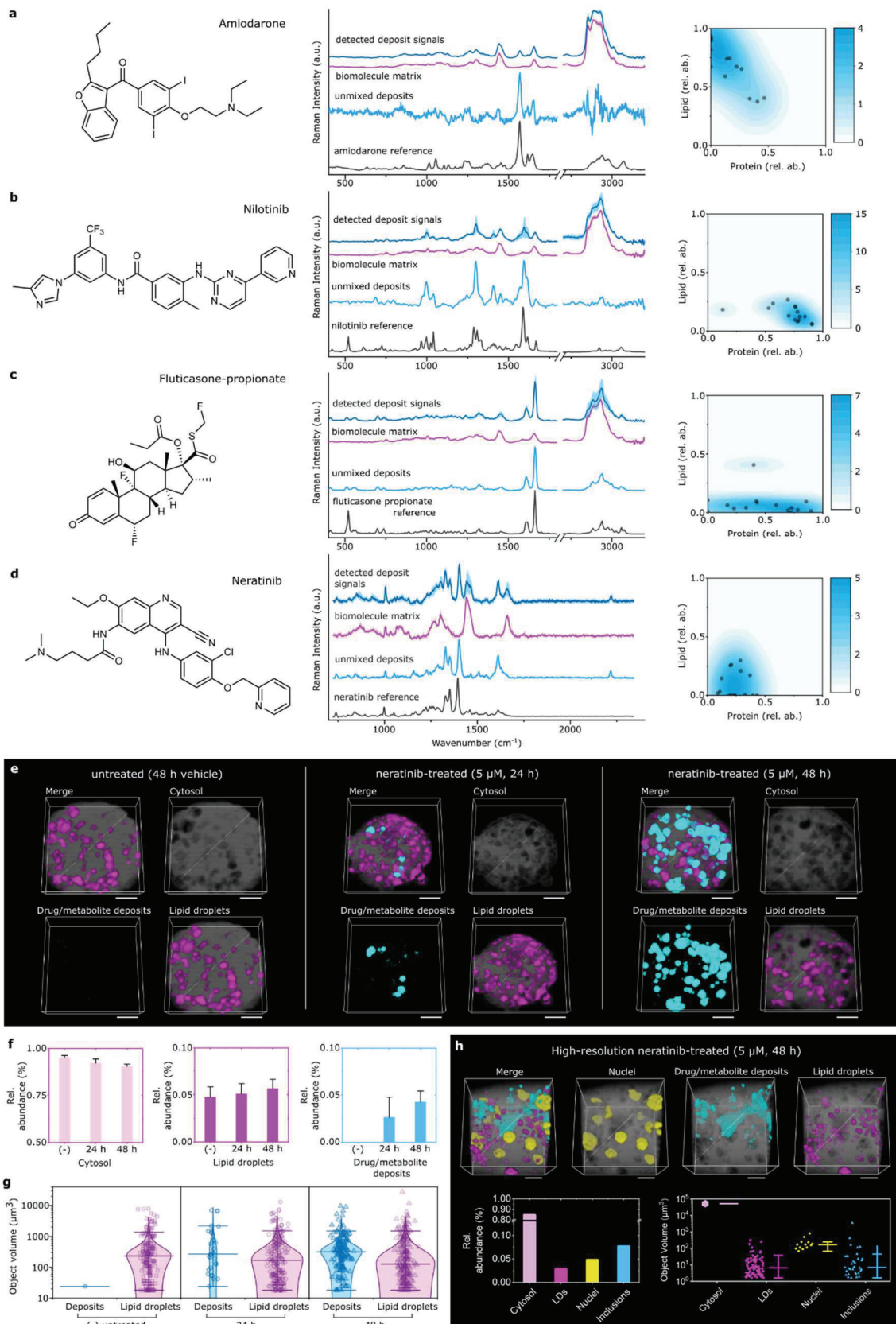
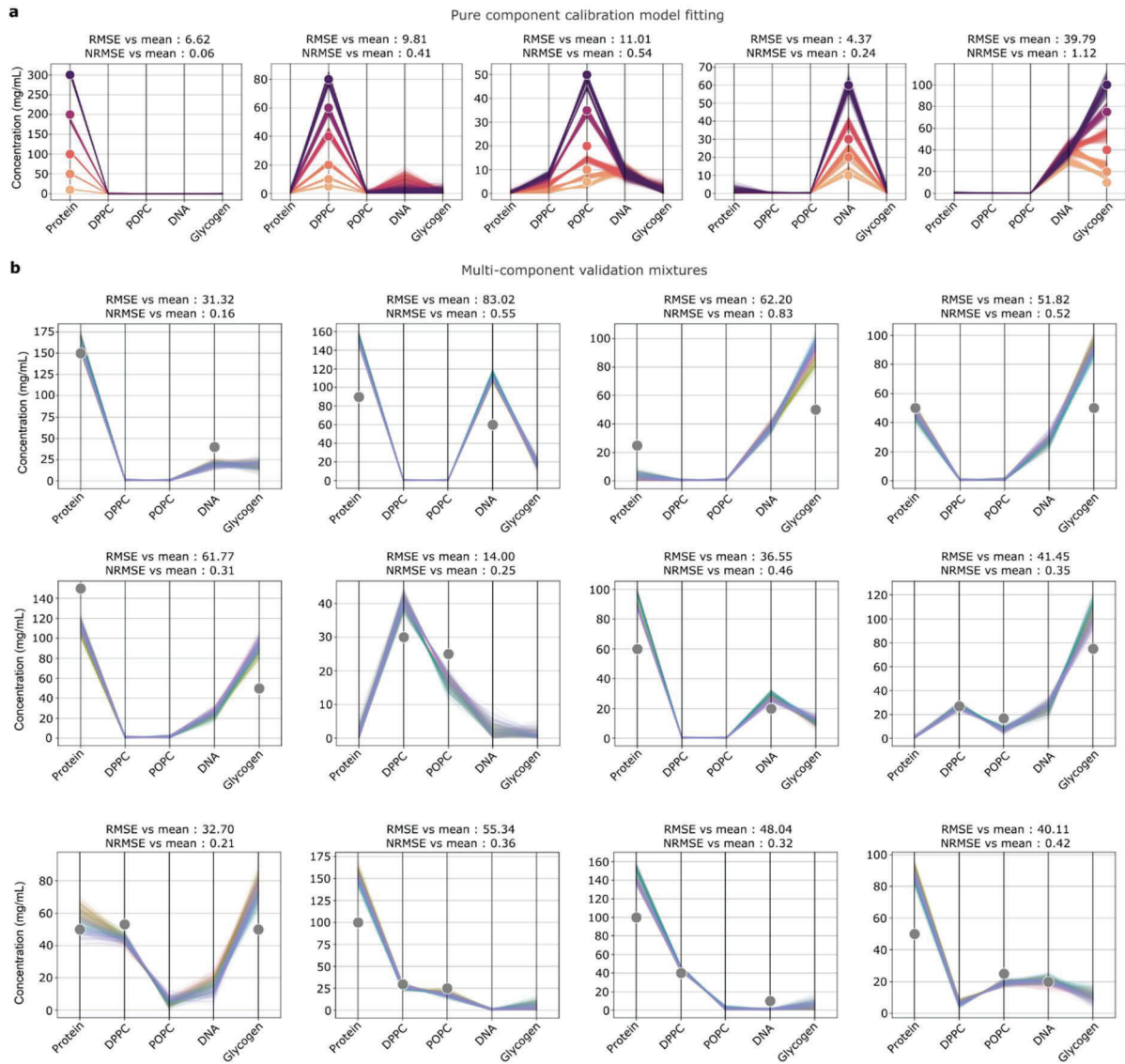
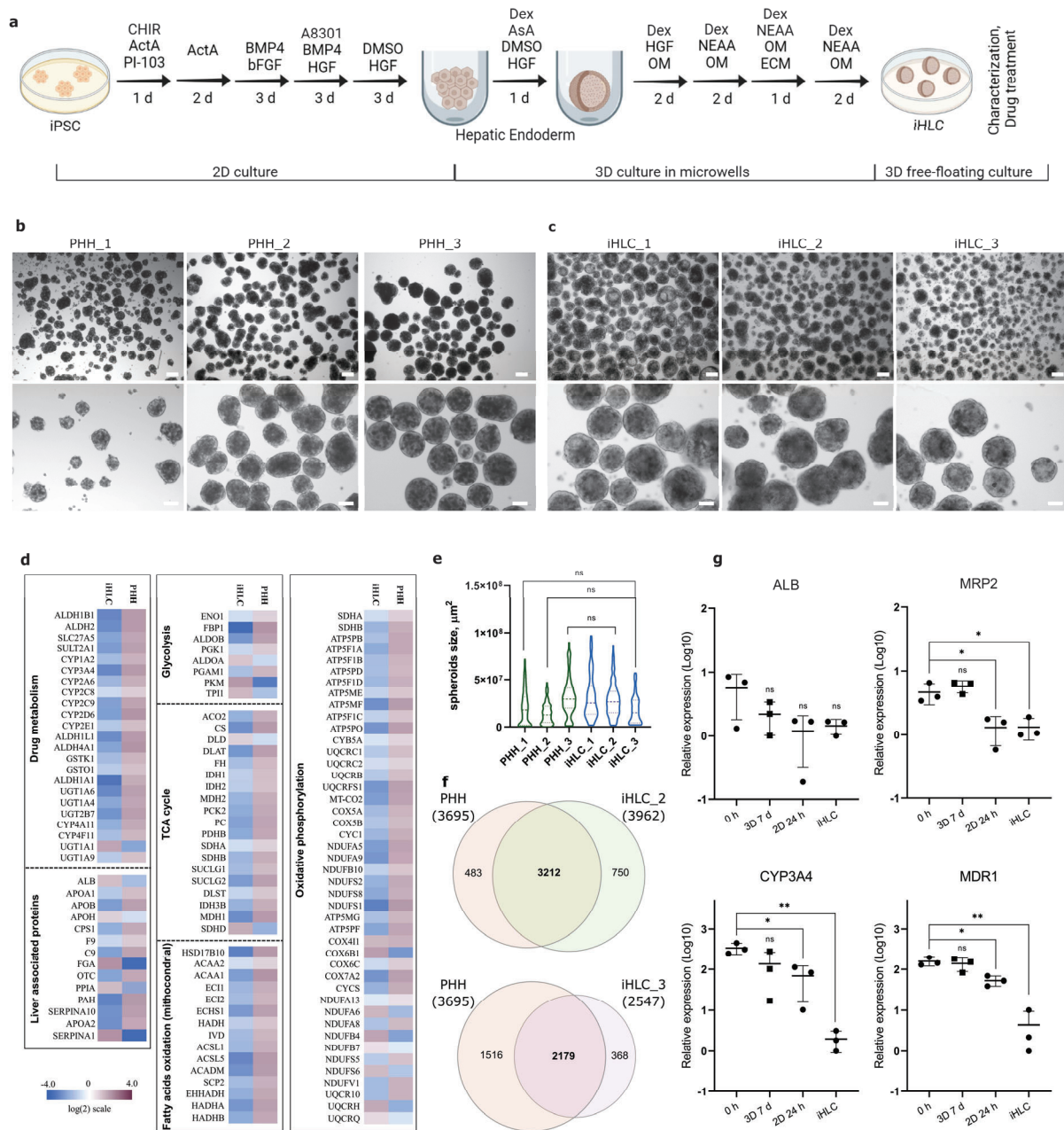


Fig. 5. Drug and drug metabolite deposits were detected within lysosomes yielding altered Raman spectral signals as compared to parent drug for drug-treated 3D iHLC organoids. **a-d**, Chemical formula for drugs for which detected deposit signals were extracted from intracellular drug and/or metabolite aggregate regions of interest (5 deposits from $n = 3$ 3D iHLCs each treatment group) for **a**, amiodarone, **b**, nilotinib, **c**, fluticasone-propionate, and **d**, neratinib-treated 3D iHLC organoids. Spectral difference between unmixed deposits and parent drug reference signals suggests metabolism of compounds. **e**, qVRI reveals distribution of drug/metabolite (cyan) and lipid droplets (magenta) for neratinib-treated 3D PHHs (scale bars = 50 μ m) and **f**, relative volumetric abundance for each component. Data shown as mean \pm SE for $n = 3$ PHH spheroids. **g**, Particle size distribution analysis of drug/metabolite deposits (inclusions) within drug-treated and control specimens ($n = 3$ organoids per group). Data shown as median \pm quartiles with each point representing an individual deposit/droplet. **h**, High-

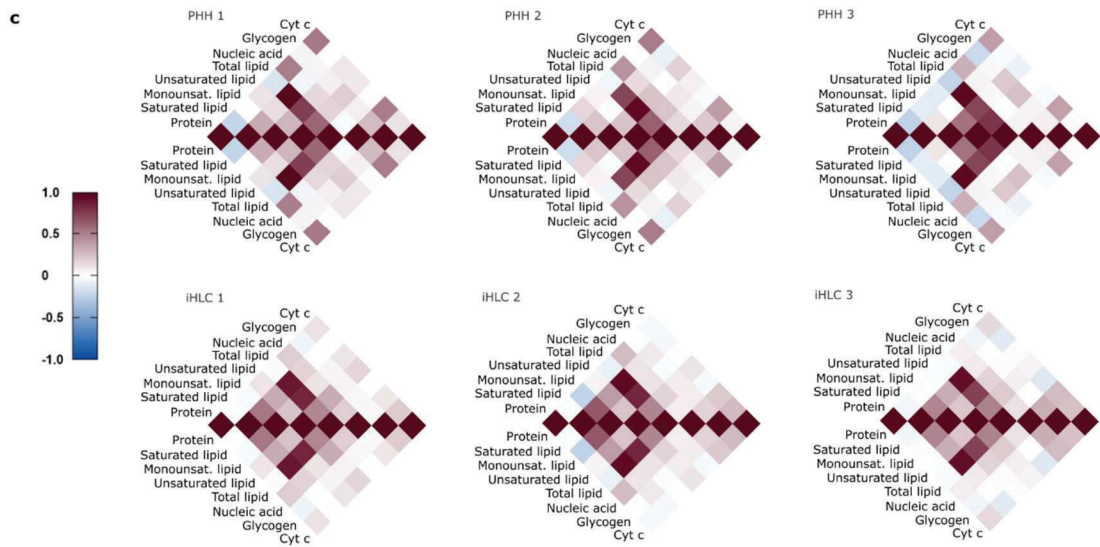
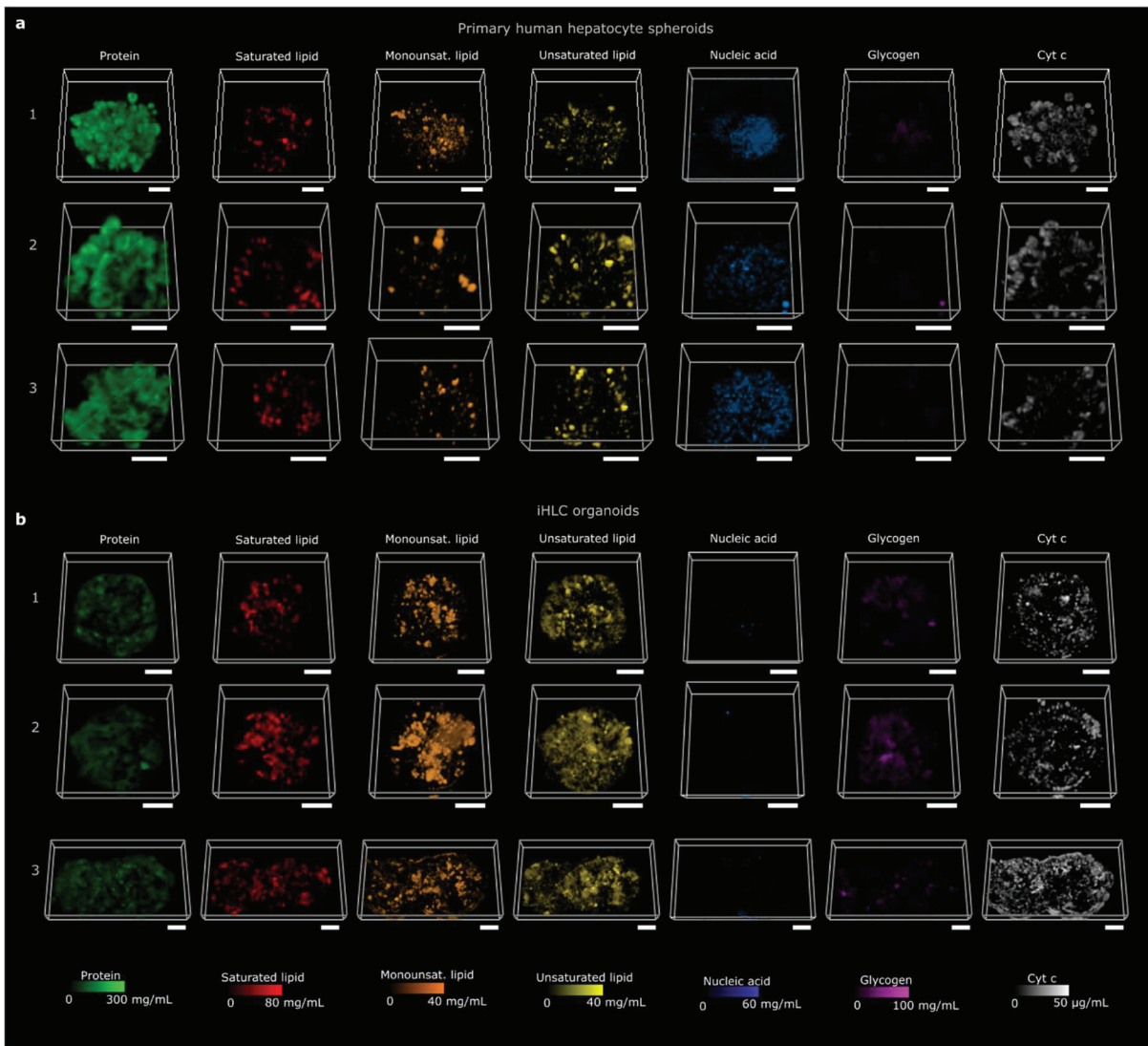
resolution 3D Raman chemical imaging suggests neratinib accumulation in lysosomes and bile canaliculi. Scale bars = 10 μm . Relative abundance data shown as volume fractions of 3D scan with each object volume point representing an individual deposit/droplet.



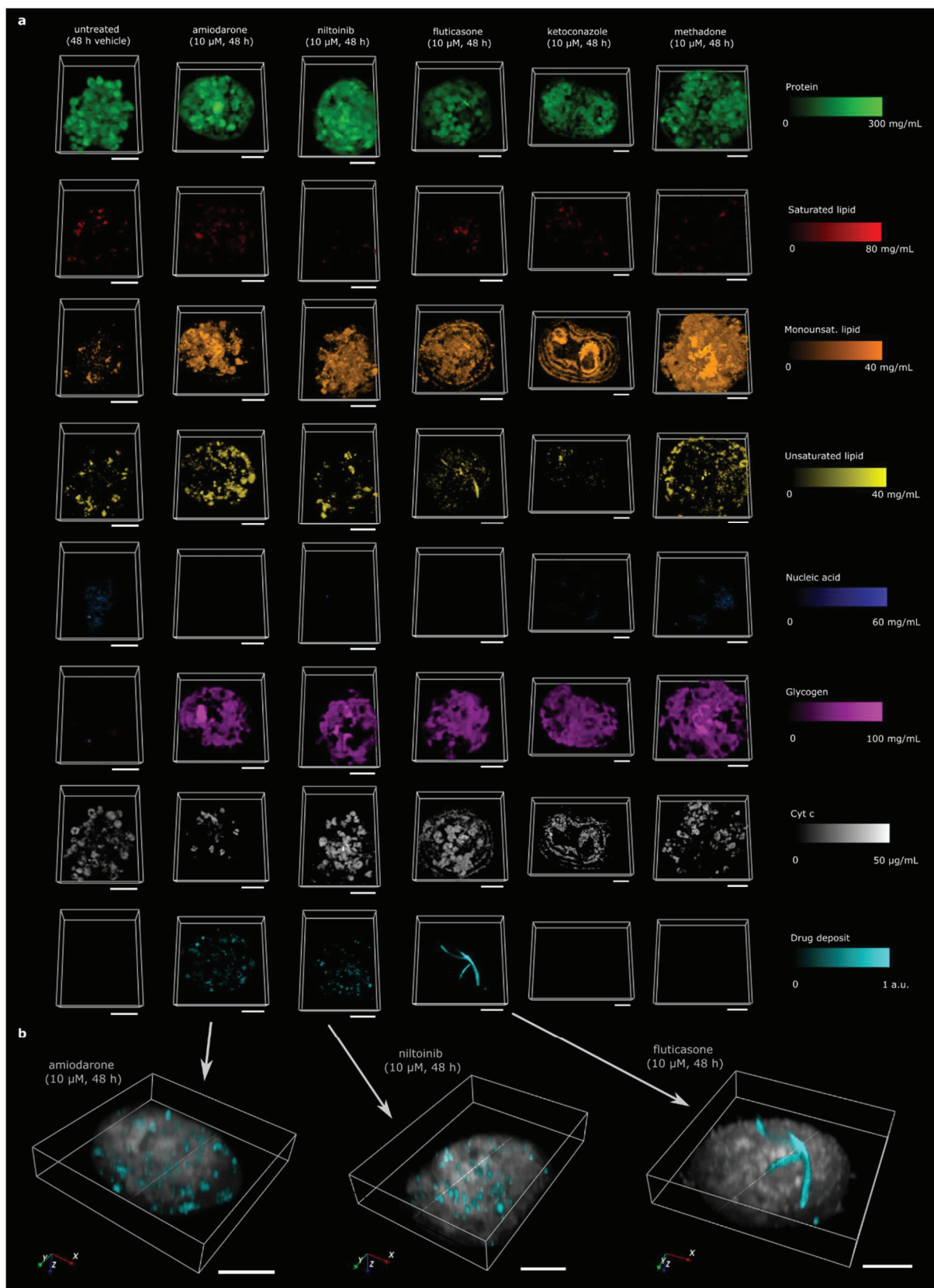
Extended Data Fig. 1. Method validation for quantitative compositional analysis in three-dimensional biospecimens using Bayesian approach to characterise model confidence. **a**, Results for pure component calibration model fitting. Datapoints reveal ground truth concentrations of analytes and shaded lines show confidence boundaries of various measurement sets. **b**, Multi-component mixtures provide measure of model confidence and accuracy to quantitatively deconvolute biomolecule spectral signatures from physiologically-relevant concentration realms.



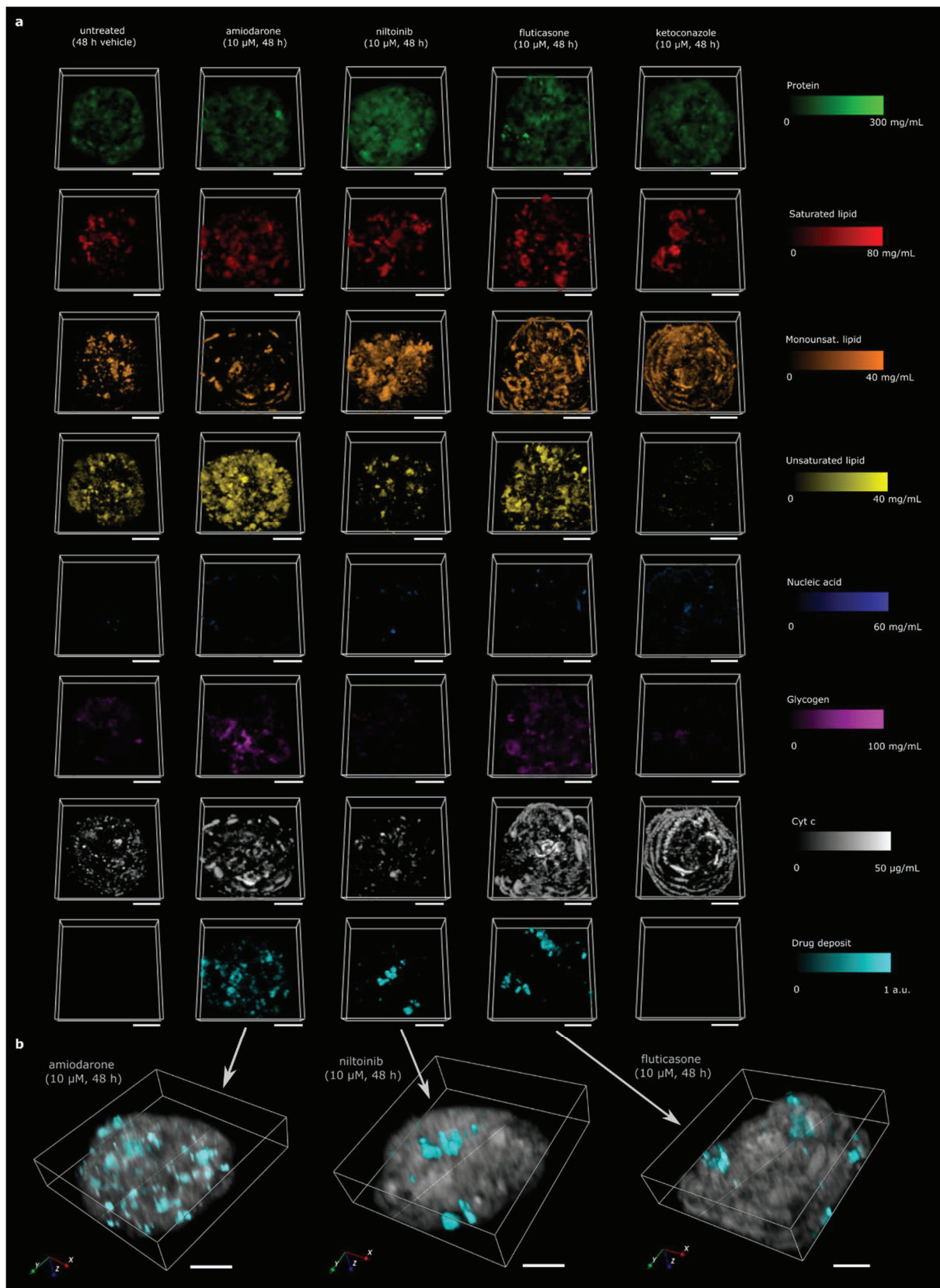
Extended Data Fig. 2. a, Schematic representation of differentiation protocol. **b-c**, Representative bright field images of PHH spheroids from 3 donors, and iHLC generated from 3 hiPSC lines. Scale bars = 100 μm . **d**, Heat map illustrating relative abundance of proteins in PHH_3 and iHLC_1. Proteins were grouped into groups related to drug-metabolism, glycolysis, TCA cycle, oxidative phosphorylation, and fatty acids phosphorylation, as well as general liver-specific proteins. **e**, Size distribution of 3D PHH and 3D iHLC, measured as an area of 3D models sections from bright field images ($n > 90$ for each group, one-way ANOVA). **f**, Venn diagram of proteins detected in PHH_3 and iHLC_2 and iHLC_3 organoids. **g**, Relative expression of selected hepatic markers in iHLC organoids, freshly thawed (0 h) PHH, PHH after 7 days and 24 h of 3D and 2D culture correspondingly. $n = 3$ donors for PHHs, $n = 3$ cell lines for iHLC organoids. Groups were compared to freshly thawed (0 h) PHH, significance was calculated using one-way ANOVA, * $p < 0.05$, ** $p < 0.01$.



Extended Data Fig. 3. qRamanomics reveals repeatable compositional phenotypic changes between different spheroids in same treatment group. a,b High-content quantitative Ramanomic imaging reveals distribution of molecular content throughout 3D PHH spheroids from a single donor ($n = 3$) and 3D iHLC organoids ($n = 3$). Scale bars = 50 µm. **c**, Pearson's correlation chemometric heatmaps illustrate colocalization of various molecular components and % difference between PHH and iHLC.

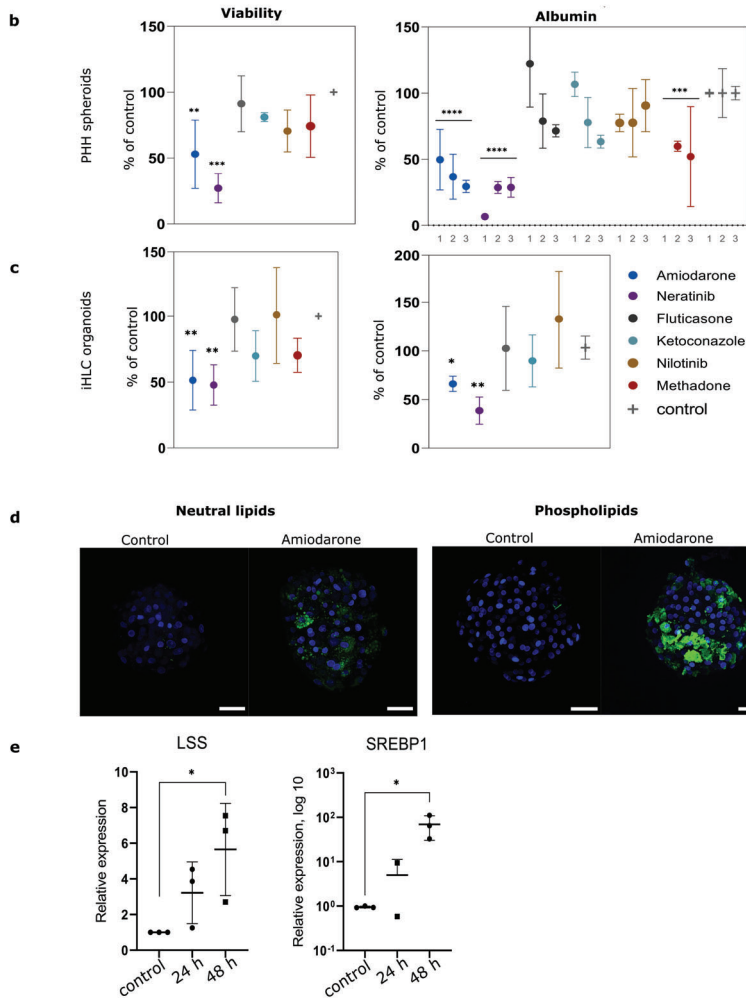


Extended Data Fig. 4. qRamanomics reveals chemotypic changes in response to drug treatment for PHH spheroids. a, High-content quantitative Ramanomic imaging reveals distribution of molecular content throughout 3D PHH spheroids from a single donor ($n = 3$). Scale bars = 50 μ m. **b**, 3D renderings of drug and/or drug metabolite deposits (shown in cyan) detected in PHH spheroids. The biomolecular matrix (i.e., protein, total lipid, and glycogen) was combined and is shown in grey (arbitrary intensity units) to reveal clear distinction between endogenous biomolecules and xenobiotic compounds present in specimens. Scale bars = 50 μ m.

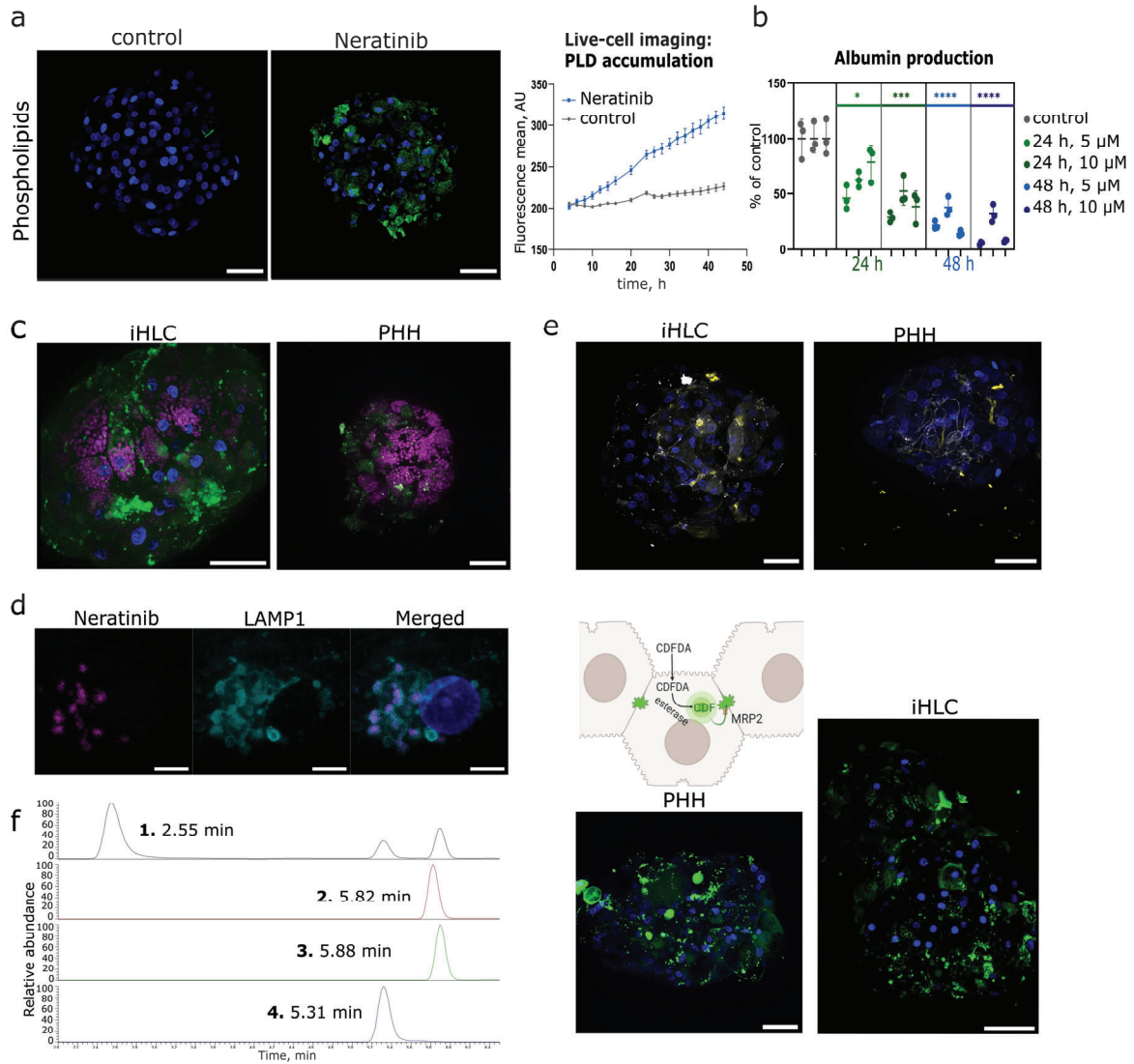


Extended Data Fig. 5. qRamanomics reveals chemotypic changes in response to drug treatment for iHLC organoids. **a**, High-content quantitative Ramanomic imaging reveals distribution of molecular content throughout 3D iHLC organoids from iHLC organoids ($n = 3$). Scale bars = 50 μ m. **b**, 3D renderings of drug and/or drug metabolite deposits (shown in cyan) detected in PHH spheroids. The biomolecular matrix (i.e., protein, total lipid, and glycogen) was combined and is shown in grey (arbitrary intensity units) to reveal clear distinction between endogenous biomolecules and xenobiotic compounds present in specimens. Scale bars = 50 μ m.

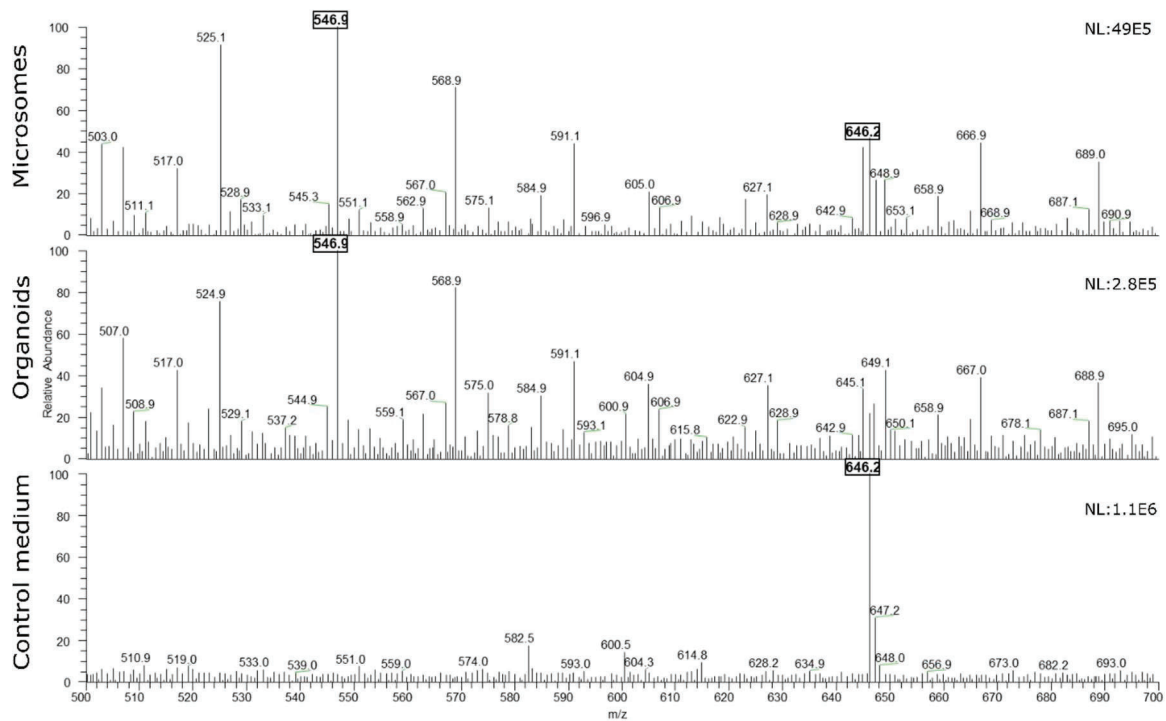
Drug	Drug Class	Hepatotoxicity likelihood score ³⁰	Mechanism of hepatotoxicity
Amiodarone	Group III antiarrhythmic	A (well-established cause of clinically apparent liver injury)	Induces microvesicular steatosis phospholipidolysis ^{39, 52, 53}
Nilotinib	BCR-ABL tyrosine kinase inhibitor	D (possible rare cause of clinically apparent liver injury)	NA
Fluticasone-propionate	Inhaled corticosteroid	No liver injury effect	NA
Ketoconazole	Azole antifungal	A (well-established cause of clinically apparent liver injury)	Inhibitor of CYP3A4 ³² . Hepatotoxicity may correlate with inhibition of mammalian sterol synthesis ^{33, 34}
Methadone	Narcotic analgesic	No liver injury effect	NA
Neratinib	EGFR & HER2 inhibitor	E* (unproven but suspected cause of clinically apparent injury)	NA



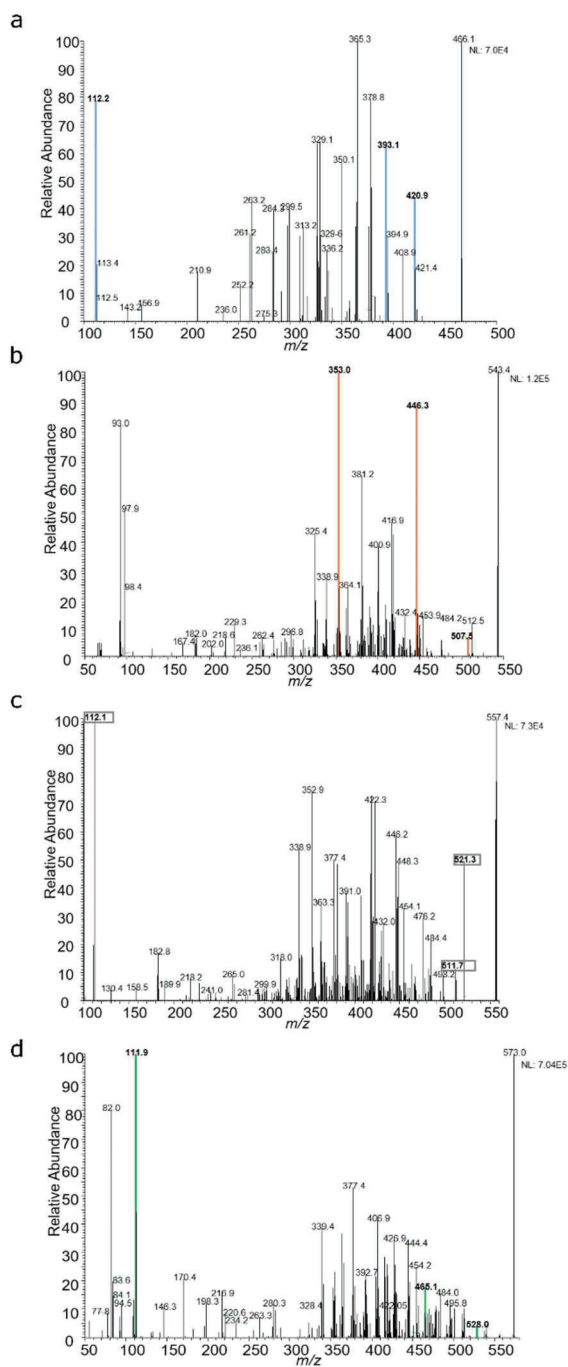
Extended Data Fig. 6. a, Table of tested compounds. **b,c**, Drug-induced changes in the viability (measured as ATP content) and albumin secretion level of PHH spheroids (**b**) and iHLC organoids (**c**) after 48h incubation with selected compounds. Data represented in % of changes from control as mean \pm SD, n= PHH from 3 donors (for methadone group – PHH from 2 donors), n = iHLC organoids from ≥ 3 independent differentiation experiments (2 – for methadone and nilotinib groups). * $p < 0,05$, ** $p < 0,01$, *** $p < 0,005$. **d**, Representative confocal images of FITC-labelled phospholipids and neutral lipids in PHH spheroids incubated for 48 h with amiodarone (10 μ M) and vehicle (control). Scale bars = 50 μ m. **e**, Relative expression of lanosterol synthase (LSS), sterol regulatory element-binding transcription factor 1 (SREBP1) in PHH spheroids after 24 and 48h of incubation with amiodarone (10 μ M), n = PHH from 3 donors. Groups were compared to non-treated group (control), significance was calculated using unpaired t-test, * $p < 0,05$.



Extended Data Fig. 7. **a**, Intracellular accumulation of phospholipids in PHH spheroids (confocal image after 48 h) and iHLC organoids (live cell imaging, Incucyte platform) in response to the incubation with 5 μ M neratinib. Scale bars = 50 μ m. **b**, Time- and concentration-dependent neratinib-induced decrease of albumin production in PHH spheroids from 3 donors. $n = 3$ replicates for each donor. Comparison performed using nested one-way ANOVA, * $p < 0,05$, ** $p < 0,01$, *** $p < 0,005$. **c**, Fluorescence of neratinib and/or associated metabolites (xenobiotics – magenta colour) and phospholipids accumulation (green) in primary hepatocytes (PHH) and iHLC in 3D organoids. Scale bars = 50 μ m. **d**, Accumulation of Neratinib and/or associated metabolites in LAMP1+ lysosomes. Scale bars = 5 μ m. **e**, Bile canaliculi-like structures with functional transporter MRP2 in PHH spheroids and iHLC organoids visualized by immunofluorescent staining for ZO1 (grey) and MRP2 (yellow), and CDFDA analysis. Scale bar 50 μ m. **f**, Representative chromatograms of neratinib and selected metabolites. Peak 1 (M3 described reference X): Selected reaction monitoring (SRM) = 466.2 [M-H⁺] -> 112.8, 393.1, 421.2. Peak 2 (M10 described in reference X): SRM = 543.200 [M-H⁺] -> 353.0, 446.1, 507.5. Peak 3 (Neratinib): SRM = 557.2 [M-H⁺] -> 112.2, 512.2, 521.3. Peak 4 (M12 described in reference X): SRM = 573.2 [M-H⁺] -> 464.3, 528.3, 111.9.



Supplementary Figure 1. MS spectra from direct injection of amiodarone incubated samples: human liver microsomes (10 μ M amiodarone, 60 min). The highlighted peak at m/z 646.2 is amiodarone, and the highlighted peak at m/z 546.9 is the detected amiodarone metabolite (44), - PHH spheroids (10 μ M amiodarone, 24 h). The highlighted peak at m/z 546.9 is the detected amiodarone metabolite (44); medium control samples without spheroids, incubated in 10 μ M amiodarone for 24 h. The highlighted peak at m/z 646.2 is amiodarone. Acquired using ESI and triple Q MS.



Supplementary Figure 2. Representative chromatograms of neratinib and selected metabolites. **a**, Peak 1 (M3 described reference 43): Selected reaction monitoring (SRM) = 466.2 [M-H]⁻ à 112.8, 393.1, 421.2. **b**, Peak 2 (M10 described in reference 43): SRM = 543.200 [M-H]⁻ à 353.0, 446.1, 507.5. **c**, Peak 3 (Neratinib): SRM = 557.2 [M-H]⁻ à 112.2, 512.2, 521.3. **d**, Peak 4 (M12 described in reference 43): SRM = 573.2 [M-H]⁻ à 464.3, 528.3, 111.9.

IV

Electromembrane Extraction and Mass Spectrometry for Liver Organoid Drug Metabolism Studies

Frøydis Sved Skottvoll, Frederik André Hansen, Sean Harrison, Ida Sneis Boger, Ago Mrsa, Magnus Saed Restan, Matthias Stein, Elsa Lundanes, Stig Pedersen-Bjergaard, Aleksandra Aizenshtadt, Stefan Krauss, Gareth Sullivan, Inger Lise Bogen, and Steven Ray Wilson*



Cite This: *Anal. Chem.* 2021, 93, 3576–3585



Read Online

ACCESS |



Metrics & More

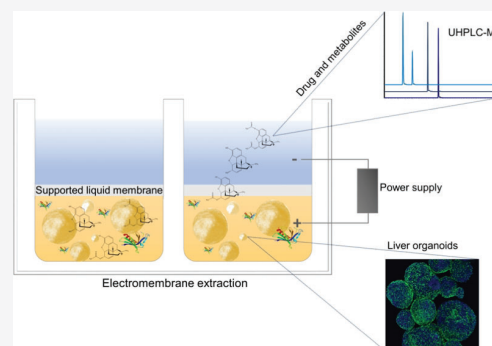


Article Recommendations



Supporting Information

ABSTRACT: Liver organoids are emerging tools for precision drug development and toxicity screening. We demonstrate that electromembrane extraction (EME) based on electrophoresis across an oil membrane is suited for segregating selected organoid-derived drug metabolites prior to mass spectrometry (MS)-based measurements. EME allowed drugs and drug metabolites to be separated from cell medium components (albumin, etc.) that could interfere with subsequent measurements. Multiwell EME (parallel-EME) holding 100 μ L solutions allowed for simple and repeatable monitoring of heroin phase I metabolism kinetics. Organoid parallel-EME extracts were compatible with ultrahigh-performance liquid chromatography (UHPLC) used to separate the analytes prior to detection. Taken together, liver organoids are well-matched with EME followed by MS-based measurements.



INTRODUCTION

The process of drug development is known to be time-consuming and bear financial uncertainties.^{1,2} It is estimated that from 5000 to 10 000 new molecular entities, only one new drug will enter the market.³ The advancement of this one drug from concept to market takes approximately 15 years and a cost of over \$1 billion, as well as the use of human resources, research skills, and technological expertise.³ As the majority of drug candidates are rejected late in the process and during clinical trials,³ one approach to reducing the assets put into the drug development may be to reject possible drug candidates early in the development process, i.e., during preclinical testing. This may be done by developing or utilizing in vitro models that adequately recapitulate the human in vivo response.

Organoids are three-dimensional tissue models derived from primary tissues, embryonic stem cells, or induced pluripotent stem cells (iPSC).^{4–6} These “mini” organs are emerging tools for studying human development and disease, serving as alternatives to cell cultures and animal models in drug development.^{7,8} A wide variety of organoids are being developed and studied, e.g., brain, heart, tumor tissue, and liver.^{9–12} Liver organoids can be valuable models for studying drug metabolism and toxicity¹³ (Figure 1A), perhaps even in a personalized fashion, as organoids can be derived from the cells of a patient.^{14,15}

Drug metabolism is a significant determinant of drug clearance and an indirect determinant of the clinical efficacy and toxicity of drugs.¹⁶ Thus, the mapping of the biotransformation pathway of drugs is crucial in the early

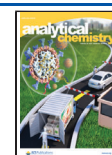
part of the drug development process.¹⁷ Clinical studies of xenobiotics in humans are subjected to constraints concerning ethical aspects. Several in vitro model systems have been developed to recapitulate human functions from the molecular level to the cellular, tissue, organ, or whole organism level. The most commonly used in vitro models for drug metabolism studies include subcellular fractions, e.g., human liver microsomes (HLMs), S-9 fractions, and human hepatocytes. However, current in vitro models has some disadvantages. For example, HLMs do not represent a complete course of metabolism as they lack soluble phase II enzymes.¹⁶ Additionally, higher biotransformation rates are obtained in HLMs compared to humans, most likely because of the enriched enzyme concentrations and the absence of competing enzymes.¹⁷ Also, animal models can have shortcomings and have frequently been shown to lead to wrong predictions of drug interaction and toxicity in humans.¹⁸

For both in vitro and in vivo models, drug metabolism studies are very often performed utilizing liquid chromatography-mass spectrometry (LC-MS). Essentially, the mass spectrometer (MS) can measure the drugs and their

Received: December 4, 2020

Accepted: January 25, 2021

Published: February 3, 2021



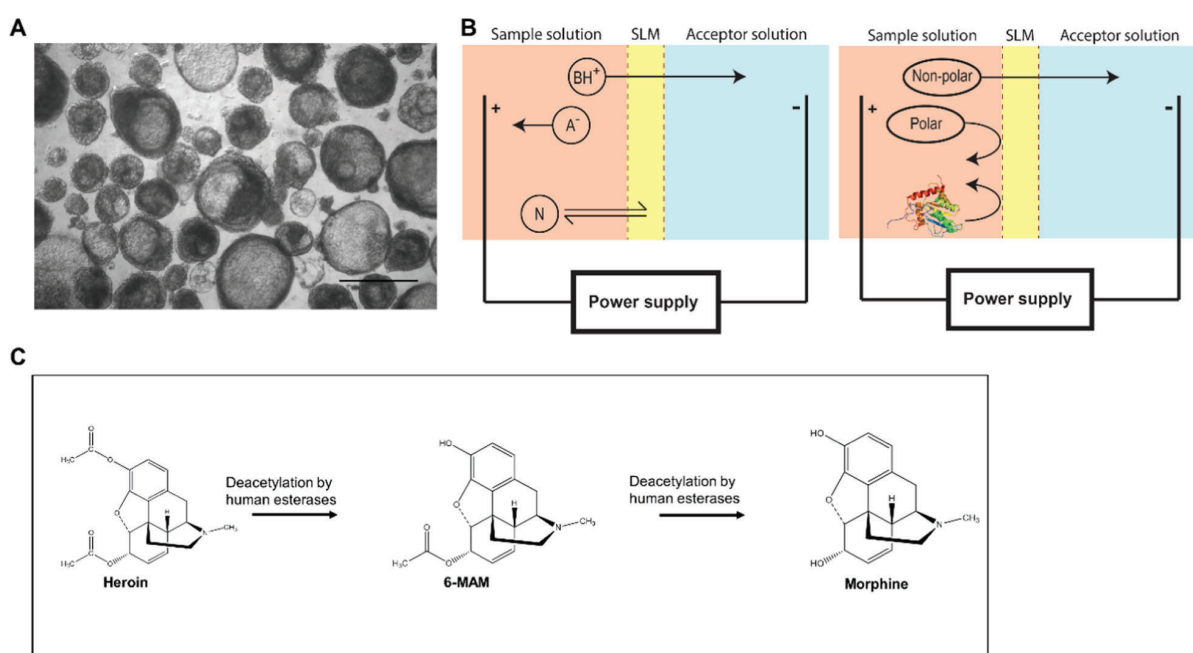


Figure 1. (A) Light microscopy picture of iPSC-derived liver organoids used in this study, scale bar 500 μm . (B) Electromembrane extraction (EME) principle. Charged analytes migrate from the donor solution (i.e., the sample solution) across the supported liquid membrane (SLM) and into the acceptor solution. Extraction selectivity is obtained by voltage polarity and partitioning into and through the SLM. Polar molecules and macromolecules are effectively discriminated from extraction by the hydrophobic SLM. (C) Illustration of well-documented liver phase I metabolism of heroin undergoing deacetylation to 6-MAM and morphine by human esterases (e.g., human liver carboxylesterase 1 and 2, hCE1 and hCE2, respectively).

metabolites with a high degree of selectivity. Prior to MS measurements, the compounds in the sample are separated by the LC system, allowing for increased sensitivity and selectivity.

There are few studies utilizing LC-MS for drug metabolism measurements of organoids.^{19–21} To the best of our knowledge, there are currently no studies dedicated to demonstrating the potential of drug metabolism studies with liver organoids and LC-MS.²² The key focus of this study is to show the potential of using liver organoids and LC-MS measurements as a methodology for drug metabolism studies. To ensure an efficient combination of organoids, LC-MS, and drug metabolism, several challenges must be addressed. The amounts of organoids can (depending on the production method) be quite limited per sample, requiring efficient sample preparation prior to analysis. It is also highly desirable that drug metabolism studies with organoids can be upscaled, which is difficult to combine with more standard sample preparation approaches which include centrifugation steps and manual pipetting (Figure S1A). In addition, liver organoids are grown in a complex medium (e.g., can contain 10% fetal bovine serum) requiring a thorough sample clean-up prior to LC-MS analysis. For extracting drugs, and the metabolites produced by organoids, we applied electromembrane extraction (EME; Figures 1B and S1B). In EME, an oil immobilized in the pores of a porous membrane (supported liquid membrane, SLM) is used to extract analytes from a cell medium (donor solution) to a protein-free MS-compatible acceptor solution. For the process, both aqueous compartments are pH-adjusted to facilitate analyte ionization, and voltage is applied across the SLM. EME is therefore essentially an electrophoretic migration of ionized analytes across an oil

membrane.^{23,24} Extraction selectivity is determined by both the partitioning of analytes into the SLM and the polarity and magnitude of the applied voltage. High clean-up efficiency of the target analytes can thus be achieved, and EME is highly successful in separating small-molecule drug substances from biological matrix substances, including salts, lipids, phospholipids, proteins, and blood cells.^{24,25} Such a clean-up is highly important prior to liquid chromatography-mass spectrometry to avoid ion suppression or enhancement. EME has recently advanced to the 96-well plate format^{26–28} (parallel-EME), and chip systems.^{29,30} Considering its documented traits regarding simple sample clean-up, we focus on using EME for organoids, which can be costly and limited in availability.

As a model system to show the potential of the methodology, we study the phase I metabolism of heroin to 6-monoacetylmorphine (6-MAM) and morphine (Figure 1C), as heroin liver metabolism is highly established, both with regards to the metabolizing enzymes^{31–33} (e.g., human liver carboxylesterase 1 and 2, hCE1 and hCE2, respectively), and the resulting metabolites. With the presented experiments, we have shown the proof of concept that liver organoids are EME compatible, and evaluate the advantages and challenges of parallel-EME/organoid/MS-based analysis for drug metabolism.

EXPERIMENTAL SECTION

Chemicals and Solutions. 2-Nitrophenyl octyl ether (NPOE), 2-nitrophenyl pentyl ether (NPPE), bis(2-ethylhexyl) hydrogen phosphite (DEHPi), bis(2-ethylhexyl) phosphate (DEHP), sodium hydroxide, ammonium formate (>99%), formic acid (FA, reagent grade 95%), L-ascorbic acid-2 phosphate (AAP) were purchased from Sigma Aldrich (St.

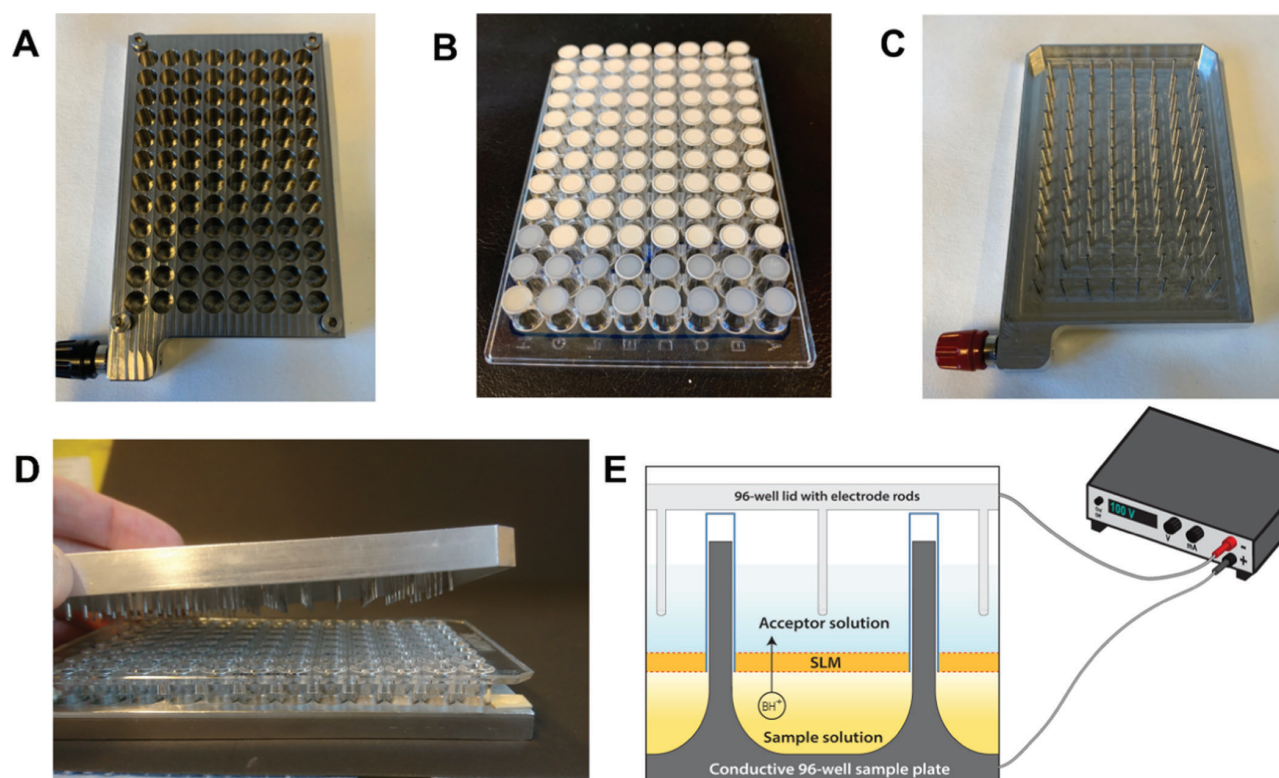


Figure 2. Experimental setup of 96-well parallel-EME. (A) Ninety-six well sample reservoir plate constituting the donor solution. (B) Ninety-six well filter plate, constituting the acceptor solution. (C) Aluminum lid with 96 electrode rods. (D) All plates clamped together. (E) Illustration of the extraction setup of parallel-EME coupled to the external power supply.

Louis, MO). LC-MS grade water and acetonitrile (ACN) were purchased from VWR (Radnor, PA). Chromasolv methanol (LC-MS grade) was from Honeywell Riedel-de Haën (Seelze, Germany). Heroin HCl, 6-MAM HCl, and morphine were purchased from Lipomed AG (Arlesheim, Switzerland). Heroin-*d*₉, 6-MAM-*d*₆, and morphine-*d*₃ were purchased from Cerilliant (Austin, TX). Unless otherwise stated, the water used was type 1 water purified by a Milli-Q water purification system from Merck Millipore (Billerica, MA).

The 5 and 10 mM ammonium formate buffer (w/v) was made by dissolving ammonium formate in LC-MS grade water followed by pH adjustment by the addition of FA to pH 3.1. A freshly made stock solution of 1 mM heroin HCl in 0.9% NaCl was made prior to each organoid experiment (stored at 4 °C) and also used to prepare heroin calibration solutions. A stock solution of 6-MAM and morphine was prepared in 5 mM ammonium formate buffer pH 3.1 at a concentration of 50 μM each and stored at 4 °C. Two stock solutions of the internal standards heroin-*d*₉, 6-MAM-*d*₆, and morphine-*d*₃ were prepared in 5 mM ammonium formate buffer pH 3.1 with analyte concentration of 1.5 μM each and 3 μM each, respectively, and stored at 4 °C.

Liver Organoid Differentiation from Induced Pluripotent Stem Cells. The iPSC cell line HPSI0114i-vabj_3 (Wellcome Trust Sanger Institute, Cambridgeshire, U.K.) was differentiated toward liver organoids using media from protocol by Ang et al.³⁴ Briefly, the HPSI0114i-vabj_3 iPSC line was differentiated toward definitive endoderm in Iscove's modified Dulbecco's medium/F12 medium (Thermo Fisher Scientific, Waltham, MA) containing 3 μM CHIR99021 (STEMCELL Technologies, Vancouver, Canada), 50 nM PI-

103 from Bio-Techne Ltd. (Abingdon, United Kingdom) and 100 ng/mL activin A (PeproTech, Cranbury, NJ) for one day and 100 ng/mL activin A for 2 more days. The definitive endoderm cells were subsequently treated with 1 μM A8301 (Bio-Techne Ltd.), 10 ng/mL FGF2 (PeproTech), 30 ng/mL BMP4 (PeproTech), and 2 μM all-trans retinoic acid (Sigma Aldrich) for one day, then with 10 ng/mL FGF2, 30 ng/mL BMP4, 1 μM forskolin (PeproTech), 1 μM Wnt-C59 (Bio-Techne Ltd.) for 2 more days and with 10 ng/mL FGF2, 30 ng/mL BMP4, 1 μM forskolin for another day. On day 8, the cells were detached and aggregated in the U bottom microwells in the presence of 20 ng/mL HGF (PeproTech), 10 ng/mL oncostatin M (OSM, PeproTech), 0.1 μM dexamethasone (Bio-Techne Ltd.), 1 μM forskolin, 10 μg/mL human recombinant insulin (Sigma Aldrich), and 100 μM AAP. After the formation of organoids at day 10, they were transferred into low attachment plates and cultured for another 10 days as free-floating organoids in William's E media (Thermo Fisher Scientific), supplemented with 10 ng/mL HGF and 10 ng/mL OSM, 10 μg/mL insulin, 100 μM AAP, 0.1 μM dexamethasone, 1 μM forskolin, and 10 μM DAPT (Bio-Techne Ltd.). The iPSC line AG27^{35–38} was differentiated using a small-molecule-driven protocol that aims to sequentially mimic in vivo liver development, resulting in hepatocyte-containing liver organoids as described by Harrison et al.³⁹

Liver Organoid Heroin Incubation. Prior to heroin incubation with organoids, 1 mM heroin was diluted in the respective cell medium and sterilized by filtration using a 0.22 μm Millex-GV syringe filter (Merck Millipore). After 20 days of differentiation, from 20 to 60 organoids per well were

treated with 10 or 50 μM heroin in cell medium for 1, 3, 6, and 24 h, respectively ($n = 3$), in separate Nunc flat-bottom 96-well microplates (Thermo Fisher Scientific). Metabolism was stopped by adding FA to a final concentration of 0.11 M, and the plates were frozen at $-80\text{ }^\circ\text{C}$. In parallel, cell medium free from organoids ($n = 3$) were used as drug degradation control samples.

Parallel Electromembrane Extraction Setup. Prior to the extraction, 50 μL of the heroin-exposed liver organoid samples (containing 0.11 M FA) was added to 40 μL of water and 10 μL of the 1.5 μM or 3 μM internal standard solution. The samples were then loaded into the wells of an in-house built 96-well stainless steel plate (Figure 2A), previously described by Restan et al.²⁸ A volume of 3 μL of DEHP/NPOE (10/90, w/w) was immobilized into the membrane pores (0.45 μm pore size) of a 96-well MultiScreen-IP poly(vinylidene fluoride) (PVDF) filter plate from Merck Millipore (Figure 2B). The steel and filter plates were subsequently clamped together and 100 μL of 10 mM ammonium formate pH 3.1 was loaded into each well of the filter plate, and thus constituting the acceptor solution. The filter plate was used to house the acceptor solution because the geometry of the steel plate wells provided better convection of the donor solution in this configuration, which improved the extraction kinetics. A conductive in-house built aluminum lid with 96 electrode rods (Figure 2C) was placed onto the filter plate, and the whole construct (Figure 2D) was placed on a Vibramax 100 Heidolph shaking board (Kellheim, Germany). The steel plate holding the organoid solution was connected to the anode of an external power supply (model ES 0300-0.45, Delta Elektronika BV, Zierikzee, The Netherlands), while the aluminum electrode lid was connected to the cathode (Figure 2E). Simultaneous extraction of all samples was performed for 15 min at 900 rpm agitation, with 30 V applied for the first 2 min and 50 V applied for the remaining extraction duration. The stepped voltage was used to ensure that the extraction current was kept below 50 μA per well, which was considered a safe limit for robust operation.⁴⁰

Ultrahigh-Performance Liquid Chromatography-Mass Spectrometry (UHPLC-MS). Determination of heroin, 6-MAM, and morphine was performed using UHPLC-MS based on a previously described method.⁴¹ The sample extracts were diluted $\times 10$ with 5 mM ammonium formate pH 3.1 and analyzed using an Acquity UHPLC pump coupled to a Xevo TQ (triple quadrupole) MS with electrospray ionization (ESI) interface, all from Waters (Milford, MA). The separation was achieved using the Acquity UPLC HSS T3 C18 column (2.1 mm \times 100 mm, 1.8 μm particles). Solvent A consisted of 10 mM ammonium formate buffer pH 3.1 and solvent B consisted of methanol. The sample injection volume was set to 7.5 μL , and the gradient elution was carried out at a flow rate of 0.5 mL/min at 65 $^\circ\text{C}$ using the following gradient profile: from 0–0.5 min; 100% solvent A, 0.5–2.7 min; 0–10% solvent B, 2.7–3.3 min; 10–20% solvent B, 3.3–4.6 min; 20–80% solvent B, 4.6–4.61 min; 80–100% solvent B, 4.61–6.60 min; 100% solvent B, 6.60–6.61 min; 100–0% solvent B, 6.61–7.50 min; and 100% solvent A. The capillary voltage was 3 kV, source temperature was 150 $^\circ\text{C}$, desolvation temperature was 500 $^\circ\text{C}$, and cone gas flow was 990 L/h. Detection was performed in positive mode using multiple reaction monitoring (MRM) with MS/MS transitions (MS/MS transition 1 being the quantifier and MS/MS transition 2 the qualifier) and collision energies for heroin (m/z 370 > 268 at 30 eV and m/z 370 >

211 at 38 eV), 6-MAM (m/z 328 > 165 at 42 eV and m/z 328 > 211 at 30 eV), morphine (m/z 286 > 201 at 24 eV and m/z 286 > 165 at 42 eV), heroin- d_9 (m/z 379 > 272 at 30 eV), 6-MAM- d_6 (m/z 334 > 165 at 42 eV), and morphine- d_3 (289 > 165 at 30 eV). Data was acquired and processed using MassLynx 4.1 software (Waters).

Nanoliquid Chromatography-Mass Spectrometry (nanoLC-MS). The nanoLC-MS setup consisted of a TSQ Quantiva, triple quadrupole MS, the nanoFlex ESI ion source, and the EASY-nLC 1000 or 1200 pump equipped with an autosampler, all from Thermo Fisher. Acclaim PepMap 100 C18 (3 μm particle size) pre- (75 μm inner diameter, ID, and 20 mm length) and analytical (75 μm ID \times 50 mm) columns from Thermo Fisher Scientific were used for the chromatographic separation. In-house made⁴² analytical columns were packed with 3 μm Atlantis T3 particles (Waters) or 2.6 μm Accucore particles (Thermo Fisher Scientific) in fused silica capillaries of 75 μm ID from Polymicro Technologies (Phoenix, AZ). The analytical column was coupled to a 40 mm stainless steel emitter (20 μm ID) purchased from Thermo Fisher. The extracted organoid samples (AG27 iPSC derived) were further diluted $\times 10^3$ in 5 mM of ammonium formate pH 3.1 buffer, and the injection volume was set to 2 μL . The nanoLC pump was equipped with two solvent compartments (A and B), where A contained 0.1% FA in the LC-MS grade water (v/v) and B contained 0.1% FA in the LC-MS grade water and ACN (10/90, v/v). The gradient elution was carried out with 3–50% B in 8 min with a constant flow rate of 500 nL/min. The spray voltage was set to 2.2 kV and the ion transfer tube temperature was set to 310 $^\circ\text{C}$. Detection was performed in positive mode using MRM with MS/MS transitions and collision energies for heroin (m/z 370 > 268 at 38 eV and 370 > 211 at 41 eV), 6-MAM (m/z 328 > 165 at 48 eV and 328 > 211 at 36 eV), morphine (m/z 286 > 181 at 48 eV and 286 > 165 at 51 eV), heroin- d_9 (m/z 379 > 272 at 38 eV and 379 > 211 at 41 eV), 6-MAM- d_6 (m/z 334 > 211 at 35 eV and 334 > 165 at 48 eV), and morphine- d_3 (m/z 289 > 181 at 48 eV and 289 > 165 at 51 eV).

For a one-column setup, the pump outlet was coupled to an external six-port valve from Valco Instruments Company Inc (VICI, Houston, TX) equipped with a 75 μm ID \times 11 cm fused silica injection loop (500 nL), a nut with a syringe sleeve and a 75 μm ID \times 10 cm fused silica capillary waste outlet. The flow outlet from the six-port valve was coupled to a stainless steel tee-piece (VICI) through a 20 μm \times 40 cm fused silica capillary from Polymicro Technologies using stainless steel nuts and vespel/graphite ferrules (VICI). The analytical column inlet was coupled to the stainless steel tee-piece, also coupled to a plug through a 550 mm nanoViper (75 μm ID, Thermo Fisher). A 500 μL syringe (51mm) from Hamilton (Reno, Nevada) was used to load the samples. Xcalibur version 2.2 was used to obtain chromatograms and mass spectra (Thermo Fisher).

Protein Profiling by Nanoliquid Chromatography-Mass Spectrometry. Acetone precipitated AG27 iPSC-derived liver organoid protein samples were subjected to sodium dodecyl sulfate-polyacrylamide gel electrophoresis (SDS-PAGE) gel electrophoresis, and the gel lanes were sliced into five sample fractions and digested with trypsin as previously described.⁴³ The peptide solutions were desalted using OMIX C18-micro solid-phase extraction (SPE) columns (Agilent, Santa Clara, CA). A Q-Exactive mass spectrometer (Thermo Fisher Scientific) equipped with a nanoFlex nano-

spray ion source was used for the nanoLC-MS analyses, coupled to an EASY-nLC 1000 pump (Thermo Fisher). Peptide separation was achieved using Acclaim PepMap 100 pre- (20 mm) and separation columns (250 mm) of 75 μm inner diameter and 3 μm particles (Thermo Fisher). Solvent A was 0.1% FA in LC-MS grade water (v/v) and solvent B was 0.1% FA in LC-MS grade water and ACN (5/95, v/v). Peptides were separated using a 180 min long gradient ranging from 3–15% solvent B (after optimization with the predigested HeLa samples from Thermo Fisher). The mass spectrometer was run in a positive mode with full MS ($m/z = 400\text{--}2000$) and data-dependent tandem mass spectrometry (ddMS2) with top N set to be 10 ions. Raw files were processed and database searches performed with Proteome Discoverer 2.3 (Thermo Fisher Scientific), using MASCOT version 2.4 to search the SwissProt database (human, 20 431 entries). Proteins were identified with the following settings; peptide identification with a false discovery rate (FDR) threshold of ≤ 0.01 , protein identification with a FDR threshold of ≤ 0.01 (strict) and ≤ 0.05 (relaxed) and digestion by trypsin with at most one missed cleavage. Dynamic modification was set to be oxidation and acetyl (N-term), static modification was set to be carbamidomethyl. Information on the elution profile and fragment match spectrum of each of the identified peptides for hCES1 (accession number P23141), hCES2 (also called cocaine esterase, accession number O00748), and UDP-glucuronosyltransferase 2B7 (accession number P16662) were obtained and verified by comparison with the raw file.

Calculation of Recovery. Recovery measurements were performed using capillary electrophoresis with ultraviolet spectroscopy detection (CE-UV) (see Supporting Information for experimental description) with an initial analyte concentration of 5 μM . The recovery (%) was calculated using the following formula

$$R (\%) = \frac{A_{\text{final}}}{A_{\text{initial}}} \times 100\%$$

where A_{final} and A_{initial} are the area of analyte collected in the acceptor solution and the area of the analyte originally present in the sample.

RESULTS AND DISCUSSION

In this study, several analytical approaches were evaluated for liver organoid drug measurements. With the future objective of advancing to online analyses, EME was assessed in a 96-well format (parallel-EME) for the high-throughput clean-up of analytes from the organoid cell medium, a method previously shown to enable selective and fast extraction from complex matrices (and also on-chip).⁴⁴ A conventional UHPLC-MS method used for clinical routine analyses was applied to explore the heroin-metabolizing properties of the parallel-EME extracted liver organoids. To get an understanding of the heroin-metabolizing liver enzymes present in the organoids, an untargeted proteomic case study using nanoLC-MS was undertaken. Lastly, two analytical approaches more suitable for online action, limited samples, and increased sensitivity were evaluated: CE, which is widely established for rapid on-chip separations,^{45–47} and nanoLC-MS, which allows high sensitivity measurements.⁴⁸

Parallel Electromembrane Extraction Optimization for Heroin and Metabolites. To evaluate the potential of MS for the analysis of liver organoids, heroin was chosen as a

model substance due to its familiar phase I metabolism to 6-MAM and morphine in the liver. To our knowledge, heroin metabolism of organoids has not previously been studied with mass spectrometric-based techniques. Although morphine extraction with EME has previously been performed,^{49–51} the extraction of heroin and 6-MAM with EME has, to our knowledge, not previously been performed. Therefore, parallel-EME conditions focusing on these three compounds were initially assessed. The experimental conditions (Figure 3) were

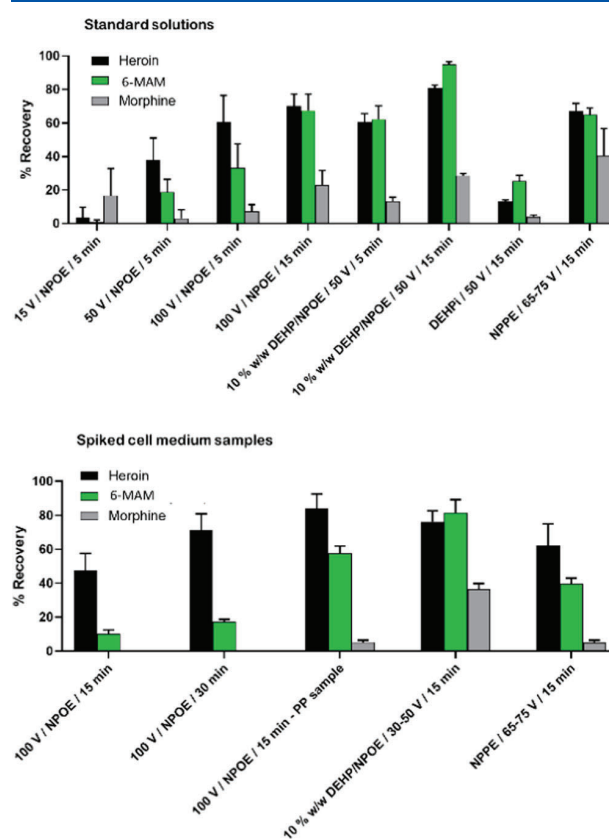


Figure 3. Analyte recovery (%) of parallel-EME under varying conditions (SLM composition, extraction voltage, and extraction time), with 5 μM standard solutions and spiked cell medium samples using CE-UV for quantitation.

selected based on previous experience and literature reports.^{49,52,53} Due to the difference in the polarity of the analytes, $>30\%$ recovery and $<15\%$ RSD were set as the acceptance criteria of extraction performance. Best recovery and repeatability for analytes in both standard solutions and spiked cell medium samples were obtained using a parallel-EME system comprising 10% (w/w) DEHP/NPOE as SLM, an extraction time of 15 min, and an extraction voltage of 50 V. From the cell medium, these conditions gave recoveries of 76% (heroin), 82% (6-MAM), and 36% (morphine) and RSD $<10\%$, which was considered acceptable for the current application. With these parameters, the average extraction current was $<50 \mu\text{A}$ per well throughout the extraction. The extraction method was therefore not optimized any further. Elevated voltages could possibly improve the recoveries but can potentially also result in analyte degradation. In addition, for increasing the accuracy, correction for nonexhaustive

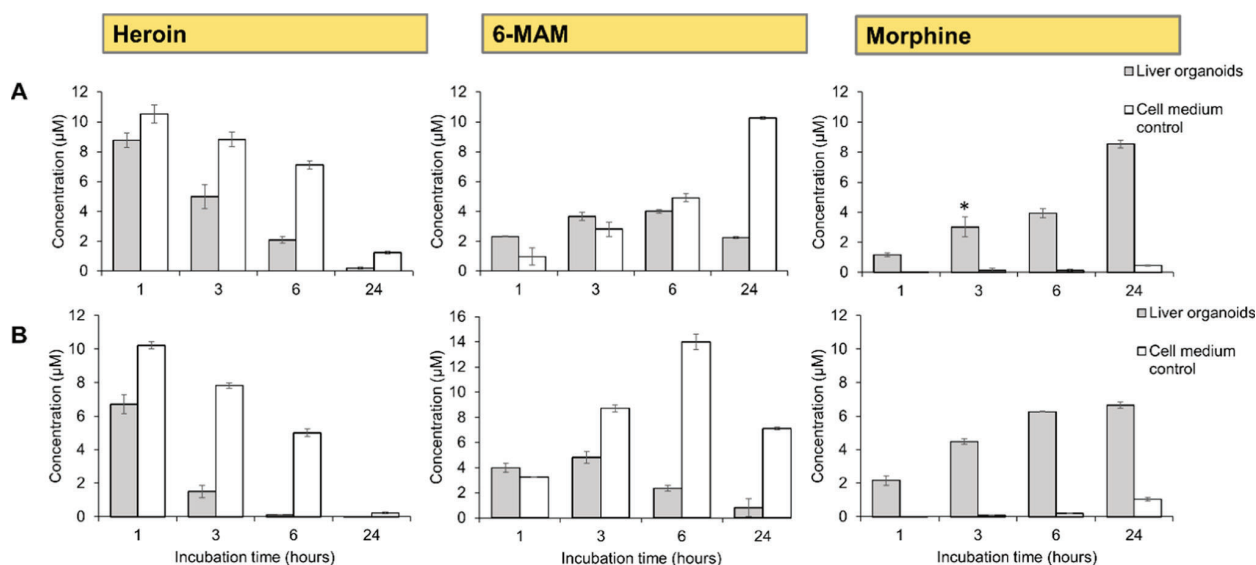


Figure 4. Concentration of heroin and metabolites in a study of liver organoid drug metabolism using parallel-EME and UHPLC-MS after incubation of liver organoids differentiated from the iPSC cell lines (A) AG27 (60 organoids) and (B) HPSI0114i-vabj_3 (20 organoids) in 10 μM heroin for 1, 3, 6, and 24 h. In parallel, cell medium free from organoids was used as the drug degradation control sample. Each bar represents the mean (\pm SD) of triplicate samples. One of the three replicates of time point 6 h liver organoids (HPSI0114i-vabj_3) was discarded. The asterisk indicates the removal of one data point due to a poor internal standard signal.

extractions was done by spiking the samples with isotopically labeled internal standards prior to extraction.

Parallel Electromembrane Extraction of Liver Organoid Heroin Metabolites. Samples containing 20 and 60 liver organoids per well were exposed to 10 μM heroin for 1, 3, 6, and 24 h. With the exception of 6-MAM and heroin at time point 24 h, the sample-to-sample repeatability was 0.4–25% with the two organoid iPSC sources (Figure 4A,B). Heroin levels decreased with time to 6-MAM (both enzymatic and nonenzymatic), and with subsequent enzymatic metabolism to morphine, adding to the confirmation that the liver organoids had traits related to human livers. Similar heroin metabolism kinetics was also observed for liver organoids derived from hepatocytes from one patient case (see Figure S2). However, the kinetics were (expectedly) substantially slower than that observed with, e.g., high enzyme-availability microsomes and S-9 fraction,^{17,54} see Figure S3; although parallel-EME and MS are compatible with phase I metabolism monitoring, we were not able to observe phase II metabolites morphine-3-glucuronide (M3G) and morphine-6-glucuronide (M6G). Traces of these metabolites could however be observed when employing more manual, centrifugation-based sample preparations (Figure S4). A key reason is a weakness of EME, that highly polar compounds have low recovery; this can in many cases be fine-tuned.^{53,55}

To complement the observations of the liver organoids enzymatic heroin-metabolizing properties, a case study using MS-based untargeted proteomics was undertaken. We could identify the presence of proteotypic peptides (FDR \leq 1%) related to the key liver enzymes^{56–60} hCES1 (9 peptides identified) and hCES2 (4 peptides identified) in the organoids differentiated from the iPSC cell line AG27 (Figure 5A–C, see also Table S1 for peptide overview). Also, one peptide was identified related to one of the heroin phase II metabolism enzymes,^{33,57} UDP-glucuronosyltransferase 2B7 (Table S1).

Compatibility of Organoid EME Extracts with Various Separation Techniques. The organoid EME extracts were

analyzed using UHPLC-MS instrumentation, which provided high-resolution separations within 5 min (Figure S5). We have also investigated other separation approaches that can be compatible with small samples and online action. Capillary electrophoresis, perhaps the most “chip-ready” of the techniques investigated, was capable of fast separations of organoid extracts (separation within 2.5 min) and low sample consumption (injection volume equivalent to 107 nL), with these initial experiments demonstrated with simple UV detection (Figure S6). However, organoid incubation in 50 μM heroin was needed to achieve detection with CE-UV, and thus no further quantification of the analytes could be performed.

The limit of quantification (LOQ) for UHPLC-MS measurements in this study was 1 nM (7 μL injection volume). NanoLC, a sensitive approach that has been mostly associated with proteomics in recent years, was seen to provide 0.95 pM detection (1 μL injection volume) for some small-molecule analytes such as heroin (results not shown). For the more hydrophobic analytes heroin and 6-MAM, the organoid extracts analyzed with nanoLC-MS could thus be 1000 times more diluted compared to that of UHPLC-MS analysis without compromising the chromatographic performance or sensitivity (Figure 6A). However, poor performance was associated with the nanoLC-MS analysis of morphine, the most polar of the metabolites observed; the chromatographic peak was completely absent in the chromatograms of the organoid extracts (Figure 6A) and sporadically very deformed or absent in that of standard solutions. This was the case for large volume injection, both using on-column injection and an SPE column. We also examined the in-house-packed nano reversed-phase (RP) LC columns which were more compatible with highly aqueous mobile phases (Accucore and Atlantis T3), but poor peak shape and breakthrough/poor retention time repeatability were still issues. Various parameters were tested, e.g., sample loading time and maximum sample loading pressure (of the Thermo nano pumps). To illustrate these

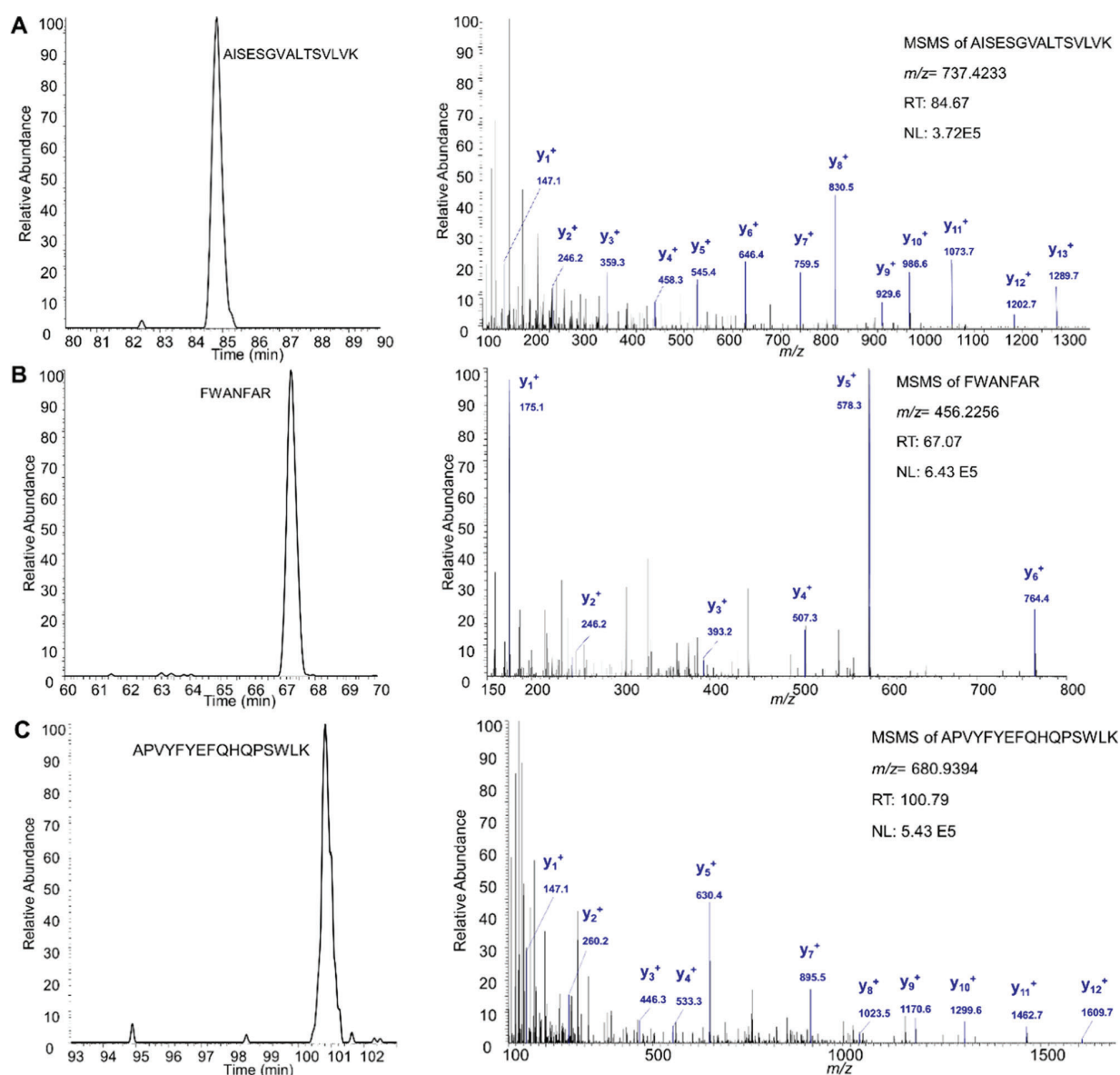


Figure 5. Total ion chromatogram of identified peptides (left) and the respective peptide fragmentation spectrum (right) of enzymes related to heroin liver phase I metabolism. (A) Peptide AISESGVALTSVLVK (m/z 737.42) from hCES1, identified at charge +2. (B) Peptide FWANFAR (m/z 456.23) from hCES1, identified at charge +2. (C) Peptide APVYFYEFQHQPSWLK (m/z 680.94) from hCES2, identified at charge +3.

effects, see Figure 6B, which shows that several loading times were suited for 6-MAM and heroin using on-column injection, but none were suited for morphine.

CONCLUSIONS

Liver organoids and LC-MS measurements are a promising concept for drug metabolism studies, here demonstrated for heroin phase I metabolism. This concept can be well suited for drug metabolism studies of other drugs, and direct measurements of drug metabolism could also provide valuable insight when optimizing organoid development protocols. A proteomic case study using nanoLC-MS identified proteotypic peptides from heroin-metabolizing enzymes, complementing the observations of the liver organoids enzymatic heroin-metabolizing properties. EME-MS was shown to be a promising combination for the liver organoid-based analysis

of drug metabolism. EME in a 96-well format (parallel-EME) was used to extract heroin and metabolites from various organoids in a complex medium, followed by UHPLC-MS measurements. In addition, the chromatographic performance was not perturbed by the initial complex matrix (analyte retention time repeatability with a maximum RSD of 0.07%), suggesting that parallel-EME was a suitable basis for organoid-derived sample preparation. It is reasonable to assume that the approach can also be applicable to other organoid variants, e.g., kidney and heart. Parallel-EME was indeed an approach that allowed multiple samples to be simply handled, more so than standard approaches to related tissues (centrifugations, several sample pipetting steps), which can allow higher throughput in larger-scale studies. We are currently developing 96-well plates made of conductive polymers, which we believe will be suited for both cell studies and EME; this will reduce yet another step

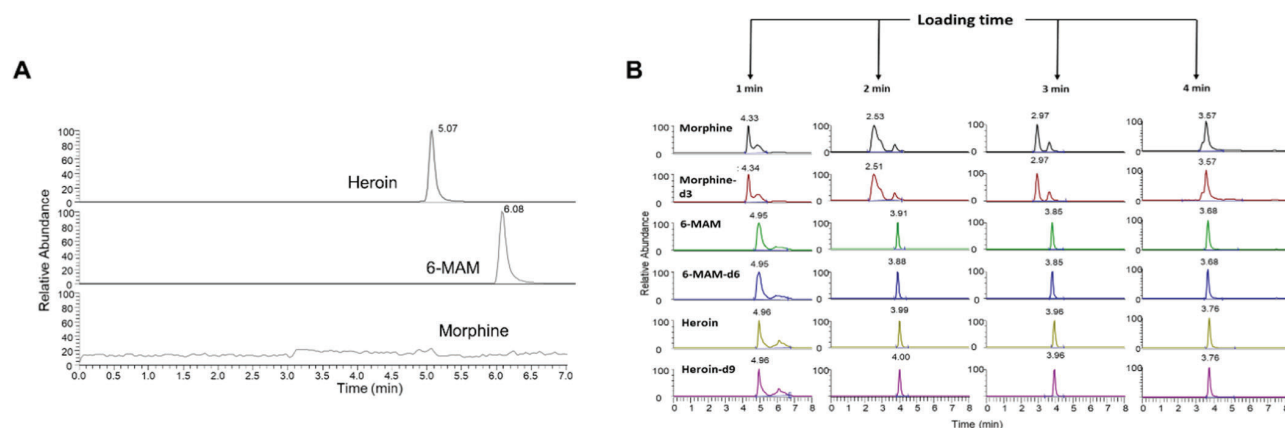


Figure 6. (A) MRM chromatograms of heroin, 6-MAM, and morphine in the extracted liver organoid sample treated with 10 μ M heroin for 1 h (AG27). The sample was analyzed using a two-column setup with Acclaim PepMap columns and injection volume of 2 μ L. (B) MRM chromatograms of a 375 nM standard solution containing heroin, morphine, 6-MAM, and their corresponding internal standards were analyzed using the one-column setup equipped with an Acclaim PepMap commercially packed analytical column with different on-column loading times (1, 2, 3, and 4 min), and injection volume of 500 nL.

of sample handling. One disadvantage that needs to be addressed is the difficulty in extracting very polar metabolites with EME, and further optimizations will therefore continue.

Following this proof-of-concept study, we will continue to explore iterations of the here presented EME configuration with the aim of further increasing the sensitivity while retaining robustness and scalability; a natural next step will be nanoliter-scale online EME-LC-MS of organoid-derived samples. Related systems have been demonstrated with microsomes,³⁰ but those systems require larger separation columns and are arguably not suited for trace samples. Due to challenges with nanoLC, we will instead likely investigate the use of capillary LC or microbore LC as a compromise between sensitivity and robustness.

■ ASSOCIATED CONTENT

SI Supporting Information

The Supporting Information is available free of charge at <https://pubs.acs.org/doi/10.1021/acs.analchem.0c05082>.

Schematic overview of the workflow of drug studies performed with the sample preparation approaches centrifugation and Pa-EME, liver organoid drug metabolism using Pa-EME and UHPLC-MS after incubation of patient-derived liver organoids in heroin, heroin metabolism in microsomes and S-9 fractions using UHPLC-MS, liver organoid drug phase I and II metabolism using centrifugation, and UHPLC-MS, a table on the peptides identified of the enzymes hCES1, hCES2, and UDP-glucuronosyltransferase 2B7, chromatogram showing the separation of the analytes M3G, M6G, morphine, 6-MAM, and heroin with the use of UHPLC-MS, electropherogram of liver organoid drug phase I metabolism using Pa-EME and CE-UV, and the following additional experimental procedures: heroin metabolism assay in S-9 fractions and microsomes, sample preparation using centrifugation, and CE-UV setup (PDF)

■ AUTHOR INFORMATION

Corresponding Author

Steven Ray Wilson – Department of Chemistry and Hybrid Technology Hub-Centre of Excellence, Institute of Basic Medical Sciences, Faculty of Medicine, University of Oslo, NO-0315 Oslo, Norway; orcid.org/0000-0002-9755-1188; Phone: +47 97010953; Email: stevnw@kjemi.uio.no

Authors

Froydis Sved Skottvoll – Department of Chemistry and Hybrid Technology Hub-Centre of Excellence, Institute of Basic Medical Sciences, Faculty of Medicine, University of Oslo, NO-0315 Oslo, Norway; orcid.org/0000-0002-5299-2502

Frederik André Hansen – Department of Pharmacy, University of Oslo, NO-0316 Oslo, Norway; orcid.org/0000-0002-1666-0447

Sean Harrison – Hybrid Technology Hub-Centre of Excellence, Institute of Basic Medical Sciences, Faculty of Medicine, University of Oslo, NO-0317 Oslo, Norway

Ida Sneis Boger – Department of Chemistry and Hybrid Technology Hub-Centre of Excellence, Institute of Basic Medical Sciences, Faculty of Medicine, University of Oslo, NO-0315 Oslo, Norway

Ago Mrsa – Department of Chemistry and Hybrid Technology Hub-Centre of Excellence, Institute of Basic Medical Sciences, Faculty of Medicine, University of Oslo, NO-0315 Oslo, Norway

Magnus Saed Restan – Department of Pharmacy, University of Oslo, NO-0316 Oslo, Norway

Matthias Stein – Institute of Medicinal and Pharmaceutical Chemistry, TU Braunschweig, DE-38106 Braunschweig, Germany

Elsa Lundanes – Department of Chemistry, University of Oslo, NO-0315 Oslo, Norway

Stig Pedersen-Bjergaard – Department of Pharmacy, University of Oslo, NO-0316 Oslo, Norway; Department of Pharmacy, Faculty of Health and Medical Sciences, University of Copenhagen, 2100 Copenhagen, Denmark; orcid.org/0000-0002-1666-8043

Aleksandra Aizenshtadt – Hybrid Technology Hub-Centre of Excellence, Institute of Basic Medical Sciences, Faculty of Medicine, University of Oslo, NO-0317 Oslo, Norway

Stefan Krauss – Hybrid Technology Hub-Centre of Excellence, Institute of Basic Medical Sciences, Faculty of Medicine, University of Oslo, NO-0317 Oslo, Norway; Department of Immunology and Transfusion Medicine, Oslo University Hospital, 0317 Oslo, Norway

Gareth Sullivan – Hybrid Technology Hub-Centre of Excellence, Institute of Basic Medical Sciences, Faculty of Medicine, University of Oslo, NO-0317 Oslo, Norway; Department of Pediatric Research, Oslo University Hospital and University of Oslo, 0317 Oslo, Norway

Inger Lise Bogen – Section for Drug Abuse Research, Department of Forensic Sciences, Oslo University Hospital, NO-0424 Oslo, Norway; Institute of Basic Medical Sciences, Faculty of Medicine, University of Oslo, NO-0317 Oslo, Norway

Complete contact information is available at:
<https://pubs.acs.org/10.1021/acs.analchem.0c05082>

Notes

The authors declare no competing financial interest.

ACKNOWLEDGMENTS

This work was supported by the Research Council of Norway through its Centre of Excellence Scheme, project number 262613. The work was also supported by the Olav Thon Foundation. Financial support from UiO:Life Science is also gratefully acknowledged. Technical assistance by Elisabeth Nerem (Department of Forensic Sciences, Oslo University Hospital, Oslo, Norway) was greatly appreciated. S.R.W. is a member of the National Network of Advanced Proteomics Infrastructure (NAPI), which is funded by the Research Council of Norway INFRASTRUKTUR-program (project number: 295910).

REFERENCES

- (1) Prakash, C.; Shaffer, C. L.; Nedderman, A. *Mass Spectrom. Rev.* **2007**, *26*, 340–369.
- (2) Au, S. H.; Chamberlain, M. D.; Mahesh, S.; Sefton, M. V.; Wheeler, A. R. *Lab Chip* **2014**, *14*, 3290–3299.
- (3) Matthews, H.; Hanison, J.; Nirmalan, N. *Proteomes* **2016**, *4*, No. 28.
- (4) Lancaster, M. A.; Knoblich, J. A. *Science* **2014**, *345*, No. 1247125.
- (5) Clevers, H. *Cell* **2016**, *165*, 1586–1597.
- (6) Rossi, G.; Manfrin, A.; Lutolf, M. P. *Nat. Rev. Genet.* **2018**, *19*, 671–687.
- (7) Pampaloni, F.; Reynaud, E. G.; Stelzer, E. H. K. *Nat. Rev. Mol. Cell Biol.* **2007**, *8*, 839–845.
- (8) Westmoreland, C.; Holmes, A. M. *Organogenesis* **2009**, *5*, 67–72.
- (9) Lancaster, M. A.; Renner, M.; Martin, C.-A.; Wenzel, D.; Bicknell, L. S.; Hurlles, M. E.; Homfray, T.; Penninger, J. M.; Jackson, A. P.; Knoblich, J. A. *Nature* **2013**, *501*, 373–379.
- (10) Stevens, K. R.; Kreutziger, K. L.; Dupras, S. K.; Korte, F. S.; Regnier, M.; Muskheili, V.; Nourse, M. B.; Bendixen, K.; Reinecke, H.; Murry, C. E. *Proc. Natl. Acad. Sci. U.S.A.* **2009**, *106*, 16568–16573.
- (11) van de Wetering, M.; Francies, Hayley, E.; Francis, Joshua, M.; Bounova, G.; Iorio, F.; Pronk, A.; van Houdt, W.; van Gorp, J.; Taylor-Weiner, A.; Kester, L.; McLaren-Douglas, A.; Blokker, J.; Jaksani, S.; Bartfeld, S.; Volckman, R.; van Sluis, P.; Li; Vivian, S. W.; Seepo, S.; Sekhar Pedamallu, C.; Cibulskis, K.; et al. *Cell* **2015**, *161*, 933–945.
- (12) Huch, M.; Dorrell, C.; Boj, S. F.; van Es, J. H.; Li, V. S. W.; van de Wetering, M.; Sato, T.; Hamer, K.; Sasaki, N.; Finegold, M. J.;

Haft, A.; Vries, R. G.; Grompe, M.; Clevers, H. *Nature* **2013**, *494*, 247–250.

(13) Park, E.; Kim, H. K.; Jee, J.; Hahn, S.; Jeong, S.; Yoo, J. *Toxicol. Appl. Pharmacol.* **2019**, *385*, No. 114790.

(14) Huch, M.; Gehart, H.; van Boxtel, R.; Hamer, K.; Blokzijl, F.; Verstegen, Monique, M. A.; Ellis, E.; van Wenum, M.; Fuchs; Sabine, A.; de Ligt, J.; van de Wetering, M.; Sasaki, N.; Boers; Susanne, J.; Kemperman, H.; de Jonge, J.; Ijzermans, J. N. M.; Nieuwenhuis, E. E. S.; Hoekstra, R.; Strom, S.; Vries, R. R. G.; et al. *Cell* **2015**, *160*, 299–312.

(15) Driehuis, E.; Kretzschmar, K.; Clevers, H. *Nat. Protoc.* **2020**, *15*, 3380–3409.

(16) Jia, L.; Liu, X. *Curr. Drug Metab.* **2007**, *8*, 822–829.

(17) Brandon, E. F. A.; Raap, C. D.; Meijerman, I.; Beijnen, J. H.; Schellens, J. H. M. *Toxicol. Appl. Pharmacol.* **2003**, *189*, 233–246.

(18) Greek, R.; Menache, A. *Int. J. Med. Sci.* **2013**, *10*, 206–221.

(19) Yoshida, S.; Miwa, H.; Kawachi, T.; Kume, S.; Takahashi, K. *Sci. Rep.* **2020**, *10*, No. 5989.

(20) Mills, R. J.; Parker, B. L.; Quaipe-Ryan, G. A.; Voges, H. K.; Needham, E. J.; Bornot, A.; Ding, M.; Andersson, H.; Polla, M.; Elliott, D. A.; Drowley, L.; Clausen, M.; Plowright, A. T.; Barrett, I. P.; Wang, Q.-D.; James, D. E.; Porrello, E. R.; Hudson, J. E. *Cell Stem Cell* **2019**, *24*, 895–907.

(21) Lu, W.; Rettenmeier, E.; Paszek, M.; Yueh, M.-F.; Tukey, R. H.; Trotter, J.; Barbier, O.; Chen, S. *Drug Metab. Dispos.* **2017**, *45*, 748–754.

(22) Lin, A.; Sved Skottvoll, F.; Rayner, S.; Pedersen-Bjergaard, S.; Sullivan, G.; Krauss, S.; Ray Wilson, S.; Harrison, S. *Electrophoresis* **2020**, *41*, 56–64.

(23) Pedersen-Bjergaard, S.; Rasmussen, K. E. *J. Chromatogr. A* **2006**, *1109*, 183–190.

(24) Drouin, N.; Kubán, P.; Rudaz, S.; Pedersen-Bjergaard, S.; Schappler, J. *TrAC, Trends Anal. Chem.* **2019**, *113*, 357–363.

(25) Gjelstad, A.; Rasmussen, K. E.; Pedersen-Bjergaard, S. *Anal. Bioanal. Chem.* **2009**, *393*, 921–928.

(26) Eibak, L. E. E.; Rasmussen, K. E.; Øiestad, E. L.; Pedersen-Bjergaard, S.; Gjelstad, A. *Anal. Chim. Acta* **2014**, *828*, 46–52.

(27) Drouin, N.; Mandscheff, J.-F.; Rudaz, S.; Schappler, J. *Anal. Chem.* **2017**, *89*, 6346–6350.

(28) Restan, M. S.; Pedersen, M. E.; Jensen, H.; Pedersen-Bjergaard, S. *Anal. Chem.* **2019**, *91*, 6702–6708.

(29) Petersen, N. J.; Jensen, H.; Hansen, S. H.; Foss, S. T.; Snakenborg, D.; Pedersen-Bjergaard, S. *Microfluid. Nanofluid.* **2010**, *9*, 881–888.

(30) Hansen, F. A.; Sticker, D.; Kutter, J. P.; Petersen, N. J.; Pedersen-Bjergaard, S. *Anal. Chem.* **2018**, *90*, 9322–9329.

(31) Kamendulis, L. M.; Brzezinski, M. R.; Pindel, E. V.; Bosron, W. F.; Dean, R. A. *J. Pharmacol. Exp. Ther.* **1996**, *279*, 713.

(32) Rook, E. J.; Alwin, D. R. H.; Brink, W. v. d.; Ree, J. M. v.; Jos, H. B. *Curr. Clin. Pharmacol.* **2006**, *1*, 109–118.

(33) Maurer, H. H.; Sauer, C.; Theobald, D. S. *Ther. Drug Monit.* **2006**, *28*, 447–453.

(34) Ang, L. T.; Tan, A. K. Y.; Autio, M. I.; Goh, S. H.; Choo, S. H.; Lee, K. L.; Tan, J.; Pan, B.; Lee, J. J. H.; Lum, J. J.; Lim, C. Y. Y.; Yeo, I. K. X.; Wong, C. J. Y.; Liu, M.; Oh, J. L. L.; Chia, C. P. L.; Loh, C. H.; Chen, A.; Chen, Q.; Weissman, I. L.; et al. *Cell Rep.* **2018**, *22*, 2190–2205.

(35) Mathapati, S.; Siller, R.; Impellizzeri, A. A. R.; Lycke, M.; Vegheim, K.; Almaas, R.; Sullivan, G. J. *Curr. Protoc. Stem Cell Biol.* **2016**, *38*, 1G.6.1–1G.6.18.

(36) Siller, R.; Greenhough, S.; Naumovska, E.; Sullivan, G. J. *Stem Cell Rep.* **2015**, *4*, 939–952.

(37) Siller, R.; Naumovska, E.; Mathapati, S.; Lycke, M.; Greenhough, S.; Sullivan, G. J. *Sci. Rep.* **2016**, *6*, No. 37178.

(38) Siller, R.; Sullivan, G. J. *Curr. Protoc. Stem Cell Biol.* **2017**, *43*, 1G.7.1–1G.7.23.

(39) Harrison, S. P.; Sillar, R.; Tanaka, Y.; Xiang, Y.; Patterson, B.; Kempf, H.; Melum, E.; Åsrud, K.; Chollet, M. E.; Andersen, E.; Sandset, P. M.; Baumgarten, S.; Bonanini, F.; Kurek, D.; Mathapati,

S.; Almaas, R.; Sharma, K.; Wilson, S. R.; Skottvoll, F. S.; Boger, I. C.; et al. *bioRxiv* **2020**, DOI: 10.1101/2020.12.02.406835.

(40) Hansen, F. A.; Jensen, H.; Pedersen-Bjergaard, S. *Anal. Chem.* **2020**, *92*, 5595–5603.

(41) Karinen, R.; Andersen, J. M.; Ripel, Å.; Hasvold, I.; Hopen, A. B.; Morland, J.; Christophersen, A. S. *J. Anal. Toxicol.* **2009**, *33*, 345–350.

(42) Berg, H. S.; Seterdal, K. E.; Smetop, T.; Rozenvalds, R.; Brandtzaeg, O. K.; Vehus, T.; Lundanes, E.; Wilson, S. R. *J. Chromatogr. A* **2017**, *1498*, 111–119.

(43) Skottvoll, F. S.; Berg, H. E.; Bjørseth, K.; Lund, K.; Roos, N.; Bekhradnia, S.; Thiede, B.; Sandberg, C.; Vik-Mo, E. O.; Roberg-Larsen, H.; Nyström, B.; Lundanes, E.; Wilson, S. R. *Future Sci. OA* **2018**, *5*, No. FSO359.

(44) Pedersen-Bjergaard, S. *Anal. Bioanal. Chem.* **2019**, *411*, 1687–1693.

(45) Chan, S. D. H.; Toyoda, H.; Sanjeeviraman, J.; Soupe, A.; Iwamoto, M.; Wu, W.; Eto, D.; Tada, T.; Kumada, T.; Zhang, J.-P. *Sci. Rep.* **2020**, *10*, No. 7379.

(46) Ou, X.; Chen, P.; Huang, X.; Li, S.; Liu, B.-F. *J. Sep. Sci.* **2020**, *43*, 258–270.

(47) Cong, H.; Xu, X.; Yu, B.; Yuan, H.; Peng, Q.; Tian, C. *J. Micromech. Microeng.* **2015**, *25*, No. 053001.

(48) Fanali, S. *Electrophoresis* **2017**, *38*, 1822–1829.

(49) Yamini, Y.; Pourali, A.; Seidi, S.; Rezazadeh, M. *Anal. Methods* **2014**, *6*, 5554–5565.

(50) Rahimi, A.; Nojavan, S.; Tabani, H. *J. Pharm. Biomed. Anal.* **2020**, *184*, No. 113175.

(51) Ahmar, H.; Tabani, H.; Hossein Koruni, M.; Davarani, S. S. H.; Fakhari, A. R. *Biosens. Bioelectron.* **2014**, *54*, 189–194.

(52) Huang, C.; Seip, K. F.; Gjellstad, A.; Pedersen-Bjergaard, S. *Anal. Chim. Acta* **2016**, *934*, 80–87.

(53) Drouin, N.; Rudaz, S.; Schappler, J. *J. Pharm. Biomed. Anal.* **2018**, *159*, 53–59.

(54) Qian, Y.; Gilliland, T. K.; Markowitz, J. S. *Chem. Biol. Interact.* **2020**, *316*, No. 108914.

(55) Román-Hidalgo, C.; Martín-Valero, M. J.; Fernández-Torres, R.; Callejón-Mochón, M.; Bello-López, M. A. *Talanta* **2017**, *162*, 32–37.

(56) Wang, X.; Liang, Y.; Liu, L.; Shi, J.; Zhu, H.-J. *Rapid Commun. Mass Spectrom.* **2016**, *30*, 553–561.

(57) Prasad, B.; Bhatt, D. K.; Johnson, K.; Chapa, R.; Chu, X.; Salphati, L.; Xiao, G.; Lee, C.; Hop, C. E. C. A.; Mathias, A.; Lai, Y.; Liao, M.; Humphreys, W. G.; Kumer, S. C.; Unadkat, J. D. *Drug Metab. Dispos.* **2018**, *46*, 943.

(58) Wang, X.; Shi, J.; Zhu, H.-J. *Proteomics* **2019**, *19*, No. 1800288.

(59) Boberg, M.; Vrana, M.; Mehrotra, A.; Pearce, R. E.; Gaedigk, A.; Bhatt, D. K.; Leeder, J. S.; Prasad, B. *Drug Metab. Dispos.* **2017**, *45*, 216–223.

(60) Sato, Y.; Miyashita, A.; Iwatsubo, T.; Usui, T. *Drug Metab. Dispos.* **2012**, *40*, 1389–1396.

Supporting Information

Electromembrane extraction and mass spectrometry for liver organoid drug metabolism studies

Frøydis Sved Skottvoll^{a,b}, Frederik André Hansen^c, Sean Harrison^b, Ida Sneis Boger^{a,b}, Ago Mrsa^{a, b}, Magnus Saed Restan^c, Matthias Stein^d, Elsa Lundanes^a, Stig Pedersen-Bjergaard^{c,e}, Aleksandra Aizenshtadt^b, Stefan Krauss^b, Gareth Sullivan^{b,f}, Inger Lise Bogen^{g,h}, Steven Ray Wilson^{a, b*}

^a Department of Chemistry, University of Oslo, P.O. Box 1033, Blindern, NO-0315 Oslo, Norway

^b Hybrid Technology Hub-Centre of Excellence, Institute of Basic Medical Sciences, Faculty of Medicine, University of Oslo, P.O. Box 1112 Blindern, NO-0317 Oslo, Norway

^c Department of Pharmacy, University of Oslo, P.O. Box 1068 Blindern, NO-0316 Oslo, Norway

^d Institute of Medicinal and Pharmaceutical Chemistry, TU Braunschweig, Beethovenstr. 55, DE-38106 Braunschweig, Germany

^e Department of Pharmacy, Faculty of Health and Medical Sciences, University of Copenhagen, Universitetsparken 2, 2100 Copenhagen, Denmark

^f Department of Pediatric Research, Oslo University Hospital and University of Oslo, PO Box 1112 Blindern, 0317 Oslo, Norway

^g Section for Drug Abuse Research, Department of Forensic Sciences, Oslo University Hospital, P.O. Box 4950 Nydalen, NO-0424 Oslo, Norway

^h Institute of Basic Medical Sciences, Faculty of Medicine, University of Oslo, P.O. Box 1103 Blindern, NO-0317 Oslo, Norway

*Corresponding author: stevenw@kjemi.uio.no, +47 97010953. <https://orcid.org/0000-0002-9755-1188>

Table of contents

Figure S-1: S Schematic overview of the workflow of drug studies performed with **(A)** a standard sample preparation approach using centrifugation and several steps of manual pipetting prior to analysis, and **(B)** parallel electromembrane extraction (Pa-EME) with fewer steps of manual pipetting and sample handling prior to analysis.

Figure S-2: Liver organoid drug metabolism using Pa-EME and UHPLC-MS, after incubation of patient derived liver organoids differentiated from primary human hepatocytes (20 organoids) in 10 μ M heroin for 1, 3, 6- and 24 hours. In parallel, cell medium free from organoids were used as drug degradation control samples. Each bar represents the mean (\pm SD) of triplicate samples.

Figure S-3: The concentration (μM) of heroin (0.1 μM final heroin concentration in incubation solution) and its phase I metabolites 6-MAM and morphine in (A) 0.01 mg microsomes and (B) 0.1 mg/mL S9-fractions after centrifugation based sample preparation. Separation and detection was performed using UHPLC-MS. Data points represent the mean (\pm SD) of triplicate samples, and the solid lines represent model prediction.

Figure S-4: Liver organoid drug phase I and II metabolism measuring the concentration (μM) of heroin, 6-MAM, morphine, morphine-3-glucuronide (M3G) and morphine-6-glucuronide (M6G) with the use of centrifugation based sample preparation and UHPLC-MS. Liver organoids differentiated from the iPSC cell line HPSI0114i-vabj_3 (20 organoids) were incubated in 10 μM heroin for 0 and 24 hours. Each bar represent the mean (\pm SD) of triplicate samples.

Table S-1: Identified peptides of the enzymes hCES1 (accession number P23141), hCES2 (accession number O00748) and UDP-glucuronosyltransferase 2B7 (accession number P16662) related to heroin liver metabolism, with annotated sequence, quality q-value, the total number (#) of protein groups identified with the peptide, number (#) of peptide spectral matches (PSMs), peptide position in the protein, number (#) of missed cleavages of the identified peptide. * The peptide is also identified in putative inactive carboxylesterase 4 (CES1P1, accession number Q9UKY3).

Figure S-5: Chromatogram showing the separation of the analytes M3G, M6G, morphine, 6-MAM and heroin with the use of UHPLC-MS.

Figure S-6: Electropherogram of liver organoid drug phase I metabolism using Pa-EME and simple capillary electrophoresis with ultraviolet spectroscopy detection (CE-UV), after incubation with liver organoids differentiated from the iPSC cell lines AG27 (60 organoids) in 50 μ M heroin for 6 hours.

Additional experimental procedures: Heroin metabolism assay in S9-fractions and microsomes, sample preparation using centrifugation, capillary electrophoresis with ultraviolet spectroscopy detection.

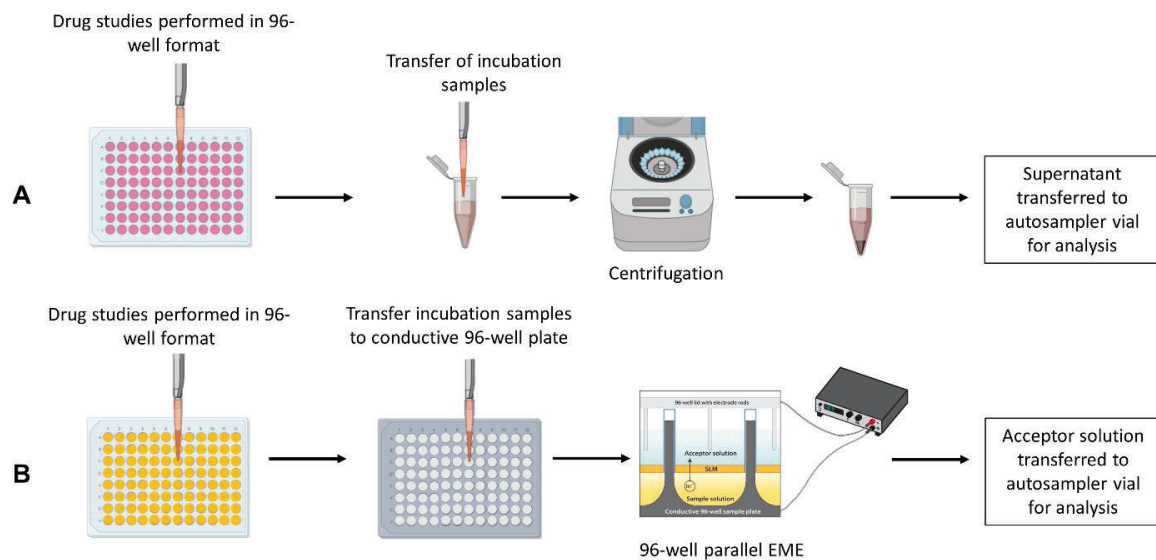


Figure S-1. Schematic overview of the workflow of drug studies performed with **(A)** a standard sample preparation approach using centrifugation and several steps of manual pipetting prior to analysis, and **(B)** parallel electromembrane extraction (Pa-EME) with fewer steps of manual pipetting and sample handling prior to analysis.

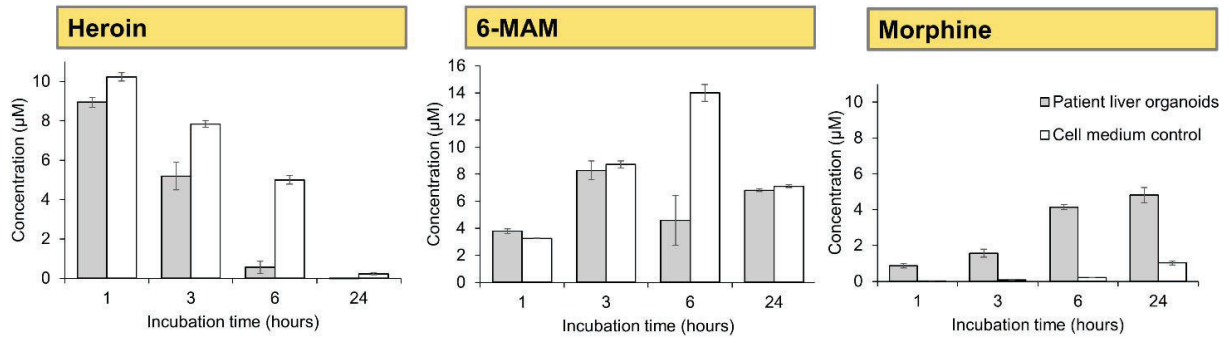


Figure S-2. Liver organoid drug metabolism using Pa-EME and UHPLC-MS, after incubation of patient derived liver organoids differentiated from primary human hepatocytes (20 organoids) in 10 µM heroin for 1, 3, 6- and 24 hours. In parallel, cell medium free from organoids were used as drug degradation control samples. Each bar represents the mean (\pm SD) of triplicate samples.

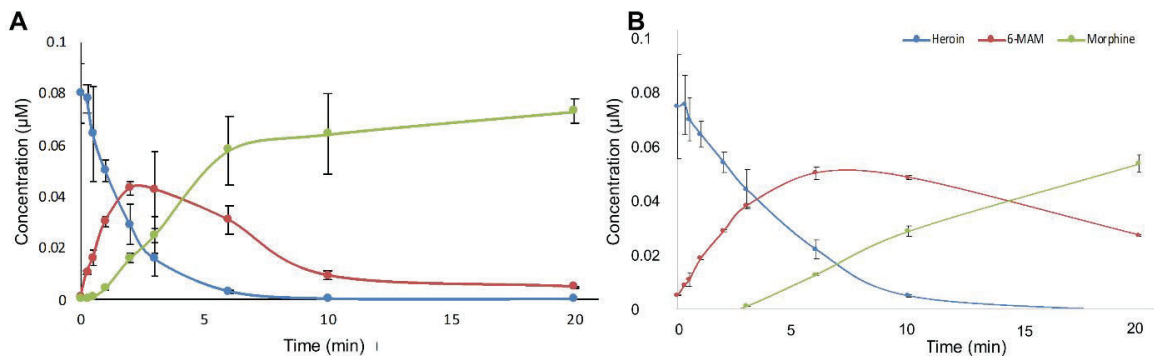


Figure S-3. The concentration (μM) of heroin (0.1 μM final heroin concentration in incubation solution) and its phase I metabolites 6-MAM and morphine in (A) 0.01 mg microsomes and (B) 0.1 mg/mL S9-fractions after centrifugation based sample preparation. Separation and detection was performed using UHPLC-MS. Data points represent the mean (\pm SD) of triplicate samples, and the solid lines represent model prediction.

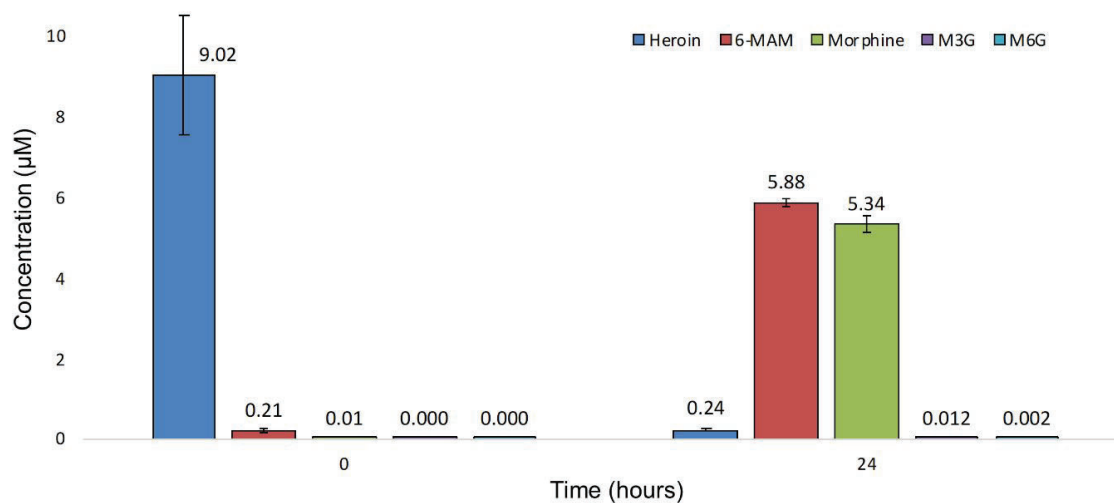


Figure S-4. Liver organoid drug phase I and II metabolism measuring the concentration (μM) of heroin, 6-MAM, morphine, morphine-3-glucuronide (M3G) and morphine-6-glucuronide (M6G) with the use of centrifugation based sample preparation and UHPLC-MS. Liver organoids differentiated from the iPSC cell line HPSI0114i-vabj_3 (20 organoids) were incubated in 10 μM heroin for 0 and 24 hours. Each bar represent the mean (\pm SD) of triplicate samples.

Table S-1. Identified peptides of the enzymes hCES1 (accession number P23141), hCES2 (accession number O00748) and UDP-glucuronosyltransferase 2B7 (accession number P16662) related to heroin liver metabolism, with annotated sequence, quality q-value, the total number (#) of protein groups identified with the peptide, number (#) of peptide spectral matches (PSMs), peptide position in the protein, number (#) of missed cleavages of the identified peptide. * The peptide is also identified in putative inactive carboxylesterase 4 (CES1P1, accession number Q9UKY3).

Annotated Sequence	Quality q-value	# Protein Groups	# PS Ms	Identified in Protein accession number [position in protein]	# Missed Cleavages
*[R].AISESGVALTSVLVK. [K]	5.45707 E-05	2	3	Q9UKY3 [244-258]; P23141 [243-257]	0
[R].FTPPQPAEPWSFVK. [N]	5.45707 E-05	1	2	P23141 [65-78]	0
[K].FVSLEGFAQPVAIFLGI PFAKPPLGPLR.[F]	5.45707 E-05	1	3	P23141 [37-64]	0
[R].GNWGHLDQVAALR. [W]	5.45707 E-05	1	7	P23141 [187-199]	0
[K].TVIGDHGDELFSVFGA PFLK.[E]	5.45707 E-05	1	3	P23141 [463-482]	0
[K].MVMKFWANFAR.[N]	0.00023 9472	1	1	P23141 [495-505]	1
[K].TAMSLWVK.[S]	0.00023 9472	1	2	P23141 [377-384]	0
[K].EGYLQIGANTQAAQK .[L]	0.00130 768	1	1	P23141 [524-538]	0
[K].FWANFAR.[N]	0.00525 625	1	1	P23141 [499-505]	0
[R].APVYFYEFQHQPSWL K.[N]	5.45707 E-05	1	2	O00748 [431-446]	0
[K].GANAGVQTFLGIPFA KPPLGPLR.[F]	5.45707 E-05	1	3	O00748 [50-72]	0
[K].ADHGDELPFVFR.[S]	0.00023 9472	1	3	O00748 [455-466]	0
[K].ALPQKIQELEPEER. [H]	0.00487 95	1	1	O00748 [541-555]	1
[K].ADVWLIR.[N]	1.5E-3	1	2	P16662 [253-259]	0

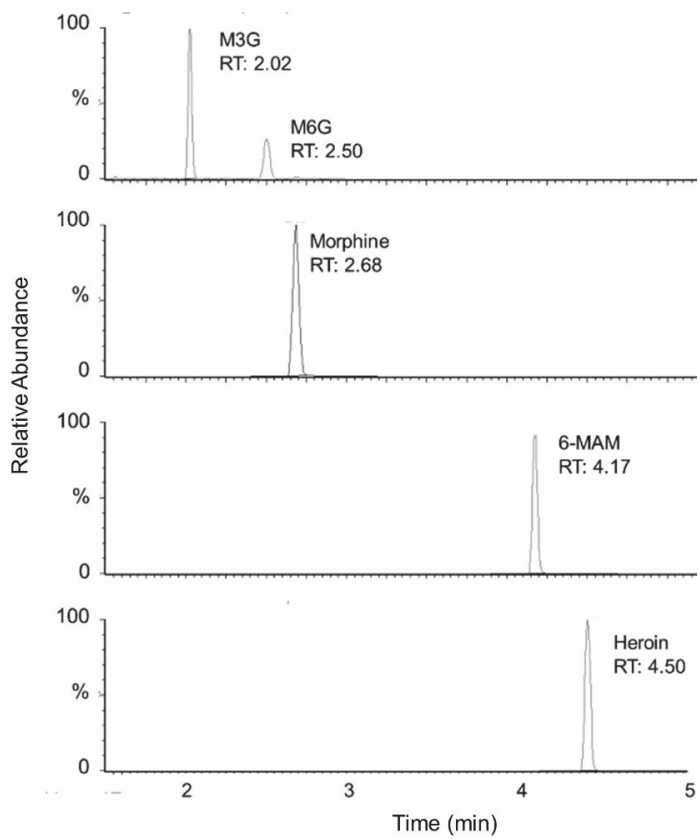


Figure S-5. Chromatogram showing the separation of the analytes M3G, M6G, morphine, 6-MAM and heroin with the use of UHPLC-MS.

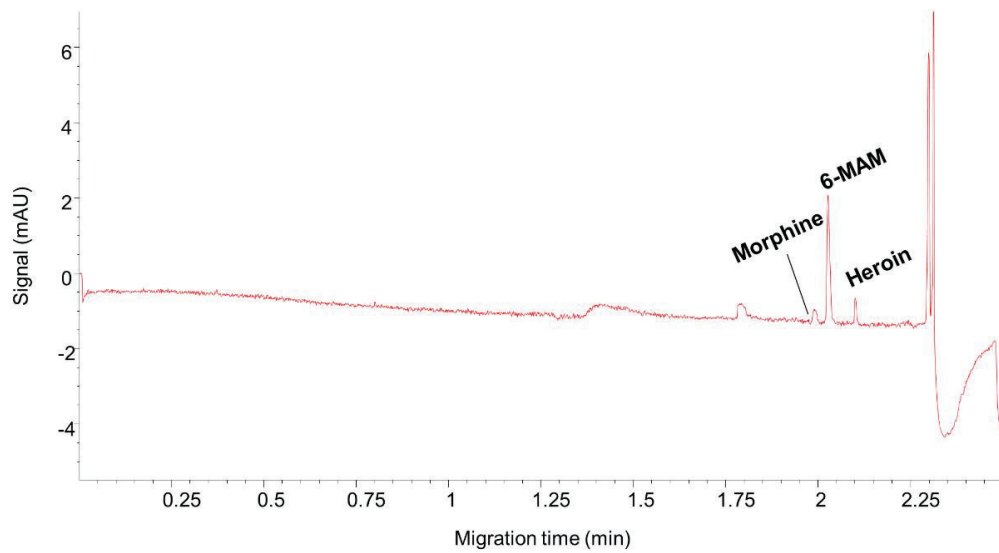


Figure S-6. Electropherogram of liver organoid drug phase I metabolism using Pa-EME and simple capillary electrophoresis with ultraviolet spectroscopy detection (CE-UV), after incubation with liver organoids differentiated from the iPSC cell lines AG27 (60 organoids) in 50 μ M heroin for 6 hours.

Additional experimental procedures

Heroin metabolism assay in microsomes and S9-fraction

A volume of 80 μL NADPH regenerating solution (Corning Incorporated, NY, USA) and 10 μL pooled human liver microsomes (XTreme 200 pool, final concentration 0.01 mg protein/sample, XenoTech, Kansas City, KS, US) or S9-fraction (Xtreme 200 pool S9 fraction, 0.01 mg protein/sample, XenoTech) were added to Eppendorf tubes and pre-incubated at 37°C for 10 min in a water bath. The heroin metabolism was initiated by adding 10 μL 1 μM heroin (final concentration 0.1 μM), and the Eppendorf tubes were vortexed before incubation at 37°C for 0-20 minutes. The metabolism was terminated by addition of 10 μL 1.2 M formic acid followed by 10 μL of a 1.5 μM mixture of internal standards (morphine-d3, 6-MAM-d6 and heroin-d9), and the samples were immediately vortexed for 30 sec. In parallel, drug degradation control samples (without microsomes or S9-fraction) were prepared.

Sample preparation using centrifugation

Centrifugation was performed using a MiniSpin plus from Eppendorf (Hamburg, Germany), or a Micro Star 17R from VWR or an Allegra X-15 R from Beckman Coulter (Brea, California, USA). The samples were centrifuged at 4°C at 14 500 g for 10 min, and the supernatants

were transferred to auto sampler vials. The vials were kept on ice if analyzed the same day as the experiment, or at -80°C until analysis.

Capillary electrophoresis with ultraviolet spectroscopy detection

The capillary electrophoresis (CE) separations with data handling were carried out using a 7100 CE instrument equipped with an on-column diode-array detector and a CE Chemstation software from Agilent Technologies (Waldbronn, Germany). Separations were performed using fused-silica capillaries from PolymicroTechnologies (Phoenix, AZ, USA), with $L_{\text{tot}} = 59$ cm and $L_{\text{eff}} = 51$ cm, $75\ \mu\text{m}$ ID and $360\ \mu\text{m}$ outer diameter (OD). The background electrolyte (BGE) consisted of 30 mM ammonium formate adjusted to pH 8 using a 1 M solution of NaOH. Initial conditioning of a new capillary was carried out at a pressure of 1000 mbar with 1 M NaOH (20 min), water (5 min) and BGE (20 min and for 5 min at +15 kV). Daily conditioning of the capillary was performed (1000 mbar) with 0.1 M NaOH (5 min), water (2 min) and BGE (10 min and for 5 min at 30 kV). Before each injection, the capillary was rinsed at a pressure of 1000 mbar with 0.1 M NaOH and water (0.5 min each), followed by the BGE (3 min). Hydrodynamic injections were performed at 50 mbar: starting with diluted BGE (9 +1, water + BGE) for 3 s, followed by the sample injection (15 s, equivalent to around 107 nL) and the BGE (3 s). Separations and measurements were performed with an applied potential of +30 kV (25°C) and at an UV-absorbance of 214 nm.

V

Direct Electromembrane Extraction-Based Mass Spectrometry: A Tool for Studying Drug Metabolism Properties of Liver Organoids

Frøydis Sved Skottvoll,^[a, b] Aleksandra Aizenshtadt,^[b] Frederik André Hansen,^[c] Mikel Amirola Martinez,^[b] Jannike Mørch Andersen,^[d] Inger Lise Bogen,^[d] Jörg P. Kutter,^[e] Stig Pedersen-Bjergaard,^[c] Elsa Lundanes,^[a] Stefan Krauss,^[b] and Steven Ray Wilson^{✉[a, b]}

This work introduces a strategy for organoid analysis - direct Electromembrane Extraction based Mass Spectrometry (dEME-MS) – for coupling liver organoids with mass spectrometry (MS). dEME-MS comprises electrophoresis of selected small molecules from a culture chamber across an oil membrane, and to a MS compatible solution. This enables clean micro-extraction of drugs and their metabolites as produced in the liver organoids to capillary liquid chromatography-mass spectrometry. Applying dEME-MS, proof-of-concept of directly measuring methadone metabolism is demonstrated on adult liver organoids. With 50 liver organoids and 1 μM methadone, methadone metabolism was monitored from 0 to 24 hours (11 time points). All analytes had <0.4% variance in retention times with > 100 measurements. dEME-MS is capable of automated and selective monitoring of drug metabolism in liver organoids, and could serve as a valuable tool for automated drug discovery efforts.

The rapidly growing attention to liver organoids (Figure 1A–B) is related to their potential in resembling human physiology and metabolism to a greater degree than conventional 2D cell cultures and animal models^[1,2] Since the cells used to develop liver organoids can be derived from individual patients, organo-

id technology is envisioned to become important for personalized medicine and it is believed that the technology has a potential to transform drug discovery and personalized medicine.^[3]

Liver organoids are typically studied/characterized with a technical repertoire including immunofluorescence microscopy, ELISA, RT PCR, and RNA-seq.^[4] For quantification of drugs and metabolites, MS is often coupled with liquid chromatography (LC), which separates compounds prior to MS measurements, enabling improved sensitivity and more reliable identifications.^[5] We have recently studied metabolism of liver organoids with conventional “off-line” manual sample preparation steps (centrifugation steps, etc.) prior to LC-MS^[6] (Figure 1C). However, such protocols are non-optimal for small samples or high throughput/automation. To our knowledge, there are currently no reports on coupling liver organoids and LC-MS in one single system. Two important technical challenges have obstructed the merging of liver organoids and MS into a directly coupled/single system.

Firstly, growth conditions for liver organoids may be operated at lower microliter scales, while conventional LC-MS is designed for larger volumes. Secondly, cell culture solutions contain salts and substantial amounts of proteins (e.g. albumin from medium) that can severely reduce sensitivity and/or contaminate the MS system, if the organoid culture chamber is connected directly (on-line) to the MS. The mismatch between LC-MS and cell culture volumes can be addressed by down-scaling the LC system. If the inner diameter (ID) of the LC column is reduced, from the conventional 2.1 mm format to 0.5 mm (capillary LC, capLC), a higher sensitivity can often be obtained, requiring far less sample amounts.^[7]

To resolve the mismatch between cell culture solutions and LC solvents, electromembrane extraction (EME) across an oil-immobilized membrane (supported liquid membrane, SLM) is an attractive choice (Figure 2).^[8,9] Solvents that can be used to immobilize the separating membrane include 2-nitrophenyl octyl ether (NPOE, highly suited for hydrophobic and basic compounds) and di (2-ethylhexyl) phosphate (DEHP, more suited for highly polar compounds).^[10] By modifying the membrane solvent and applying voltage polarity/magnitude, EME can be tuned to allow selective extraction and enrichment of drugs and/or metabolites (even for complex samples such as full blood, see reference^[11]).

[a] F. S. Skottvoll, Dr. E. Lundanes, Dr. S. R. Wilson
Department of Chemistry
University of Oslo
E-mail: stevenw@kjemi.uio.no


[b] F. S. Skottvoll, Dr. A. Aizenshtadt, M. A. Martinez, Dr. S. Krauss,
Dr. S. R. Wilson
Hybrid Technology Hub Centre of Excellence, Faculty of Medicine
University of Oslo

[c] Dr. F. A. Hansen, Dr. S. Pedersen-Bjergaard
Department of Pharmacy
University of Oslo

[d] Dr. J. M. Andersen, Dr. I. L. Bogen
Section for Drug Abuse Research
Department of Forensic Sciences
Oslo University Hospital, Norway

[e] Dr. J. P. Kutter
Department of Pharmacy
University of Copenhagen

 Supporting information for this article is available on the WWW under <https://doi.org/10.1002/anse.202100051>

 © 2021 The Authors. *Analysis & Sensing* published by Wiley-VCH GmbH. This is an open access article under the terms of the Creative Commons Attribution Non-Commercial License, which permits use, distribution and reproduction in any medium, provided the original work is properly cited and is not used for commercial purposes.

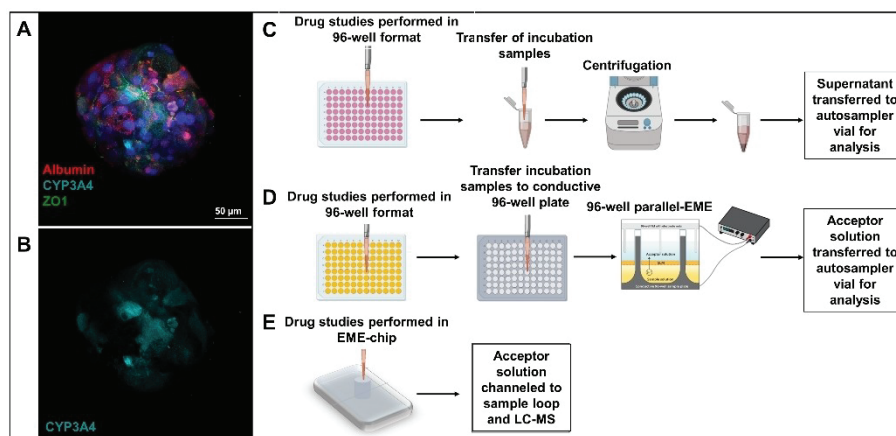


Figure 1. A–B) Representative images of the whole-mount staining of liver organoids formed from adult hepatocytes, albumin (red), CYP3A4 (turquoise) and ZO1 (green), Scale bar 50 μm . C) Schematic overview of drug studies performed with simple sample handling using centrifugation and manual pipetting prior to analysis [6]. D) Drug studies performed with high throughput sample handling using parallel-EME with reduced steps of sample handling prior to analysis (multi-sample EME) [12]. E) Drug studies performed on chip (single-sample dEME) with continuous EME extraction and no manual sample handling prior to LC-MS analysis (this Communication). Figure adapted/expanded from our previous work [12] (further permissions related to the material excerpted should be directed to the American Chemical Society).

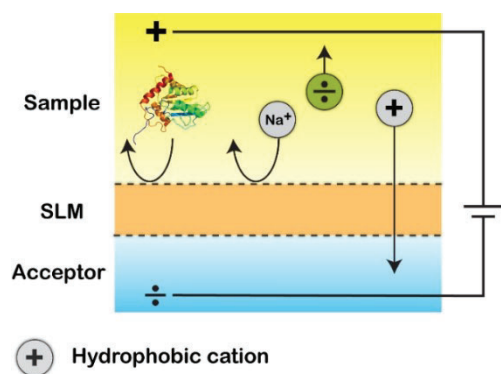


Figure 2. Principle of EME. Sample extraction is performed by electro-assisted partitioning of ions into and across the SLM and to the acceptor solution. Proteins and salts in the donor solution are discriminated by the hydrophobicity of the SLM.

We have recently shown that off-line EME is excellent for simple and parallel extraction of drugs and metabolites from organoids in a 96-well format, reducing sample preparation steps (Figure 1D).^[12] However, on-line coupling of EME and MS would allow for a substantially higher degree of automation and throughput. EME has been briefly explored for on-line coupling to MS for microsome-based studies,^[13–15] encouraging us to hypothesize that EME is a potential tool for the bridging of liver organoids and MS.

In this communication, we describe our prototype on-line dEME-MS system, which features liver organoids, chip-EME, capillary LC, electrospray ionization, and a triple quadrupole mass spectrometer. The system is reduced to one single manual step, namely adding a drug or reagent to the organoid culture chamber prior to automated analysis of molecules including the drug and its metabolites that pass the membrane (Figure 1E). We then demonstrate the system in a proof-of-concept study of methadone metabolism.

See Supporting Information for experimental details.

The dEME-MS chip (Figure 3A–B) allowed for liver organoids to be exposed to small molecule drugs, and derived metabolites + drugs could subsequently be extracted on-line into a microfluidic channel with a flow-through of LC-MS compatible solution. Methadone was chosen as a model drug due to the well-established EME conditions, and to the hydrophobic nature of the methadone metabolites 2-ethylidene-1,5-dimethyl-3,3-diphenylpyrrolidine (EDDP) and 2-ethyl-5-methyl-3,3-diphenylpyrrolidine (EMDP) also previously studied using EME.^[15,16] In addition, methadone metabolism is predictive for CYP3A4 activity, a major enzyme in drug metabolism. The chip structure was fabricated from thiol-ene polymer, adapting the same design as previously reported.^[17] Thiol-ene is a highly cross-linked thermoset polymer composed of two monomers with free thiol and allyl (or “-ene”) functionalities, respectively. Polymerization can be initiated by UV-radiation, and is characterized by fast click-chemistry with near 100% monomer conversion.^[18] Thiol-ene additionally offers low shrinkage upon polymerization, and is compatible with cell culture.^[19] Some modifications were made compared to previous chip-designs: The chamber system was modified to feature an inner chamber which the liver organoids were placed in, preventing direct contact with the electrode. The polycarbonate membrane bottom (5 μm pore size) of the inner chamber enabled analyte diffusion to the extraction chamber, while preventing contact between the organoids and the SLM. The membrane may also have provided a limited clean-up of macromolecules, such as proteins, while small molecules (like salts) were free to diffuse into the extraction chamber. Another modification included an increase in the thickness of the upper chip layer, and an extraction chamber to contain the donor solution, all casted in thiol-ene as one piece. The use of thiol-ene differed from the previous study,^[17] where the extraction chamber composed of glass resulted in high methadone adsorption. To avoid clogging observed under stagnant conditions, the acceptor

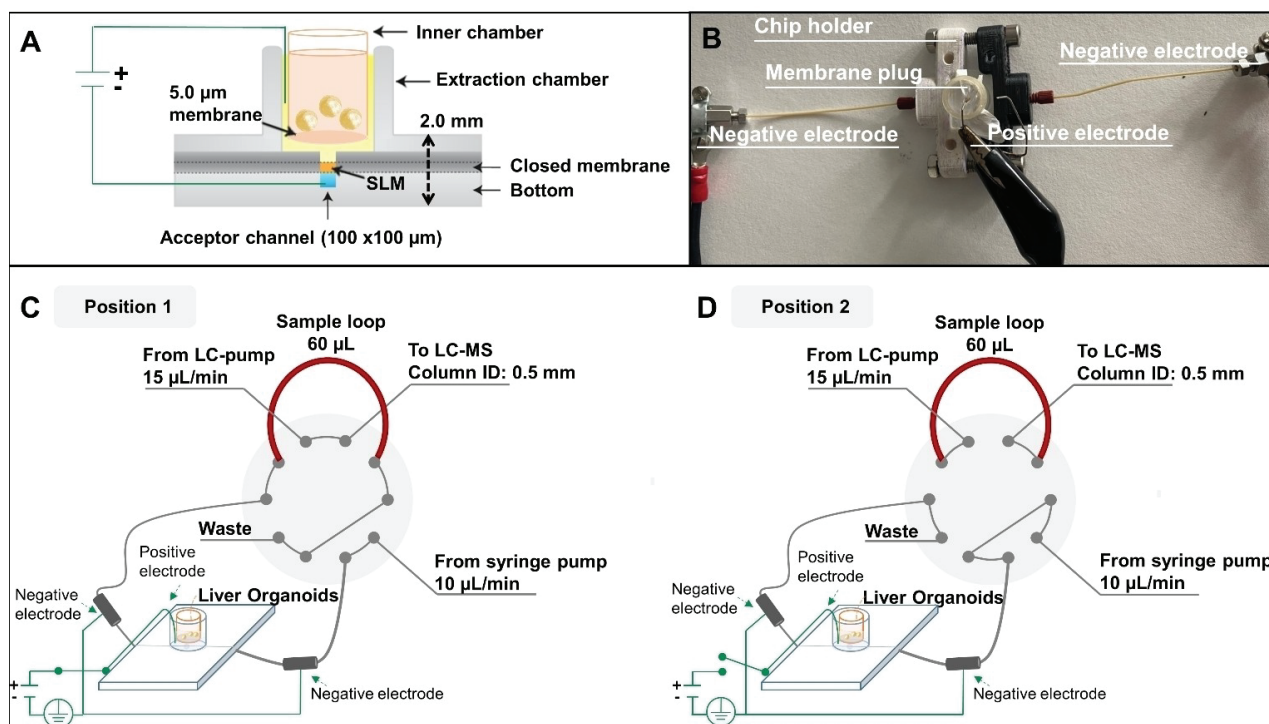


Figure 3. A) Illustration of a side-viewed cross-section of the SLM at the center of the chip. B) Top-down photograph of the EME chip assembly. C) Valve system for collecting EME extracts in a 60 μL loop, and subsequent transfer to LC-MS. In position 1- EME is performed and sample transfer to sample loop. D) In position 2- sample loading and LC-MS analysis.

solution was continuously pumped through the acceptor channel. NPOE was chosen as the solvent for SLM, due to the excellent methadone extraction capabilities when using NPOE.^[16,20] Preparation of the SLM was performed by placing a small droplet NPOE onto the dry porous membrane of the chip. The solvent penetrated the pores and became completely immobilized by strong capillary forces. This enabled flow of the acceptor solution without loss of NPOE. The voltages applied during EME of methadone and metabolites are often preferably in the 15–50 V range.^[17] The voltage applied in this study, shown to be favorable with regards to recovery, was 40 V after initial evaluation of 20 V, 30 V and 40 V.

During EME, the acceptor solution was pumped to a valve system that bridges the EME-chip and the LC-MS system (Figure 3C–D). A platinum electrode was placed in the extraction chamber (positive electrode). To provide a robust electrical field, the two reducing unions on either side of the SLM were constituting the negative electrode. Importantly, the set-up allows for acceptor solution fractions to be collected under low-pressure conditions, so that the high-pressures LC is operated under would not affect chip integrity. In this system, the collection loop was 60 μL, allowing for an “under-filling” of the 50 μL fraction (5-minute collection time) from the EME chip.

Due to the highly selective nature of EME,^[21,22] the valve system and subsequent LC step was not exposed to unwanted compounds, e.g. salts and proteins from the liver organoids and medium. This is a clear advantage, as we have experienced severe clogging with non-EME capillary LC systems when used to analyze liver organoids. Since the fractioning time, loop

volumes and sampling intervals can be widely varied/adjusted, an LC-MS method does not need to be compromised regarding time needed for re-equilibration, solvent gradient programming, and other steps.

A capillary LC column (0.5 mm ID) was employed in the present study. The MS instrument used was a triple quadrupole-MS, which is the standard approach for targeted measurements of drugs and metabolites. The capillary LC set-up used was also compatible with high resolution MS (Orbitrap, etc.), which can be important for structural elucidation of undetermined metabolites.

After successful initial tests, the cell culture chamber would be filled with 50 liver organoids and mixed with methadone, typically in the low μM range, in accordance with our previous work.^[6,12] The system was used to test drug metabolism of methadone to its metabolites EDDP and EMDP by liver organoids. Figure 4 shows clean LC-MS chromatograms of the methadone, EDDP and EMDP 24 hours after liver organoid exposure to 1 μM methadone, illustrating activity of the CYP3A4 enzyme. The overall liver organoid viability after 24 hours of dEME was visually inspected to be over 50% (Figure S1), which we considered satisfactory at this stage. All our analytes had <0.4% variance in retention times with >100 measurements, and together with characteristic mass spectrometric properties of the analytes, allowed for selective measurements of similar/related compounds (Figure 4).

Secondly, methadone metabolism in liver organoids was monitored from 0 to 24 hours (11 time points), where time point 0 min corresponded to the first 5 minutes of EME-

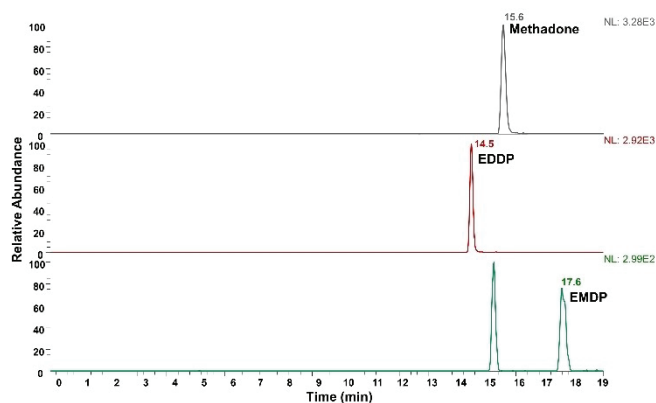


Figure 4. Extracted ion chromatogram of methadone, EDDP and EMDP in on-chip EME extracted liver organoids after 24 hours of incubation in 1 μM methadone.

sampling, after the addition of methadone to the inner chamber (containing liver organoids) and the extraction chamber (see Figure 5A). The measured methadone peak area and the metabolite formation in liver organoids were compared to the methadone metabolism of two conventional model systems for drug metabolism studies, namely human liver microsomes, and rat liver metabolism analyzed with conventional LC-MS/MS. As shown in Figure 5A, the measured peak area curves of methadone and the main metabolite EDDP in organoids resembled the *in vivo* metabolism in rats (Figure 5B) and humans^[23,24] more closely than the metabolism profile in human liver microsomes (Figure 5C). The initial formation of EDDP observed after addition/administration of methadone (in organoids and in rats), can be explained by the methadone-induced activation of the pregnane X receptor (PXR) and constitutive androstane receptor (CAR), consequently leading to an upregulation of the drug-metabolizing enzymes expression^[25] which is not possible to observe with the human liver microsomes. Trace levels of the methadone metabolite EMDP were also successfully measured in liver organoids and human liver microsomes (see Figure S2, see also Table S1 for methadone stability evaluation).

For four individual organoid batches, variances were anticipated at this prototype stage (see Figure S3). The variances could derive from factors such as drift in MS signal intensity or chip-to-chip extraction efficiency, and the use of adult liver organoids from different donors. The expression level and metabolic activity of CYP3A4 and other drug metabolizing enzymes are highly donor-specific, thus leading to variances in the formation of methadone metabolites between donors. Regardless of the high variances measured with dEME-MS, the similar profile of the methadone metabolite formation in organoids from different donors demonstrated the reproducibility of the method.

In summary, dEME-MS is capable of automated and selective monitoring of drug metabolism in liver organoids. Further technical steps to improve repeatability will include addition of internal standards in the acceptor solution for absolute quantification and modification of our chip design to

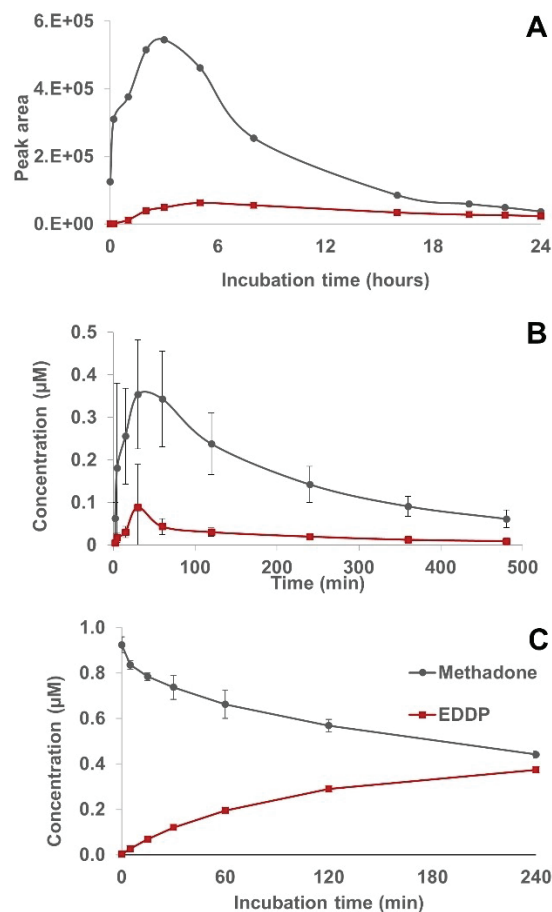


Figure 5. A) Peak area of methadone and EDDP from a representative study of liver organoid drug metabolism in 1 μM methadone using incubation and dEME, continuous sample transfer and capLC-MS/MS measurements. Measurements were undertaken at the following time points; 0 hours, 20 min, 1, 2, 3, 5, 8, 16, 20, 22 and 24 hours. B) Metabolism of methadone in rats given a single dose of methadone (2.5 mg/kg, s.c.). Data points represent the mean (\pm SD) blood concentrations (in μM) of methadone and EDDP ($n=5$). The animal experiments (Project ID: 1649) were approved by the Norwegian Animal Research Authority (Norwegian Food Safety Authority, Oslo, Norway) and performed in accordance with the laws and regulations controlling experiments on animals in Norway. C) Metabolism of 1 μM methadone in human liver microsomes. Data points represent the mean (\pm SD) concentration (in μM) of methadone and EDDP ($n=3-4$).

be compatible with commercial LC fittings. Next, the system will be assessed for other drugs/metabolites of telltale traits of enzyme activity, and ultimately as a tool for automated drug discovery efforts.

Acknowledgements

Financial support from the UiO:Life Science Convergence Environment grant is gratefully acknowledged. SRW is a member of the National Network of Advanced Proteomics Infrastructure (NAPI), which is funded by the Research Council of Norway INFRA-STRUKTUR-program (project number: 295910). SRW, SK, AA, FSS, MAM are supported by the Research Council of Norway through its Centre of Excellence scheme; project number 262613. Technical assistance with human liver microsomes studies by Elisabeth

Nerem (Department of Forensic Sciences, Oslo University Hospital, Oslo, Norway) was greatly appreciated.

Conflict of Interest

The authors declare no conflict of interest.

Keywords: drug metabolism · electromembrane extraction · liquid chromatography · mass spectrometry · organoids.

- [1] J. Kim, B.-K. Koo, J. A. Knoblich, *Nat. Rev. Mol. Cell Biol.* **2020**, *21*, 571–584.
- [2] M. Hofer, M. P. Lutolf, *Nat. Rev. Mater.* **2021**, *6*, 402–420.
- [3] B. Zhang, A. Korolj, B. F. L. Lai, M. Radisic, *Nat. Rev. Mater.* **2018**, *3*, 257–278.
- [4] A. Lin, F. Sved Skottvoll, S. Rayner, S. Pedersen-Bjergaard, G. Sullivan, S. Krauss, S. Ray Wilson, S. Harrison, *Electrophoresis* **2020**, *41*, 56–64.
- [5] A. Rubiano, A. Indapurkar, R. Yokosawa, A. Miedzik, B. Rosenzweig, A. Arefin, C. M. Moulin, K. Dame, N. Hartman, D. A. Volpe, M. K. Matta, D. J. Hughes, D. G. Strauss, T. Kostrzewski, A. J. S. Ribeiro, *Clin. Transl. Sci.* **2021**, *14*, 1049–1061.
- [6] S. P. Harrison, R. Sillar, Y. Tanaka, Y. Xiang, B. Patterson, H. Kempf, E. Melum, K. Åsrud, M. E. Chollet, E. Andersen, P. M. Sandset, S. Baumgarten, F. Bonanini, D. Kurek, S. Mathapati, R. Almaas, K. Sharma, S. R. Wilson, F. S. Skottvoll, I. C. Boger, I. L. Bogen, T. A. Nyman, J. J. Wu, A. Bezrouk, D. Cizkova, J. Mokry, R. Zweigerdt, I.-H. Park, G. J. Sullivan, *bioRxiv* **2020**, 2020.2012.2002.406835.
- [7] S. R. Wilson, T. Vehus, H. S. Berg, E. Lundanes, *Bioanalysis* **2015**, *7*, 1799–1815.
- [8] S. Pedersen-Bjergaard, K. E. Rasmussen, *J. Chromatogr. A* **2006**, *1109*, 183–190.
- [9] N. Drouin, P. Kubáň, S. Rudaz, S. Pedersen-Bjergaard, J. Schappler, *TrAC Trends Anal. Chem.* **2019**, *113*, 357–363.
- [10] F. A. Hansen, P. Kubáň, E. L. Øiestad, S. Pedersen-Bjergaard, *Anal. Chim. Acta* **2020**, *1115*, 23–32.
- [11] A. Gjelstad, K. E. Rasmussen, S. Pedersen-Bjergaard, *Anal. Bioanal. Chem.* **2009**, *393*, 921–928.
- [12] F. S. Skottvoll, F. A. Hansen, S. Harrison, I. S. Boger, A. M. S. Restan, M. Stein, E. Lundanes, S. Pedersen-Bjergaard, A. Aizenshtadt, S. Krauss, G. Sullivan, I. L. Bogen, S. R. Wilson, *Anal. Chem.* **2021**, *93*, 3576–3585.
- [13] N. J. Petersen, J. S. Pedersen, N. N. Poulsen, H. Jensen, C. Skonberg, S. H. Hansen, S. Pedersen-Bjergaard, *Analyst* **2012**, *137*, 3321–3327.
- [14] D. Fuchs, H. Jensen, S. Pedersen-Bjergaard, C. Gabel-Jensen, S. H. Hansen, N. J. Petersen, *Anal. Chem.* **2015**, *87*, 5774–5781.
- [15] D. Fuchs, C. Gabel-Jensen, H. Jensen, K. D. Rand, S. Pedersen-Bjergaard, S. H. Hansen, N. J. Petersen, *Anal. Chim. Acta* **2016**, *905*, 93–99.
- [16] M. S. Restan, Ø. Skjærvø, Ø. G. Martinsen, S. Pedersen-Bjergaard, *Anal. Chim. Acta* **2020**, *1104*, 1–9.
- [17] F. A. Hansen, D. Sticker, J. P. Kutter, N. J. Petersen, S. Pedersen-Bjergaard, *Anal. Chem.* **2018**, *90*, 9322–9329.
- [18] C. E. Hoyle, T. Y. Lee, T. Roper, *J. Polym. Sci. Part A* **2004**, *42*, 5301–5338.
- [19] D. Sticker, R. Geczy, U. O. Häfeli, J. P. Kutter, *ACS Appl. Mater. Interfaces* **2020**, *12*, 10080–10095.
- [20] L. Vårdal, E. L. Øiestad, A. Gjelstad, H. Jensen, S. Pedersen-Bjergaard, *Bioanalysis* **2019**, *11*, 755–771.
- [21] N. C. Domínguez, A. Gjelstad, A. M. Nadal, H. Jensen, N. J. Petersen, S. H. Hansen, K. E. Rasmussen, S. Pedersen-Bjergaard, *J. Chromatogr. A* **2012**, *1248*, 48–54.
- [22] M. S. Restan, H. Jensen, X. Shen, C. Huang, Ø. G. Martinsen, P. Kubáň, A. Gjelstad, S. Pedersen-Bjergaard, *Anal. Chim. Acta* **2017**, *984*, 116–123.
- [23] J. De Vos, J. Ufkes, H. van Wilgenburg, P. Geerlings, W. van den Brink, *Eur. J. Clin. Pharmacol.* **1995**, *48*, 361–366.
- [24] A. Ferrari, C. P. R. Coccia, A. Bertolini, E. Sternieri, *Pharmacol. Res.* **2004**, *50*, 551–559.
- [25] A. H. Tolson, H. Li, N. D. Eddington, H. Wang, *Drug Metab. Dispos.* **2009**, *37*, 1887–1894.

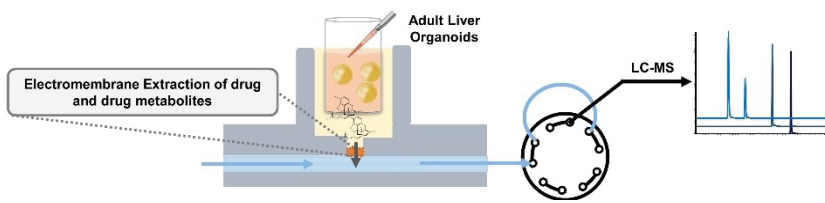
Manuscript received: October 6, 2021

Revised manuscript received: December 20, 2021

Accepted manuscript online: December 21, 2021

Version of record online: ■■■, ■■■■

COMMUNICATIONS



Liver organoids have been predicted to serve as valuable models in drug analysis. Here, liver organoids are coupled with mass spectrometry (MS), through direct Electromembrane Ex-

traction sample preparation on chip (dEME-MS). As a proof-of-concept, methadone metabolism was continuously monitored for 24 hours using adult liver organoids.

*F. S. Skottvoll, Dr. A. Aizenshtadt, Dr. F. A. Hansen, M. A. Martinez, Dr. J. M. Andersen, Dr. I. L. Bogen, Dr. J. P. Kutter, Dr. S. Pedersen-Bjergaard, Dr. E. Lundanes, Dr. S. Krauss, Dr. S. R. Wilson**

1 – 6

Direct Electromembrane Extraction-Based Mass Spectrometry: A Tool for Studying Drug Metabolism Properties of Liver Organoids



Analysis & Sensing

Supporting Information

Direct Electromembrane Extraction-Based Mass Spectrometry: A Tool for Studying Drug Metabolism Properties of Liver Organoids

Frøydis Sved Skottvoll, Aleksandra Aizenshtadt, Frederik André Hansen, Mikel Amirola Martinez, Jannike Mørch Andersen, Inger Lise Bogen, Jörg P. Kutter, Stig Pedersen-Bjergaard, Elsa Lundanes, Stefan Krauss, and Steven Ray Wilson*

Table of Contents

Table of Contents.....	S1
Experimental Procedures.....	S1
Results and Discussion.....	S4
References.....	S6
Author Contributions.....	S6

Experimental Procedures

Chemicals and Solutions

2-Nitrophenyl octyl ether (NPOE), ammonium formate (>99%), methadone hydrochloride (>98%), 2-Ethylidene-1,5-dimethyl-3,3-diphenylpyrrolidine (EDDP) perchlorate and formic acid (FA, reagent grade 95%) were purchased from Sigma Aldrich (St. Louis, MO). LC-MS grade water and acetonitrile (ACN) were purchased from VWR (Radnor, PA). For UHPLC-MS, methadone hydrochloride, EDDP perchlorate, methadone d3 and EDDP d3 was purchased from Chiron AS (Trondheim, Norway). Human liver microsomes (Xtreme pool 200) were from XenoTech (Kansas City, KS), and NADPH regenerating solution from Corning Incorporated (Corning, NY). Heparin was purchased from LEO Pharma (Lysaker, Norway).

5 mM ammonium formate buffer (w/v) was made by dissolving ammonium formate in LC-MS grade water followed by pH adjustment by the addition of FA to pH 3.1. A stock solution of 53 mM EDDP (w/v) was made by dissolving one ampule of 10 mg EDDP perchlorate in 500 μ L ACN (stored at -20 °C). A stock solution of 40 mM methadone (w/v) was made by dissolving 15 mg methadone in 1000 μ L ACN (stored at -20 °C). Working solutions of methadone (2 μ M =WSM) were prepared freshly by diluting stock solution in FBS free medium. Low concentration standards were prepared by diluting stock solution in 5 mM ammonium formate pH 3.1 or 0.1% FA (v/v).

Adult Liver Organoids

Cell culture: Cryopreserved primary human hepatocytes (PHH) (Lot HUM180201A from Lonza, Basel, Switzerland and Lot HU8287 from Thermo Fisher Scientific, Waltham, MA) were thawed according to vendor protocol. For the formation of liver organoids, PHH were plated into Elplasia ultra-low attachment plates with microwells (Corning, NY) at the concentration 500 viable PHH/microwell. PHH aggregation was facilitated by short centrifugation (100 g, 2 min). Adult liver organoids were cultured in Williams E medium (Thermo Fisher Scientific) supplemented with 1% insulin-transferrin-selenium mix (ITS, Thermo Fisher Scientific), 10% fetal bovine serum (FBS), and 0.1 μ M dexamethasone (Bio-Techne Ltd., Abingdon, United Kingdom) for the first 3 days in culture. From day 4, half of the medium was daily exchanged for the FBS-free media with the same formulation. 24h prior to the EME-chip experiments adult liver organoids were incubated in FBS-free medium supplemented with 5 μ M rifampicin (Sigma Aldrich) for induction of CYP3A4 activity.

Whole-organoid Immunofluorescence Staining and Confocal Microscopy

Adult liver organoids were washed in phosphate buffered saline (PBS, Thermo Fisher Scientific) and fixed with 4% formaldehyde (Sigma Aldrich) for 20 min. Permeabilization and blocking was performed by incubation in PBS with 1% bovine serum albumin (BSA, Sigma Aldrich), 0.2% Tritox-X100 (Sigma Aldrich) and 0.5% DMSO at RT for 2h with constant mixing, followed by 24 hours (at 4°C) incubation with primary (anti-human serum albumin (PN ab2406, Abcam, Cambridge, United Kingdom) antibodies, and subsequently with 2h incubation with CyTM3 AffiniPure Donkey Anti-Rabbit secondary antibodies (1:400, at RT) (Jackson Immuno Research, West Grove, PA) diluted with 1% BSA, 0.1% Tritox-X100 in PBS. Nuclear counterstaining was performed with 1 μ g/mL DAPI for 5 min at RT (PN D9542, Sigma Aldrich). Confocal microscopy was performed on a Meta 710 laser scanning confocal microscope from Zeiss (Oberkochen, Germany) using standard filters sets and laser lines with a 40X oil immersion objective. Images were acquired using Zen software (Zeiss) as Z-stacks with 0.9 μ m spacing between stacks. The confocal images were analyzed using Fiji software [1]. Confocal image was displayed as a resulting Z-stack of half of spheroid.

Adult Liver Organoid Functionality Test

Functionality of adult liver organoids was probed by analysis of albumin secretion and CYP3A4 activity. Culture medium of organoids that were used for EME chip experiments was collected and albumin concentrations were determined by ELISA (Bethyl Laboratories, Montgomery, TX). Albumin values were normalized to organoids number and size as determined from bright field imaging. CYP3A4 activity in rifampicin-treated and control organoids was measured by P450-Glo CYP3A4 cell-based Assay with Luciferin-IPA (Promega, Madison, WI) according to the manufacturer's protocol. Results were normalized to ATP measured CellTiter-Glo 3D Cell Viability Assay (Promega) according to the manufacturer's protocol.

Electromembrane Extraction Chip

SUPPORTING INFORMATION

EME chips/set-up were prepared similar to that described in Hansen et al. [2], but with a series of modifications allowing for more rugged analysis of organoids. The chip was constructed with four layers, with the first three layers fabricated according to above-mentioned previous report. The bottom layer had a microchannel (0.1 x 0.1 x 15 mm) that held the acceptor solution, while the second layer contained a porous polypropylene membrane (25 μm thick, Celgard 2500, Celgard, Charlotte, NC) laminated on top of the bottom layer. For the third layer, thiol-ene was casted onto the porous membrane and sealed the pores, except a circular area of 0.28 mm² above the acceptor channel that was kept free. The thiol-ene free porous membrane area was used to hold the SLM for EME. The final layer comprised a layer to increase the thickness of the chip, and a reservoir to hold the donor solution (outer EME chip reservoir), casted in thiol-ene as one piece. A separate well reservoir (inner EME chip reservoir) was made by laser cutting a sterile Corning® HTS Transwell-96 Permeable Support, constituting the organoid chamber (5.0 μm pore polycarbonate membrane, Sigma Aldrich). The total inner/outer chamber volume used in this study was 280 μL , while only 6 nL acceptor solution was in contact with the SLM. This large difference in volume enabled the desirable combination of soft extraction and analyte enrichment.

Prior to use, a few microliters of NPOE was added to the porous membrane, and excess NPOE was removed with a wipe. The PEEK tubing on the in/outlet of the EME chip channel was 0.39 μm ID and cut to be 80 mm (1/32 inch OD, IDEX Health & Science LLC, Oak Harbor, WA), as 100 μm ID was also associated with clogging at 37 °C. The chip channel inlet/outlet was connected to the PEEK tubing using #6-32 coned fittings (Microtight, IDEX), a 3D-printed chip holder and cylindrical PDMS O-ring both fabricated in-house [2]. The 1/32 inch OD PEEK tubing was connected to the valve system using stainless steel reducing unions (Valco, Schenkon, Switzerland) and Viper™ stainless steel capillaries (0.18 mm ID, 350 mm) from Thermo Fisher Scientific. A number of 50 organoids were placed in the inner EME chip reservoir in 50 μL FBS free medium + 50 μL WSM (final concentration of 1 μM methadone). A volume of 90 μL WSM was added to the outer EME chip reservoir, together with 90 μL FBS free medium (final concentration of 1 μM methadone). A platinum electrode was placed in the outer EME chip reservoir (positive electrode) and the two reducing unions were constituting the negative electrode, all connected to an external power supply from Delta Elektronika (Zierikzee, Netherlands). A gas permeable membrane plug (originally a part of an Agilent 1200 solvent degasser from Agilent Technologies, Santa Clara, CA) was capped onto the reservoir construction to avoid sample evaporation.

The extraction voltage was controlled on and off via a relay from Sensata/Crydom (San Diego, CA) controlled by the LC software (Agilent Chemstation). Voltage (40 V) was applied at 5 min for soft extraction of drugs and metabolites across the SLM and into the acceptor solution (5 mM ammonium formate pH 3.1). The acceptor solution was continuously pumped through the microchip channel (10 $\mu\text{L}/\text{min}$), using a syringe pump (World Precision Instruments, Sarasota, FL). The chip assembly was placed on a closed metal tray on a modified Thermoshaker (PSC-20, Grant-bio, Cambridge, UK) for temperature control (250 rpm, 37 °C), monitored using a Temptec thermometer. The bottom of the tray was filled with water to prevent medium evaporation.

Valve System

The acceptor solution was continuously pumped to a 2-position 10-port stainless steel valve (VICI, Houston, TX). When voltage was applied (extraction), the acceptor solution (5 min X 10 $\mu\text{L}/\text{min}$ = 50 μL) was collected in a ~60 μL loop (0.5 x 300 mm PEEK tubing, IDEX). After collection, the loop was connected to the capillary LC-MS system (described in the next section), where the LC mobile phase would pump the contents to the column for separation and detection. During LC-MS and other non-extraction events, the acceptor solution was pumped to waste.

Capillary Liquid Chromatography and Electrospray Mass Spectrometry

Determination of methadone, EDDP and EMDP after EME-sampling was performed with an Agilent 1100 series pump equipped with an Agilent 1200 autosampler from Agilent Technologies. The autosampler and pump was coupled to Quantiva (triple quadrupole) MS with an electrospray ionization (ESI) interface from Thermo Fisher Scientific. The extracted sample was pumped from the sample loop and to the analytical column through a nanoViper™ fitting (50 μm , 550 mm, Thermo Scientific). Separation was performed using a HotSep® Sunniest C18 analytical column (150 x 0.5 mm, 3 μm particles and 120 Å pores) from GT Septech Teknolab (Ski, Norway). The Agilent 1100 series pump was equipped with two solvent compartments (A and B), where A contained 5 mM ammonium formate pH 3.1 (w/v) and B contained 0.1% FA in LC-MS grade water and ACN (5/95, v/v). The solvent compartment composition was initially kept constant at 40% B during sample loading and refocusing. Then, a linear gradient was applied ranging from 40% to 85% B in 3.5 min at a flow rate of 15 $\mu\text{L}/\text{min}$. The ion spray voltage was set to 3.5 kV and the vaporizer temperature was set to 33 °C. The MS operated in positive mode, with multiple reaction monitoring (MRM) transitions and collision energies (ce) for methadone (m/z 265.1 > 310.1 at 15 V and m/z 105 > 310.1 at 29 V), EDDP (m/z 234.1 > 278.1 at 31 V and m/z 186 > 278.1 at 36 V) and EMDP (m/z 219.1 > 264.1 at 31 V). Solvent gradients, valve positioning and MS acquisition was controlled by the Agilent LC software (Chemstation).

Live/Dead Staining

The viability of liver organoids after 24h incubation in the chip was tested using a Live/Dead assay (ThermoFisher Scientific) as described by the manufacturer. Briefly, organoids were collected from EME chip, washed in D-PBS and incubated for 30 min at 37 °C in a 5% CO₂ incubator in 1 mL of culture media containing 1 μL of calcein AM solution and 5 μL of ethidium homodimer-1 solution. Stained organoids were analyzed using a fluorescence microscope (Zeiss).

Metabolism Studies in Human Liver Microsomes

Human liver microsomes were stored at -80 °C. Eppendorf tubes added NADPH regeneration solution (final concentration 1.3 mM NADP⁺, 3.3 mM glucose-6-phosphate, 0.4 U/ml glucose-6-phosphate dehydrogenase, 3.3 mM MgCl₂) and human liver microsomes

SUPPORTING INFORMATION

(final concentration 1 mg protein/mL) were pre-incubated to 37 °C for 15 minutes in a shaking water bath. The reaction was initiated by addition of methadone HCl (final concentration of 1 µM in a total volume of 100 µL) and stopped after 0, 5, 15, 30, 60, 120 and 240 min by addition of ice-cold formic acid (final concentration 0.1 M). Internal standards (methadone-d3 and EDDP-d3) were added and the samples mixed by immediate vortexing. The samples were centrifuged at 14500 × g and 4°C for 10 min and the supernatants were transferred to autosampler vials. Drug degradation control samples, without human liver microsomes, were performed in parallel to evaluate the stability of methadone at the incubation conditions.

The samples were analyzed by UHPLC-MS/MS using an Acquity UPLC system coupled to a TQ-MS with an electrospray ionization interface (Waters, Milford, MA). Methadone, EDDP and EMDP were separated on an Acquity HSS T3 column (2.1 x 100 mm, 1.8 µm; Waters) using gradient elution with a mobile phase consisting of 10 mM ammonium formate buffer, pH 3.1 (solvent A) and MeOH (solvent B), a flow rate of 0.5 ml/minute and a column temperature of 65°C. The gradient had a total run time of 6 minutes with the following profile: 0-0.5 minutes; 20% B, 0.5-1.0 minutes; 20-50% B, 1.0-4.0 minutes; 50-85% B, 4.0-4.1 minutes; 85-100% B, 4.1-5.0 minutes; 100% B, 5.0-5.1 minutes; 20% B. The injection volume was 5 µL. MS analysis was performed with positive ionization using MRM mode. A capillary voltage of 1 kV, source temperature of 150°C, desolvation gas temperature of 500°C, cone gas flow of 60 L/hour and desolvation gas flow of 1100 L/hour were used. The MRM transitions for the compounds had the following values: methadone: m/z 310.0 > 265.0 (cone voltage (cv) 40 V, ce 18 eV) and m/z 310.0 > 223.0 (cv 40 V, ce 18 eV), methadone d3: m/z 313.0 > 268.0 (cv 40 V, ce 18 eV), EDDP: m/z 278.1 > 249.2 (cv 44 V, ce 24 eV) and m/z 278.1 > 234.1 (cv 44 V, ce 30 eV), EDDP d3 m/z 281.2 > 249.2 (cv 44, ce 24) EMDP: m/z 264.3 > 220.2 (cv 38 V, ce 32 eV) and m/z 264.3 > 235.2 (cv 38 V, ce 22 eV). Acquisition and processing were performed using Masslynx software (version 4.1, Waters).

Metabolism Studies in Rats

Male Wistar rats (Møllegaard Breeding Laboratories, Denmark) were injected with methadone (2.5 mg/kg, s.c.). At specified times after injection (5–480 min) blood samples were taken from the tail vein. The blood samples were immediately transferred to microcentrifuge tubes containing sodium fluoride (final conc. 4 mg/ml) dissolved in heparin (100 IU/ml), and frozen in liquid nitrogen. The blood samples were analyzed by LC-MS/MS using a previously described method [3] with the inclusion of the analyte EDDP (m/z: 278.1 > 234.1). The animal experiments (Project ID: 1649) were approved by the Norwegian Animal Research Authority (Norwegian Food Safety Authority, Oslo, Norway) and performed in accordance with the laws and regulations controlling experiments on animals in Norway.

SUPPORTING INFORMATION

Results and Discussion

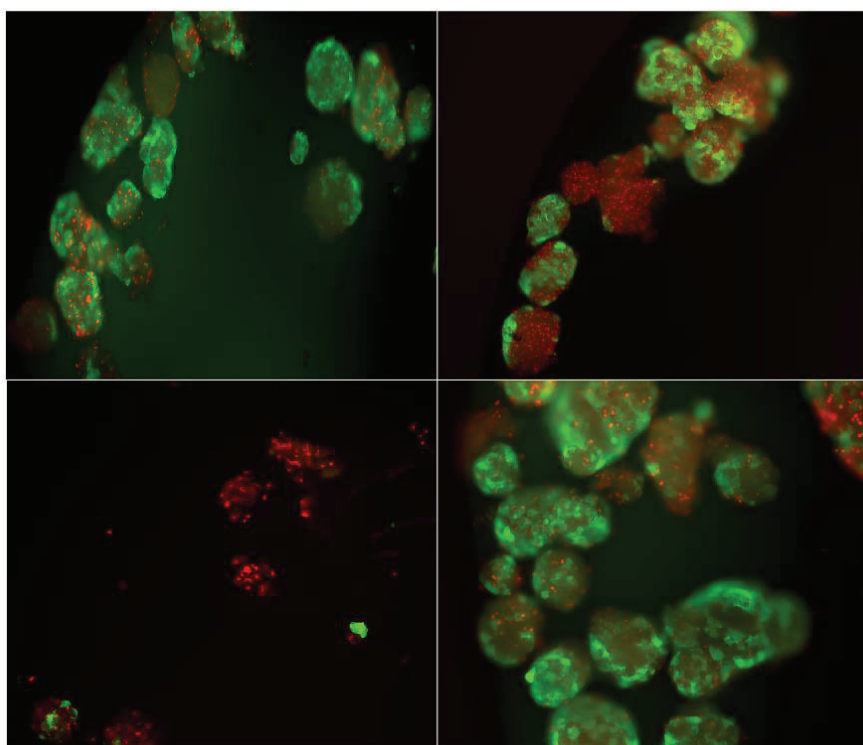


Figure S1. Live (green)/Dead (red) staining of adult liver organoids after 24 hours of incubation on-chip using a fluorescence microscope.

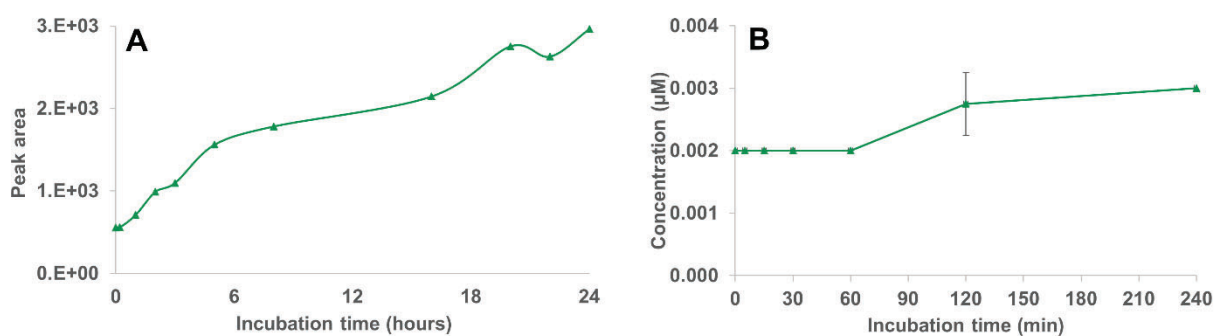


Figure S2. **A)** Peak area of the methadone metabolite EMDP from a representative study of liver organoid drug metabolism in 1 μM methadone using incubation and EME on-chip, continuous sample transfer and capLC-MS/MS measurements. Measurements were undertaken at the following time points; 0 hours, 20 min, 1, 2, 3, 5, 8, 16, 20, 22 and 24 hours. **B)** Metabolism of 1 μM methadone in human liver microsomes. Data points represent the mean (\pm SD, $n=3-4$) EMDP concentration (μM).

SUPPORTING INFORMATION

Table S1. Measured concentration (μM) of methadone, EDDP and EMDP in drug degradation control samples, performed in parallel with the human liver microsomes studies.

Time of incubation	Concentration methadone (μM)	Concentration EDDP (μM)	Concentration EMDP (μM)
C-1 - 0 min	0.902	0.002	0
C-2 - 0 min	0.921	0.002	0
C-3 - 0 min	0.972	0.002	0
C-4 - 120 min	0.905	0.001	0
C-5 - 120 min	0.9	0.001	0
C-6 - 120 min	0.844	0.001	0
C-7 - 240 min	0.832	0.001	0
C-8 - 240 min	0.825	0.002	0
C-9 - 240 min	0.875	0.002	0

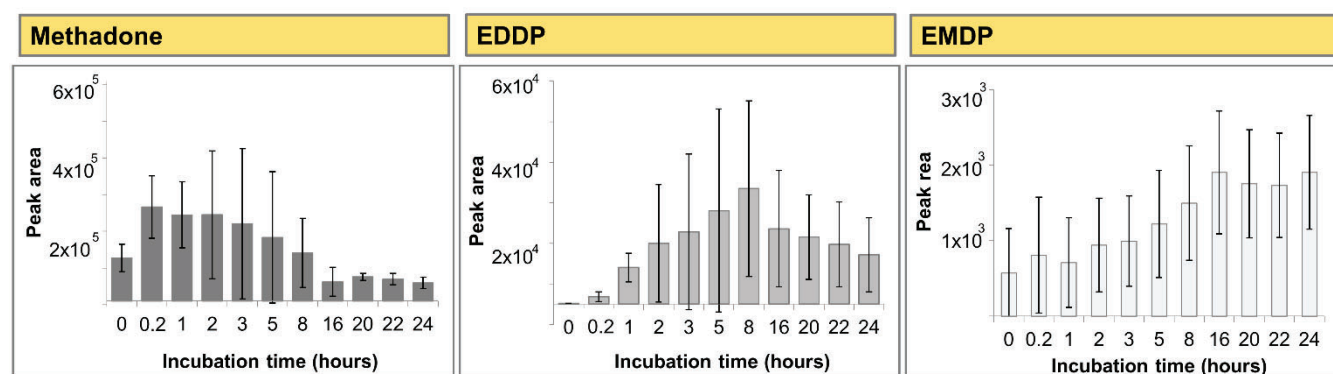


Figure S3. Mean peak area (\pm SD) of methadone and metabolites from the four studies of adult liver organoids drug metabolism in $1 \mu\text{M}$ methadone using incubation and EME on-chip, and continuous sample transfer and capLC-MS measurements. Measurements were undertaken at the following time points; 0 hours, 20 min, 1, 2, 3, 5, 8, 16, 20, 22 and 24 hours. Time point 8, 20, 22 and 24 was not measured in one of the four studies due to operational difficulties.

References

- [1] Schindelin, J., Arganda-Carreras, I., Frise, E., Kaynig, V., Longair, M., Pietzsch, T., Preibisch, S., Rueden, C., Saalfeld, S., Schmid, B., Tinevez, J.-Y., White, D. J., Hartenstein, V., Eliceiri, K., Tomancak, P., Cardona, A., *Nat. Methods* **2012**, 9, 676-682.
- [2] Hansen, F. A., Sticker, D., Kutter, J. P., Petersen, N. J., Pedersen-Bjergaard, S., *Anal. Chem.* **2018**, 90, 9322-9329.
- [3] Andersen, J. M., Olaussen, C. F., Ripel, A., Mørland, J., *Pharmacol., Biochem. Behav.* **2011**, 98, 412-416.

Author Contributions

SRW and FSS conceived the project and directed the research. FAH fabricated the chip. AA prepared the adult liver organoids, FSS conducted the EME on-chip experiments. MAM conducted the live/dead staining of spheroids. JMA conducted the rat experiments and ILB supervised the microsome experiment. SRW and FSS contributed to the writing of the manuscript. All the authors discussed the results and commented on the manuscript.